



UNIVERSITAT DE
BARCELONA

UNIVERSITY OF BARCELONA

Faculty of Pharmacy and Food Sciences

DEPARTAMENT OF PHARMACY, PHARMACEUTICAL
TECHNOLOGY AND PHYSICAL CHEMISTRY

**Pioglitazone dosage forms for the treatment of inflammation
associated with skin, ocular and neurodegenerative diseases**

MARCELLE SILVA DE ABREU
BARCELONA, 2018



UNIVERSITAT DE
BARCELONA

UNIVERSITY OF BARCELONA

Faculty of Pharmacy and Food Sciences

DEPARTAMENT OF PHARMACY, PHARMACEUTICAL
TECHNOLOGY AND PHYSICAL CHEMISTRY

DOCTORAL PROGRAM: RESEARCH, DEVELOPMENT AND
CONTROL OF DRUGS

**Pioglitazone dosage forms for the treatment of inflammation
associated with skin, ocular and neurodegenerative diseases**

Report presented by Marcelle Silva de Abreu to obtain the title of doctor
from the University of Barcelona

Directors

Dra. María Luisa García López

Dra. Marta Espina García

PhD Candidate

Marcelle Silva de Abreu

Tutor

Dra. María Luisa García López

MARCELLE SILVA DE ABREU
BARCELONA, 2018

To my best friend *Jesus*

ACKNOWLEDGMENTS

Firstly, I would like to say thanks to GOD for guiding me each day of my life, giving me peace, health and strength to overcome daily challenges.

Also, I wish to express my gratitude to the *Coordenação de Aperfeiçoamento de Nível Superior* (CAPES) Brazil, for the scholarship they granted me over the time while I was developing this thesis.

I would also like to thank:

My thesis directors Professor Dr. María Luisa García and Professor Dr. Marta Espina for giving me the opportunity to develop this doctoral thesis and to work in their research group, and for making me aware of the world of nanostructured systems.

Professor Dr. Ana Calpena, who has been fundamental in the development of this thesis: thank you for your friendship, encouragement, perseverance and active collaboration every day.

Dr. María Antonia Egea for her knowledge and the bright cheer she gave me. Also, my thanks go to Dr. María Dolores Ricart for her words of support she always heartened me with.

I would like to thank my family in a special way, because they are the basis for all I have achieved so far. My mother Carmem, a wonderful woman who makes my days happier and I find her motivation and strength to move on, she always made me believe that I could get here. My sister Michelle, her prayers and love kept me strong every day, none of them were in vain, thank you for always supporting me and to be a strong arm by my side. To my father Francisco "*in memorian*" who made me see since I was a child that I was capable. He supported me and encouraged me every day of his life. My heart is filled with pride for having had so wonderful, honest and loving parents, who even in little things have always taught us the way we should walk. Thanks also to my brother-in-law Nilson for all his words of encouragement and prayers. To my brother, Givanildo, "*in memorian*" for so many unforgettable moments shared.

I cannot leave out all my laboratory partners during these years, so much time together, working nights and weekends: Alexandre, Amanda, Elena, Lilian, María, Mireia, Marta and Paulina. Especially to Roberto (for his good friendship and help in the laboratory), Camila (for her friendship and friendly conversations in Portuguese to relax) Gladys (for so many shared moments together), and Sukran (the beautiful Turkish girl).

Also, to the master students that I had over these years, Sussy, Rubén and Ana, thank you for supporting me in the laboratory.

I also value and am grateful for other numerous collaborations:

My special thanks to Dr. Alvaro and Lúdia from Animal Facility, Bellvitge Health Sciences Campus, University of Barcelona: without your help it would not have been possible to achieve so many results.

Professor Dr. David Male, an incredible person and excellent immunologist from The Open University (Milton Keynes, UK), who has given me the opportunity to know so much about world of brain endothelial cells, during my PhD internship. It has been a wonderful and unforgettable experience.

Professor Dr. Nacho Romero for giving me the opportunity to carry out studies on the passage of the nanoparticles through the blood brain barrier and enable me to enter into contact with Dr. David Male.

Dr. María José Fábrega for her help in the toxicity studies in the HaCat cell line and for her friendship.

Professor Dr. María José Rodríguez from the department of physiology, University of Barcelona for her collaboration in histological studies: thank you for your willingness to help and support.

Professor Dr. Lyda Halbaut, of the department of pharmaceutical technology, University of Barcelona for her contribution in rheological studies and for always being willing to lend a hand.

Professor Dr. Amelia Silva of Trás-os-Montes University (Portugal) for ocular toxicity studies in the retinoblastoma cell line.

I am also grateful to the group CIBERNED, Centro de Investigación Biomédica en Red de Enfermedades Neurodegenerativas, Instituto de Salud Carlos III, Spain and Servei d'Anatomia Patològica, IDIBELL-Hospital Universitari de Bellvitge, University of Barcelona, to Isidre Ferrer, Esther Aso and Pol Andrés. Thank you for all your support with the *in vivo* studies in the transgenic mice model with Alzheimer's Disease.

All these collaborations were fundamental to get me here. Thank you!

I could not forget Josefina, my roommate for 3 years: thanks for your friendship and for the many times you have been like a mother to me.

I would also like to thank my roommates Juan and Cira, for so many good times shared. Especially Cira, for your friendship, help and the many times you have been like a sister. Moreover, I am grateful to my friend Genildo for all the technical support during these years.

I could not fail to remember Carolina and Faviola, "powerpuff girls", for their friendship, a gift from God in my life. Thank you for so many shared moments of laughter together, trips and the things that are still to come.

Finally, thanks to all who were directly or indirectly involved in the years of this doctoral thesis. I believe that words are too few for me to describe my great affection for all of you.

Marcelle Abreu

INDEX

1.	INTRODUCTION	3
1.1	INFLAMMATION	3
1.2	SKIN INFLAMMATION DISORDERS	5
1.2.1	STRUCTURE AND FUNCTION OF THE SKIN	5
1.2.2	ROSACEA	10
1.3	OCULAR INFLAMMATORY DISEASES	12
1.3.1	STRUCTURE AND FUNCTION OF THE EYE	12
1.3.2	UVEITIS	13
1.4	BRAIN NEUROINFLAMMATORY DISEASES.....	16
1.4.1	CENTRAL NERVOUS SYSTEM: STRUCTURE AND FUNCTION	16
1.4.2	BRAIN ADMINISTRATION ROUTES.....	19
1.4.3	ALZHEIMER’S DISEASES	23
1.5	PEROXISOME PROLIFERATOR ACTIVATED RECEPTOR γ (PPAR γ)	26
1.5.1	PIOGLITAZONE.....	29
1.6	PIOGLITAZONE DOSAGE FORMS	30
1.6.1	LIQUID PHARMACEUTICAL FORMS	30
1.6.2	NANOCARRIERS FOR DRUG DELIVERY.....	32
2.	OBJECTIVES.....	41
3.	RESULTS.....	45
3.1	Article 1	47
	Human Skin Permeation Studies with PPAR γ Agonist to Improve Its Permeability and Efficacy in Inflammatory Processes.....	47
3.2	Article 2	71
	Optimization, Biopharmaceutical Profile and Therapeutic Efficacy of Pioglitazone-loaded PLGA-PEG Nanospheres as a Novel Strategy for Ocular Inflammatory Disorders	71
3.3	Article 3	93
	Comparative Study of Ex Vivo Transmucosal Permeation of Pioglitazone Nanoparticles for the Treatment of Alzheimer’s Disease	93
3.4	Article 4	109
	PPAR γ agonist-loaded PLGA-PEG nanocarriers as a potential treatment for Alzheimer’s disease: <i>in vitro</i> and <i>in vivo</i> studies.....	109
3.5	Article 5	141
	Thiazolidinedione as alternative to facilitate oral administration in geriatric patients with Alzheimer’s Disease.....	141

4.	DISCUSSION	163
4.1	DEVELOPMENT, OPTIMIZATION AND CHARACTERIZATION OF DOSAGE FORMS	163
4.2	BIOPHARMACEUTICAL BEHAVIOUR	165
4.3	TOLERANCE AND CYTOTOXICITY	167
4.4	INTERNALIZATION, TRANSPORT AND PERMEABILITY STUDIES.....	168
4.5	THERAPEUTIC EFFICACY OF DOSAGE FORMS.....	168
5.	CONCLUSIONS	173
6.	REFERENCES	177

ABBREVIATION

AA: Arachidonic acid

AD: Alzheimer's disease

A β : Amyloid beta protein

BBB: Blood brain barrier

BRB: Blood-retinal barrier

CECs: Cerebral endothelial cells

CNS: Central nervous system

COX: Cyclooxygenase

C_{ss}: Steady-state plasma concentration

DEGEE: Diethylene glycol monoethyl ether

DMSO: Dimethylsulfoxide

DSC: Differential Scanning Calorimetry

EE: Encapsulation Efficiency

EMA: European medicine agency

FDA: Food and drug administration

FTIR: Fourier transform infrared spectroscopy

HaCat: Immortalized human keratinocytes cell line

hCMEC/D3: Immortalized human cerebral microvascular endothelial cell line

HPLC: High performance liquid chromatography

HRP: horseradish peroxidase

IFN γ : Interferon gamma

IL: Interleukin

J_{ss}: Permeability flux

K_p: Permeability coefficient

NF- κ B: Nuclear factor kappa-light-chain-enhancer of activated B cells

NPs: Nanoparticles

P₂: Diffusion coefficient

PEG: Polyethylene glycol

PGs: Prostaglandins

PGZ: Pioglitazone

PI: Polydispersity index

PLGA: Poly(d,l-lactic-co-glycolic acid)

PNPs: Polymeric nanoparticles

PPARs: Peroxisome proliferator activated receptors

PPAR γ : Peroxisome proliferator activated receptor gamma

Q_{ret}: Retained drug

RES: Reticuloendothelial system

ROS: Oxygen species

RXR-receptor: Retinoic acid X-receptor

SA: Sodium arachidonate

Tg: Glass transition

Th: T helper cells

TJs: Tight junctions

TNF α : Tumor necrosis factor alpha

TZDs: Thiazolidinediones

Y-79: Retinoblastoma cell line

ZP: Zeta potential

CHAPTER 1

INTRODUCTION

1. INTRODUCTION

1.1 INFLAMMATION

The inflammatory process can start in any vascularized part of the body. It consists of a series of stages and follows a course that is generally uniform in its sequence, but it can vary in intensity and duration, depending on the type and degree of the initial stimulus. Moreover, inflammation is a generic response, and therefore it is considered as a mechanism of innate immunity, as compared to adaptive immunity, which is specific for each pathogen (1).

The five signs of inflammation, described as heat, redness, swelling, pain and loss of function, and represent the external signs of a vascular, immunological and cellular reaction, which involves a variety of locally produced molecules (2). These inflammatory mediators include substances which are present in blood plasma such as the enzyme plasmin and other components involved in blood coagulation and histamine release. Besides, there are cellular mediators released by the white blood cells and they include various substances such as leukotrienes, prostaglandins (PGs), cytokines, interleukins (IL), and many others (3). Many anti-inflammatory drugs work by preventing the formation of those mediators or by blocking their actions on the target cells whose behaviour is modified by the mediators.

Inflammation can be classified as either *acute* or *chronic*. *Acute inflammation* is the initial response of the body to harmful stimuli and is achieved by the increased movement of plasma and leukocytes (especially granulocytes) from the blood into the injured tissues. *Chronic inflammation* leads to a progressive shift in the type of cells present at the site of inflammation, such as mononuclear cells, and is characterized by simultaneous destruction and healing of the tissue throughout the inflammatory process (4).

The inflammation process gives rise to a cascade, in which the mediators of inflammation are expressed by a catalysis of enzymes. They are known as Cyclooxygenase (COX-1 and COX-2) (5). COX-1 was the first enzyme to be identified, it is present in almost all tissues at constant levels. Its metabolites from arachidonic acid (AA) are responsible for maintaining the basic physiological conditions of the organism, for example, the protection of the gastric mucosa and homeostasis (6,7). On the other hand, COX-2 present in limited tissues, it is involved in the synthesis of PGs that participate in inflammatory, pathological and stress processes (8). It is expressed as a response to pro-inflammatory

stimuli, growth factors or tumorigenic agents (9-11). The activation of the enzyme phospholipase A₂, in response to various stimuli (biological, physical, chemical, traumatic, vascular or immune), hydrolyses membrane phospholipids, releases AA that catalyse the synthesis of eicosanoids and in turn release various mediators such as PGs, leukotrienes and thromboxanes. The production of each biochemical mediator depends on the action of other enzymes on the AA itself. For example, there is COX which generates PG H₂, which stimulates the formation of several prostanoids, including various PGs (PGI₂, PGD₂, PGE₂, PGF₂α) and thromboxane A₂. In addition, AA catalysed by lipoxygenase can be converted to leukotrienes or eicosanoids (Figure 1).

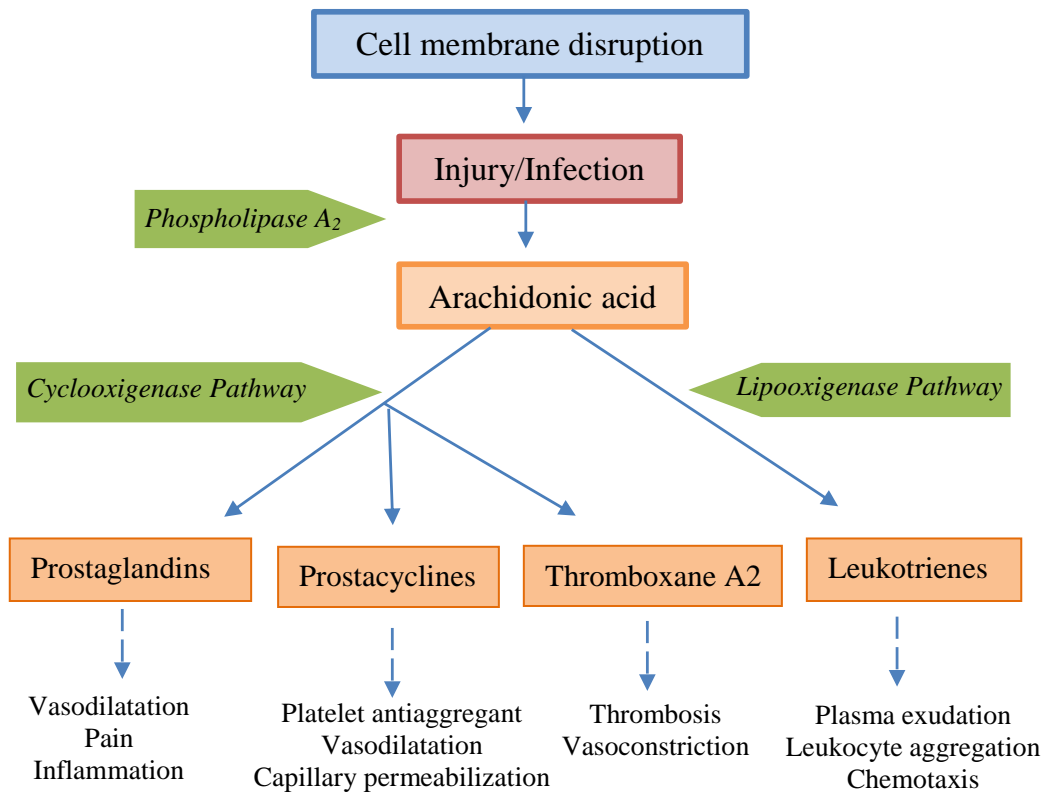


Figure 1: Inflammation cascade.

1.2 SKIN INFLAMMATION DISORDERS

1.2.1 STRUCTURE AND FUNCTION OF THE SKIN

1.2.1.1 Structure

The skin is the outer tissue covering vertebrates. In mammals, this organ is made up of multiple layers and covers the underlying muscles, bones, ligaments and internal organs. As the interface with the environment, it helps maintain homeostasis by protecting the organism against loss of water, abrasion, temperature changes, and several external factors such as UV-radiation, pathogens, as well as the entrance of other substances (12,13). In humans, the skin is the largest organ in the body, comprising about 15% of the body weight, with a surface between 1.5 to 2 m² in adults. In terms of chemical composition, the skin is about 70 % water, 25 % protein and 2 % lipids and consists of three main layers: epidermis, dermis, and hypodermis (Figure 2) (14).

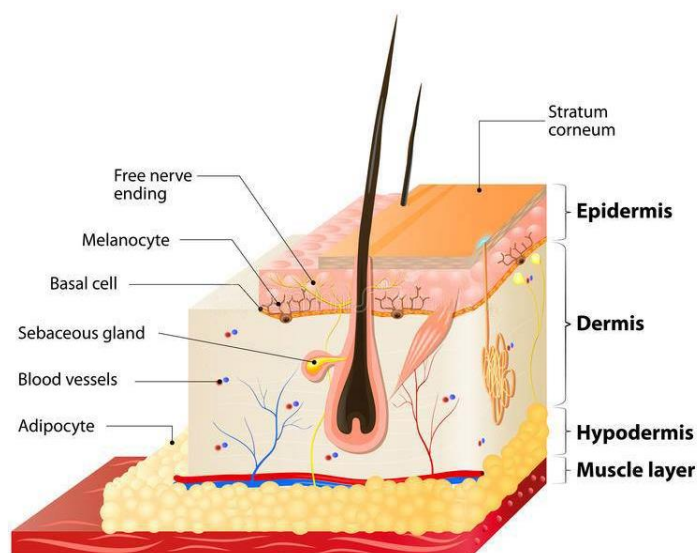


Figure 2: Structure of the skin and their different components.

The **epidermis** is the outer part of the skin. It has a width varying from 0.04 to 1.6 mm, depending on the body zone. The main cells in the epidermis are keratinocytes, though other cells are present, such as melanocytes, Langerhans cells and Merkel cells. Also, three appendices can be found in epidermis: sweat glands, hair follicles, sebaceous glands, and nails. The epidermis is comprised of 4 different layers: *stratum basale*, *stratum spinosum*, *stratum granulosum* and *stratum corneum*.

The *stratum basale*, the inner layer, is attached to the dermis, and is formed of a single layer of keratinocyte stem cells which produce new keratinocytes by mitosis. The new

keratinocytes migrate superficially to form the *stratum spinosum*, characterized by the active production of keratin. Finally, the *stratum granulosum* is formed of keratinocytes with characteristic granules of keratin. In zones of thicker skin such as the palms and soles, an extra layer is found called the *stratum lucidum*, a homogeneous layer of transparent cells without nucleus (15).

The *stratum corneum* is the outer layer of the epidermis, a 10-20 μm thick hydrophobic (13 % of water) and forms a rough structure mainly comprised of corneocytes, which are terminally differentiated keratinocytes, and are biologically dead (16). The main role of this layer is to protect the skin against the loss of water and the entrance of external substances. Due to its hydrophobic nature, highly hydrophilic substances cannot penetrate into the *stratum corneum*, while highly hydrophobic ones can, but they remain retained within, without permeating into deeper layers, and are eventually taken out of the skin through the desquamation process (12,15).

The corneocytes in this layer are bridged together through specialized junctions called corneodesmosomes, which are being constantly cleaved by serine proteases such as Kallikrein, permitting the desquamation of dead cells, as the main step in the renewal of the cells of the skin (15,17). The structure of the epidermis layers is constantly being renewed. In a healthy epidermis, the rotation period is around 28 days (14).

The **dermis** is located between the epidermis and the hypodermis, and its thickness ranges from 0.3 to 3 mm, depending of the zone of the body. It has a hydrophilic nature and is formed by 90 % of a net of collagen and elastin fibres (that provide mechanical resistance to the skin), blood flow and lymphatic vessels, hair follicles, sebaceous glands, sweat glands, and some muscle fibres. The remaining 10 % is composed of other cells, including fibrocytes, monocytes, histiocytes, lymphocytes, eosinophils, and associated lymphatic cells. Any substance that reaches the dermis can enter the blood systemic circulation (16).

The **hypodermis** (which sometimes is not considered by many as a part of the skin) is one of the three skin layers that help in the attachment of the skin to the muscles and bone. It also supplies the skin with blood vessels and nerves. The hypodermis is formed of loose connective tissue and contains mainly adipocytes and also fibroblasts and macrophages. The thickness of this layer is reported to be 4 to 9 mm on average (18).

1.2.1.2 Skin permeation

The term “transdermal permeation” refers to the passage of substances through the skin, and is divided into three main steps: penetration, permeation, and absorption:

- **Penetration** is the process through which the drug enters the first layer of the skin (*stratum corneum*). The process implies an initial dissolution of the drug and a diffusion to the vehicle-*stratum corneum* interphase, with a subsequent release of the drug from the vehicle and a partition between the vehicle-*stratum corneum*. Thereby, an adequate vehicle is needed so as to permit the drug release (19,20).
- **Permeation** is the step in which the drug crosses subsequent skin layers through a passive diffusion mechanism, from the compartment with the highest concentration, to the one with the lowest concentration. The crossing of the epidermis can occur by two different routes:

a) *Appendicular pathway*, also called the trans-appendageal route. It occurs when the substances pass mainly through the hair follicles and sebaceous glands. Even though hair follicles occupy only 0.1 % of the total surface area of the skin, the appendicular pathway constitutes a significant route for steroidal drugs and molecules with a similar structure, hydrophilic substances, slowly diffusing compounds, and drugs with a high molecular weight (20).

b) *Epidermal pathway*. It is the major route, and the passage of drugs depends on the drug’s physicochemical properties such as its molecular weight, solubility in water and lipids (partition coefficient [logP]), and pKa. Other aspects influencing the epidermal pathway are the metabolism of the drug, the stratum corneum thickness, the hydration and integrity of the skin, and the excipients. The passage of substances through the epidermis may in turn take place through two routes (21):

- The *intracellular* route, or transcellular route, is mostly used by hydrophilic substances, and happens when the drug crosses the cell.
- The *intercellular* route, happens when the drug goes through the lipid matrices, between the cells in the *stratum corneum*, and is mostly used by hydrophobic substances.

Therefore, amphiphilic substances can use both routes.

- **Absorption** is the passage of the drug to blood vessels, through which it reaches systemic circulation.

1.2.1.3 Factors influence skin permeation

Skin physicochemical factors:

- *Temperature.* An increase in the temperature of the skin implies an increase in blood flow and, subsequently, the speed of permeation and absorption of the drug. Moreover, the increase of the temperature from 32 °C to 35 °C changes the packing of the lipids in the *stratum corneum*, from an orthorhombic to a hexagonal packing, increasing the permeability (16).
- *pH.* The normal pH values of the skin (4.0 – 6.0) can affect the degree of dissociation of the drug (according to their pKa values), and therefore their ability to cross membranes. For instance, non-ionized substances can permeate the skin more easily (22)
- *Hydration.* The hydration of the skin generally increases transdermal absorption, though the precise mechanism is still unclear (23).

Drug physicochemical factors:

- *Partition coefficient* is defined as the proportion of drug that is dissolved in two immiscible solvents. In this case, the proportion dissolved between the *stratum corneum* and the vehicle is of major importance as the corneal layer behaves as a lipidic membrane. When the partition coefficient value is near 1, the permeation is adequate (24). The experimental calculation of the partition coefficient between the *stratum corneum* and the vehicle is not easy. Therefore, a commonly used value for predicting the permeability of a drug is the partition coefficient between octanol (as an apolar solvent) and water (as a polar solvent). As this value can vary widely, a common way of expressing it is as a logarithm (log Pow or log P). It is well-known that molecules with a log P ranged between 1 and 3 (a predominant solubility in lipids), and with good solubility in oils and water, show adequate skin permeation (20).
- *Permeability coefficient* is a constant proportional to the partition coefficient and the diffusion coefficient (P_2) of the drug. In turn, the P_2 is inversely proportional to the molecular weight. It is well-known that the molecular weight is a determinant factor

in the permeation of drugs, being those smaller than 500 Da the ones that can permeate the skin (25,26).

Vehicle factors:

- *Excipients.* The nature of the vehicle can modify skin permeation of the drug because the vehicle can affect the structure of the *stratum corneum*, through an increase in the hydration, an increase of the temperature, or a disruption of the lipids packing, thus leading to a change in skin permeation (23,27). Also, the interaction vehicle-drug plays an important role in several ways. For example, the pH of the formulation affects the degree of dissociation of molecules according to their pKa, which in turn affects the partition coefficient of the substance.
- *Rheological properties.* A vehicle with a viscoelastic behaviour is optimum because it should have a fluidic behaviour at the application (where a shear stress is applied) in order to extend the drug over an area wide enough for the treatment, but the vehicle should remain adhered on the skin after application in order to maintain a concentration gradient that favours permeation (28).
- *Drug concentration.* Since the penetration and permeation of the drug occurs through a passive diffusion mechanism, they depend on the concentration gradient between the vehicle and the layers of the skin (16,20,27,29).

Physiopathological factors:

Different factors such as age, integrity of the skin, blood flow, zone of application, and metabolism, influence the skin permeation (28). Also, any lesion, eruption or pathology affecting the integrity of the skin modifies in the permeability. As well, an increase in blood flow leads to a faster absorption of the drug into the systemic circulation, creating in turn a higher concentration gradient, and thus, increasing the drug permeation. The skin thickness and the degree of vascularization changes the permeability, and this varies throughout different zones of the skin (23). Finally, as the skin is a metabolically active organ, some oxidation-reduction, hydrolysis or conjugation reactions can occur to the drug during permeation.

1.2.2 ROSACEA

Rosacea is a common, chronic inflammatory skin disease with poorly understood etiology. It is a condition of vasomotor instability that primarily affects blood vessels and pilosebaceous units of the central facial skin (cheeks, chin, nose, and central forehead), causing transient or persistent erythema, telangiectasias, papules, pustules, phymatous changes and ocular involvement (30). Complex pathomechanisms involving dysregulation in the immune, vascular, and nervous systems, as well as barrier function impairments, are suggested (17,31). The knowledge about rosacea immunology is still very limited and most studies have focused on the involvement of the vascular or innate immune system.

According to the *National Rosacea Society Expert Committee*, rosacea can be classified into four subtypes based on the signs and symptoms, and patients can present more than one subtype (32):

a) *Erythematotelangiectatic rosacea* is characterized by permanent erythema (redness) with a tendency to flush and blush easily. The presence of telangiectasias (small, widened, visible blood vessels) near the surface of the skin is observed, and possibly intense burning, stinging, or itching. People with this type of rosacea often have sensitive skin(33).

b) *Papulopustular rosacea* presents permanent redness with papules (red bumps) and pustules (pus-filled papules). This subtype is often confused with acne vulgaris (34).

c) *Phymatous rosacea* is most commonly associated with rhinophyma (enlargement of the nose). Signs include skin thickening, irregular surface nodularities, and enlargement. Phymatous rosacea can also affect the chin, forehead, cheeks, eyelids, and ears (35).

d) *Ocular rosacea* is associated with redness of the eyes and eyelids due to telangiectasias and inflammation. Other symptoms include sensitivity to light. Patients with ocular rosacea present more susceptibility to infection (36).

Due to its etiology, which is not completely known yet, some recent discoveries in the biochemical pathway have been reported. Sensitivity to rosacea triggers through the upregulation of trigger-responsive receptors and is a logical first step in the initiation and perpetuation of rosacea. Some hypotheses on the mechanisms for rosacea have been described and represented in Figure 3.

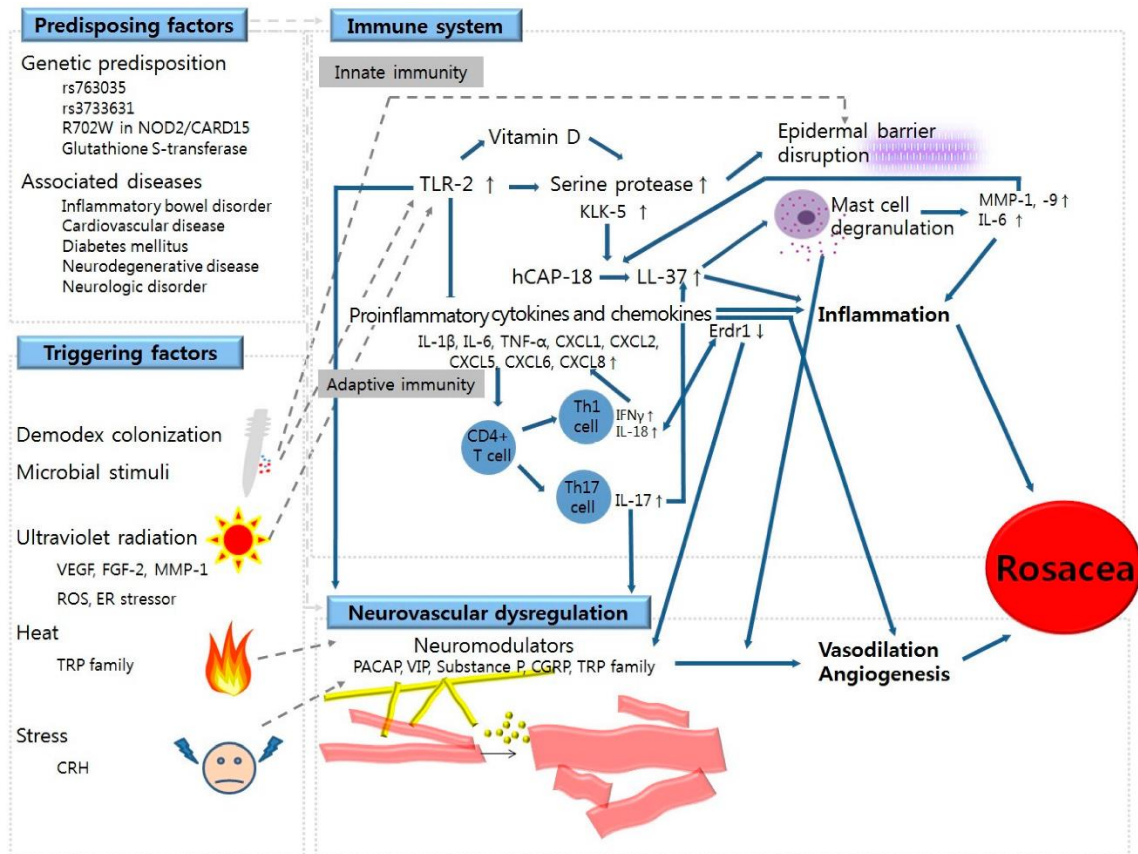


Figure 3: Mechanisms for rosacea production (37).

Besides trigger avoidance, the most common approach to rosacea is pharmacologic treatment. Oral tetracycline-class antibiotics are commonly used to treat papulopustular rosacea, and a 40 mg modified-release doxycycline capsule is approved for its treatment. Topical ivermectin is a recently approved molecule for the treatment of inflammatory lesions of rosacea. Dermal Azelaic acid and metronidazole have proven clinical efficacy in the treatment of papulopustular rosacea. Topical brimonidine is approved for the symptomatic relief of the erythema of rosacea (34,35). Current therapeutics give great importance to targeting inflammatory pathways such as agonists peroxisome proliferator activated receptor gamma (PPAR γ), since they could act as negative regulators in T cell differentiation and in the activation to attenuate inflammatory responses and inhibiting different proinflammatory cytokines (38). Moreover, Pioglitazone (PGZ) inhibits the signalling pathways involved in inflammatory process (39,40). However, development of new therapeutics that inhibit neural and vascular components of disease, as well as sensitive and specific diagnostic tests, is required for the improved, long-term control of rosacea and for individualized treatment.

1.3 OCULAR INFLAMMATORY DISEASES

1.3.1 STRUCTURE AND FUNCTION OF THE EYE

1.3.1.1 Structure

The eye is a major sensory organ that includes a variety of barriers to drug delivery due to its complex anatomy and physiology. It measures approximately 22 to 27 mm in its antero-posterior diameter and 69 to 85 mm in circumference (Figure 4). The eye consists of three layered structure, with each of these three layers being sub-dividable (41).

- The outermost supporting layer of the eye, which consists of clear cornea, opaque sclera, and their zone of interdigitation, is designated as the limbus.
- The middle uveal layer of the eye, constituting of the central vascular layer of the globe, is composed of the iris, ciliary body, and choroid.
- The interior layer of the eye, commonly designated as the retina, is the neural layer.

However, the eye is segmented into two parts, the anterior and posterior segment. The anterior eye consists of the cornea, iris, lens, ciliary body, and sclera (anterior). The posterior eye consists of the vitreous humour, retina, choroid, sclera (posterior), and optic nerve. Aqueous humour permeates both segments (42). Orbit, lids and sclera are the protective structures of the eye. The optic nerve, optic tracts and visual cortex are the visual signal pathways to the brain.

The eyes are equipped with several defence barriers that restrict the entry of exogenous substances. These barriers make difficult the passing through of different molecules including microorganism right through to medicines, it being difficult to treat different diseases of the eye.

Ocular administration of drugs is commonly used for the treatment of superficial and/or internal disorders of the eye. The pathologies that weaken the eyes are: cataracts, retinal problems such as macular degeneration or retinitis pigmentosa, glaucoma, uveitis, ocular dryness, bacterial conjunctivitis, ocular allergies, or inflammations. However, the low bioavailability of drugs in classical dosage forms is mainly linked to the anatomical and physiological structure of the ocular pathway. The main challenge of ocular therapy is to reach an optimal concentration of the drug in the place of action and to enable the drugs to overcome the anatomical and physiological barriers that protect the eye (43,44).

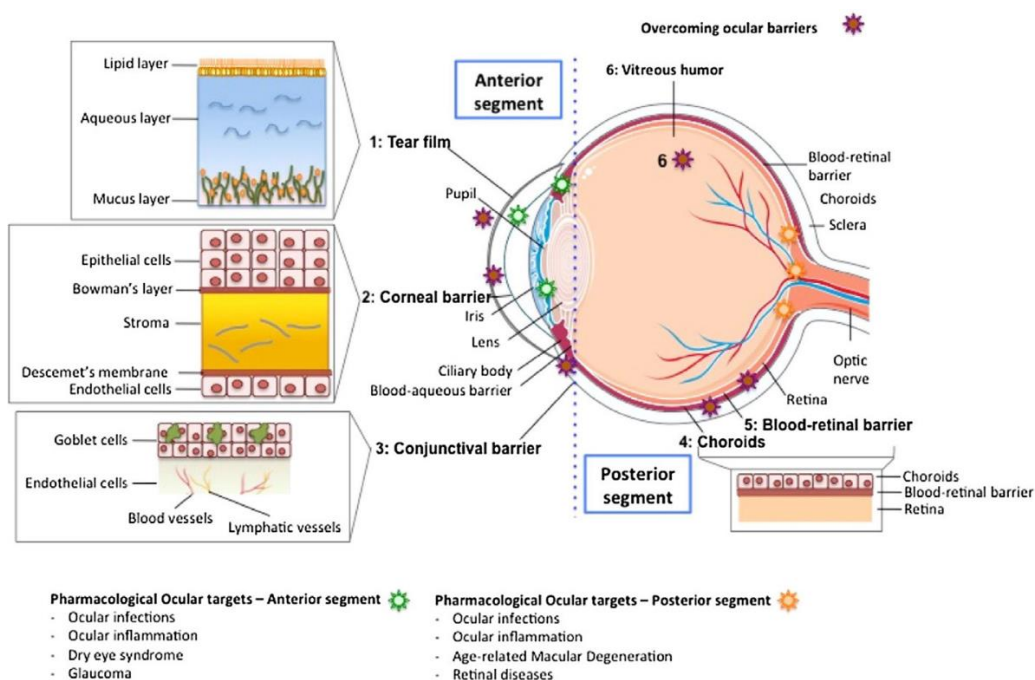


Figure 4: Different structures from anterior and posterior segment of the eye. The different barriers that drugs need to overcome after topical installation are indicated with a red star, and a detailed representation is also provided. The ocular targets to treat a specific disease are indicated with a green star, if they are in the anterior segment, or with a yellow star, if they are located in the posterior segment (45).

1.3.2 UVEITIS

The inflammation of the eye, including uveitis, was known to the ancient Egyptians (46). The uvea is composed of the iris, ciliary body and choroid. Each of these components has a unique histology, anatomy and function. The uvea is the intermediate of the three coats of the eyeball. It is sandwiched between the sclera and the retina in its posterior portion (choroid) (47,48). Moreover, it is consistently involved in intraocular inflammation, transporting more than 80 % of the ocular blood volume. Uveitis may occur as a consequence of different stimuli. The immune systems play a key role in this process, as inflammation and repair are closely intertwined (49). The inflammation may be acute, subacute or chronic.

Specialists categorize uveitis etiologically as either infectious or non-infectious (47). Infections are proven causes of some cases of uveitis (50,51). In others, the activation of innate immune processes in response to infection may cause tissue damage through a mechanism of autoinflammation.

Non-infectious uveitis is not synonymous with autoimmune uveitis. The autoimmune hypothesis for non-infectious uveitis derives from the experimental models of retinal

inflammation that create blood-retinal barrier (BRB) breakdown and stimulate adaptive immunity directed towards retinal antigenic targets. In nonretinal tissues, autoinflammatory or innate immune-mediated mechanisms may prevail. As infectious agents usually drive autoinflammation, infection may be behind the pathogenesis of most uveitis, either through cytolytic tissue damage or through uncontrolled and dysregulated host immune responses that continue after infection subsides.

The current classification of uveitis is an anatomic classification, as set forth by the international uveitis study group then confirmed by the standardization of uveitis nomenclature (52). This classification is based upon the concept of the “primary” or “initial” site of inflammation. It is thus based on the place where the inflammation predominates. It distinguishes between anterior uveitis with iris and ciliary body involvement, intermediate uveitis with peripheral chorioretinal involvement, posterior uveitis with choroidal and retinal involvement and panuveitis (53).

Uveitis results from the imbalance between inflammatory mechanisms and regulatory mechanisms. Acute inflammation is initiated by those cells that have been present previously in affected tissues, mainly resident macrophages and dendritic cells (54). In autoimmune uveitis, self-reactive T cells leave the thymus and when they reach the eye they come in contact with retinal antigens. Myeloid dendritic cells present a sturdy ability in the capturing of antigens, which enables them to stimulate T cells. Therefore, T-lymphocytes may differentiate into Tregs, T helper cells (Th) 1, Th17 or Th2 as a precise immune response in function of the antigen encountered and cytokine presence. Th1 and Th17 cells participate in inflammatory and autoimmune uveitis, which produce pro-inflammatory cytokines such as IL-2, interferon gamma (INF γ), IL-17, IL-23 and tumor necrosis factor alpha (TNF α), and these recruit leukocytes from circulation and result in tissue damage. Th1 cells are crucial for the development of uveitis, whereas Th17 cells play a relevant role in the late/chronic phase of uveitis. However induced Treg cells defeat both Th1 and Th17 cell responses (55–57). Furthermore, the migration of Th1 and Th17 to the eye also results in the breaking down of the BRB and, consequently, different leukocytes from the circulation are recruited. In figure 5, it is possible to see the main specific targets in uveitis.

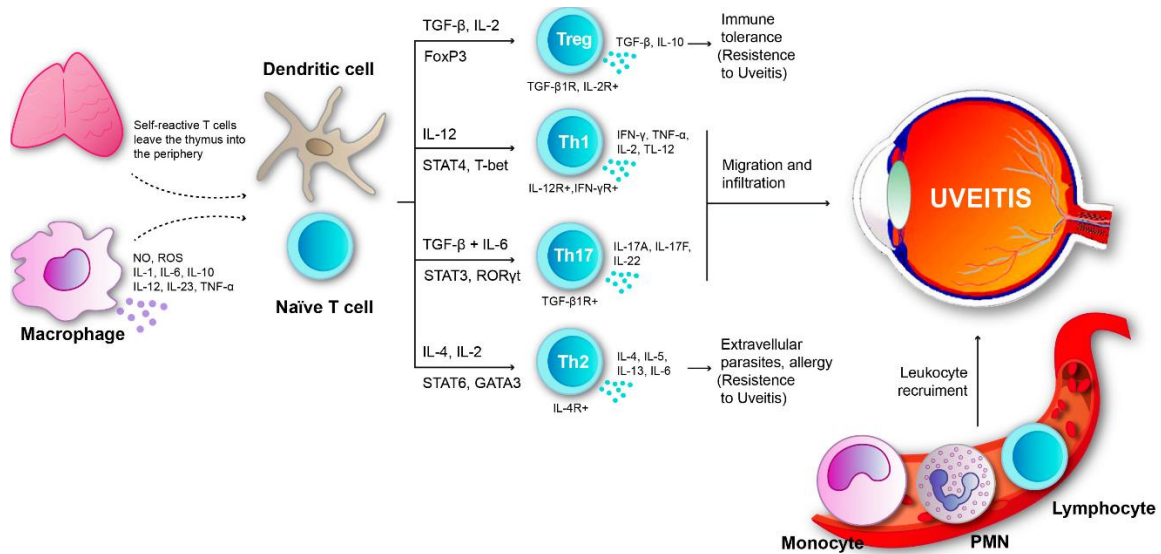


Figure 5: Uveitis results from imbalance between inflammatory mechanisms and regulatory mechanisms (54).

The treatment of uveitis depends on the cause of inflammation. In those causes of infectious origin, treatment with antibiotics can be curative. The corticosteroids are the basis of treatment in the acute phase, used in eye drops, injections around or inside the eye or systemically (orally, intramuscularly or intravenously). In some uveitis of immunological origin, chronic, difficult to manage or with complications derived from the use of corticosteroids, it may be necessary to use immunomodulatory drugs to control inflammation. Some of these drugs can have side effects requiring frequent monitoring. Due to the activity of PPAR γ agonists in the pathway of inflammation, and apart from their original indication as antidiabetic agents, multiple functions such as anti-inflammatory, antitumor, and antiangiogenic effects, as well as neuroprotection, have been investigated recently (58). The PPAR γ in different studies (59–61) on activated T cells and also treatment with PPAR γ agonists have shown that the latter inhibit antigen-specific T cell proliferation and promotes the apoptosis of activated T cells, suggesting a role for PPAR γ in the regulation of T cell-mediated immune and inflammatory responses (62). Interestingly, recent studies have also shown the importance of PPAR γ in the regulation of immune and inflammatory responses in animal models (63–67).

1.4 BRAIN NEUROINFLAMMATORY DISEASES

1.4.1 CENTRAL NERVOUS SYSTEM: STRUCTURE AND FUNCTION

1.4.1.1 Structure

The central nervous system (CNS) is a highly vascularized system and is comprised of three different segments of endothelial cells that differ in their anatomical, morphological, biochemical and functional organization (Table 1) (68,69). The human brain can be divided into three major parts, namely, forebrain, midbrain and hindbrain. These broad divisions are comprised of different smaller divisions, with each having a specific role to play.

- Forebrain is considered as the most important part of brain because, on account of its functioning, it distinguishes human from other animals. This part is responsible for processing sensory information, collected by different sensory organs, such as eyes, nose, ears, tongue and skin.
- Midbrain acts as a bridge to transmit signals from hindbrain and forebrain. These signals mostly come from the senses of touch and hearing, collected by the specialized organs, i.e. skin and ears, respectively.
- Hindbrain can be further divided into three parts: medulla oblongata, pons and cerebellum. The main function of this human brain structure is to control certain visceral functions in body (including heart rate, breathing and blood pressure).

Besides this, the cerebrum is the largest part of the human brain, associated with higher brain functions such as thought and action. The cerebral cortex is divided into four lobes: the frontal, parietal, occipital and temporal lobe (Figure 6). The principal arteries that irrigate the brain with arterial blood are the internal carotid artery and the vertebral-basilar system which terminates in the circle of Willis whereas cerebral venous blood is collected into the superior sagittal sinus and from there it exits the brain. Between these two main circulatory systems, the exchange of O₂ and nutrients occur mainly at the level of the cerebral microvasculature which comprises, sequentially: (1) arterioles (10-100 μm diameter) that penetrate the cerebral parenchyma; (2) capillaries (4-10 μm diameter) that constitute the largest surface area for the exchange of blood with the brain and cerebral endothelial cells (CECs) show the most highly organized tight junctions (TJs); (3) venules (10-100 μm diameter) which constitute the main area of leukocyte infiltration and CECs which show a loose arrangement of TJs. (70).

Table 1: Cellular composition and differential expression of BBB-related properties along the brain microvascular endothelium.

<i>Cells and features</i>	<i>Arterioles</i>	<i>Capillaries</i>	<i>Venules</i>
<i>Smooth muscle cells</i>	+	-	+
<i>Pericytes</i>	+	+	+
<i>Endothelial TJs</i>	n.d	Belts of TJ	Non-specialized
<i>Permeability for BBB Markers</i>	n.d	No	Yes
<i>Intimate contact between astrocytic endfeet and the vascular wall</i>	No	Yes	No
<i>Presence of perivascular spaces</i>	Yes	No	Yes
<i>Perivascular macrophage</i>	+	+	+
<i>P-glycoprotein</i>	?	+++	?
<i>Alkaline phosphatase</i>	+++	++	+
<i>Mg+ ATPase</i>	+++	+	+
<i>Na+ K+ ATPase</i>	+++	+	+
<i>Surface anionic sites</i>	+++	+++	+

+, present; -, absent; n.d., not determined. Relative expression of properties is indicated by +, ++, and +++, from lowest to highest. The question mark refers to the fact that P-glycoprotein expression has been confirmed at high levels in capillaries but not in arterioles or venules. Adapted from (68,69).

1.4.1.2 Blood Brain Barrier

The blood brain barrier (BBB) can be defined as a highly specialized complex cellular structure comprised of CECs, pericytes, the perivascular extremities of the astrocytic glia, nerve terminals and perivascular microglia/macrophages. More recently, this cellular structure has also been termed the neurovascular unit due to the complexity of the cellular interactions thereby giving rise to a coordinated response necessary to maintain a functional BBB (Figure 6) (71–73).

In 1900 Lewandowski introduced the term “blood-brain barrier (BBB)” in his studies on neurotoxic agents where he demonstrated that some compounds could be highly neurotoxic when injected directly into the brain but not when injected intravenously (69). These results led him to conclude that the cerebral capillaries are capable of limiting the entrance of certain blood-borne molecules into the CNS. Further experimental evidence of the BBB's existence was provided a few years later by Edwin Goldman (74) who reported that Trypan Blue dye neither stained the brain nor the spinal cord when administered through the bloodstream. However, it quickly stained these structures when administered into the cerebrospinal fluid. These experiments led to the idea of a cellular

barrier that restricts the free exchange of hydrophilic molecules from blood to brain at the site of the cerebral vasculature (75). In the 1960s with the development of electron microscopy techniques, the anatomical localization of the BBB was identified by Reese, Karnovsky and Brightman (in two separate studies) using the electron-dense marker horseradish peroxidase (HRP) (76,77). Their collective observations established two important paradigms in the BBB field of research: (1) the BBB is localized at the level of the CECs and (2) the presence of interendothelial TJs, highly expressed along the brain capillaries, allows the physical restriction to the HRP flux between the brain and blood (68,72).

Three barriers are recognized as part of the brain's isolating system and which allows for the maintenance of brain homeostasis: the BBB, the blood-cerebrospinal fluid barrier, and the arachnoid epithelium (78,79). The consequence of this intricate interplay is a controlled and restricted transport of molecules across the BBB. Only very small (< 400 Da), lipophilic molecules can diffuse through the BBB, while the crossing of lipid insoluble or larger hydrophilic molecules is very limited. However, in addition to lipophilicity, other factors, such as the affinity, contribute to the available transport system and further control the BBB crossing (80,81).

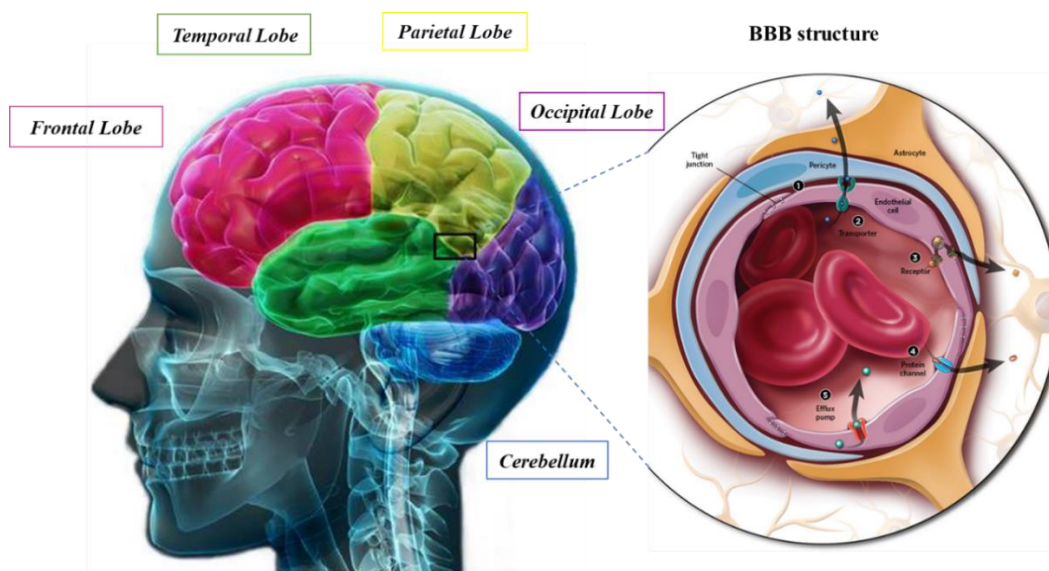


Figure 6: Lobes of the brain and BBB structure. The blood vessel CECs of the BBB are cemented together by TJs (1). CECs display transporters (2), receptors (3), and channels (4) that facilitate selective transport of vital nutrients into the CNS. They also possess efflux pumps, such as P-glycoprotein, that expel most small, amphiphilic molecules that are soluble in the blood and in cell lipid membranes (5). Pericytes and astrocyte pseudopods serve as an additional physical barrier between the blood vessel and brain tissue, and support the expression of endothelial cell genes required to maintain the BBB (82).

1.4.2 BRAIN ADMINISTRATION ROUTES

Up to the present day many different drug delivery methods have been developed. Few of them have been able to deliver the drugs neurologically, are invasive and have been found to be unsafe for drug delivery. No review of drug delivery across BBB is complete without looking at the broad picture of administration routes. Generally, most therapeutics of CNS diseases in conventional administration enter the CNS via the systemic blood circulation. To reach effective drug concentrations at the CNS disease sites, it is necessary to raise the systemic drug levels by substantially an enhanced dose or extended administration.

Researchers are looking for more ways to transfer therapeutic agents into the CNS without the need to increase the systemic levels of these agents and decreasing the risk of systemic toxicity. A direct drug administration to the brain region, painless and safe, will definitively improve the scenario. However, in the meantime intravenous administration is the most popular choice in clinical studies. Some approaches have been developed to enhance drug delivery to the CNS have been gaining considerable attention, such as oral route, inhalation or intra-tracheal instillation, intranasal drug delivery, convection-enhanced diffusion and intrathecal/intraventricular drug delivery systems, using non-invasive, invasive, and recent techniques for drug delivery (Figure 7).

Hence, for therapeutic purposes active transfer of the drug is very necessary for the advantages it could offer. However, whatever the circumstances, both drug composition and its delivery methods must be taken into account so that effective drug formulations are achieved in order to treat the CNS disease (83,84).

One must take into mind that the effect of topically applied medications can be of two types: topical and/or systemic. After the administration of an active agent on the mucosa, it can exert its effect only on the local tissues or superficial layers and/or on any of the tissues of the body, as if its application were orally or parenterally. Therefore, transmucosal drug administration represents a more practical, safe and less invasive route than conventional routes. Although, the transmucosal administration of drugs has not yet been investigated enough, its potential advantages over other routes of administration have already been established and are innumerable, including:

Their liberation is in a specific place, and there is control of the absorption percentage; they can be formulated as a delayed-release compound. They provide a constant dose,

reduce systemic side effects, application is easy, allows substantial concentrations of the drug to be found inside the soft tissues of the application site, and is easily accessible from the surface (possibility to control and/or eliminate the pharmaceutical form).

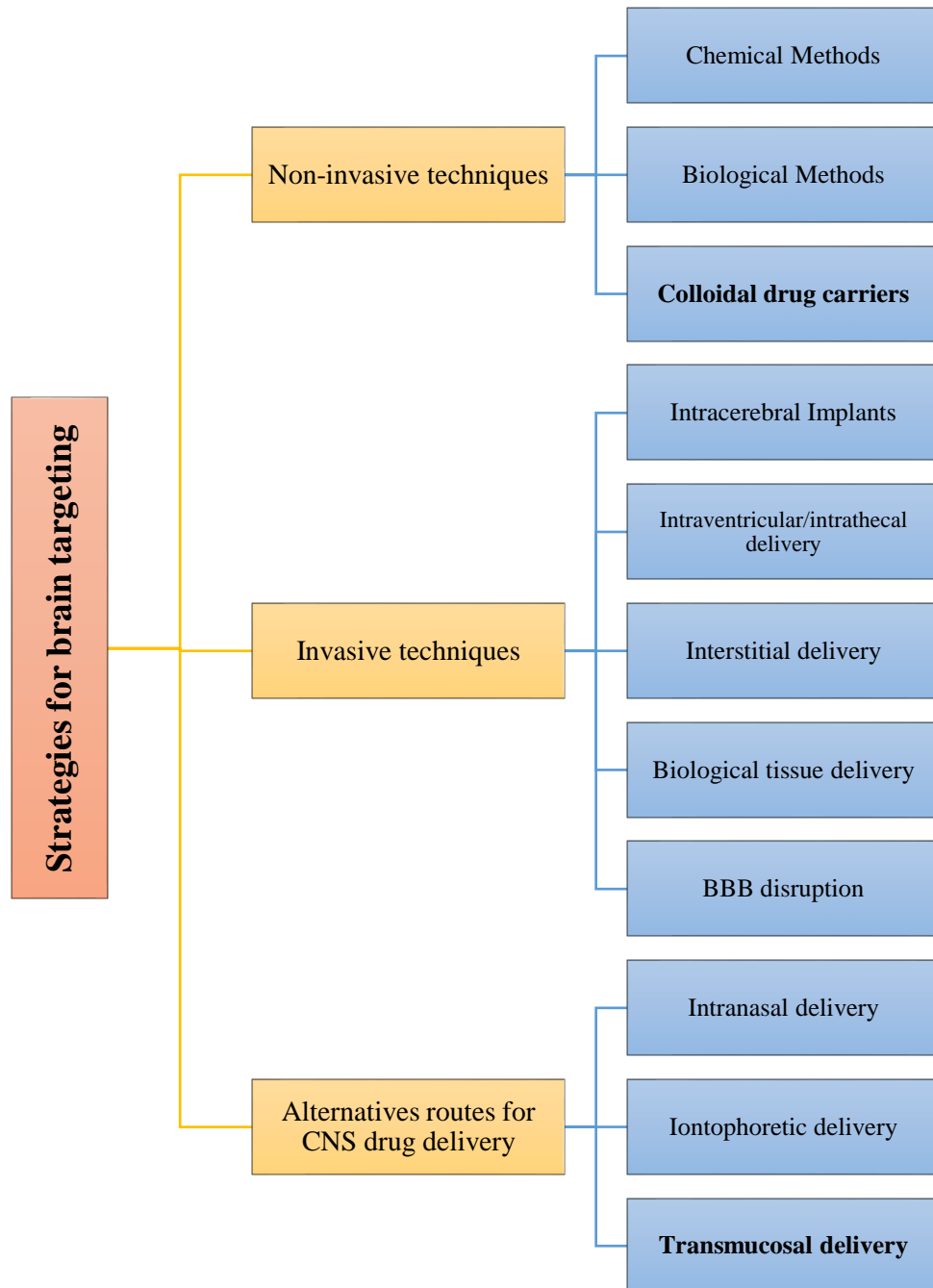


Figure 7: Current approaches for CNS drug delivery. Modified from (85)

1.4.2.1 Oral route

The oral mucosa is a very popular administration route due to its good accessibility and high patient acceptance (86). Moreover, it is routinely exposed to different compounds and mechanical stress, so it is assumed to be more robust and less sensitive to irritation by the drug or pharmaceutical form, use of absorption promoters, etc., in comparison with other routes.

However, it should be taken into account that there is also metabolism in the mucosa, and although its metabolic load is much less than that in the liver, it can be an inconvenience for the administration of certain drugs in this way. On the other hand, the great variety of microorganisms present in the mucous membranes can also alter some drugs (87). As an advantage of the oral transmucosal versus the transdermal route, it can be said that it is more permeable, more vascularized and has greater hydration, which allows the solubilization of the drug. These factors make the oral mucosa an interesting administration route for drugs that require a rapid onset of action at systemic level (88).

It is considered that most drugs pass through the mucosa by passive diffusion and two permeations pathways can be used:

- Transcellular route: involve the crossing of the cellular membranes with a polar and a lipid domain.
- Paracellular route: imply the passive diffusion through the extracellular lipid domain.

Apart from this, the epithelium of the oral cavity (buccal mucosa) is well suited for its many unique functions, having regional differences in the keratinization of the mucosa (89). The oral mucosa is composed mainly of two layers: the epithelium and the underlying connective tissue (basal lamina, lamina propria and submucosa). Both layers are separated by the basement membrane. Its primary function is to protect underlying tissues from mechanical and chemical damage and against the entry of foreign substances (90). It is estimated that the thickness of the buccal mucosa epithelium is 500 to 800 μm (500 to 600 μm in its non-keratinized part). It has a cell turnover rate of 5-7 days, a total area of 50 cm^2 and a flow blood of 20.3 ml/min/100 g tissue approximately (91).

On the other hand, the sublingual mucosa has a thickness of 100-200 μm , a cell turnover rate of 20 days, a total area of 26 cm^2 and a blood flow of 12.2 ml/min/100 g tissue approximately (92). In the layers of more superficial epithelial cells membranous granules can be observed that seem to fuse with the membrane of the epithelial cell, expelling the

lipids that contain the extracellular space. These granules are spherical and of about 0.2 μm (91). Independently of the degree of keratinization of the oral mucosa, it does not have a corneum stratum proper. Due to this it is much more permeable than the skin (4 to 4000 times) (93).

The intestine is other important tissue for the delivery of drug by the oral route. It is considered as an important site that exerts a huge effect on the metabolism of many xenobiotics, due to the presence of numerous enzymes produced by the gut microbiota (94). The mean total mucosal surface of the digestive tract interior averages around 32 m^2 , of which about 2 m^2 refers to the large intestine (95). The intestinal mucosal barrier is a heterogeneous entity composed of physical, biochemical, and immune elements. The central component is the intestinal epithelial layer, which provides physical separation between the lumen and the body. Its role in protecting the mucosal tissues and circulatory system from exposure to pro-inflammatory molecules, such as microorganisms, toxins, and antigens, is vital for the maintenance of health and well-being (96–98).

Its composition is of a simple layer of columnar epithelial cells, as well as the underlying lamina propria and muscular mucosa. The TJs, a component of the apical junctional complex, seals the paracellular space between epithelial cells.

1.4.2.2 Intranasal route

The intranasal route is an alternative route bypassing the cardiovascular system. As shown in Figure 8, the neural pathways connecting the nasal mucosa and the brain provide potential routes for non-invasive drug delivery to the CNS. The surface, or epithelium, of this mucosa contains the cells which produce mucus and the ciliated cells, covered with fine hairs called cilia. The nose is responsible for olfaction and respiration and it is the first line of defence of the respiratory system. It is comprised of two symmetric cavities, divided by the septum which lies along the midsagittal plane. The cavities are lined with a layer of mucosa, and the total area of both cavities is around 150 cm^2 (99,100). These cavities can be further divided into three regions.

- Vestibular region: it is relatively small with a total surface area of 0.6 cm^2 , and contains the nasal hairs which serve for filtering inhaled particles.
- Respiratory region: covers the lateral walls of the nasal cavities, including the three projecting turbinate (conchae). This region has the largest area at around 130 cm^2 , and is also the most vascular (101).

- Olfactory region: it is located on the superior aspect of the nasal cavities, covering the inferior surface of the cribriform plate of the ethmoid bone. This region is small at 10 cm², but varies in proportionate size by species: while this is only around 10% of the area in humans, this region can be up to 50% of the total area in rodents a common model for intranasal administration studies (102,103).

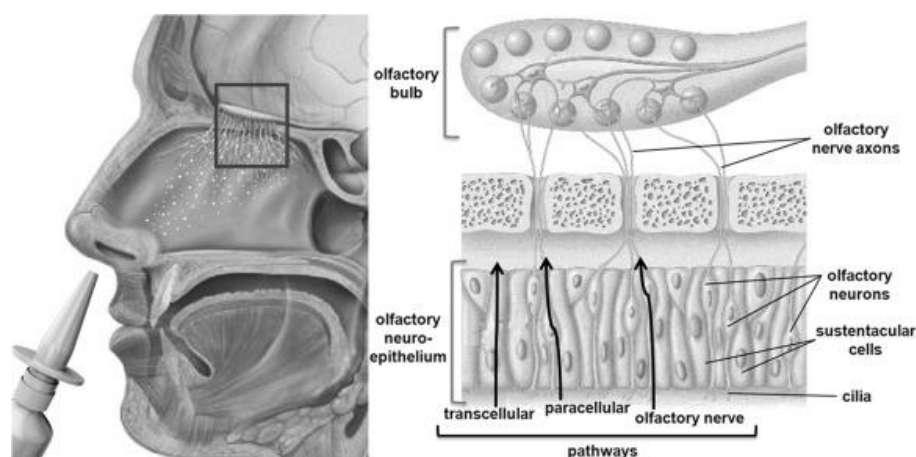


Figure 8: Cross section of the human nasal cavity with the olfactory region and its structures labelled. Pathways of nose-to-brain transport of drug after administration of formulation are also indicated (104).

1.4.3 ALZHEIMER'S DISEASES

Alzheimer's diseases (AD) is an age-associated neurodegenerative disorder characterized by progressive memory and cognitive impairment that eventually leads to death. It is estimated that in the United States in 2050 the total number of people with AD dementia is projected to be 13.8 million (105). This disease is characterized by atrophy of cerebral cortex and loss of hippocampal and neocortical neurons.

Several theories have been proposed concerning the pathogenesis of AD at the molecular level. These theories are based on the roles of "amyloid, cholinergic, tau, glutamate and oxidative stress hypotheses". The pathophysiological basis of neurodegeneration is related to two main hallmarks, these being the prevalent neuritic plaques which are accumulations of amyloid beta protein (A β) and intracellular neurofibrillary tangles (106,107). A β is a short polypeptide of about 42 amino acids produced by the abnormal proteolytic cleavage of amyloid precursor protein, which involves enzymes like gamma-secretase (108,109). Production and deposition of A β is the central event triggering oxidation, lipid peroxidation, excessive excitotoxicity of glutamatergic neurons,

inflammation, apoptotic cell death and formation of neurofibrillary tangles (110). Neurofibrillary tangles are paired helical filaments composed of tau protein which in normal cells are essential for axonal growth and development (111). However, when hyperphosphorylated, the tau protein forms tangles that are systematically deposited within neurons located in the hippocampus and medial temporal lobe, the parieto-temporal region, and the frontal association cortices leading to cell death (112,113). Moreover, impaired glucose metabolism in older patients with or without diabetes a direct association between dementia and glycaemia has been demonstrated (114,115). Further, lower hippocampal function, memory and executive function in older adults without diabetes was linked to poor glucose metabolism (116).

The inflammation is another important hallmark in the AD, as it leads to neuroinflammation. The activated microglia secrete a large number of molecules, including proinflammatory cytokines, PGs, the reducing oxygen species (ROS) and nitric oxide synthetase. These factors lead to a state of perpetual chronic stress and consequently neuroinflammation, which can lead to the neuronal death (117,118). Indeed, PPAR γ activation has shown protective effects in many models of disease and shows the ability to protect against inflammation and stimulate recovery. It is related to oxidative stress response as well as antioxidant activity (119,120). In addition, PPAR γ agonists have proven to reduce oxidative damage through the reduction of ROS production in several tissues, including the brain, liver, and blood vessels, among others, due to the interaction of peroxisome proliferator activated receptors (PPARs) with anti-inflammatory pathways such as nuclear factor kappa-light-chain-enhancer of activated B cells (NF- κ B) and nuclear factor (erythroid-derived 2)-like 2, the reduction of COX-2 expression or the interaction with antiapoptotic pathways such as B-cell lymphoma 2 (121–127). However, the mechanisms of action as well as the interactions with different cell signalling pathways of the PPAR γ remain to be fully elucidated.

Different drugs have been proposed for AD (Figure 9), but none have been able to cure the disease or modify its course. The main objectives of pharmacological treatment are focused on delaying the appearance of clinical manifestations and controlling cognitive, non-cognitive, behavioural and psychological symptoms in order to prevent, maintain and improve the quality of life of these patients. Recent researches are looking for new technologies and drugs to act in the different pathways of the disease.

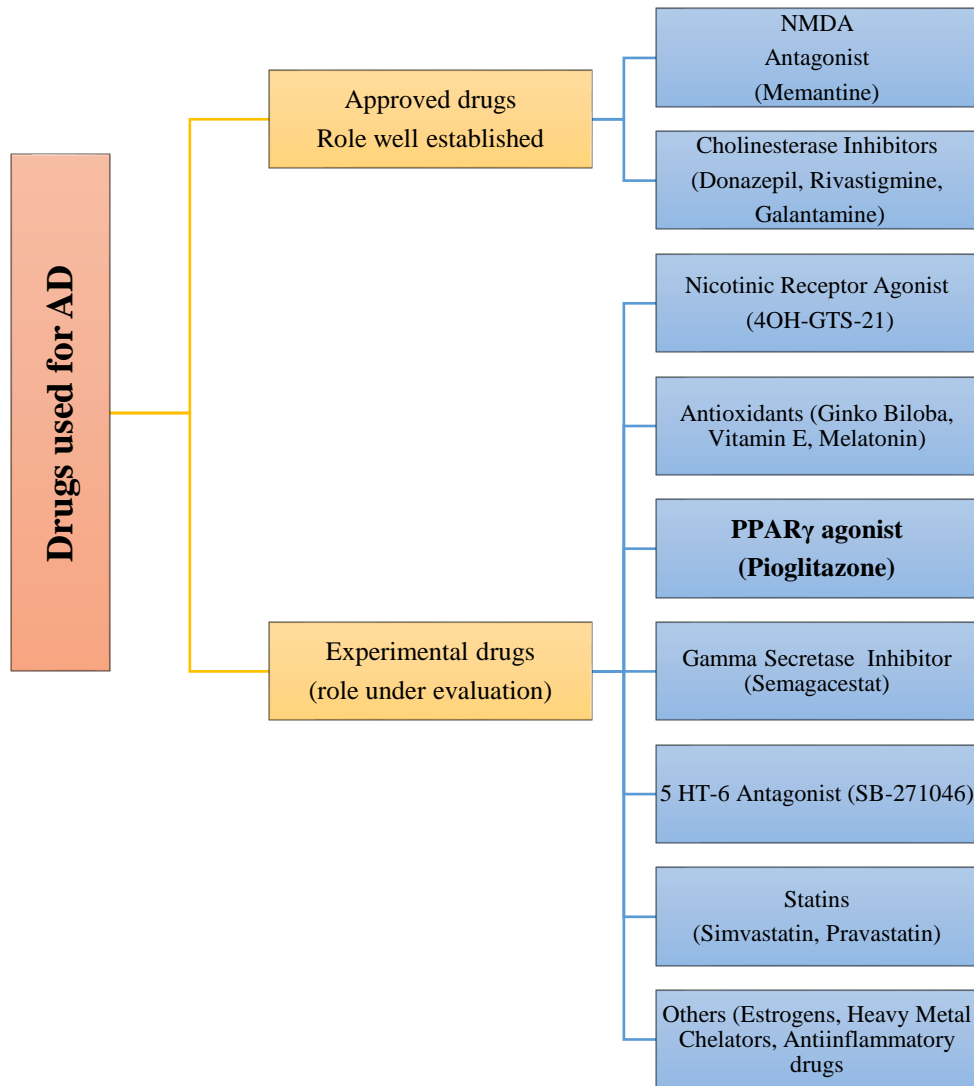


Figure 9: Pharmacological approach for Alzheimer's disease treatment. Modified from (128).

1.5 PEROXISOME PROLIFERATOR ACTIVATED RECEPTOR γ (PPAR γ)

PPARs are a subset of the nuclear receptor superfamily. These receptors reside in the nucleus bound to DNA response elements. Its location is typical of metabolite-activated nuclear receptors with three isoforms, PPAR α , PPAR β and PPAR γ , all of which form obligate heterodimers with the retinoic acid X-receptor (RXR-receptor). Otherwise, to activate PPARs, it is also necessary to activate RXR. Thus, RXR is activated by the vitamin A found in animals (retinol), not plants. In general, PPAR γ apparently prefers polyunsaturated fatty acids such as linoleic acid, AA and eicosapentaenoic acid (129).

PPAR γ has a wide variety of biological roles, including regulating fatty acid synthesis, storage and glucose metabolism, promoting adipogenesis and inhibiting inflammatory signalling through NF- κ B. Moreover, it is activated, not only by ligand (agonist) binding, but also by phosphorylation, which increases the ligand-independent transcriptional activity (62). Apart from its role as a transcription factor, PPAR γ also acts as a trans-repressor of macrophage inflammatory and gene regulator (Table 2) (130,131).

Nowadays, the role of PPAR γ in mediating responses to inflammation has been of particular interest since its agonists have been shown to exert a broad spectrum of anti-inflammatory effects. PPAR γ is expressed on numerous immune cells, including monocytes/macrophages, platelets, lymphocytes, dendritic cells (132–134), regulating different pathways signalling, among them anti-inflammatory activity (Figure 10). Overall, PPAR γ is a healthy protein (transcription factor) that lowers inflammation and increases insulin sensitivity. A wide diversity of ligands has been identified which bind to and activate PPAR γ receptor in different tissues. These ligands include thiazolidinediones (TZDs), which are antidiabetic drugs, as well as several PGs (PG D2 and its metabolite, 15-deoxy PG J2), oleanolic acids, and other eicosanoids (62). However, TZDs are also known to exert several PPAR γ independent effects.

Importantly, ligand activation of PPAR γ has been shown to exert potent anti-inflammatory effects. In addition, several of these molecules have effects independent of PPAR γ , many of which are also anti-inflammatory. The degree to which these ligands act in an independent manner varies. PPAR γ research has begun to focus on these anti-inflammatory effects and to investigate the role that PPAR γ and its ligands play in the resolution of inflammation (135).

Table 2: Genes regulated by PPAR γ agonists.

<i>Gene</i>	<i>Function</i>
<i>Adipophilin</i>	Fatty acid transport and storage
<i>L-FABP</i> ¹	Fatty acid transport and storage
<i>Regeneration gene IA</i>	Proliferation of pancreatic β and acinar cells
<i>Gob-4 (hAG-2)</i> ²	Maturation of intestinal goblet cells
<i>NGAL</i> ³	Anti-inflammatory, lipid metabolism
<i>NF-kappaB</i> ⁴	Pro-inflammatory, development
<i>TNF-α</i> ⁵	Pro-inflammatory, development
<i>IL-2</i> ⁶	Pro-inflammatory cytokine
<i>Catalase</i>	Anti-oxidatant enzyme
<i>Cu/Zn SOD</i> ⁷	Anti-oxidatant enzyme
<i>CD36</i>	Macrophage scavenger receptor
<i>SOCS3</i>	Cytokine negative modulator

¹Liver fatty acid binding protein; ²human homologue of anterior gradient-2; ³neutrophil; gelatinase-associated lipocalin; ⁴nuclear factor-kappaB; ⁵tumor necrosis factor- α ; ⁶interleukin-2; ⁷copper/zinc superoxide dismutase (131).

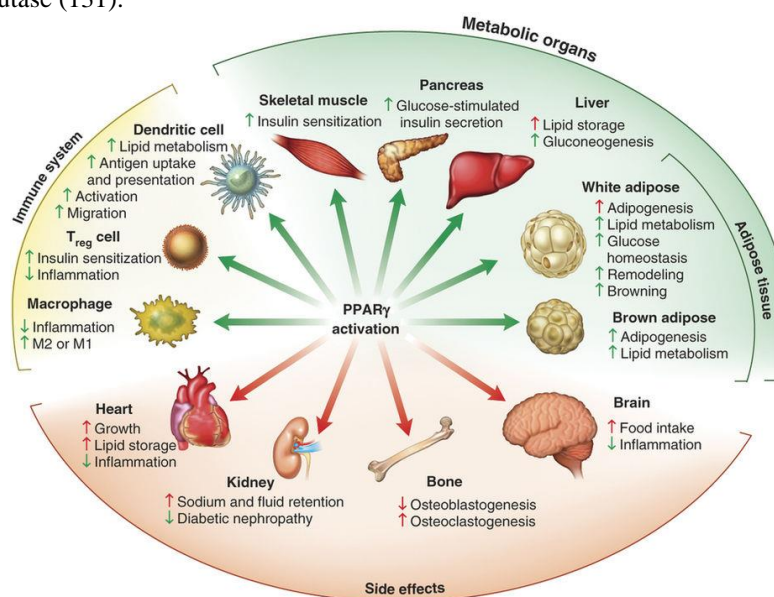


Figure 10: Known effects of PPAR γ activation (136).

Although TZDs are best recognized for their insulin sensitizing activity, they also have potent anti-inflammatory activity in tissues and inflammatory cells. It has been proposed that this may occur through both PPAR γ receptor-mediated and receptor-independent mechanisms (107). Numerous studies have shown that TZDs can repress activator protein 1 and NF- κ B dependent expression of inflammatory genes, and this may occur in large

part via PPAR γ -mediated stabilization of the nuclear receptor corepressor complex. TZDs may also drive expression of a variety of anti-inflammatory genes, such as adiponectin, hemeoxygenase-1, and IL-10 (137–139).

Given the diverse mechanisms by which TZDs may reduce inflammation, it is not surprising that therapy with TZDs has been shown to reduce multiple plasma markers of inflammation, although it is unclear whether these *in vivo* effects are attributable to effects on mononuclear cells or other tissues (140).

Animal studies and human trials of PPAR γ activating drugs, normally used to treat diabetes, have shown these compounds to have great potential as anti-inflammatory drugs. In a mouse model of asthma, PGZ, a PPAR γ activator, was found to be as effective as dexamethasone, a corticosteroid commonly used in asthma treatment (141). Using Type II diabetic rats as a model of inflammatory renal disease, PGZ reduced nephropathy by an anti-inflammatory mechanism (142). PPAR γ agonists inhibit inflammatory gene expression, alter A β homeostasis and exhibit neuroprotective effects (125). Also, there are several studies involving clinical trials with PPAR γ and most of them used PGZ for a trial of different inflammatory diseases (143,144). Taken together, these studies brought to light strong evidence of the anti-inflammatory function of PPAR γ through its ability to suppress inflammatory factors and the mechanisms by which PPAR γ activators may ameliorate inflammatory disease are discussed (Figure 11). Moreover, this receptor remains an attractive therapeutic target for treatment of many diseases with underlying inflammatory pathology.

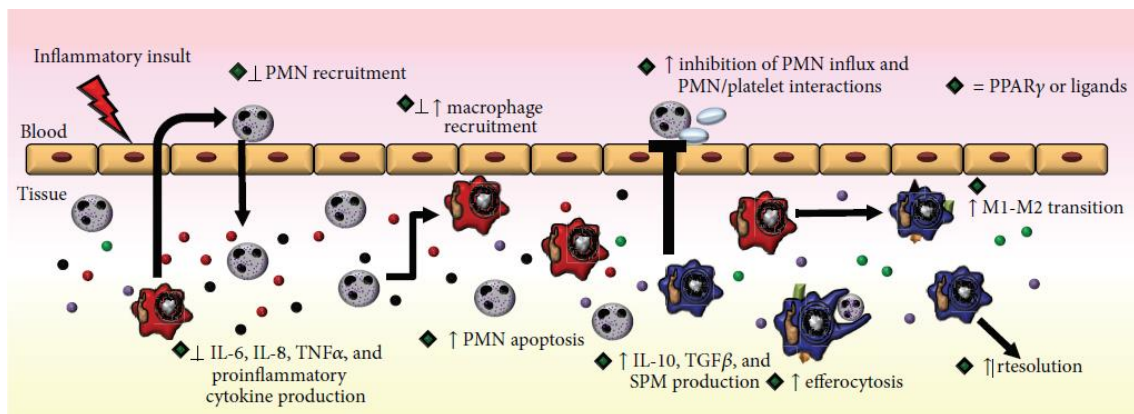


Figure 11: PPAR γ and the resolution of inflammation. PPAR γ and PPAR γ ligands (denoted by green diamond) play roles in all stages of inflammation. Early on, PPAR γ and its ligands decrease neutrophil recruitment and proinflammatory cytokine production. PPAR γ and its ligands then act to promote neutrophil apoptosis and efferocytosis and induction from proinflammatory to anti-inflammatory production. Finally, macrophages move to an M2 phenotype and tissue repair is initiated to return to homeostasis (62).

1.5.1 PIOGLITAZONE

PGZ is a selective synthetic PPAR γ agonist and approved by food and drug administration (FDA), used to treat diabetes type 2 (Figure 12). PGZ [(±)-5-[[4-[2-(5-ethyl-2-pyridinyl)ethoxy] phenyl] methyl]-2,4] TZD monohydrochloride contains one asymmetric carbon, and the compound is synthesized and used as the racemic mixture. The two enantiomers of PGZ interconvert *in vivo*. No differences were found in the pharmacologic activity between the two enantiomers (145). PGZ is an odourless white crystalline powder that has a molecular weight of 392.90 Da. This drug is soluble in N,dimethylformamide, dimethylsulfoxide (DMSO) and methanol, slightly soluble in anhydrous ethanol, very slightly soluble in acetone and acetonitrile, practically insoluble in water, and insoluble in ether. The pharmaceutical form is a tablet and it presents doses from 15 mg up to 45 mg once daily based on the glycaemic response of each patient.

Nowadays, it has been reported that PGZ modulates different pathways of inflammatory responses, such as decreasing the infiltration of inflammatory cells and cytokines (146), antifibrotic, anti-angiogenic, antifibrotic, anti-tumour effects, and neuroprotection (58,67,147). In addition, PGZ has the capacity to inhibit the local development of several inflammatory factors: these included IFN γ and IL-6 *in vivo*. Therefore, PGZ through its activation of PPAR γ and subsequent anti-inflammatory response, may prove to be a novel therapeutic in different inflammatory disorders such as rosacea, uveitis and Alzheimer's disease.

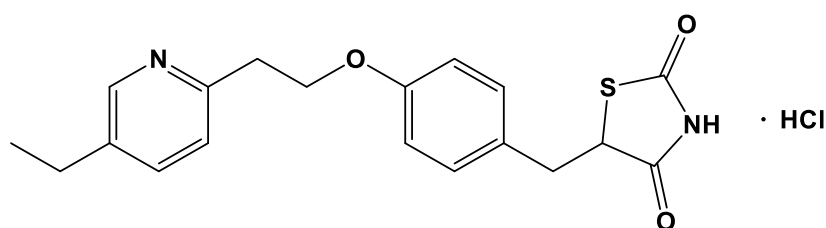


Figure 12: Chemistry structure of PGZ.

Mechanism of action

PGZ is a potent and highly selective agonist at PPAR γ in target tissues for insulin action such as adipose tissue, skeletal muscle, and liver. Being metabolized mainly by CYP2C8, CYP3A4 and CYP2C9. The activation of PPAR γ receptor increases the transcription of insulin-responsive genes involved in the control of glucose production, transport, utilization and lipid metabolism. One question is that PGZ enhances tissue sensitivity to

insulin and reduces the production of glucose via the liver (hepatic gluconeogenesis). Thus, insulin resistance associated with type 2 diabetes mellitus is improved without an increase in insulin secretion by pancreatic β cells. Basically, the PGZ reduces the glucose by two main mechanisms (145).

- increased glucose disposal in peripheral tissues (the principal effect)
- decreased hepatic glucose production.

The main adverse effects of the PGZ are weight gain (typically 3–4 kg of weight gain in the first year of use), fluid retention (with peripheral edema in 3–4 % of patients) and decreased bone density. The use of PGZ is associated with a small increased risk of bladder cancer, and therefore it is not recommended in patients with a history of bladder cancer or un-investigated haematuria.

1.6 PIOGLITAZONE DOSAGE FORMS

Drugs are rarely administered as pure chemical substances alone and are almost always given as formulated preparations or medicines. These can vary from relatively simple solutions to complex drug delivery systems through the use of appropriate additives or excipients in the formulation (148). It is important for pharmacists to appreciate the different properties of the varying dosage forms in order that the most appropriate or most acceptable formulation is prescribed to the patient (149). There are numerous dosage forms including solutions, suspensions, emulsions, gels, powders, granules, capsules, tablets, ointments, pastes, etc. into which a drug can be incorporated for the convenient and efficacious treatment of a disease. They can be taken orally or injected, as well as being applied to the skin or inhaled (148).

1.6.1 LIQUID PHARMACEUTICAL FORMS

Are medicines composed of a homogeneous one-phase system consisting of two or more components (148). They contain one or more solutes dissolved in one or more solvents, usually solids dissolved in liquids (149). Since molecules in solutions are uniformly dispersed, the use of solutions as dosage forms generally provide a way to assure the dosage is uniform on administration, and good accuracy when diluting or otherwise mixing solutions.

Dosage forms categorized as “Solutions” are classified according to route of administration, such as “Oral Solutions” and “Topical Solutions,” or by their solute and solvent systems, such as “Spirits,” “Tinctures,” and “Waters.” Liquid pharmaceutical forms intended for parenteral administration are officially entitled “Injections” (150).

Moreover, the oral solutions are liquid preparations, intended for oral administration, that contain one or more substances with or without flavoring, sweetening, or coloring agents dissolved in a suitable vehicle (150). Pharmaceutical solutions for oral administration offer several advantages:

- Therapeutic agents can easily be administered orally to individuals who have difficulty in swallowing, e.g. elderly patients, infants.
- The therapeutic agent is dissolved in the formulation and is therefore immediately available for absorption. Providing the drug does not precipitate within the gastrointestinal tract, the bioavailability of pharmaceutical solutions is greater than that of oral solid-dosage forms.
- Taste-masking of bitter therapeutic agents may be readily achieved.

Sometimes the poor solubility of certain therapeutic agents may make difficult their formulation as pharmaceutical solutions, as example of PGZ. However, certain techniques are available to enhance the solubility of poorly soluble drugs (151). The aqueous solubility of insoluble or sparingly soluble drugs can be enhanced by the addition of water-soluble cosolvents such as ethanol, glycerol or propylene glycol, which are suitable for oral administration. The solubility of poorly soluble drugs may also be improved by the addition of solubilizing agents such as the nonionic surfactants, by the addition of acid or alkali to form salts, or by complexation (152).

Among the solubilizing agents, Transcutol is a purified diethylene glycol monoethyl ether (DEGEE) and it is an interesting compound due to its low toxicity and high biocompatibility. DEGEE, is an ethylene oxide derivative used as a solvent in many products, including pharmaceuticals, cosmetics, and food applications. Its appearance is a clear, colorless, hygroscopic liquid with a mild, pleasant odor. It is produced by condensation of ethylene oxide and alcohol, followed by a purification distillation (153). DEGEE is soluble in water and miscible in acetone, benzene, chloroform, ethanol (95%), ether, and pyridine. It is partially soluble in vegetable oils and insoluble in mineral oils (154). The primary supplier in the US for pharmaceutical grade DEGEE is Gattefossé,

under the trade name Transcutol (155). Current pharmaceutical grade Transcutol-P (topical route) and Transcutol-HP (oral route) are 99.8% and 99.9% pure, respectively.

1.6.2 NANOCARRIERS FOR DRUG DELIVERY

Nanotechnology is the application of scientific knowledge to manipulate and control matter at the nanoscale in order to make use of size and structure dependent properties and phenomena. It has given numerous options in the delivery of bioactives and it has benefited in the formulation of delivery in several modes i.e. reduced side effects, targeting, improved patient compliance, etc (156). This field presents new opportunities for the development of everyday products with enhanced performance in drug delivery, reduced production cost and using less raw material. The concept of drug delivery deals with the use of approaches to help a pharmaceutical compound reach its target for achieving its therapeutic effect. Such approaches include the use of formulations, alternative routes of administration, prodrugs that act once they are metabolized, or more complex systems for transporting the pharmaceutical compound (carriers) (157–159).

The development of new nanomaterials for medical applications, including therapy, has been of great importance in the recent years due to the useful properties which are specific of the materials of nanometric size, such as the light absorption or light dispersion, the surface/volume ratio, or the size itself as the majority of biomacromolecules are of nanometric size (160,161). A wide variety of nanomaterials with medical purposes have been described, including nanoparticles (NPs) of different materials, liposome, dendrimer, nanostructured gels, nanotubes, etc (Figure 13).

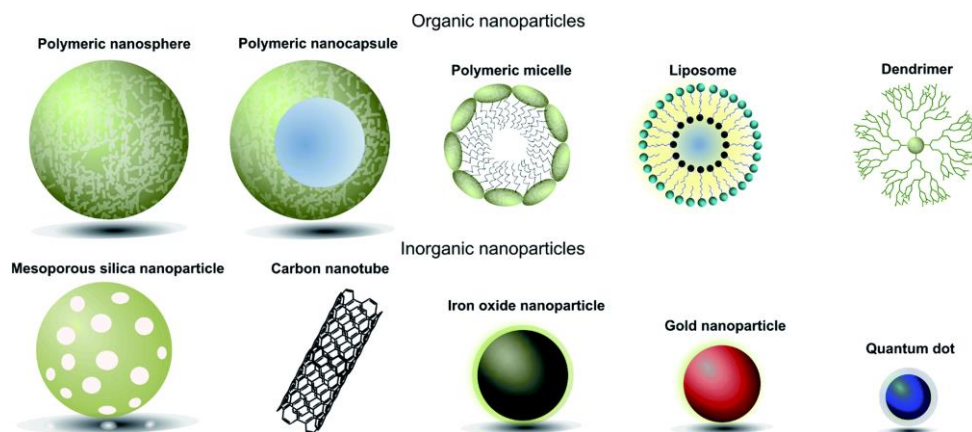


Figure 13: Some types of nano delivery systems (162).

1.6.2.1 Polymeric Nanoparticles

Polymeric nanoparticles (PNPs) have attracted considerable interest over the last few years due to their unique properties and behaviours resulting from their small size. As asserted by different authors, these nanoparticulate materials show potential for a wide range of applications such as diagnostics and drug delivery (163–166). PNPs are solid colloid matrix-like particles sizing from 10 to 1000 nm, made of polymers of a different nature (natural and synthetic), and encapsulating molecules during the preparation process, chosen depending on both the polymers and the drug to be delivered. The drug may be attached to a nanoparticle matrix, or dissolved, encapsulated and entrapped, giving rise to different terminologies as NPs, nanospheres or nanocapsules (Figure 14) (167). The nanospheres have a matrix structure, whose entire mass is solid and the molecules can be adsorbed on the surface of the sphere or encapsulated within the particle. On the other hand, nanocapsules are vesicular systems, which act as a kind of deposit, in which the drug is trapped in a cavity consisting of an oily or aqueous core surrounded by a shell of solid material (167).

Considering the stringent request of FDA guidelines in terms of biodegradability and biocompatibility for *in vivo* administration, the list of polymers, that could be used to prepare PNPs systems, results very short with few polymers available for drug delivery system preparation and approved for systemic administration. The most useful are biodegradable polymer of natural origin (albumin, gelatine, lysine, collagen and chitosan) (168) and synthetic as poly(alkyl cyanoacrylates) and polyesters poly(ϵ -caprolactone) and copolymers of poly(d,l-lactic-co-glycolic acid) (PLGA) (169).

PLGA is also approved by the European medicine agency (EMA) in various drug delivery systems for humans, being commercially available with different molecular weights and copolymer compositions (170–172). It is one of the most successfully used biodegradable polymers because its hydrolysis leads to metabolite monomers, lactic acid and glycolic acid. Because these two monomers are endogenous and easily metabolized by the body via the Krebs cycle, a minimal systemic toxicity is associated with the use of PLGA for drug delivery or biomaterial applications (173). Moreover, it can modify the release of the drug and/or its bioavailability. However, it allows incorporation molecules hydrophilic and hydrophobic and obtains a sustained release of the drug, as well as protecting it from degradation.

Advantages of these systems as carriers include controlled release, the ability to combine both therapy and imaging (theragnostics), the protection of drug molecules and its specific targeting, facilitating improvements in the therapeutic index (174,175).

In particular, it is a common opinion that the toxicology of a nanodevice is related both to morphological and structural parameters of the systems (size, surface charge, shape) and the polymers used (80).

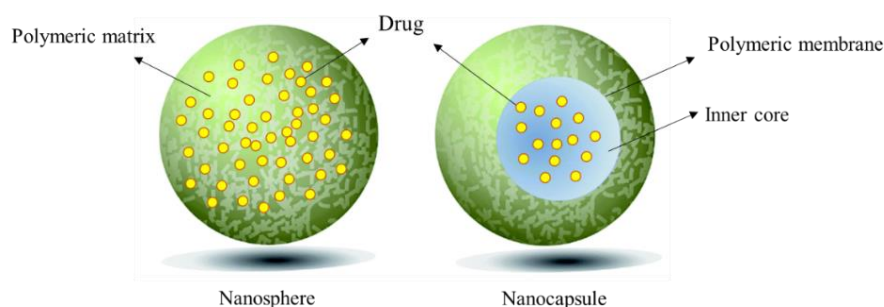


Figure 14: Polymeric nanoparticles. Adapted from (162).

To target organs with PNPs to increase selective cellular binding and internalization through receptor-mediated endocytosis and to avoid the reticuloendothelial system (RES) to eliminate these from the blood stream and take them up in the liver or the spleen (171), the surface of these systems is modified. NPs can be coated with molecules that hide the hydrophobicity by providing a hydrophilic layer at the surface. The most common way for the surface modification is the hydrophilic and non-ionic polymer polyethylene glycol (PEG). It has been well demonstrated that the “PEGylation” increases their blood circulation half-life by several orders of magnitude (176). Moreover, PEG exhibits an excellent biocompatibility. Poloxamer, poloxamines or chitosan have also been studied for surface modification (173,177). These groups can block the electrostatic and hydrophobic interactions that help opsonin to bind to particles surfaces. Moreover, the surface charge of NPs also has an important influence on their interaction with cells and on their uptake.

NPs can be targeted to organs such as liver, spleen, lung and lymph, and because of their very small volume, they can pass through the narrowest capillaries. They can remain in the blood stream for prolonged times because of their ability to avoid the phagocytes, and as a consequence, they are amenable to controlled release properties (172).

Preparation methods

Several preparation methods have been developed and these can be divided into two groups, namely, the conventional and advanced (Figure 15). NPs have been fabricated depending on the requirements of their application and the physicochemical characteristics of the drug by using various techniques such as solvent evaporation, spontaneous emulsification/solvent diffusion, salting out/emulsification–diffusion, interfacial polymerization and nanoprecipitation. The choice of the most suitable method plays a vital role in order to obtain PNPs with the desired properties for a particular application (163).

The typical method used to encapsulate drugs into of a polymeric matrix is the displacement technique, described first by Fessi *et al.*, (178) (Figure 16). It has been a successful method to deliver the lipophilic drug (179), and it consists of two phases. The organic phase consists in dissolving the polymer and the drug in an organic solvent and an aqueous phase with surfactant and water. After that, the organic phase is added drop by drop, gently mixing it into a known volume of an aqueous phase. After the formation of NPs the solvent is evaporated and the NPs dispersion is concentrated at the initially set volume under reduced pressure.

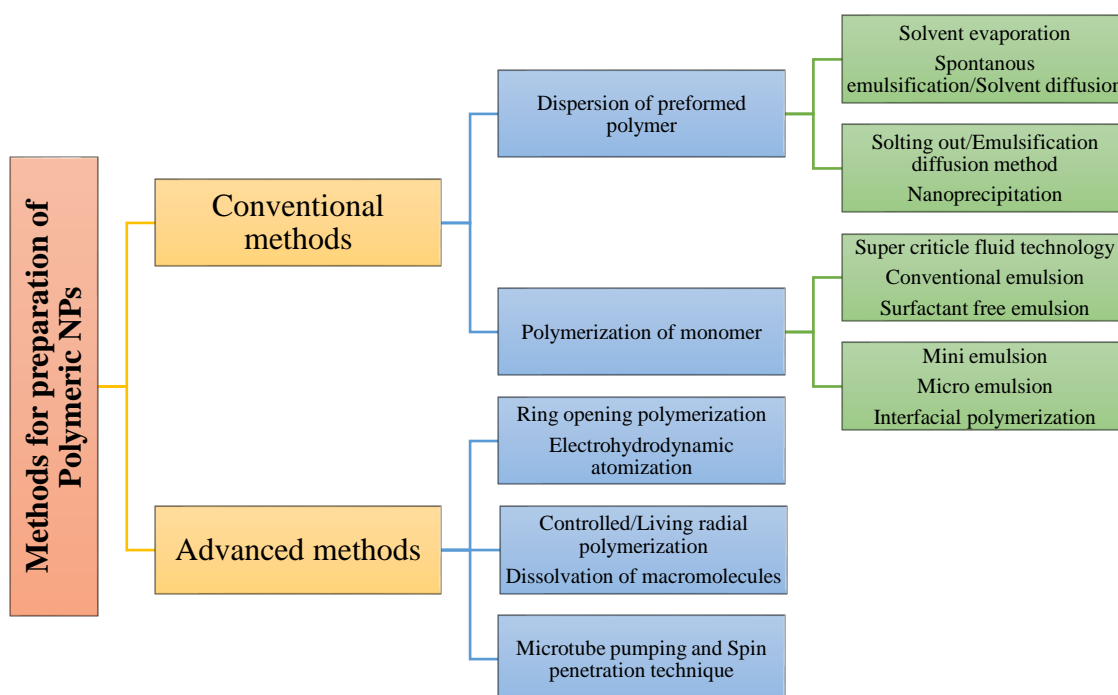


Figure 15: Conventional method of preparation of PNPs. Adapted from (180).

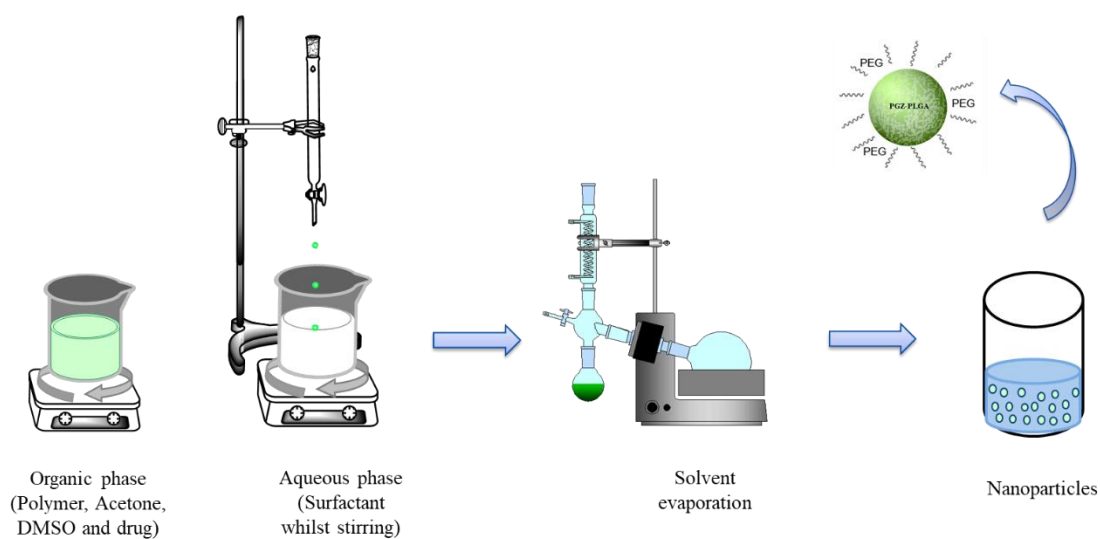


Figure 16: Method of preparation of NPs by solvent displacement technique.

Physicochemical Characterization of PNPs

NPs are usually characterized in the literature by size distribution, morphology, surface properties, stability and drug-polymer interactions. The various techniques involved in the physicochemical characterization of PNPs are summarized in Table 3 with only some common characterization methods.

Table 3: Principal techniques for evaluation of the physicochemical characteristics of PNPs (163). Adapted from (181).

<i>Techniques</i>	<i>Physicochemical characteristics analysed</i>
<i>Atomic force microscopy (AFM)</i>	Size and size distribution Shape Structure Aggregation Surface properties (modified AFM)
<i>Differential Scanning Calorimetry (DSC)</i>	Physicochemical state and possible interactions of the drug and the polymer
<i>Dynamic light scattering (DLS)</i>	Hydrodynamic size distribution Critical association concentration (CAC)
<i>Fluorescence spectroscopy</i>	determination Drug content <i>In vitro</i> drug release
<i>High Performance Liquid Chromatography (HPLC)</i>	Drug content <i>In vitro</i> drug release
<i>Infrared spectroscopy (IR)</i>	Structure and conformation of bioconjugates Functional group analysis
<i>Mass spectrometry (MS)</i>	Molecular weight Composition Structure Surface properties (secondary ion MS)
<i>Near-field scanning optical microscopy (NSOM)</i>	Size and shape of nanomaterials
<i>Nuclear magnetic resonance (NMR)</i>	Structure Composition Purity Conformational charge
<i>Scanning electron microscopy (SEM) and Scanning tunnelling microscopy (STM)</i>	Size and size distribution Shape Aggregation
<i>Transmission electron microscopy (TEM)</i>	Size and size distribution Shape heterogeneity Aggregation
<i>X-ray photoelectron spectroscopy (XPS)</i>	Elemental and chemical composition at the surface
<i>Zeta potential (ZP)</i>	Stability referring to surface charge

CHAPTER 2

OBJECTIVES

2. OBJECTIVES

The main objective of this research is the development and characterization of different dosage forms of Pioglitazone able to reduce the inflammation associated with rosacea, uveitis and Alzheimer disease's.

To achieve this goal the research work has been divided into several stages (specific objectives):

- Optimization by factorial design of polymeric nanostructured systems of PLGA-PEG able to cross different tissues barriers, analysing drug-vehicle interactions (by spectroscopic and thermal methods) and short time stability.
- Biopharmaceutical behaviour studies analysing *in vitro* drug release from dosage forms and *ex vivo* permeation of the drug across different biological membranes.
- Dosage forms tolerance and *in vitro* cytotoxicity assay in cell culture from immortalized human keratinocytes (HaCat), retinoblastoma (Y-79) and immortalized human cerebral microvascular endothelial (hCMEC/D3).
- Internalization, transport and permeability studies of PGZ-NPs in hCMEC/D3 cell line.
- *In vivo* evaluation therapeutic efficacy of the dosage forms developed in animal model for rosacea, uveitis and Alzheimer's disease.

CHAPTER 3

RESULTS

3. RESULTS

Below is a summary of the results obtained from the research work in the form of articles which deal with the subject of this doctoral thesis.

3.1 Article 1: Human Skin Permeation Studies with PPAR γ Agonist to Improve Its Permeability and Efficacy in Inflammatory Processes. *International Journal of Molecular Science*, 2017.

3.2 Article 2: Optimization, Biopharmaceutical Profile and Therapeutic Efficacy of Pioglitazone-loaded PLGA-PEG Nanospheres as a Novel Strategy for Ocular Inflammatory Disorders. *Pharmaceutical Research*, 2018.

3.3 Article 3: Comparative Study of Ex Vivo Transmucosal Permeation of Pioglitazone Nanoparticles for the Treatment of Alzheimer's Disease. *Polymers*, 2018.

3.4 Article 4: PPAR γ agonist-loaded PLGA-PEG nanocarriers as a potential treatment for Alzheimer's disease: in vitro and in vivo studies. *International Journal of Nanomedicine*, 2018 (Accepted).

3.5 Article 5: Thiazolidinedione as an alternative to facilitate oral administration in geriatric patients with Alzheimer's Disease. *European Journal of Pharmaceutical Science* (Submitted).

3.1 Article 1

Human Skin Permeation Studies with PPAR γ Agonist to Improve Its Permeability and Efficacy in Inflammatory Processes

Marcelle Silva-Abreu, Lupe Carolina Espinoza, María José Rodríguez-Lagunas, María-José Fábrega, Marta Espina, María Luisa García and Ana Cristina Calpena.

International Journal of Molecular Science

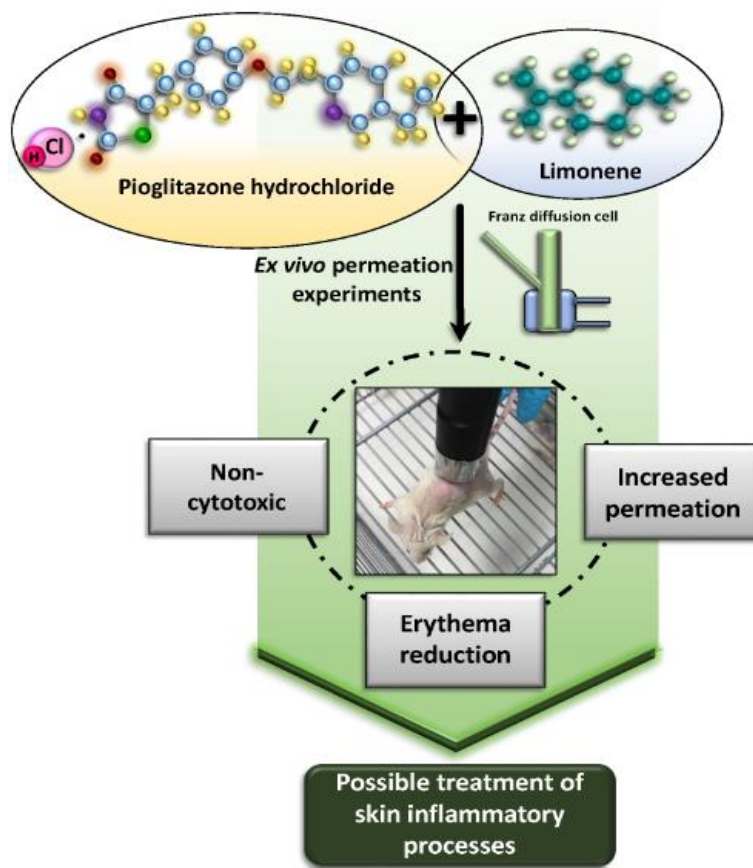
Year: 2017

ISSN: 1422-0067

IF: 3.687

DOI: 10.3390/ijms18122548

Graphical abstract





Article

Human Skin Permeation Studies with PPAR γ Agonist to Improve Its Permeability and Efficacy in Inflammatory Processes

Marcelle Silva-Abreu ^{1,2} , Lupe Carolina Espinoza ^{1,3} , María José Rodríguez-Lagunas ^{4,5} ,
María-José Fábrega ^{4,6} , Marta Espina ^{1,2}, María Luisa García ^{1,2} and Ana Cristina Calpena ^{1,2,*}

¹ Department of Pharmacy, Pharmaceutical Technology and Physical Chemistry, Faculty of Pharmacy and Food Sciences, University of Barcelona, 08028 Barcelona, Spain; marcellesabreu@gmail.com (M.S.-A.); lcespinoza@utpl.edu.ec (L.C.E.); m.espina@ub.edu (M.E.); rdc@ub.edu (M.L.G.)

² Institute of Nanoscience and Nanotechnology (IN2UB), University of Barcelona, 08028 Barcelona, Spain

³ Departamento de Química y Ciencias Exactas, Universidad Técnica Particular de Loja, Loja 1101608, Ecuador

⁴ Department of Biochemistry and Physiology, Faculty of Pharmacy and Food Sciences, University of Barcelona, 08028 Barcelona, Spain; mjrodriguez@ub.edu (M.J.R.-L.); mjfabrega@ub.edu (M.-J.F.)

⁵ Institut de Recerca en Nutrició i Seguretat Alimentària (INSA), Universitat de Barcelona (UB), 08028 Barcelona, Spain

⁶ Institute of Biomedicine, University of Barcelona, 08028 Barcelona, Spain

* Correspondence: anacalpena@ub.edu; Tel.: +34-93-402-4560

Received: 30 October 2017; Accepted: 21 November 2017; Published: 28 November 2017

Abstract: Rosacea is the most common inflammatory skin disease. It is characterized by erythema, inflammatory papules and pustules, visible blood vessels, and telangiectasia. The current treatment has limitations and unsatisfactory results. Pioglitazone (PGZ) is an agonist of peroxisome proliferator-activated receptors (PPARs), a nuclear receptor that regulates important cellular functions, including inflammatory responses. The purpose of this study was to evaluate the permeation of PGZ with a selection of penetration enhancers and to analyze its effectiveness for treating rosacea. The high-performance liquid chromatography (HPLC) method was validated for the quantitative determination of PGZ. Ex vivo permeation experiments were realized in Franz diffusion cells using human skin, in which PGZ with different penetration enhancers were assayed. The results showed that the limonene was the most effective penetration enhancer that promotes the permeation of PGZ through the skin. The cytotoxicity studies and the Draize test detected cell viability and the absence of skin irritation, respectively. The determination of the skin color using a skin colorimetric probe and the results of histopathological studies confirmed the ability of PGZ-limonene to reduce erythema and vasodilation. This study suggests new pharmacological indications of PGZ and its possible application in the treatment of skin diseases, namely rosacea.

Keywords: skin permeation; PPAR- γ ; pioglitazone; limonene; rosacea; inflammation

1. Introduction

Rosacea is a chronic inflammatory disease of the skin [1–3]. The clinical features appear principally in the central region of the face and include the presence of facial erythema, inflammatory papules and pustules, telangiectasia, and edema [4–6]. It predominantly affects women and fair-skinned people and can occur at any age but is more frequent in middle-aged individuals [7,8]. The estimated prevalence of rosacea among the population of Europe and United States has a wide range from less than 1% to more than 20%, likely due to differences in the methods used and the populations studied [9,10]. Furthermore, it has been associated with several comorbidities such as depression and anxiety [11,12], dyslipidemia, hypertension, cardiovascular diseases, and metabolic diseases [13–15].

The pathogenesis of the disease has not been totally clarified but several factors implicated in the etiology of the disease have been reported, such as genetic predisposition, alterations of the neurovascular system, and dysregulation of the innate and adaptive immune system [16,17]. Studies about the pathophysiological mechanisms of rosacea suggest activation of pattern recognition receptors (PRRs) that identify components from foreign microorganisms and immunostimulatory products [18,19]. An increase in Toll-like receptors-2 (TLR-2) expression, a family of PRRs, has been observed in inflammatory skin diseases such as rosacea. When TLR-2 is stimulated by triggering factors, it induces the release of antimicrobial peptides (cathelicidin LL-37) or proinflammatory cytokines such as IL-8, IL-1 β , and TNF- α [18,20]. In addition, the characterization of inflammatory infiltrate in this disease has revealed the activation of T lymphocytes, particularly T-helper 1 (Th1) and T-helper 17 (Th17) cells, as well as the presence of macrophages and mast cells, which mediate the inflammatory reactions and development of the disease [21,22].

Topical treatments like sodium sulfacetamide, azelaic acid, metronidazole, and the alpha-adrenergic agonist are recommended when there are few papules and pustules [23,24]. If the skin lesions are more extensive, systemic medications like tetracyclines are prescribed [25,26]. Despite these pharmacological options, rosacea remains incurable, and thus its treatment focuses mainly on controlling the symptoms [27]. These limitations, coupled with unsatisfactory therapeutic results, demonstrate the need to develop more targeted and efficacious treatments [23,28].

Recent studies have suggested that the peroxisome proliferator-activated receptor-gamma (PPAR- γ), a nuclear receptor that regulates glucose homeostasis and lipid metabolism, has an important role in adaptive immunity by regulating genes expression involved in inflammatory processes [29]. Therefore, it has been proposed that PPAR- γ agonists could act as negative regulators in T cell differentiation and activation to attenuate inflammatory responses of autoimmune diseases [30]. Pioglitazone (PGZ) is a member of the thiazolidinediones, which is useful to treat type 2 diabetes mellitus (DM) [31,32]. Moreover, previous studies have demonstrated that this drug has the capacity to inhibit the signaling pathways involved in inflammatory and immunologic processes [33,34], suggesting that its application could be an effective treatment of inflammatory processes.

Penetration enhancers are used with the aim to improve the transdermal drug delivery [35]. Several chemicals such as sulphoxides, azones, pyrrolidones, alcohols, glycols, surfactants, fatty acids, essential oils, and terpenes have been proposed for their ability to reversibly decrease the barrier resistance, allowing drug penetration into the skin at a greater rate [36,37]. As a result, penetration enhancers represent an alternative to improve the permeability and, consequently, the duration of drug action.

After having taken into consideration the role of PPAR- γ as an important immunomodulator with anti-inflammatory properties, the aim of this study was to evaluate the efficacy of the PGZ solution with a selection of penetration enhancers to improve its permeability for treating rosacea using an *in vivo* model.

2. Results

2.1. Validation of the Analytical Method

All the analytical method data can be found in Supplementary materials. The linearity of the method was evaluated by the obtained equation and regression values from the calibration curves determined by least-squares linear regression analysis of the peak-area ratios of the PGZ standards solutions *versus* concentration. Three calibration curves were made in the range of 1.5–110 $\mu\text{g}/\text{mL}$ (Table S1). No single calibration standard point was dropped during the validation and the data indicate good linearity of the proposed method. The equation obtained from the average calibration curves and the correlation coefficient value are shown Figure S1. Precision of the method was evaluated at concentrations of 3, 60, and 110 $\mu\text{g}/\text{mL}$ for the linearity range. Obtained results are shown in Table S2. Data are expressed as percentage of coefficient of variation (CV) and precision of method. The accuracy

of the method was evaluated in small, medium, and large concentrations of the range of linearity studied by comparing the tested concentration with the theoretical concentration. Obtained results are shown in Table S3. Data are expressed as percentage of relative error and accuracy. Robustness examines the effect that operational parameters have on the results and provides an indication of its reliability during normal usage. It was determined by evaluating retention time with tolerance variations in the flow and mobile phase that are shown in Table S4. Specificity was proven by the analysis of blank control of mobile phase (Figure S2), standard of 30 ppm (Figure S3), blank of the skin as control (Figure S4), and sample of skin permeated with PGZ-limonene (Figure S5). Chromatogram did not show interference at the retention time of PGZ. From the lowest concentration standard (1.5 ppm), the detection limit (LOD) and the limit of quantification (LOQ) were determined based on signal-to-noise ratios of 3:1 and 10:1, respectively. Hence, the LOD for PGZ was set at 0.12 ± 0.28 ng/mL and the LOQ at 0.40 ± 0.52 ng/mL.

2.2. Permeation Studies in Human Skin

The permeation profiles of PGZ with and without penetration enhancers were estimated. The cumulative permeated amount of PGZ (μg) per cm^2 of human skin in each time interval is shown in Figure 1.

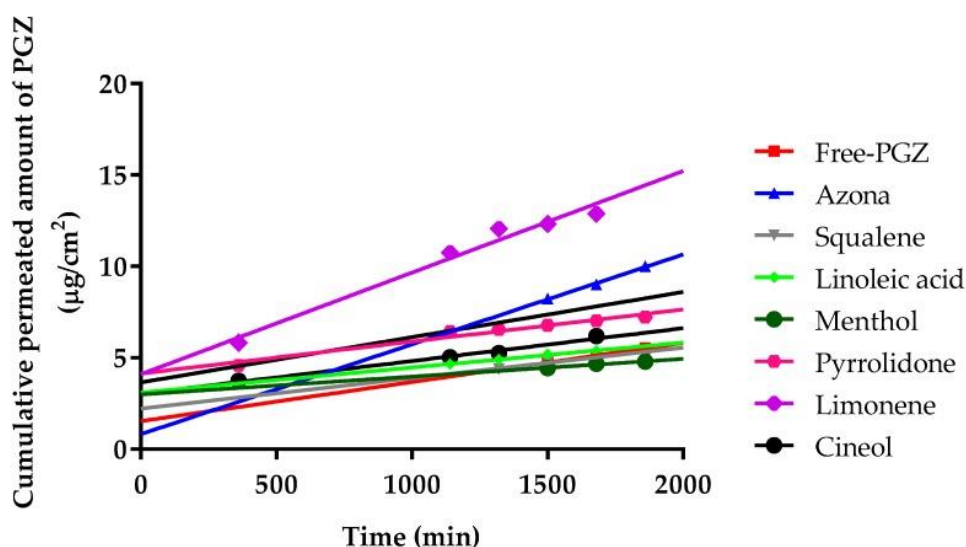


Figure 1. Median cumulative permeated amount of pioglitazone (PGZ) with and without penetration enhancers through human skin, expressed as $\mu\text{g}/\text{cm}^2$.

Furthermore, the permeation and prediction parameters of PGZ with permeation enhancers were calculated. The flow (J_{ss}) and permeability coefficient (K_p) were determined from the cumulative amount of the drug permeated through the skin plotted *versus* time in steady state. Table 1 shows that the limonene presented the highest values for J_{ss} , k_p , Q_{ret} , and C_{ss} .

Table 1. Permeation and prediction parameters of PGZ and penetration enhancers.

Permeation and Prediction Parameters	Free-PGZ	Azona	Squaleno	Linoleic Acid	Menthol	Pyrrolidone	Limonene	Cineol
J_{ss} ($\mu\text{g}/(\text{h}/\text{cm}^2)) \times 10^4$	8.42 ^{a,c,d,f,g} (7.68–9.36)	19.40 ^{b,c,d,e} (17.4–23.3)	6.56 ^{f,g} (5.81–7.22)	5.38 ^{f,g} (4.74–6.02)	3.83 ^{e,f,g} (3.44–4.31)	6.89 ^{f,g} (6.30–7.58)	21.90 ^g (19.7–25.1)	18.00 (15.2–20.8)
K_p ($\text{cm}/\text{h}) \times 10^5$	4.92 ^{a,c,d,f,g} (4.33–5.41)	12.10 ^{b,c,d,e} (11.90–14.30)	3.62 ^{f,g} (3.16–3.98)	3.21 ^{f,g} (2.69–3.53)	2.33 ^{e,f,g} (2.20–2.66)	4.21 ^{f,g} (3.69–4.53)	13.20 ^g (12.90–16.50)	2.53 (2.38–2.78)
Q_{ret} ($\mu\text{g}/\text{g skin}/\text{cm}^2$)	42.61 ^{a,c,d,e,f,g} (38.34–46.86)	8.42 ^{b,d,f,g} (7.67–9.36)	53.61 ^{c,d,e,f,g} (47.24–57.97)	14.84 ^{d,f,g} (14.35–16.32)	101.82 ^{e,f} (90.63–112.00)	18.04 ^{f,g} (15.23–20.84)	207.65 ^g (186.88–229.41)	94.74 (85.26–105.21)
C_{ss} ($\text{ng}/\text{mL}) \times 10^4$	3.73 ^{a,c,d,f,g} (3.45–4.20)	8.57 ^{b,c,d,e,g} (7.71–9.52)	2.90 ^{f,g} (2.41–3.29)	2.38 ^{f,g} (2.04–2.62)	1.69 ^{e,f,g} (1.44–1.96)	3.05 ^{f,g} (2.84–3.35)	9.68 (8.81–10.50)	9.60 (8.54–11.60)

^a = Azona; ^b = Squaleno; ^c = Linoleic acid; ^d = Methol; ^e = Pyrrolidone; ^f = Limonene; ^g = Cineol. No differences found for Free-PGZ. Results are expressed by median and range of three replicates. One-way Analysis of Variance (ANOVA) with Tukey's Multiple Comparison Tests were performed to assess the statistical significance between groups at ($p < 0.05$).

2.3. Cytotoxicity Studies and Skin Tolerance Studies

The in vitro cytotoxicity assay by 3-(4,5-dimethylthiazol-2-yl)-2,5-diphenyltetrazolium bromide (MTT) was carried out using HaCaT cells after incubation with PGZ-limonene and limonene. Six concentrations were selected according to the level of concentration of each formulation studied. The results showed cell viability greater than 80% in the dilutions assayed from 0.001 to 0.02 mg/mL (Figure 2).

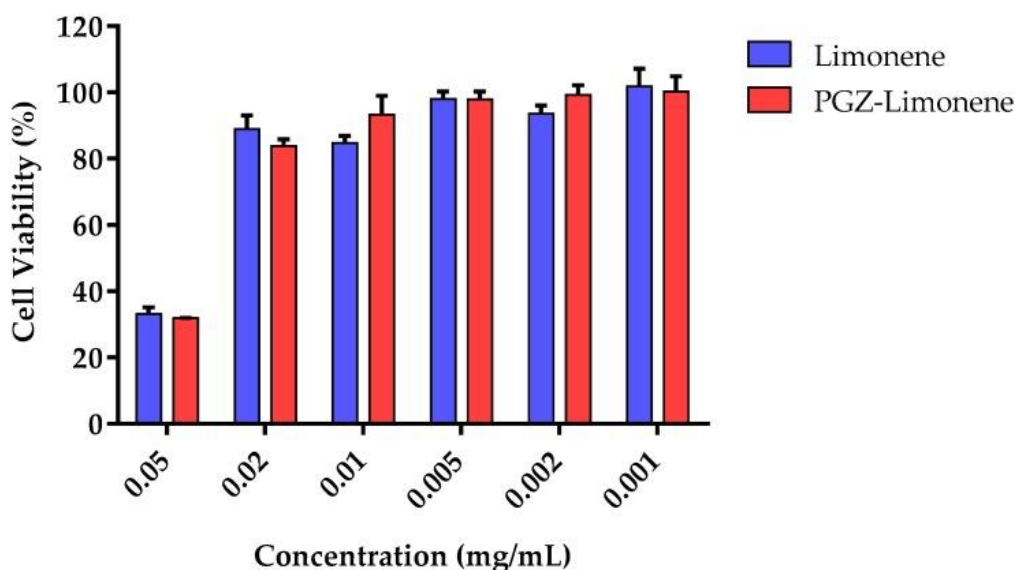


Figure 2. Percentage of cellular viability of immortalized human keratinocytes (HaCaT) cell line exposed to PGZ-limonene and limonene.

The Draize test was performed in order to evaluate the skin irritation potential of PGZ-limonene and limonene. It had a duration of 72 h using a concentration of 1 mg/mL of PGZ and 5% of limonene. The resulting primary irritation index value of the tested groups were: Control (0.9% NaCl): 0; PGZ-limonene: 0.32 and limonene: 0.43, thereby indicating that PGZ-limonene and limonene are non-irritant.

2.4. Efficacy Studies

2.4.1. Colorimetric Parameters

The pharmacological efficacy of PGZ-limonene was evaluated by skin color differences from the backs of mice with respect to basal color. The evolution of erythema can be seen in Figure 3 and Figure S6, which displays the reproduction of the color codes as a sequence through different steps: basal color, induction of inflammation/vasodilation, and treatment after 5, 10, and 20 min. The results showed significant differences between the relative erythema (%) of the topical treatment with PGZ-limonene and limonene with respect to positive control. PGZ combined with limonene reduced the relative erythema below the basal value at 20 min (Figure 4a–c).

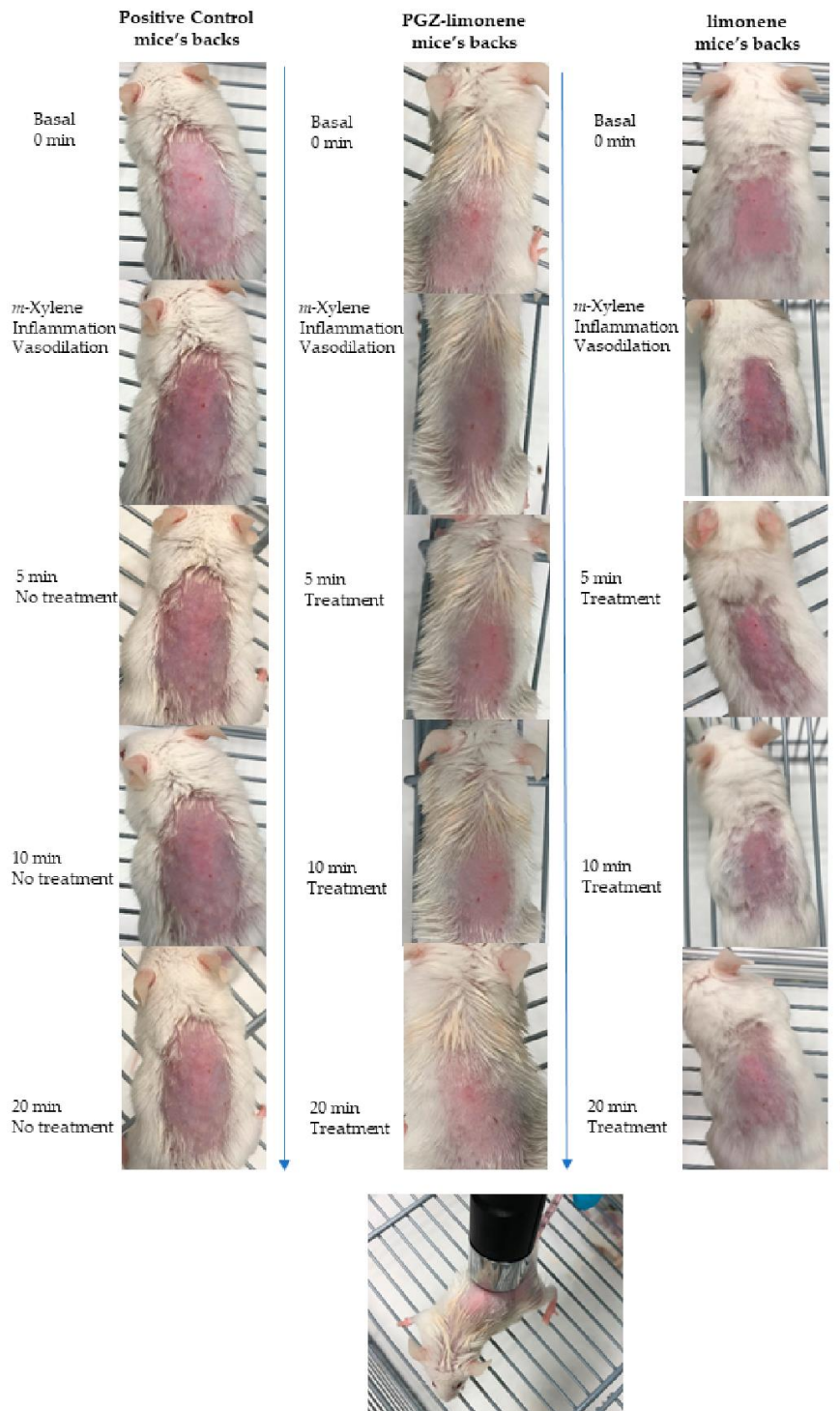


Figure 3. Evolution of erythema shown as skin color sequence on mice's backs, using PGZ-limonene and limonene compared with positive control. Colors are reproduced from the average values of three basic light components, red, green, and blue (RGB) codes using a Multi Probe Adapter (MPA) 5 Multi Probe adapter from Courage + Khazaka electronic GmbH (Cologne, Germany), equipped with a CL400.

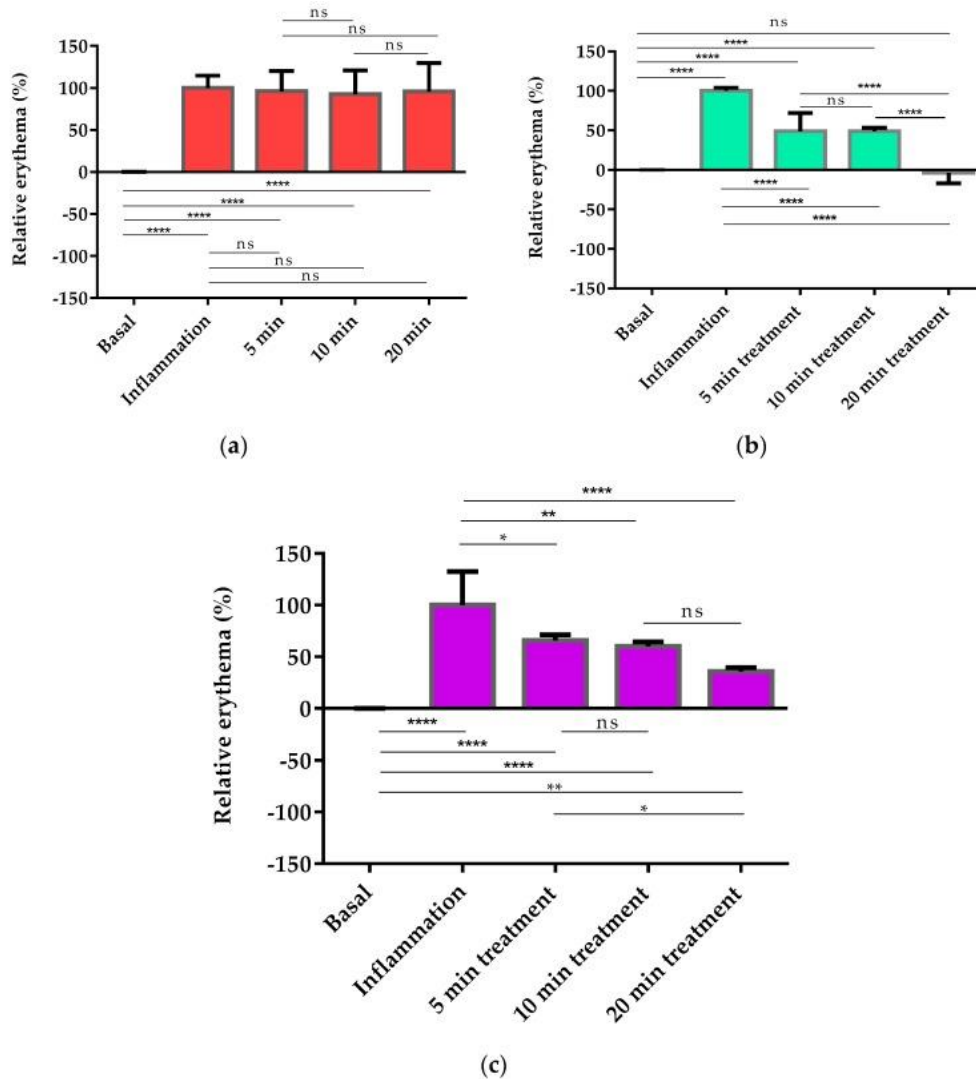


Figure 4. Colorimetric studies for pharmacological evaluation. (a) Statistical differences of positive control with respect to basal values (0 min); (b) relative erythema (%) of PGZ-limonene at different time intervals with respect to the basal stage (0 min); (c) relative erythema (%) of limonene at different time intervals with respect to the basal stage (0 min). Horizontal bars represent the average value. Significant statistical differences: * $p < 0.05$, ** $p < 0.01$, **** $p < 0.0001$, ns = non-significant.

2.4.2. Histological Analysis

Histologically, control skin consisted of a relatively thin epidermis with a contiguous stratum corneum and normal dermal appendages (Figure 5A). A similar pattern of staining was observed in the PGZ-limonene treated skin (Figure 5D). Loss of the stratum corneum was evident in the *m*-Xylene treated mice (*, Figure 5B), along with a prominent leukocyte infiltrate (arrow, Figure 5B) accompanied by a general loss of dermal appendages, including sebaceous glands and hair follicles. PGZ-limonene skin was limited to less infiltrating leukocytes compared to the *m*-Xylene skin and a normal epidermis with a contiguous stratum corneum (Figure 5C).

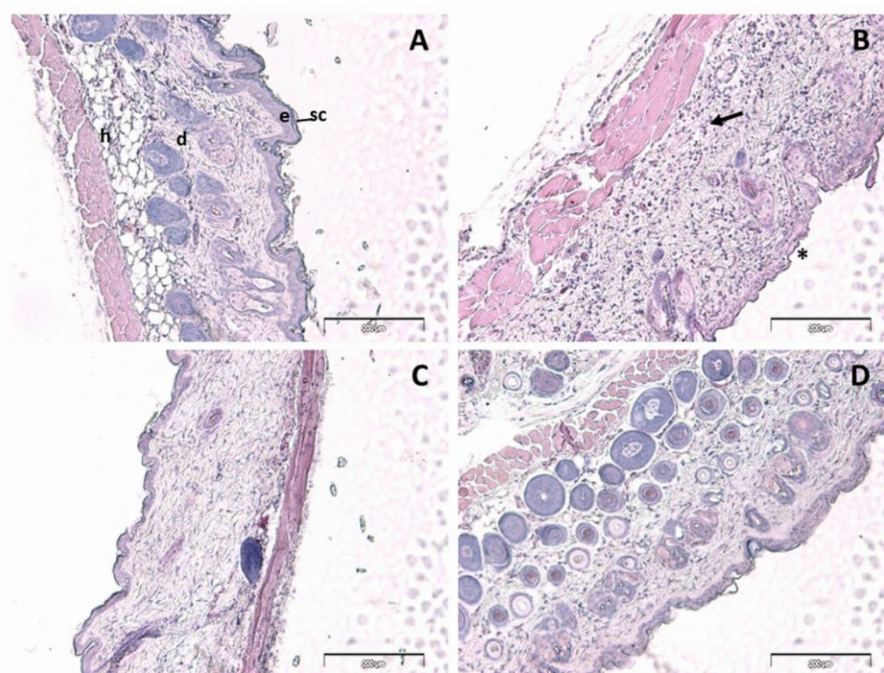


Figure 5. Hematoxylin and eosin staining of control (A), *m*-Xylene (B), PGZ-limonene (C), and limonene (D) mice's back skin from affected area ($\times 10$ magnification). Hematoxylin stains nuclei blue/black, and eosin stains keratin and cytoplasm red/orange. Bars = 200 μm . sc = stratum corneum, e = epidermis, d = dermis, h = subcutaneous layer Arrow = leucocyte infiltrate, * = loss of stratum corneum.

3. Discussion

Rosacea is an inflammatory skin disease which remains incurable because the current treatment has limitations and a significant number of patients are unresponsive to it or have unsatisfactory results [28]. Mounting evidence suggests that PPAR- γ activation is a promising target to regulate pro-inflammatory cytokines expression [38]. Therefore, PPAR- γ agonists such as PGZ could promote an anti-inflammatory effect to treat several diseases [39]. In the present study, the possible application of PGZ in rosacea treatment was evaluated. Validation of the analytical method was carried out in accordance with international conference on harmonization (ICH) guidelines, for which the following criteria were analyzed: linearity, precision, accuracy, robustness, specificity, limits of detection, and quantification. The objective of validating an analytical method is to confirm that the analytical procedure employed for a specific test is suitable for its intended use [40,41]. Spectra showed maximum absorbance at a wavelength of 269 nm and the calibration curve was found to be linear in the concentration range of 1.5–110 $\mu\text{g}/\text{mL}$, with a correlation coefficient (r^2) value of 0.0998 (Figure S1). The obtained values for accuracy did not exceed $\pm 5\%$ (Table S3), and precision was maintained below $\pm 3\%$ (Table S2), thus proving that the analytical method is accurate and precise within the determined concentration range.

Furthermore, the human skin was analyzed as a possible route for PGZ delivery, because topical treatment offers important advantages that include reduced side effects and ease of product use over the target areas [42]. However, poor permeation of the drug through the skin is the primary challenge in the development of topical formulations [43]. The use of penetration enhancers is a common strategy to increase drug flux through the stratum corneum, which is the upper layer of the skin and the major barrier for drug permeation [44,45]. In this study, ex vivo permeation experiments through human skin

using PGZ with different penetration enhancers evidenced that terpenes (menthol, cineole, and mainly limonene) were the most effective.

Ex vivo permeation experiments through human skin using PGZ with different penetration enhancers (Figure 1) evidenced that the permeation flow of PGZ without enhancers was relatively low: 0.84 ng/(h/cm²). The addition of azone, squalene, linoleic acid, menthol, pyrrolidone, limonene, and cineole changed the permeation flow to 1.94, 0.66, 0.54, 0.38, 0.69, 2.19, and 1.8 ng/(h/cm²), respectively. Therefore, limonene was the most effective penetration enhancer that promoted the permeation of PGZ through human skin. As shown in Table 1, limonene presents the highest values for J_{ss} , k_p , Q_{ret} , and C_{ss} [44]. Some studies suggest that hydrocarbon terpenes like limonene (log p value of 4.53) are more effective to enhance skin penetration of lipophilic drugs like PGZ (log p value of 2.3) [45,46]. Terpenes consist of isoprene units that enhance the permeation of hydrophilic and lipophilic drugs [47]. The mechanism of action of limonene as a penetration enhancer is based on changing the structure of lipids between the stratum corneum, with a consequent increase of intercellular diffusivity and improvement of drug partitioning into the tissue [48]. Researchers have found that limonene has anti-inflammatory properties in a murine dermal model, as well as healing effects on the epidermal barrier [49]. However, some researchers have suggested limonene could be toxic for human skin [50,51], whereas others do not consider the research significant enough to invalidate its use [52–54]. In addition, topical treatment of normal mouse skin with PPAR does not affect basal transepidermal water loss. In other words, permeability barrier function is not altered [55]. Furthermore, the high retention of PGZ in the human skin (207.65 µg/g of tissue) indicates that limonene promotes the retention of drug in the skin, which could prolong the duration of drug action and increase efficacy in the treatment of rosacea, thus favoring the likelihood of a reduction of the dosing frequency in clinical practice.

The in vitro cytotoxicity studies were made using HaCaT cells after 24 h of incubation with different dilutions of PGZ-limonene and limonene. Figure 2 shows similar results in both cases with cell viability greater than 80% in five of the six dilutions tested. Therefore, PGZ-limonene did not affect cell viability, which suggests the absence of apparent toxicity and suitability for topical use [56,57].

The irritancy test was performed in male albino rabbits. The possibility of causing skin damage is of vital importance in the development of topical treatments [58]. The result after 24 and 72 h of exposure to the formulation at a concentration of 1 mg/mL of PGZ and 5% of limonene was obtained in accordance with previous studies [59,60], showing a primary irritation index below 0.5 in all cases, which indicates that PGZ-limonene and limonene are non-irritant.

Moreover, the relative erythema (%) was determined in order to confirm the ability of PGZ-limonene to reduce erythema and vasodilation, which are the main clinical features of rosacea. Recent studies using animal models of inflammatory skin diseases have confirmed that topical administration of PPAR-γ ligands like PGZ decreases epidermal hyperplasia, enhances permeability barrier function, and reduces the inflammation mediated by T lymphocytes [61]. In this study, a skin colorimetric assay was performed in order to measure the skin color of the mice's backs after inducing inflammation and treating it with PGZ-limonene and limonene. Topical application of *m*-Xylene immediately leads to vasodilation and erythema. The positive control showed significant differences ($p < 0.0001$) with respect to basal values during the 20 min of assay, though without significant changes over time (Figure 4a). Treatment with PGZ-limonene and limonene (Figure 4b,c) decreased the level of vasodilatation, but not at the same proportion. PGZ associate with limonene significantly reduced the relative erythema in all the time intervals tested ($p < 0.0001$), and at 20 min the differences intensified, decreasing below the basal value with notably reduced erythema, thus resulting in a lighter color. (Figures 3 and 4b). This is likely attributed to limonene because of its drug-enhancing effect [62]. Finally, the application of limonene also significantly decreased redness, reaching a relative erythema of about 40% at 20 min without reaching the basal state, revealing that the benefits of limonene go far beyond its use as a penetration enhancer, because it also has an anti-inflammatory

effect. Consequently, its combined use with PGZ constitutes a strategy to increase the pharmacological efficacy of rosacea treatment.

The back skin from mice was used to obtain sections 6 μm in thickness that were stained with hematoxylin and eosin in order to evaluate leukocyte infiltration, as well as histopathological changes after treatment. Control skin exhibited normal morphology (Figure 5A). Dermal papillae created a clearly demarcated border between the epidermis and dermis. The topical application of *m*-Xylene (Figure 5B) caused a loss of the stratum corneum, an absence of epidermal ridges, and dermal papillae, thus resulting in a diminished definition of the border between the epidermis and dermis. Additionally, general loss of dermal appendages such as sweat glands, sebaceous glands, and hair follicles was observed. Moreover, the presence of prominent leukocyte infiltration was evidently manifested as a result of the inflammatory process. In accordance with other studies, the treatment with PGZ-limonene after inducing inflammation notably improved the structural characteristics of the mice skin where a contiguous stratum corneum was observed [63,64]. This treatment significantly attenuated the inflammatory response, which was evident with less leukocyte infiltration compared to the *m*-Xylene skin (Figure 5C). A similar structure to the control was observed in the skin treated with limonene (Figure 5D), which showed normal skin layers and an absence of pathological changes. Therefore, the results of histological and colorimetric studies suggested that PGZ-limonene may be used as a promising therapeutic treatment for rosacea. In summary, the experimental assays carried out in this study indicated the efficacy and the capability of PGZ-limonene to regulate the signaling pathways involved in inflammatory processes.

4. Materials and Methods

4.1. Materials

The PGZ was purchased from Capot Chemical (Hangzhou, China), and the penetration enhancers and *m*-Xylene were obtained from Sigma-Aldrich (Madrid, Spain). Transcutol was supplied from Gattefossé (Barcelona, Spain). Reagents for histological procedures were purchased from Sigma and Thermo Fisher Scientific (Barcelona, Spain). Reagents for cell culture were obtained from Gibco (Carcavelos, Portugal). The HaCat was acquired from Cell Lines Service (CLS, Eppelheim, Germany) and MTT used for cell viability was obtained from Invitrogen Alfacene[®] (Carcavelos, Portugal). Water Millipore MilliQ system (Millipore Corporation, Bedford, MA, USA) was used for all the experiments, and all reagents used were of analytical grade.

4.2. Validated Analytical Method

To validate the new analytical method, high-performance liquid chromatography (HPLC) was performed. The HPLC system is composed of a Waters 1525 pump and a 2487 UV-Visible detector (Waters, Milford, CT, USA). Data were collected and processed using Empower Pro software (Waters, Milford, CT, USA). The analysis was carried out by a chromatographic column 100 C18 (250 mm \times 4.6 mm \times 5 μm). The composition of the mobile phase was acetonitrile: ammonium acetate: glacial acetic acid (75:25:2 (*v/v/v*)). The mobile phase was filtered using a membrane filter PVDF of 0.45 μm (Millipore Corp., Madrid, Spain). The mobile phase was pumped through the chromatography column with a flow rate of 0.7 mL/min and 10 μL of injection volume. Detection was performed by UV spectrophotometry at λ of 269 nm.

Conditions Analyzed

The standard PGZ stock solution (200 $\mu\text{g}/\text{mL}$) was prepared daily in methanol. The calibration curve was prepared by dilutions in mobile phase in a range of concentration from 1.5 to 110 $\mu\text{g}/\text{mL}$. The method was validated in terms of linearity, precision, accuracy, robustness, sensitivity, and specificity. The validation was carried out according to the ICH Q2A and ICH Q2B.

- Linearity

The calibration curve was prepared from nine different concentrations of PGZ (1.5 to 110 µg/mL). Three calibration curves were prepared, evaluating the linearity according to the determination coefficient (r^2) of each curve, the y-intercept, the slope of the regression line, and the residual and sum of the squares.

- Precision

Instrument precision was determined by intermediate precision (inter-day). It was expressed according to the standard deviation (SD) and the % coefficient of variation (CV). The precision was evaluated to analyze sets of three standard samples of 3, 60, and 110 µg/mL within three intercalated days (inter-day). The selected concentrations correspond to the lowest, the intermediate, and the highest concentrations of the calibration curve.

- Accuracy

The accuracy was determined by measuring the degree of approach between the real value and the experimental data. Accuracy was assessed for concentrations of PGZ (3, 30, 60, and 110 µg/mL) and analyzed in triplicate. The margin of error was calculated for each concentration between the theoretical value (χ_a) and the experimental value (χ_r) by Equation (1):

$$\chi_d = \frac{\chi_a - \chi_r}{\chi_a} \cdot 100 \quad (1)$$

- Robustness

Robustness was determined by changing experimental flow conditions and the composition of the mobile phase. The flow was varied at ± 0.1 mL/min, and the concentration of the mobile phase was varied at $\pm 3\%$ acetonitrile and $\pm 3\%$ ammonium acetate. The effects of these variations on the experimental conditions were tested for retention time. Standard deviation (SD) was calculated.

- Specificity

The specificity of the method was evaluated by analyzing the possible interferences due to the components of the skin that are released during the passing of the drug with the penetration enhancer. Four different samples were evaluated: blank of mobile phase, standard of 30 ppm, blank of skin as a control, and sample of skin permeated with PGZ-limonene. A volume of 10 µL of each sample was injected, and then the chromatogram profiles (wavelength 269 nm) were analyzed.

- Sensitivity

Sensitivity was analyzed by the limit of detection (LOD) and the limit of quantification (LOQ). LOD is the lowest concentration of analyte that can be determined, and LOQ is the lowest concentration that can be quantified with adequate accuracy and precision. The signal-to-noise ratio was found by comparing signals from samples of known low concentrations of drug with the signals of blank samples and then establishing the lowest concentration of drug that can be reliably detected, in addition to being reliably quantified. A signal-to-noise ratio of 3:1 for LOD and 10:1 for LOQ were ultimately determined.

4.3. Permeation Studies in Human Skin

A healthy 38-year old woman donated a skin sample from her abdominal region and, with written informed consent, facilitated the use of this sample for permeation studies. The consent was obtained in accordance with the Ethical Committee of the Hospital of Barcelona and was assigned the number 001, (dated 20 January 2016). Free-PGZ solution (1 mg/mL), diluted with transcutol/water 4:5.5 (v/v) and

mixed with 5% of different penetration enhancers, were assayed. The penetration enhancers studied were: linoleic acid, squalene, menthol, pyrrolidine, azone, limonene, and cineole ($n = 3$). The study was performed in Franz diffusion cells with diffusion area of 2.54 cm^2 . The experiment was carried out in triplicate using the sample of skin from the same donor to reduce variability due to biological factors. Skin was assessed by measuring transepidermal water loss (TEWL) (TEWL-meter TM210 Courage & Khazaka, Koln, Germany), exhibiting values below $10 \text{ g/m}^2 \cdot \text{h}$. Dermatomed skin slices of 0.4 mm thickness were placed between the receptor and donor compartments. Samples of 0.3 mL were placed in the donor compartment and the same volume of samples were extracted from receptor compartment at established time intervals for 31 h and replaced with fresh receptor medium (transcutol/water, 60:40) at $32 \pm 0.5 \text{ }^\circ\text{C}$ under continuous stirring to simulate sink conditions. The quantitative determination of permeated PGZ was analyzed in triplicate by HPLC. Kinetic parameters were estimated using GraphPad Prism[®] 6.0 (GraphPad Software Inc., San Diego, CA, USA).

4.4. Permeation Parameters

The accumulated amounts of PGZ (μg) that were penetrated per cm^2 of skin were analyzed for the collected samples and plotted against time (h). Permeation profiles were analyzed based on a diffusion model for an infinite dose condition. PGZ flow (J_{ss} , $\mu\text{g}/(\text{h}/\text{cm}^2)$) through the skin was calculated by plotting the cumulative amount of drug permeating the skin *versus* time, determining the slope of the linear portion of the curve by analysis of linear regression using GraphPad Prism[®] 6.0 (GraphPad Software Inc.) and dividing by the diffusion area. The permeability coefficients (K_p , cm/h) were obtained by dividing J_{ss} (by the initial concentration of drug (C_0) in the donor compartment. The steady-state plasma concentration (C_{ss}) of drug, which would penetrate the dermal barrier after topical application, was obtained using the following Equation (2):

$$C_{ss} = \frac{J_{ss} \times A}{Clp} \quad (2)$$

where C_{ss} is the steady-state plasma concentration, J_{ss} is the flow, A is the area of application, and Clp is the plasma clearance. The calculations are based on a maximum area of application of 1 cm^2 and human Clp value of $2.26 \text{ L/h} \pm 1.22$ [65], in order to ensure the local action of the formulation.

When the permeation study finished, the skin was removed from the Franz cells, cleaned with distilled water, and dried with filter paper. These samples of skin were used to determine the amount of PGZ retained.

The permeated area of the skin was cut and weighed. The PGZ retained in these skin fragments was extracted with 2 mL of methanol after 20 min in an ultrasonic processor. The resulting solutions were analyzed by HPLC, determining the amount of PGZ retained in the skin Q_{ret} ($\mu\text{g}/\text{g skin}/\text{cm}^2$).

4.5. Toxicity in HaCat Cell Line and Skin Tolerance

The effect of PGZ on cell viability was evaluated using the MTT cytotoxicity assay (reduction of tetrazolium salt carried out by intracellular dehydrogenases of viable living cells). To develop this assay, immortalized human keratinocytes (HaCaT) cell line (2×10^5 cells/mL) were plated in 96-wells plates (Corning) and cultured in a humidified incubator at $37 \text{ }^\circ\text{C}$ in a $5\% \text{ CO}_2$ atmosphere for 24 h to allow adhesion. Experiments were performed at $80\text{--}90\%$ of confluence (passes between $n = 85\text{--}95$). Cells were grown in high-glucose Dubelcco's Modified Eagle's medium (DMEM) supplemented with 25 mM hepes, 1% non-essential amino acids, 100 U/mL penicillin, $100 \mu\text{g/mL}$ streptomycin, and 10% heat inactivated foetal calf serum (FCS). HaCaT were treated with different concentrations from 0.5 to 0.01 mg/mL of PGZ-limonene and limonene for 24 h and then incubated with fresh medium in presence of 10% MTT (5 mg/mL in phosphate buffered saline) for 2 h at $37 \text{ }^\circ\text{C}$. After this, the medium was removed carefully and $100 \mu\text{L}$ of DMSO 99% purity was added to lysate the cells and the purple insoluble crystals of MTT were dissolved. The cell lysate was transferred to a 96-well new plate and then the absorbance was read using a Microplate Autoreader at excitation/emission of $540/630 \text{ nm}$

(Modulus Microplate Multicode Reader-Turner Biosystems, Sunnyvale, CA, USA). In parallel, a negative control (cells without any stimulation or treatment) was processed for comparison. Absorbance values were considered directly proportional to cell viability, and the percentage cell viability was calculated by Equation (3).

$$\text{Cell viability} = \left[\frac{A \text{ sample}}{A \text{ control}} \right] \times 100 \quad (3)$$

The potential of skin irritation by PGZ-limonene was assessed by the Draize skin irritation test on New Zealand albino male rabbits (2 kg), which were purchased from San Bernardo farm (Navarra). This test was performed according to the Ethical Committee for Animal Experimentation of University of Barcelona (UB) and followed the respective guidelines [66]. The rabbits were acclimatized for 7 days before the study, after the dorsal area of the trunk was shaved with clippers 24 h before the beginning of the assay. Three groups of animals were analyzed ($n = 3/\text{group}$): Group 1: 0.9% (w/v) NaCl solution (Control); Group 2: PGZ-limonene; Group 3: limonene. Two squares were drawn on each side of the back of each rabbit, and a volume of 0.5 mL of each solution was applied on the hair-free skin on each square. This area was covered with gauze and polyethylene film (parafilm[®]) and secured with hypoallergenic sticking plaster. The formation of edema and erythema were analyzed after 24 h and 72 h of exposure. The edema and erythema scores were established according to the degree of severity (graded 0–4). The primary irritation index value was calculated, and the mean value was registered. The treatment was classified according the reported specifications: “non-irritant” (<0.5), “irritant” (2–5), or “highly irritant” (5–8) [66]. The Draize test allowed us to estimate the skin irritation potential but it is not a predictor for skin sensitization potential.

4.6. Efficacy Studies

An *in vivo* model was performed in order to evaluate the efficacy of PGZ for rosacea treatment using the BALB/c backs of mice (four months old). The study protocol was approved by the Animal Experimentation Ethics Committee of the UB with date 28/01/2016 (CEEA/UB ref. 4/16 and Generalitat ref. 8756). Three groups of mice ($n = 5$), including the control group, were assayed. The groups were: positive control (*m*-Xylene), PGZ-limonene, and limonene. The skin color of the backs of the mice was determined using a MPA 5 Multi Probe adapter from Courage + Khazaka electronic GmbH, equipped with a CL400, (Cologne, Germany) The device emits a white LED light that illuminates a circular part of the skin homogeneously. The light scattered by the skin is detected by the colorimeter probe and is expressed as the intensity of light in terms of the three basic light components, R, G, and B (red, green, and blue), on a scale of 0 to 255 each. The skin colorimeter was measured before and after induced vasodilation and erythema by applying *m*-Xylene on the backs of the mice with the help of a sterile gauze. Next, 400 μL of each formulation was promptly applied and PGZ was used at drug concentration of 1 mg/mL and limonene at 5%. Skin color determinations were performed after 5, 10, and 20 min of treatment. Colors were reproduced using Microsoft Excel[®] software (Version 2016, Microsoft Corporation, Redmond, WA, USA) from the RGB codes and plotted as a sequence and evaluated in accordance with previously mentioned equations [67].

The difference values were calculated between each measurement and the average of basal values. The corrected difference obtained between the basal color and the one after inducing vasodilation (vasodilation difference) was considered 100% erythema. Relative erythema (%) values were calculated by dividing each corrected difference by the vasodilation difference and were plotted as a sequence of the different stages in order to see the evolution of erythema. One-way Analysis of Variance (ANOVA), along with Tukey’s Multiple Comparison Tests, were performed for assessing the statistical significance of both the evolution of erythema and the comparison between treatment and basal values. Statistical analysis was performed using GraphPad Prism[®] software version 6.0.

4.7. Histological Analysis

For histological observation of skin structure, the animals were sacrificed immediately after colorimeter assay by cervical dislocation, and then the skin of the backs of the mice was carefully collected and set overnight in 4% buffered formaldehyde at room temperature. Their back skin was then embedded in paraffin, cut into 6 μm sections, stained with hematoxylin and eosin, and then viewed under a microscope for the evaluation of skin structure and possible inflammatory responses.

4.8. Statistics

All the values are expressed as mean \pm standard deviation. Statistical analysis was performed using GraphPad Prism[®] software version 6.0 (GraphPad Software Inc.).

5. Conclusions

In summary, our study suggest that PGZ-limonene could be used as a therapeutic treatment for rosacea by improving the underlying inflammatory processes. However, further studies are needed to determine the underlying mechanisms for the anti-inflammatory effect of the drug in addition to providing greater assurance of its safety prior to use in clinical practice.

Supplementary Materials: Supplementary materials can be found at www.mdpi.com/1422-0067/18/12/2548/s1.

Acknowledgments: This work was supported by the Coordination for the Improvement of Higher Education Personnel (CAPES)—Brazil, the Spanish Ministry of Science and Innovation (MAT2014-59134R), Secretaría de Educación Superior, Ciencia, Tecnología e Innovación (Sensescyt – Ecuador), and Universidad Técnica Particular de Loja—Ecuador. Marcelle Abreu also acknowledges her Ph.D. scholarship—CAPES, Brazil. The authors would like to thank Jonathan Proctor for his review of the use of the English language.

Author Contributions: Marcelle Silva-Abreu carried out all the experiments, analyzed the data/results, and wrote the paper; Lupe Carolina Espinoza carried out in vivo experiments, analyzed the data/results, and wrote the paper; María José Rodríguez-Lagunas analyzed the in vivo experiments histologically; María-José Fábrega carried out toxicity studies and contribution with reagents; Marta Espina examined the statistical analysis; María Luisa García corrected and analyzed the validation of analytical method and Ana Cristina Calpena conceived and designed all the experiments.

Conflicts of Interest: The authors declare no conflict of interest.

Abbreviations

PGZ	Pioglitazone
PPARs	Peroxisome proliferator-activated receptors
HPLC	Liquid chromatography of high resolution
TLR	Toll-like receptors
IL-8	Interleukin 8
IL-1 β	Interleukin 1 β
TNF- α	Tumor necrosis factor α
LOD	Detection limit
LOQ	limit of quantification
J_{ss}	Permeability flow
k_p	Permeability coefficient
Q_{ret}	Retained drug
C_{ss}	Steady-state plasma concentration
GRAS	Generally regarded as safe
ICH	International conference on harmonization

References

1. Wu, C.Y.; Chang, Y.T.; Juan, C.K.; Shieh, J.J.; Lin, Y.P.; Liu, H.N.; Lin, J.T.; Chen, Y.J. Risk of inflammatory bowel disease in patients with rosacea: Results from a nationwide cohort study in Taiwan. *J. Am. Acad. Dermatol.* **2017**, *76*, 911–917. [[CrossRef](#)] [[PubMed](#)]

2. Egeberg, A.; Hansen, P.R.; Gislason, G.H.; Thyssen, J.P. Clustering of autoimmune diseases in patients with rosacea. *J. Am. Acad. Dermatol.* **2016**, *74*, 667–672. [[CrossRef](#)] [[PubMed](#)]
3. Alcantara-Reifs, C.M.; Salido-Vallejo, R.; Garnacho-Saucedo, G.; Velez Garcia-Nieto, A. Otophyma: A rare variant of phymatous rosacea. *Am. J. Otolaryngol.* **2016**, *37*, 251–254. [[CrossRef](#)] [[PubMed](#)]
4. Hopkinson, D.; Moradi Tuchayi, S.; Alinia, H.; Feldman, S.R. Assessment of rosacea severity: A review of evaluation methods used in clinical trials. *J. Am. Acad. Dermatol.* **2015**, *73*, 138–143. [[CrossRef](#)] [[PubMed](#)]
5. Two, A.M.; Wu, W.; Gallo, R.L.; Hata, T.R. Rosacea: Part I. Introduction, categorization, histology, pathogenesis, and risk factors. *J. Am. Acad. Dermatol.* **2015**, *72*, 749–758. [[CrossRef](#)] [[PubMed](#)]
6. Awais, M.; Anwar, M.I.; Iftikhar, R.; Iqbal, Z.; Shehzad, N.; Akbar, B. Rosacea—the ophthalmic perspective. *Cutan. Ocul. Toxicol.* **2015**, *34*, 161–166. [[CrossRef](#)] [[PubMed](#)]
7. Di Nardo, A.; Holmes, A.D.; Muto, Y.; Huang, E.Y.; Preston, N.; Winkelman, W.J.; Gallo, R.L. Improved clinical outcome and biomarkers in adults with papulopustular rosacea treated with doxycycline modified-release capsules in a randomized trial. *J. Am. Acad. Dermatol.* **2016**, *74*, 1086–1092. [[CrossRef](#)] [[PubMed](#)]
8. Egeberg, A.; Hansen, P.R.; Gislason, G.H.; Thyssen, J.P. Assessment of the risk of cardiovascular disease in patients with rosacea. *J. Am. Acad. Dermatol.* **2016**, *75*, 336–339. [[CrossRef](#)] [[PubMed](#)]
9. Picardo, M.; Eichenfield, L.F.; Tan, J. Acne and Rosacea. *Dermatol. Ther.* **2017**, *7*, 43–52. [[CrossRef](#)] [[PubMed](#)]
10. Margalit, A.; Kowalczyk, M.J.; Zaba, R.; Kavanagh, K. The role of altered cutaneous immune responses in the induction and persistence of rosacea. *J. Dermatol. Sci.* **2016**, *82*, 3–8. [[CrossRef](#)] [[PubMed](#)]
11. Moustafa, F.; Lewallen, R.S.; Feldman, S.R. The psychological impact of rosacea and the influence of current management options. *J. Am. Acad. Dermatol.* **2014**, *71*, 973–980. [[CrossRef](#)] [[PubMed](#)]
12. Cardwell, L.A.; Farhangian, M.E.; Alinia, H.; Kuo, S.; Feldman, S.R. Psychological disorders associated with rosacea: Analysis of unscripted comments. *J. Dermatol. Dermatol. Surg.* **2015**, *19*, 99–103. [[CrossRef](#)]
13. Rainer, B.M.; Fischer, A.H.; Luz Felipe da Silva, D.; Kang, S.; Chien, A.L. Rosacea is associated with chronic systemic diseases in a skin severity-dependent manner: Results of a case-control study. *J. Am. Acad. Dermatol.* **2015**, *73*, 604–608. [[CrossRef](#)] [[PubMed](#)]
14. Akin Belli, A.; Altun, I. Assessment of Framingham risk score and systemic coronary risk evaluation in rosacea patients. *Dermatol. Sin.* **2017**, *35*, 127–130. [[CrossRef](#)]
15. Hua, T.C.; Chung, P.I.; Chen, Y.J.; Wu, L.C.; Chen, Y.D.; Hwang, C.Y.; Chu, S.Y.; Chen, C.C.; Lee, D.D.; Chang, Y.T.; et al. Cardiovascular comorbidities in patients with rosacea: A nationwide case-control study from Taiwan. *J. Am. Acad. Dermatol.* **2015**, *73*, 249–254. [[CrossRef](#)] [[PubMed](#)]
16. Egeberg, A.; Fowler, J.F., Jr.; Gislason, G.H.; Thyssen, J.P. Rosacea and risk of cancer in Denmark. *Cancer Epidemiol.* **2017**, *47*, 76–80. [[CrossRef](#)] [[PubMed](#)]
17. Tuzun, Y.; Wolf, R.; Kutlubay, Z.; Karakus, O.; Engin, B. Rosacea and rhinophyma. *Clin. Dermatol.* **2014**, *32*, 35–46. [[CrossRef](#)] [[PubMed](#)]
18. Woo, Y.R.; Lim, J.H.; Cho, D.H.; Park, H.J. Rosacea: Molecular Mechanisms and Management of a Chronic Cutaneous Inflammatory Condition. *Int. J. Mol. Sci.* **2016**, *17*, 1562. [[CrossRef](#)] [[PubMed](#)]
19. Cao, X. Self-regulation and cross-regulation of pattern-recognition receptor signalling in health and disease. *Nat. Rev. Immunol.* **2016**, *16*, 35–50. [[CrossRef](#)] [[PubMed](#)]
20. Steinhoff, M.; Schaubert, J.; Leyden, J.J. New insights into rosacea pathophysiology: A review of recent findings. *J. Am. Acad. Dermatol.* **2013**, *69*, S15–S26. [[CrossRef](#)] [[PubMed](#)]
21. Buhl, T.; Sulk, M.; Nowak, P.; Buddenkotte, J.; McDonald, I.; Aubert, J.; Carlván, I.; Deret, S.; Reiniche, P.; Rivier, M.; et al. Molecular and Morphological Characterization of Inflammatory Infiltrate in Rosacea Reveals Activation of Th1/Th17 Pathways. *J. Investig. Dermatol.* **2015**, *135*, 2198–2208. [[CrossRef](#)] [[PubMed](#)]
22. Tan, J.; Almeida, L.M.; Bewley, A.; Cribier, B.; Dlova, N.C.; Gallo, R.; Kautz, G.; Mannis, M.; Oon, H.H.; Rajagopalan, M.; et al. Updating the diagnosis, classification and assessment of rosacea: Recommendations from the global ROSacea Consensus (ROSCO) panel. *Br. J. Dermatol.* **2017**, *176*, 431–438. [[CrossRef](#)] [[PubMed](#)]
23. Two, A.M.; Wu, W.; Gallo, R.L.; Hata, T.R. Rosacea: Part II. Topical and systemic therapies in the treatment of rosacea. *J. Am. Acad. Dermatol.* **2015**, *72*, 761–770. [[CrossRef](#)] [[PubMed](#)]
24. Chang, Y.; Kurian, A. Rosacea: An Update on Medical Therapies. *Skin Ther. Lett.* **2014**, *19*, 1–4.
25. Layton, A.M. Pharmacologic treatments for rosacea. *Clin. Dermatol.* **2017**, *35*, 207–212. [[CrossRef](#)] [[PubMed](#)]

26. Holmes, A.D.; Steinhoff, M. Integrative concepts of rosacea pathophysiology, clinical presentation and new therapeutics. *Exp. Dermatol.* **2017**, *26*, 659–667. [[CrossRef](#)] [[PubMed](#)]
27. Webster, G.; Schaller, M.; Tan, J.; Jackson, J.M.; Kerrouche, N.; Schafer, G. Defining treatment success in rosacea as ‘clear’ may provide multiple patient benefits: Results of a pooled analysis. *J. Dermatol. Treat.* **2017**, *28*, 469–474. [[CrossRef](#)] [[PubMed](#)]
28. Zhong, S.; Sun, N.; Liu, H.; Niu, Y.; Chen, C.; Wu, Y. Topical tranexamic acid improves the permeability barrier in rosacea. *Dermatol. Sin.* **2015**, *33*, 112–117. [[CrossRef](#)]
29. Sun, H.; Zhu, X.; Cai, W.; Qiu, L. Hypaphorine Attenuates Lipopolysaccharide-Induced Endothelial Inflammation via Regulation of TLR4 and PPAR- γ Dependent on PI3K/Akt/mTOR Signal Pathway. *Int. J. Mol. Sci.* **2017**, *18*, 844. [[CrossRef](#)] [[PubMed](#)]
30. Park, H.J.; Park, H.S.; Lee, J.U.; Bothwell, A.L.; Choi, J.M. Sex-Based Selectivity of PPAR γ Regulation in Th1, Th2, and Th17 Differentiation. *Int. J. Mol. Sci.* **2016**, *17*, 1347. [[CrossRef](#)] [[PubMed](#)]
31. Jia, C.; Huan, Y.; Liu, S.; Hou, S.; Sun, S.; Li, C.; Liu, Q.; Jiang, Q.; Wang, Y.; Shen, Z. Effect of Chronic Pioglitazone Treatment on Hepatic Gene Expression Profile in Obese C57BL/6J Mice. *Int. J. Mol. Sci.* **2015**, *16*, 12213–12229. [[CrossRef](#)] [[PubMed](#)]
32. Radenkovic, M. Pioglitazone and Endothelial Dysfunction: Pleiotropic Effects and Possible Therapeutic Implications. *Sci. Pharm.* **2014**, *82*, 709–721. [[CrossRef](#)] [[PubMed](#)]
33. El-Zaher, A.A.; Elkady, E.F.; Elwy, H.M.; Saleh, M. Simultaneous spectrophotometric determination of glimepiride and pioglitazone in binary mixture and combined dosage form using chemometric-assisted techniques. *Spectrochim. Acta* **2017**, *182*, 175–182. [[CrossRef](#)] [[PubMed](#)]
34. Suzuki, S.; Mori, Y.; Nagano, A.; Naiki-Ito, A.; Kato, H.; Nagayasu, Y.; Kobayashi, M.; Kuno, T.; Takahashi, S. Pioglitazone, a Peroxisome Proliferator-Activated Receptor γ Agonist, Suppresses Rat Prostate Carcinogenesis. *Int. J. Mol. Sci.* **2016**, *17*, 2071. [[CrossRef](#)] [[PubMed](#)]
35. Kumar, S.; Zakrewsky, M.; Chen, M.; Menegatti, S.; Muraski, J.A.; Mitragotri, S. Peptides as skin penetration enhancers: Mechanisms of action. *J. Controll. Release* **2015**, *199*, 168–178. [[CrossRef](#)] [[PubMed](#)]
36. Mansour, R.S.H.; Sallam, A.A.; Hamdan, I.I.; Khalil, E.A.; Yousef, I. Elucidation of penetration enhancement mechanism of Emu oil using FTIR microspectroscopy at EMIRA laboratory of SESAME synchrotron. *Spectrochim. Acta* **2017**, *185*, 1–10. [[CrossRef](#)] [[PubMed](#)]
37. Xie, F.; Chai, J.K.; Hu, Q.; Yu, Y.H.; Ma, L.; Liu, L.Y.; Zhang, X.L.; Li, B.L.; Zhang, D.H. Transdermal permeation of drugs with differing lipophilicity: Effect of penetration enhancer camphor. *Int. J. Pharm.* **2016**, *507*, 90–101. [[CrossRef](#)] [[PubMed](#)]
38. Zhu, W.; Yan, H.; Li, S.; Nie, W.; Fan, F.; Zhu, J. PPAR-gamma agonist pioglitazone regulates dendritic cells immunogenicity mediated by DC-SIGN via the MAPK and NF- κ B pathways. *Int. Immunopharmacol.* **2016**, *41*, 24–34. [[CrossRef](#)] [[PubMed](#)]
39. Wang, F.; Liu, Y.; Bi, Z. Pioglitazone inhibits growth of human retinoblastoma cells via regulation of NF- κ B inflammation signals. *J. Recept. Signal Transduct. Res.* **2017**, *37*, 94–99. [[CrossRef](#)] [[PubMed](#)]
40. Mirza, A.Z.; Arayne, M.S.; Sultana, N. HPLC method development, validation and its application to investigate in vitro effect of pioglitazone on the availability of H 1 receptor antagonists. *J. Assoc. Arab Univ. Basic Appl. Sci.* **2017**, *22*, 70–75. [[CrossRef](#)]
41. Satheeshkumar, N.; Shantikumar, S.; Srinivas, R. Pioglitazone: A review of analytical methods. *J. Pharm. Anal.* **2014**, *4*, 295–302. [[CrossRef](#)]
42. Hagen, M.; Baker, M. Skin penetration and tissue permeation after topical administration of diclofenac. *Curr. Med. Res. Opin.* **2017**, *33*, 1623–1634. [[CrossRef](#)] [[PubMed](#)]
43. Vijayakumar, A.; Baskaran, R.; Yoo, B.K. Skin permeation and retention of topical bead formulation containing tranexamic acid. *J. Cosmet. Laser Ther.* **2017**, *19*, 68–74. [[CrossRef](#)] [[PubMed](#)]
44. Calpena, A.C.; Lauroba, J.; Suriol, M.; Obach, R.; Domenech, J. Effect of d-limonene on the transdermal permeation of nifedipine and domperidone. *Int. J. Pharm.* **1994**, *103*, 179–186. [[CrossRef](#)]
45. Sugita, M.; Kataoka, M.; Sugihara, M.; Takeuchi, S.; Yamashita, S. Effect of excipients on the particle size of precipitated pioglitazone in the gastrointestinal tract: Impact on bioequivalence. *AAPS J.* **2014**, *16*, 1119–1127. [[CrossRef](#)] [[PubMed](#)]
46. Krishnaiah, Y.S.; Raju, V.; Shiva Kumar, M.; Rama, B.; Raghuramurthy, V.; Ramana Murthy, K.V. Studies on optimizing in vitro transdermal permeation of ondansetron hydrochloride using nerodilol, carvone, and limonene as penetration enhancers. *Pharm. Dev. Technol.* **2008**, *13*, 177–185. [[CrossRef](#)] [[PubMed](#)]

47. Jiang, Q.; Wu, Y.; Zhang, H.; Liu, P.; Yao, J.; Yao, P.; Chen, J.; Duan, J. Development of essential oils as skin permeation enhancers: Penetration enhancement effect and mechanism of action. *Pharm. Biol.* **2017**, *55*, 1592–1600. [[CrossRef](#)] [[PubMed](#)]
48. Yang, Z.; Teng, Y.; Wang, H.; Hou, H. Enhancement of skin permeation of bufalin by limonene via reservoir type transdermal patch: Formulation design and biopharmaceutical evaluation. *Int. J. Pharm.* **2013**, *447*, 231–240. [[CrossRef](#)] [[PubMed](#)]
49. d'Alessio, P.; Mirshahi, M.; Bisson, J.; Béné, M. Skin Repair Properties of d-Limonene and Perillyl Alcohol in Murine Models. *Anti-Inflamm. Anti-Allergy Agents Med. Chem.* **2014**, *13*, 29–35. [[CrossRef](#)]
50. Pesonen, M.; Suomela, S.; Kuuliala, O.; Henriks-Eckerman, M.L.; Aalto-Korte, K. Occupational contact dermatitis caused by d-limonene. *Contact Dermat.* **2014**, *71*, 273–279. [[CrossRef](#)] [[PubMed](#)]
51. Basketter, D.; McFadden, J.; Evans, P.; Andersen, K.; Jowsey, I. Identification and classification of skin sensitizers: Identifying false positives and false negatives. *Contact Dermat.* **2006**, *55*, 268–273. [[CrossRef](#)] [[PubMed](#)]
52. Kim, Y.W.; Kim, M.J.; Chung, B.Y.; Bang du, Y.; Lim, S.K.; Choi, S.M.; Lim, D.S.; Cho, M.C.; Yoon, K.; Kim, H.S.; et al. Safety evaluation and risk assessment of d-Limonene. *J. Toxicol. Environ. Health Part B* **2013**, *16*, 17–38. [[CrossRef](#)] [[PubMed](#)]
53. Lu, W.C.; Chiang, B.H.; Huang, D.W.; Li, P.H. Skin permeation of D-limonene-based nanoemulsions as a transdermal carrier prepared by ultrasonic emulsification. *Ultrason. Sonochem.* **2014**, *21*, 826–832. [[CrossRef](#)] [[PubMed](#)]
54. Api, A.M.; Ritacco, G.; Hawkins, D.R. The fate of dermally applied [14C]d-limonene in rats and humans. *Int. J. Toxicol.* **2013**, *32*, 130–135. [[CrossRef](#)] [[PubMed](#)]
55. Schmutz, M.; Jiang, Y.J.; Dubrac, S.; Elias, P.M.; Feingold, K.R. Thematic review series: Skin lipids. Peroxisome proliferator-activated receptors and liver X receptors in epidermal biology. *J. Lipid Res.* **2008**, *49*, 499–509. [[CrossRef](#)] [[PubMed](#)]
56. Thangavel, S.; Yoshitomi, T.; Sakharkar, M.K.; Nagasaki, Y. Redox nanoparticle increases the chemotherapeutic efficiency of pioglitazone and suppresses its toxic side effects. *Biomaterials* **2016**, *99*, 109–123. [[CrossRef](#)] [[PubMed](#)]
57. Yoon, W.; Lee, N.; Hyun, C. Limonene suppresses lipopolysaccharide-induced production of nitric oxide, prostaglandin E2, and pro-inflammatory cytokines in RAW 264.7 macrophages. *J. Oleo Sci.* **2010**, *59*, 415–421. [[CrossRef](#)] [[PubMed](#)]
58. Parra, A.; Clares, B.; Rossello, A.; Garduno-Ramirez, M.L.; Abrego, G.; Garcia, M.L.; Calpena, A.C. Ex vivo permeation of carprofen from nanoparticles: A comprehensive study through human, porcine and bovine skin as anti-inflammatory agent. *Int. J. Pharm.* **2016**, *501*, 10–17. [[CrossRef](#)] [[PubMed](#)]
59. Prasad, P.S.; Imam, S.S.; Aqil, M.; Sultana, Y.; Ali, A. QbD-based carbopol transgel formulation: Characterization, pharmacokinetic assessment and therapeutic efficacy in diabetes. *Drug Deliv.* **2016**, *23*, 1057–1066. [[CrossRef](#)] [[PubMed](#)]
60. Rangari, N.T.; Kalyankar, T.M.; Puranik, P.K.; Chaudhari, S.R. Permeation studies of pioglitazone HCl from ficus carica fruit mucilage matrix transdermal Patches. *IJPSR* **2012**, *3*, 3927–3931.
61. Mastrofrancesco, A.; Kovacs, D.; Sarra, M.; Bastonini, E.; Cardinali, G.; Aspate, N.; Camera, E.; Chavatte, P.; Desreumaux, P.; Monteleone, G.; et al. Preclinical studies of a specific PPAR γ modulator in the control of skin inflammation. *J. Investig. Dermatol.* **2014**, *134*, 1001–1011. [[CrossRef](#)] [[PubMed](#)]
62. Takayama, K.; Nagai, T. Limonene and Related Compounds as Potential Skin Penetration Promoters. *Drug Dev. Ind. Pharm.* **2008**, *20*, 677–684. [[CrossRef](#)]
63. Kandeel, S.; Balaha, M. The possible protective effect of simvastatin and pioglitazone separately and in combination on bleomycin-induced changes in mice thin skin. *Tissue Cell* **2015**, *47*, 159–170. [[CrossRef](#)] [[PubMed](#)]
64. Lappas, C.M.; Lappas, N.T. D-Limonene modulates T lymphocyte activity and viability. *Cell. Immunol.* **2012**, *279*, 30–41. [[CrossRef](#)] [[PubMed](#)]
65. Wittayalertpanya, S.; Chompootaweep, S.; Thaworn, N. The Pharmacokinetics of Pioglitazone in Thai Healthy Subjects. *J. Med. Assoc. Thail.* **2006**, *89*, 2116–2122.
66. Draize, J.; Woodard, G.; Calvery, H. Methods for the study of irritation and toxicity of substances applied topically to the skin and mucous membranes. *J. Pharmacol. Exp. Ther.* **1994**, *82*, 377–390.

67. Limón, D.; Jiménez-Newman, C.; Rodrigues, M.; González-Campo, A.; Amabilino, D.; Calpena, A.; Pérez-García, L. Cationic Supramolecular Hydrogels for Overcoming the Skin Barrier in Drug Delivery. *ChemistryOpen* 2017, 6, 585–598. [CrossRef] [PubMed]



© 2017 by the authors. Licensee MDPI, Basel, Switzerland. This article is an open access article distributed under the terms and conditions of the Creative Commons Attribution (CC BY) license (<http://creativecommons.org/licenses/by/4.0/>).

Supplementary Materials

Table S1. Standards of PGZ to analyze the linearity

Standards ($\mu\text{g/mL}$)	Area 1 ($\mu\text{V}\cdot\text{sec}$)	Area 2 ($\mu\text{V}\cdot\text{sec}$)	Area 3 ($\mu\text{V}\cdot\text{sec}$)	A(Average) ($\mu\text{V}\cdot\text{sec}$)	SD
1.5	34167	31506	32387	32387	1355.57
3	48311	46324	48380	48311	1167.62
5	65374	64878	63891	64878	754.92
10	124741	116434	119389	119389	4210.74
15	189224	171933	170119	171933	10545.69
30	366468	314375	329348	329348	26819.66
60	702444	665092	678080	678080	18962.52
80	972119	921532	943514	943514	25365.65
110	1292669	1309338	1314170	1309338	11280.49

SD: Standard deviation

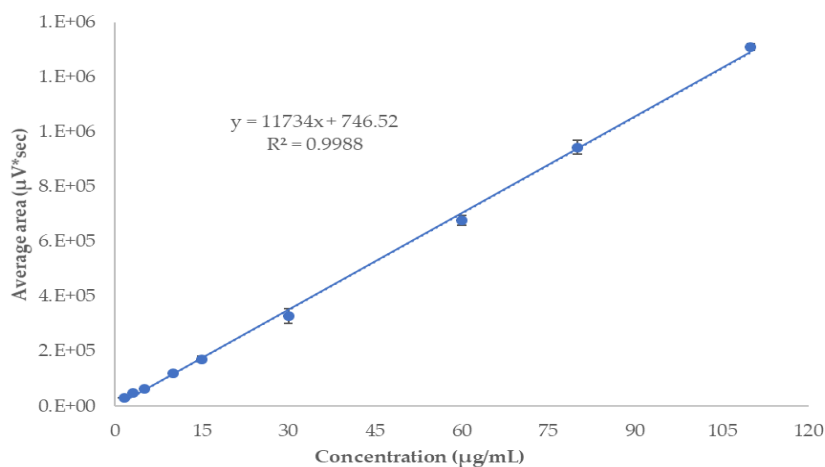


Figure S1: Linearity of the average of 3 calibrate curve. Runs test showed that deviation from linearity is not significant ($p=0.1071$)

Table S2. Precision inter-day

Day 1		Day 2		Day 3		SD	CV (%)	Method Precision (%)
Area (μV*Sec)	C (μg/mL)	Area (μV*Sec)	C (μg/mL)	Area (μV*Sec)	C (μg/mL)			
45104	3	42679	3	43376	3	1248.49	2.87	97.15
713066	60	711243	60	702444	60	5679.97	0.79	99.19
1295099	110	1293630	110	1292669	110	1223.81	0.09	99.90

C: Concentration; SD: Standard deviation; CV: Coefficient of variation

Table S3. Accuracy of the analytical method

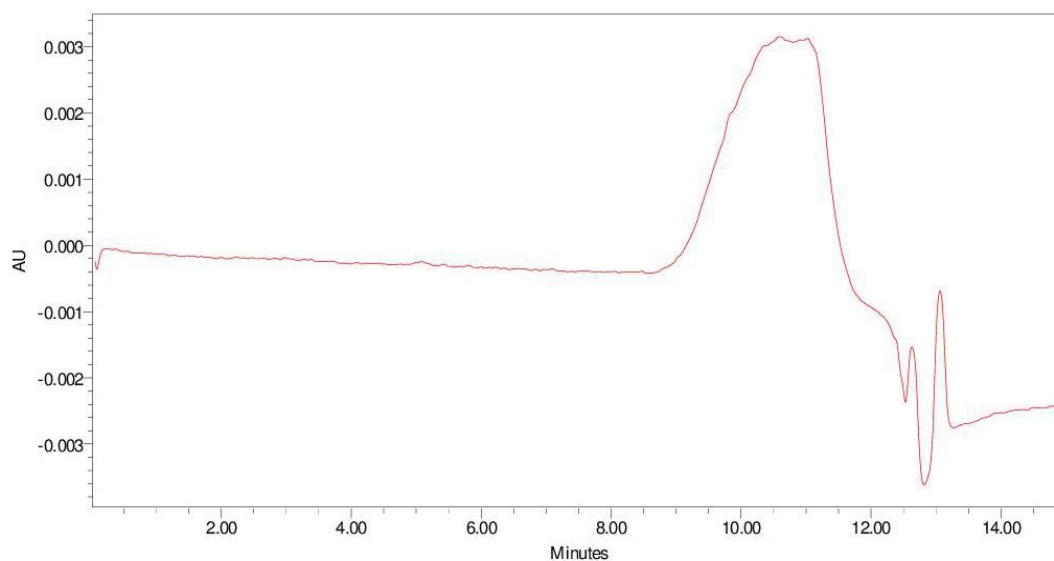
Theor. C. (μg/mL)	Tested C. (μg/mL)	Theor. C. (μg/mL)	Tested C. (μg/mL)	Theor. C. (μg/mL)	Tested C. (μg/mL)	Average (μg/mL)	SD	CV (%)	Relative error (%)	Accuracy (%)
3	3.263	3	3.057	3	3.116	3.145	106.086	3.40	-4.83	104.83
30	30.088	30	29.957	30	30.178	30.074	111.132	0.36	-0.24	100.24
60	59.897	60	59.742	60	57.442	59.027	1374.83	2.30	1.62	98.38
110	109.245	110	109.121	110	110.656	109.674	852.693	0.78	0.29	99.71

SD: Standard deviation; CV: Coefficient of variation

Table S4. Robustness of the analytical method: Effect of the change of flow (mL/min) and variations in the concentration (V/V) of the mobile phase to determine robustness.

Flux (mL/min)	C (μg/mL)	Average retention time (min) ± SD	C (v/v)	Average retention time (min) ± SD
0.6	30	6.2 ± 0.002	A:78	5.1 ± 0.002
	60	6.2 ± 0.007	B:22	5.1 ± 0.002
0.7	30	5.3 ± 0.004		
	60	5.4 ± 0.016		
0.8	30	4.6 ± 0.008	A:72	6.1 ± 0.002
	60	4.5 ± 0.016	B:22	6.1 ± 0.002

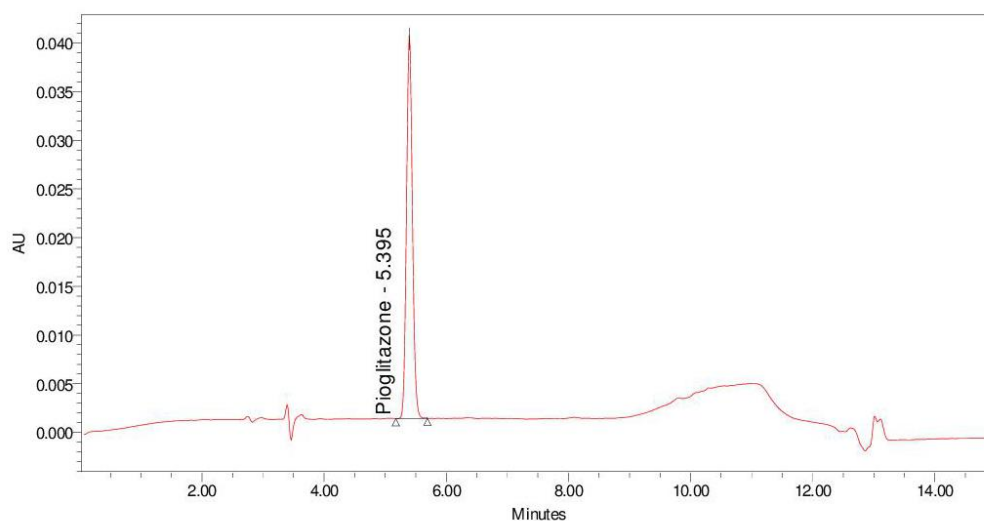
SD: Standard deviation



Peak Results

SampleName	Name	RT	Height	Amount	Units	Area (μV*sec)
1 Blank_control	Pioglitazone	5.390		Missing		

Figure S2: Chromatogram of blank control sample (Mobile phase)



Peak Results

SampleName	Name	RT	Height	Amount	Units	Area (μV*sec)
1 30 ppm	Pioglitazone	5.395	39301	30.000	ppm	268716

Figure S3: Standard sample 30 ppm.

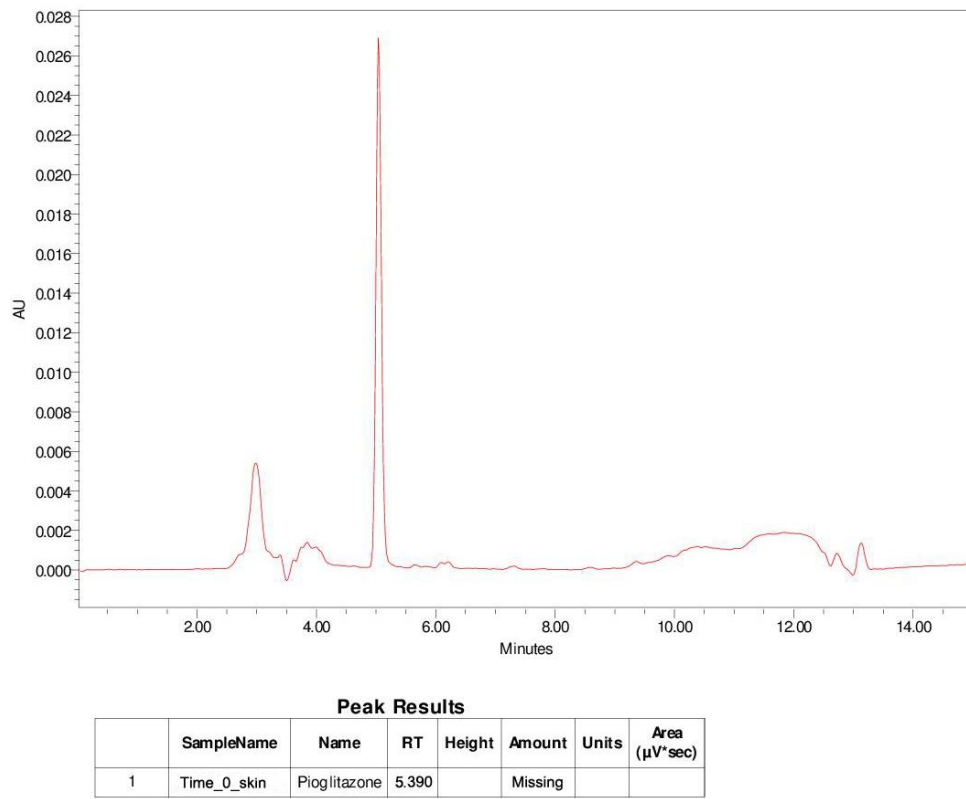


Figure S4: Skin blank sample of permeation study as control.

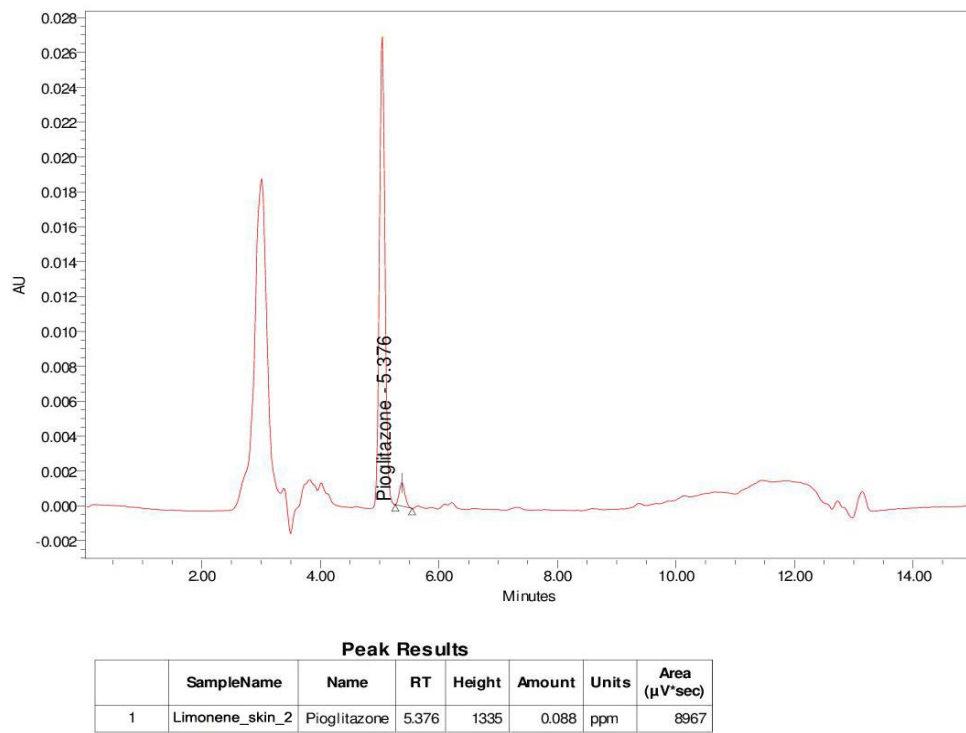


Figure S5: Skin sample permeation study of PGZ-limonene.

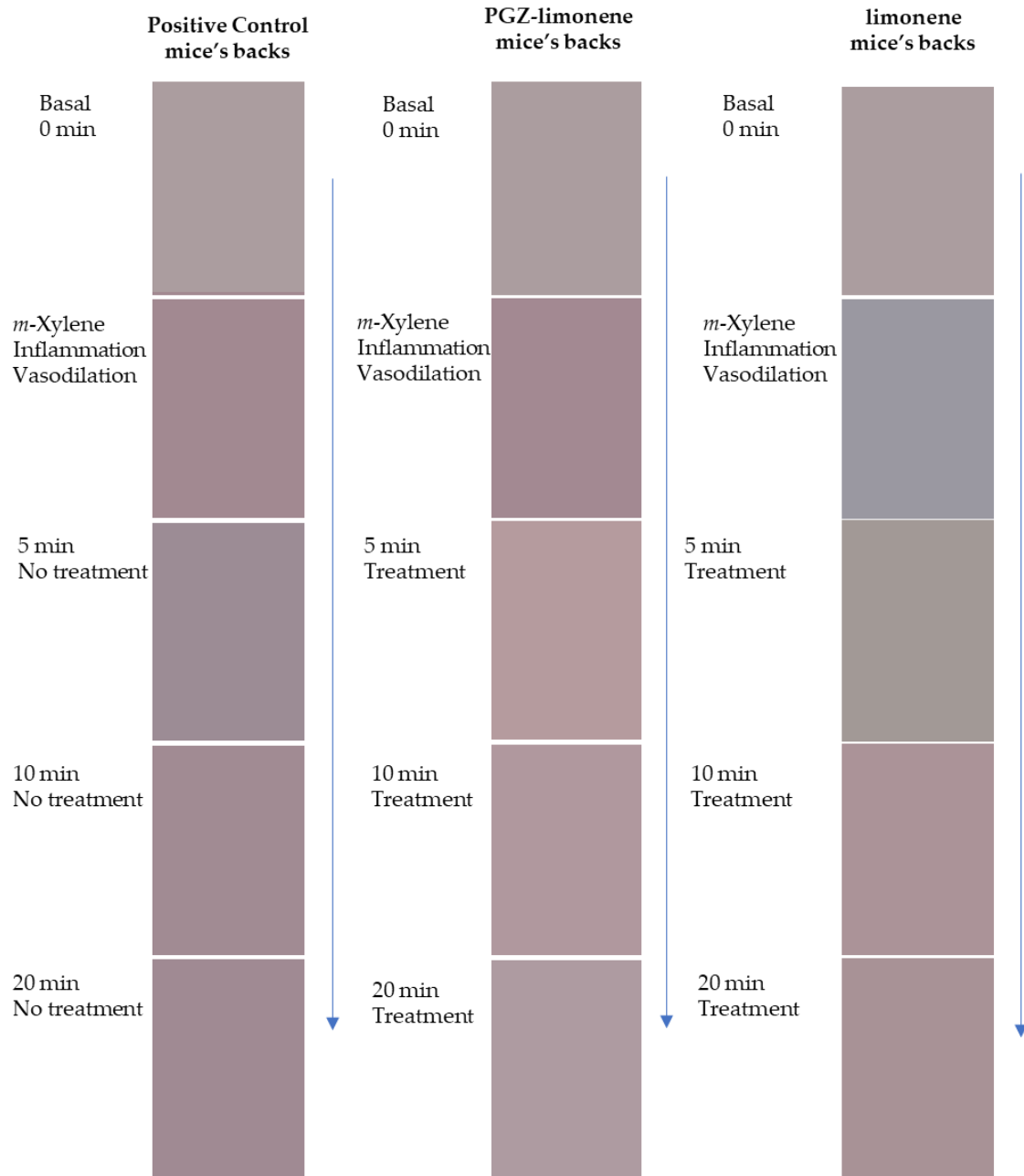


Figure S6.: Evolution of erythema shown as skin color sequence, using PGZ-limonene, limonene, compared with positive control. Colors are reproduced from the average values of RGB codes.

3.2 Article 2

Optimization, Biopharmaceutical Profile and Therapeutic Efficacy of Pioglitazone-loaded PLGA-PEG Nanospheres as a Novel Strategy for Ocular Inflammatory Disorders

Marcelle Silva-Abreu, Ana Cristina Calpena, Marta Espina, Amelia M. Silva, Alvaro Gimeno, Maria Antonia Egea and María Luisa García

Pharmaceutical Research

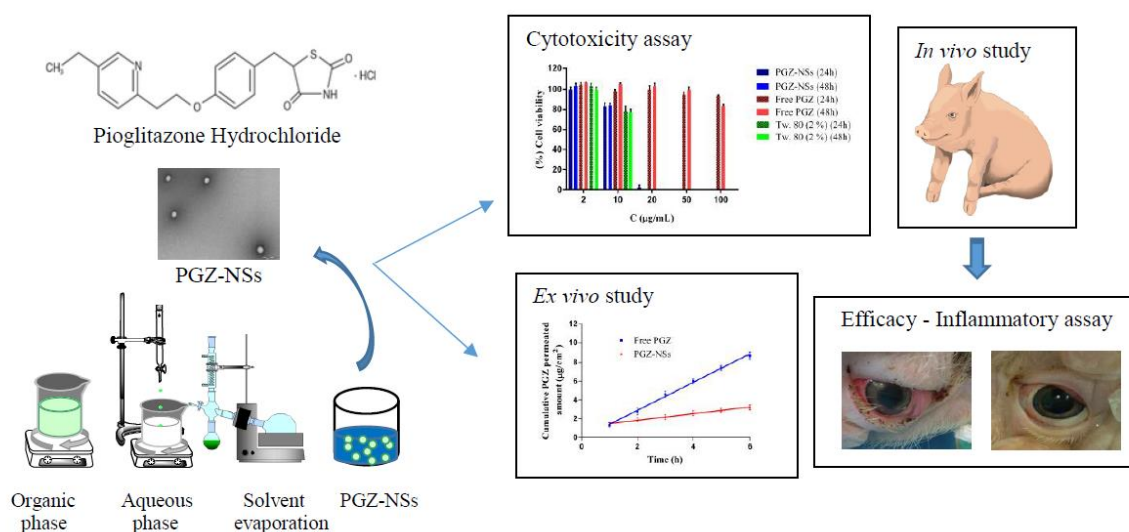
Year: 2018

ISSN: 0724-8741

IF: 3.335

DOI: 10.1007/s11095-017-2319-8

Graphical abstract





Optimization, Biopharmaceutical Profile and Therapeutic Efficacy of Pioglitazone-loaded PLGA-PEG Nanospheres as a Novel Strategy for Ocular Inflammatory Disorders

Marcelle Silva-Abreu^{1,2} · Ana Cristina Calpena^{1,2} · Marta Espina^{1,2} · Amelia M. Silva^{3,4} · Alvaro Gimeno⁵ · María Antonia Egea^{1,2} · María Luisa García^{1,2}

Received: 22 August 2017 / Accepted: 21 November 2017
© Springer Science+Business Media, LLC, part of Springer Nature 2018

ABSTRACT

Purpose The main goal of this study was to encapsulate Pioglitazone (PGZ), in biodegradable polymeric nanoparticles as a new strategy for the treatment of ocular inflammatory processes.

Methods To improve their biopharmaceutical profile for the treatment of ocular inflammatory disorders, nanospheres (NSs) of PGZ were formulated by factorial design with poly (lactic-co-glycolic acid) polyethylene glycol (PLGA-PEG). Interactions drug-polymer have been carried out by spectroscopic (X-ray spectroscopy, FTIR) and thermal methods (DSC). The PGZ-NSs were tested for their *in vitro* release profile, cytotoxicity, and ocular tolerance (HET-CAM® test); *ex vivo* corneal permeation, and *in vivo* inflammatory prevention and bioavailability.

Results The optimized system showed a negative surface charge of -13.9 mV, an average particle size (Z_{av}) of around

160 nm, a polydispersity index (PI) below 0.1, and a high encapsulation efficiency (EE) of around 92%. According to the DSC results, the drug was incorporated into the NSs polymeric matrix. The drug release was sustained for up to 14 h. PGZ-NSs up to 10 µg/ml exhibited no retinoblastoma cell toxicity. The *ex vivo* corneal and scleral permeation profiles of PGZ-NSs showed that retention and permeation through the sclera were higher than through the cornea. Ocular tolerance *in vitro* and *in vivo* demonstrated the non-irritant character of the formulation.

Conclusion The *in vivo* anti-inflammatory efficacy of developed PGZ-NSs indicates this colloidal system could constitute a new approach to prevent ocular inflammation.

KEY WORDS drug delivery · nanospheres · ocular anti-inflammatory efficacy · pioglitazone · PLGA-PEG

Electronic supplementary material The online version of this article (https://doi.org/10.1007/s11095-017-2319-8) contains supplementary material, which is available to authorized users.

✉ María Luisa García
rdcm@ub.edu

- ¹ Department of Pharmacy, Pharmaceutical Technology and Physical Chemistry, Faculty of Pharmacy and Food Sciences, University of Barcelona, 08028 Barcelona, Spain
- ² Institute of Nanoscience and Nanotechnology (IN2UB), University of Barcelona, Barcelona, Spain
- ³ Department of Biology and Environment, School of Life and Environmental Sciences, (ECVA, UTAD), University of Trás-os-Montes and Alto Douro, Quinta de Prados, 5001-801 Vila Real, Portugal
- ⁴ Centre for the Research and Technology of Agro-Environmental and Biological Sciences, University of Trás-os-Montes and Alto Douro CITAB-UTAD, 5001-801 Vila-Real, Portugal
- ⁵ Animal Facility, Bellvitge Health Sciences Campus, University of Barcelona, 08907 Barcelona, Spain

ABBREVIATIONS

DSC	Differential Scanning Calorimetry
NSs	Nanospheres
PEG	Polyethylene glycol
PGZ	Pioglitazone
PI	Polydispersity index
PLGA	Poly(lactic-co-glycolic acid)
PPAR γ	Peroxisome proliferator-activated receptor
TEM	Transmission electron microscopy
ZP	Zeta potential

INTRODUCTION

Pioglitazone (PGZ) (5-[[4-[2-(5-ethylpyridin-2-yl)ethoxy]phenyl]methyl]-1,3-thiazolidine-2,4-dione) belongs to the class of the thiazolidinediones (TZDs) for clinical treatment of type 2 diabetes. This drug is an agonist of the peroxisome proliferator-activated receptor (PPAR γ), it is

significantly important in the regulation of the immune and inflammatory responses. The anti-inflammatory effects are induced as a response to a negative regulation of macrophage activation and differentiation. Previous studies into PPAR γ receptors have reported functions such as: anti-inflammatory, anti-angiogenic, antifibrotic, anti-tumor effects, and neuro-protection. Moreover, it has a protective effect on inflammatory ocular process [1–4].

PGZ has the capacity to inhibit the local development of several inflammatory factors: these included IFN- γ and IL-6 *in vivo*. This effect was made clear in the measurement of intraocular cytokines and chemokines [3]. The activation of PPAR γ may suppress the production of inflammatory factors. This may work through the direct inhibition of their production by intraocular monocytes or T cells. PGZ may also operate by inhibiting corneal fibroblast migration, thus cutting down on corneal fibroblast-induced collagen contraction as the cornea heals [1]. In ocular therapies, one of the difficulties is for an adequate drug concentration to be delivered to the site of action and sustained. Normally, in the cases when ophthalmic formulations are used, less than 5% of the applied drug actually permeates the cornea and arrives to the intraocular tissues [5]. This problematic performance means that it is necessary to instill the formulation several times a day in order to achieve the therapeutic efficacy, which is often associated with adverse effects. When the drug is retained in the pre-corneal area and the penetration is through to the cornea, this is of great benefit to the ophthalmic therapy [5].

In past studies it has been indicated that controlled release systems have an interesting potential for ocular drug delivery [6–10]. These systems may intensify the ocular retention through prolonging it. Therefore, different ocular distributions in colloidal carriers greatly aid in achieving satisfactory treatment of eye pathologies, with the possibility of targeting different eye regions [11]. Liposomes and polymeric nanoparticles (NPs) including nanospheres (NSs) and nanocapsules, are among the most successful approaches for ocular delivery systems. Numerous studies have reported on the effectiveness of encapsulation drugs with biodegradable polymers to treat ocular disorders. This is because of their biocompatibility and biodegradability, and they show an appropriate drug delivery in different tissues of the eye [6, 10, 12, 13].

Much attention has been focused on polymeric NPs as potential therapeutic delivery systems. Biodegradable polymers, including polylactic-co-glycolic acid (PLGA), (approved by European Medicine Agency (EMA) and Food and Drug Administration (FDA)) used in various drug delivery systems in humans, exhibit good biocompatibility, small and non-toxic particles can be produced [12]. All the foregoing renders them optimal carriers for

entrapping biologically active macromolecular drugs, such as polypeptides, proteins, nucleic acids, and vaccine vectors [5]. Therefore, they could be a valid alternative for the delivery of drugs into the eye. The addition of a second ingredient such as Polyethylene glycol (PEG) may make them more versatile in terms of the encapsulation and delivery of proteins, and more susceptible to interact with the biological surface [14]. Thus, studies have shown that PEG coated NPs have crucial therapeutic potential ensuring a more controlled release of drugs. The PEG associated with the surface of PLGA-NPs creates a hydrophilic coating at the hydrophobic NPs surface, with the advantage that these systems are working their (beneficial) effect over a greater time period, thus avoiding being recognized by the reticuloendothelial system (RES). PEG coating polyester also facilitates the transport of the NPs across the corneal epithelium [15].

The aim of this study was to develop a new ocular delivery system of PGZ loaded PLGA-PEG NSs determining which factors influence the physicochemical properties of the particles and drug entrapment efficiency (EE). The NSs were optimized by a factorial design.

The *in vitro* release profile, *ex vivo* transcorneal and transcleral permeations and *in vivo* assays were performed to demonstrate that pioglitazone nanospheres (PGZ-NSs) are suitable for the prevention of ocular inflammatory process. Assays of cellular toxicity, HET-CAM[®] and Draize test were carried out to confirm that these systems do not induced eye irritation and they could present novel targets so as to act more effectively against ocular inflammatory diseases.

EXPERIMENTAL

Materials

The PGZ was purchased from Capot Chemical (Hangzhou, P.R. China) and diblock copolymer PLGA-PEG 5% (50:50) Resomer[®] was obtained from Evonik Corporation (Birmingham, USA). Tween (Tw) 80 and acetone were purchased from Sigma-Aldrich (Madrid, Spain) and Fisher Scientific (Pittsburgh, USA), respectively. The dialysis membrane MWCO 12,000–14,000 Da. was obtained from Medicell International Ltd. (London, UK). Fertilized hens' eggs were obtained from the GALLSA farm (Tarragona, Spain). Reagents for cell culture were obtained from Gibco (Alfagene, Portugal). The Y-79 was acquired from Cell Lines Service (CLS, Eppelheim, Germany) and Alamar Blue from Invitrogen Alfagene[®] (Portugal) was used in order to estimate the cell viability. Water filtered through a Millipore MilliQ system was used throughout all the experiments. All reagents were up to analytical grade.

Methods

Optimization and Characterization of PGZ-NSs

PGZ-NSs were obtained by the solvent displacement technique described in accordance with Fessi *et al.*, [16]. This technique consists of dissolving the polymer and the compound in an organic solvent, it being a successful method to deliver the lipophilic drug [13].

PGZ was previously solubilized in dimethyl sulfoxide (DMSO) [17], then the PLGA-PEG was dissolved in 5 ml of acetone. Once completely dissolved, they were then mixed together. This organic phase was added drop by drop, gently mixing into 10 ml of an aqueous solution of Tw 80 (2%), used as a surfactant to achieve pH 4.5. DMSO, and acetone were evaporated. The NSs dispersion was concentrated to 10 ml under reduced pressure (Büchi B-480, Flawil, Switzerland).

The factorial design was set up so as to optimize in that the PGZ-NSs needed as few experiments to be carried out as possible. A five-levels central rotatable composite design $2^3 + \text{star}$ was selected to study the main effects and interactions of three independent variables (PGZ, PLGA-PEG and Tw 80 concentrations), on four dependent variables (average particle size (Z_{av}), polydispersity index (PI), zeta potential (ZP) and EE). A pH of 4.5 was kept constant for all the assays. A total of 16 experiments (8 factorial points, 6 axial points and 2 replicated center points) to estimate the pure error sum of squares were required using Statgraphics Plus 5.1 software (Table I). The individual influences and the interactions of the three independent variables led to the results and responses observed in the experiments, and following on from this the full second-order polynomial equation below was used to model them (Eq. 1):

$$Y = \beta_0 + \beta_1 X_1 + \beta_2 X_2 + \beta_3 X_3 + \beta_{11} X_1^2 + \beta_{22} X_2^2 + \beta_{33} X_3^2 + \beta_{12} X_1 X_2 + \beta_{13} X_1 X_3 + \beta_{23} X_2 X_3 \quad (1)$$

where Y is the measured response, β_0 to β_{23} are the regression coefficients and X_1 , X_2 and X_3 are the three independent variables. To identify the significance of the effects and interactions between them, analysis of variance (ANOVA) was performed for each parameter.

Morphology of PGZ-NSs dispersions was analyzed by transmission electronic microscopy (TEM). Prior to negative staining, UV light was used to activate copper grids and samples were placed on the grid surface. Samples were diluted (1:3) placed in the grids and negative stain was employed with a 2% (v/v) uranyl acetate solution. They were then dried at room temperature and the samples were examined by TEM on a Jeol 1010 (Tec-nai Spirit TEM, FEI) at 80 kV.

Morphometry (Z_{av} and PI) of NSs was determined by photon correlation spectroscopy (PCS) (after 1:10 dilution) with a Zetasizer Nano ZS (Malvern Instruments, Malvern, UK) at 25°C, in a disposable quartz cells (Malvern Instruments).

Surface charge of developed NSs, measured as ZP, was determined by laser-Doppler electrophoresis with the M3 PALS system in Zetasizer Nano ZS. ZP measurements can give information about the possibility of particles aggregation. A greater ZP (in absolute value) results in there being less aggregation coming from repulsion forces between the particles. To calculate this, the Henry equation was used [18], according to (Eq. 2):

$$\mu_E = \frac{\epsilon Z P f(Ka)}{6\pi\eta} \quad (2)$$

where μ_E is the electrophoretic mobility, ϵ is the dielectric constant of the medium, ZP is the Zeta potential, η is the viscosity of the medium, K is the Deybye-Hückel parameter and $f(Ka)$ is a correction factor fully adjusted for the thickness of the electrical double layer ($1/K$) and the particle diameter (a). The reported values are the average \pm SD of at least three different formulation batches [19].

To indirectly determine the EE of PGZ-NSs the concentration of the free drug in the dispersion medium has been determined previous filtration/centrifugation technique (1:10 dilution) by using Ultracell-100 K (Amicon® Ultra; Millipore Corporation, Billerica, Massachusetts) centrifugal filter devices at 12,000 rpm for 15 min. The EE was made clear as in (Eq. 3):

$$EE(\%) = \frac{\text{Total amount of PGZ} - \text{Free amount of PGZ}}{\text{Total amount of PGZ}} \cdot 100 \quad (3)$$

High performance liquid chromatography (HPLC) was used in the evaluation of the samples. The mobile phase was: acetonitrile, ammonia acetate 0.1 M and glacial acetic acid, with a flux of 0.7 ml/min and a volume of injection of 10 μ l. The reported values are the average \pm SD, there being at least three different batches of the formulation.

Interaction Studies

To assess the physical state of the PGZ and the possible interactions between the drug and the polymer, X-ray spectroscopy came into play, backed by FTIR spectral measurements and differential scanning calorimetry (DSC) analysis.

X-ray spectroscopy was used to analyse the state (amorphous or crystalline) of the PGZ-NSs. Powder of PGZ, PLGA-PEG, and NSs was sandwiched between films of

Table 1 Coded and values of the three experimental factors according to the matrix designed by 2^3 + star central composite rotatable factorial design and measured responses

Factorial points	C_{PGZ}		$C_{PLGA-PEG}$		$C_{TW 80}$		Measured response			
	Coded level (mg/ml)		Coded level (mg)		Coded level (%)		Z_{av} (nm)	PI	ZP (mV)	EE (%)
F1	-1	0.8	-1	90	-1	1.5	152.1 ± 2.4	0.11 ± 0.01	-13.9 ± 0.4	93.97 ± 0.22
F2	1	1.2	-1	90	-1	1.5	152.9 ± 1.1	0.09 ± 0.01	-10.5 ± 0.1	85.82 ± 1.56
F3	-1	0.8	1	100	-1	1.5	165.1 ± 2.6	0.16 ± 0.17	-13.0 ± 0.3	91.66 ± 2.13
F4	1	1.2	1	100	-1	1.5	158.4 ± 0.8	0.12 ± 0.03	-10.9 ± 0.1	84.87 ± 2.31
F5	-1	0.8	-1	90	1	2.5	151.0 ± 1.1	0.11 ± 0.01	-12.8 ± 0.3	91.15 ± 1.54
F6	1	1.2	-1	90	1	2.5	152.4 ± 0.8	0.10 ± 0.01	-10.7 ± 0.1	82.01 ± 0.21
F7	-1	0.8	1	100	1	2.5	165.4 ± 1.7	0.12 ± 0.02	-13.3 ± 0.3	94.47 ± 0.17
F8	1	1.2	1	100	1	2.5	148.9 ± 2.3	0.10 ± 0.03	-10.9 ± 0.4	81.19 ± 2.32
F9	1.68	1.34	0	95	0	2.0	161.5 ± 0.6	0.13 ± 0.01	-10.1 ± 0.4	80.45 ± 0.17
F10	-1.68	0.66	0	95	0	2.0	148.9 ± 0.8	0.12 ± 0.02	-15.6 ± 0.5	92.89 ± 1.23
F11	0	1	1.68	103.4	0	2.0	152.5 ± 0.1	0.12 ± 0.00	-12.4 ± 0.2	88.24 ± 2.42
F12	0	1	-1.68	86.6	0	2.0	162.1 ± 0.4	0.12 ± 0.03	-12.5 ± 0.4	93.95 ± 1.32
F13	0	1	0	95	1.68	2.84	165.0 ± 0.3	0.17 ± 0.01	-12.8 ± 0.2	87.94 ± 1.12
F14	0	1	0	95	-1.68	1.16	155.0 ± 1.8	0.10 ± 0.01	-13.0 ± 0.5	90.84 ± 1.35
F15 ^a	0	1	0	95	0	2.0	158.6 ± 1.7	0.08 ± 0.00	-13.6 ± 0.5	90.17 ± 0.31
F16 ^a	0	1	0	95	0	2.0	160.7 ± 2.1	0.10 ± 0.02	-13.9 ± 0.7	91.61 ± 1.72

^a Centre points

polyester and exposed to CuK α radiation (45 kV, 40 mA, $\lambda = 1.5418 \text{ \AA}$) in the range $2\theta/\theta$ scans from 2° to $60^\circ 2\theta$ with a step size of $0.026^\circ 2\theta$. The measuring time was 200 s per step.

To obtain FTIR spectra of PGZ, PLGA-PEG, and NSs a Thermo Scientific Nicolet iZ10 with an ATR diamond and DTGS detector were used. The scanning range was $525\text{--}4000 \text{ cm}^{-1}$.

DSC analysis was performed using a DSC 823e System (Mettler-Toledo, Barcelona, Spain). A pan with indium (purity $\geq 99.95\%$; Fluka, Switzerland) proved ideal to check the calibration of the calorimetric system. An empty pan served as a reference. The DSC measurements were carried out on the PGZ, PLGA-PEG and NSs. On heating the samples (2.32–2.95 mg) from 25°C to 235°C at $10^\circ\text{C}/\text{min}$ in a nitrogen atmosphere it was possible to evaluate the data from the peak areas using the Mettler STARe V 9.01 dB software (Mettler-Toledo).

Release Profile of PGZ-NSs

The Franz diffusion cell technique enabled PGZ release studies from NSs to be carried out giving models that explained the release of the drug from the polymer matrix. Behind this there is the direct dispersion of the NSs in the dialysis medium complying with sink conditions [20]. For 24 h a dialysis membrane was hydrated and then placed in the Franz diffusion cell. The temperature of the medium and speed of the paddle were set at $32.0 \pm 0.5^\circ\text{C}$ and 100 rpm, respectively. The

comparisons of the PGZ-NSs formulations were made with free drug (1 mg/ml) dissolved in DMSO and a phosphate buffer solution (PBS) (60:40), receptor solution (RS) at pH 7.4 for 15 h to allow an estimated modeling. A volume of 0.3 ml of formulations was put in the donor compartment and the same medium was introduced for the solubilization of free drug in the receptor compartment. A volume of 0.3 ml was withdrawn from the receptor compartment at marked times and its place taken by an equivalent volume of RS at the same temperature. HPLC provided the released PGZ concentration. Values are reported as the average \pm SD using six replicates. At each point of time, the released PGZ content was evaluated and the data were adjusted to the most common kinetic models [21]. In each case Akaike's information criterion (AIC) was determined: it was to be an indicator of the model's suitability for a given set of data [22].

Corneal and Scleral Permeation Studies

Ex vivo corneal and scleral permeation experiments were carried out with pigs (male, weight 30–40 kg and group $n = 6$). These were supervised by veterinary officials and were in accordance with the ethics committee of animal experimentation at the University of Barcelona. The pigs were anesthetized with intramuscular administration of ketamine HCl (3 mg/kg), xylazine (2.5 mg/kg) and midazolam (0.17 mg/kg). Once sedated, the Propofol (3 mg/kg) was administered by auricular vein and immediately afterwards they were

Pioglitazone Nanoparticles to Treat Ocular Inflammatory Disorders

intubated and maintained under anesthesia inhaled with isoflurane. In order to induce pig euthanize, 250 mg/Kg of sodium pentobarbital were administered through the auricular ear vein under deep anesthesia. The cornea and sclera of the animals were cut away and placed in an artificial tear solution. The assay was carried out using Franz diffusion cells and the tissue was fixed between the donor and receptor compartment. The area in which the permeation could work was 0.64 cm². The receptor compartment was filled with a freshly prepared transcutol/water solution (60/40 v/v) and kept at 32.0 ± 0.5°C and stirred continuously for 6 h. Volumes of 0.2 ml from a solution containing 1 mg/ml of PGZ-NSs and free drug solution (solubilized at the same receptor medium) were added to the donor compartment (covered with parafilm so that there should be no evaporation). A volume of 0.2 ml was taken from the receptor compartment at pre-determined times and in its place an equivalent volume of transcutol/water solution was introduced at the same temperature. The cumulative PGZ amount permeated per unit area (μg/cm²) was worked out at each time in point from the PGZ concentration in the receiving medium and a graph drawn up as a function of time (h). All experiments were carried out under sink conditions. Samples were analyzed by HPLC.

PGZ Amount Retained in the Cornea

PGZ quantification in the ocular tissues was realized after 6 h of the experiment. The cornea and sclera were cleaned using a 0.05% solution of sodium lauryl sulfate and thoroughly rinsed with distilled water. They were weighed and during 30 min PGZ was extracted with methanol under sonication using an ultrasound bath. PGZ levels were expressed as μg/(g·cm²) of the cornea or sclera permeated and retained through the tissues. HPLC determined the PGZ. Results are reported as the average ± SD for the PGZ amount permeated and retained on each tissue, respectively.

Ocular Permeation Parameters

At every marked time the cumulative drug amounts (Q_t) permeated through the cornea and sclera per unit area were noted. The retained amount (Q_{ret}) was calculated working from the amount extracted and the recovery percentage - information already available. The amount extracted (Q_{ext}) was calculated at the end of the experiment from the contact area vs tissue weight, after sonication. PGZ flux (J_{ss}) through the cornea and sclera from each formulation was calculated setting out on a graph the cumulative drug amount permeating the cornea and sclera over time. The slope of the linear portion of the curve was found by linear regression analysis and dividing it by the diffusion area. The permeability coefficient of

the drug at the steady state (K_{ps}) from formulations was worked out using (Eq. 4):

$$K_{ps} = \frac{J_{ss}}{c_o} \tag{4}$$

being J_{ss} the flux and c_o the initial drug concentration in the donor phase.

Ocular Hydration Levels

At the end of the corneal permeation assays, the level of ocular hydration (HL (%)) of cornea assessed was determined. Then, each cornea was gently released from the sclera ring, washed, weighed and desiccated at a constant weight and dried at 80°C and then reweighed. HL (%) was arrived at in line with a previous study [9] using (Eq. 5):

$$HL (\%) = [1 - (w_d/w_w)] \cdot 100 \tag{5}$$

where w_d is weight of the cornea after being dried and w_w is the weight before being dried. Results are reported as the average ± SD of six replicates.

Studies of Ocular Tolerance: In vitro and In vivo

HET CAM®. When it came to evaluating the ocular tolerability of the developed formulation, the modified hen's egg chorioallantoic membrane (HET-CAM) test was carried out. The potential irritancy of compounds may be detected by observing adverse changes that occur in the CAM of the egg after exposure to test chemicals [23]. Briefly, fertilized hens' eggs were maintained at a temperature of 12 ± 1°C not less than 24 h before placing them in the incubator at a controlled temperature (37.8°C) and humidity (50–60%), to stay there over the days of incubation.

The shell was cut a little above the marked line of the chorioallantoic membrane (first this section of shell was removed). The inner membrane directly in contact with the CAM was dampened with 1 ml of 0.9% saline solution, added with a pipette. The inner membrane was then removed with great care. It was important that no harm was done to the blood vessels, then it was possible to see the chorioallantoic membrane below. A volume of 0.3 ml of the studied formulation was then added directly by pipette onto the CAM. Analysis, hemorrhaging and/or coagulation at different times over a 5 min period after the application of the test solution were written down, and any effect that stood out was compared with the controls: saline (negative) and sodium hydroxide (positive) solutions. Each test was performed 6 times. Data were analyzed as the average ± SD of the time at which the injury had happened (n = 6/group). The scores were recorded

according to the scoring schemes as described previously [7]. (Table S2: a. [Supplementary data](#)).

Draize Test. Tests on pigs (male, weight 30–40 kg) revealed the extent of the irritancy of the PGZ-NSs formulations. This assay was the primary eye irritation test following the methods set down by Draize (1944) and Kay *et al.*, (1962), ($n = 6/\text{group}$) [24, 25]. A volume of 0.05 ml of the sample from a concentration of 1 mg/ml, was administered in the conjunctival sac of the right eye: the untreated contra-lateral eye was a control. The level of irritation was assessed 1 h after application of the formulation. An analysis was carried out of ocular lesions in the cornea (opacity), iris (swelling, hemorrhage) and conjunctiva (inflammation, congestion, chemosis and discharge) guided by the ocular irritation index (OII) by visual assessment looking for any changes in the cornea, conjunctiva and iris. (Table S2: b. [Supplementary data](#)).

In vivo Bioavailability Study. In order to investigate ocular bioavailability and disposition of PGZ, 6 h after topical administration of 0.05 ml of PGZ-NSs from a concentration of 1 mg/ml, the pigs were euthanized and the ocular tissues, including the retina, cornea, lens, sclera, choroid, iris, aqueous humor and vitreous humor were isolated from the eyes and kept at -80°C until liquid chromatography quantification of the PGZ amount - mass spectrometry (LC-MS) as the average \pm SD ($n = 6/\text{group}$).

Cell Culture Cell Line (Y-79). The cytotoxicity of PGZ-NSs in comparison to the free PGZ was carried out in the Y-79 cell line, exposed to different concentrations which went from 2 to 100 $\mu\text{g}/\text{ml}$, using the Alamar blue (AB) assay. AB (resazurin) is a sensitive oxidation-reduction metabolic indicator. Once it has entered the cells and in the presence of metabolic reducing equivalent molecules (originating from cell metabolism), it changes its coloration from blue to rose (and thus the absorbance spectra shifts). The Y-79 cells were kept in RPMI-1640, supplemented with 10% (v/v) fetal bovine serum (FBS), 2 mM L-glutamine, and antibiotics (100 U/ml penicillin and 100 $\mu\text{g}/\text{ml}$ of streptomycin) in an atmosphere of 5% CO_2 in air at 37°C . The cells were centrifuged, re-suspended in culture media, the number recorded and seeded, once the appropriate dilution had been made, at $1 \cdot 10^5$ cells/ml in poly-L-lysine pre-coated 96-well plates (100 $\mu\text{g}/\text{well}$) for adherence, which was achieved in about 24 h. After adherence, the culture medium was taken away and test solutions added in. PGZ-NSs and free PGZ were diluted with FBS-free culture medium to achieve the desired final concentrations (test solutions), and then introduced to the cells (0.1 ml/well). Microplates were placed in the incubator, and the cells were in contact with the test solutions for 24 or 48 h. Once the exposure time was over, the media containing the NSs and the control were taken away and replaced by FBS-free

medium supplemented with 10% (v/v) of AB. The absorbance readings took place about 4–5 h after AB addition, at 570 nm (reduced form) and 620 nm (oxidized form). A Multiskan EX microplate reader was employed (MTX LabSystems, USA). The cell viability was worked out by the percentage of AB reduction, using equations as recommended by AB manufacturers as described previously [26].

In vivo Anti-inflammatory Assay. To assess inflammation prevention, PGZ-NSs were tested in pigs ($n = 6/\text{group}$). Firstly, there was just one instillation of a single dose administered at 0.05 ml of PGZ-NSs (concentration of 1 mg/ml) or 0.9% (w/v) isotonic saline solution (control) in the conjunctival sac of the right eye. The contralateral eye acted as the untreated control. After 30 min, ocular inflammation was induced administering 0.05 ml of SA 0.5% (w/v) dissolved in a phosphate buffer solution (pH 7.4) instilled in the right eye. From the first reading after 30 min, thereafter every 30 min a new reading was made of the inflammation to measure it up to three hours (180 min) after the instillation of SA. The level of inflammation was quantified through ocular changes, in line with a modified Draize scoring system [27], which are shown as the sum of the inflammation scores expressed as the average \pm SD of six replicates.

Statistical Analysis. The GraphPad Prism[®] 6.0 software package was used to analyze the data. The student's *t*-test was used for two-group comparisons and Statgraphics Plus 5.1 software. To analyze the factorial design, statistical evaluation of data was carried out using a one-way analysis of variance (ANOVA) test. Differences were taken as statistically significant when the *p*-value fell below 0.05. All of the data are presented as the average \pm SD.

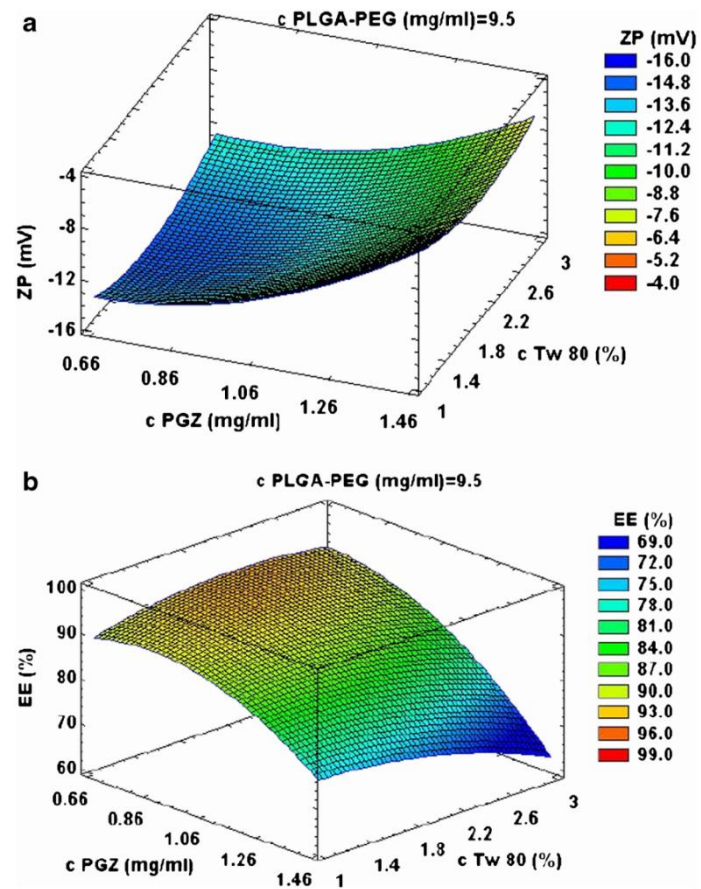
RESULTS AND DISCUSSION

Factorial Design and Characterization of PGZ-NSs

The experiments design was used to optimize the parameters, in order to obtain particles suitable for ocular administration. The results of factorial design ranged from Z_{av} 148.9 to 165.4 nm with monomodal distribution, PI values between 0.08 and 0.17 (Table I). There were no statistically significant effects noticeable when morphometric properties were indicated as responses. ZP values ranged from -10.1 to -15.6 mV, and were greatly influenced by PGZ concentration (Fig. 1a), with a coefficient of determination of 0.93. A low PGZ concentration allows the obtaining of high negative ZP values which can increase the stability of these systems. In the Pareto diagram (Fig. S1: B. [Supplementary data](#)) the influence of PGZ concentration on the ZP was observed. The EE values

Pioglitazone Nanoparticles to Treat Ocular Inflammatory Disorders

Fig. 1 Surface response of PGZ-NSs at 9.5 mg/ml PLGA-PEG concentration. **(a)** PGZ and Tw 80 concentrations influence on the ZP NSs. **(b)** PGZ and Tw 80 concentrations influence on the EE NSs.



ranged from 81.19% to 94.47%, and showed a significant decrease at high PGZ concentrations (Fig. 1b). This could be put down to the fact that the PGZ concentration indirectly influences encapsulation ($r^2 = 0.94$). For these reasons, in order to obtain an equilibrium between stability and high EE, the replicate formulation (F15 and F16) was selected (1 mg/ml of PGZ, 95 mg of polymer, 2% of Tw 80 and pH of 4.5).

The optimized PGZ loaded PLGA-PEG NSs, made by solvent displacement technique, showed a Z_{av} around 160.0 ± 1.3 nm, with PI values in the range of monodisperse systems ($PI < 0.1$) and high association efficiency (92%), which is suitable for ophthalmic application. The ZP that could be considered as a parameter of stability and mucoadhesion of these systems was -13.9 mV, indicating an adequate short-time stability. To determine the size and surface morphology of the optimized PGZ-NSs TEM was the method chosen (Fig. 2), evidencing that PGZ-NSs are spherical in morphology.

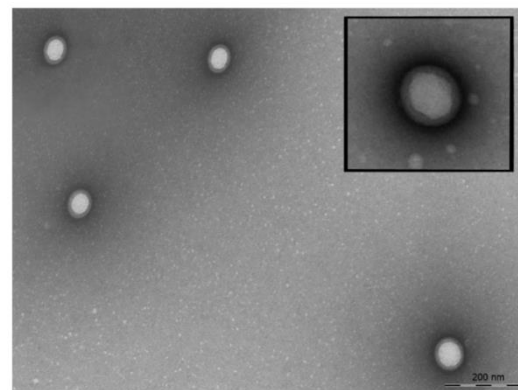


Fig. 2 Transmission electron microphotograph of the PGZ-NSs.

Interaction Studies

The *in vivo* and *in vitro* release of drugs from delivery systems could be influenced by the physical state of drugs in the colloidal systems. Therefore, different combinations of drug/polymer could coexist in the bulk, and these would be: (i) amorphous drug in either an amorphous or a semi-crystalline polymer or (ii) crystalline drug in either an amorphous or a semi-crystalline polymer. This leads on to it being possible that the drug may be present as either a solid solution or as a solid dispersion in an amorphous or semi-crystalline polymer [19]. Herein lies why it is necessary to be aware of the interactions between the polymer and the drug.

Fig. 3a sets out the X-ray diagrams of PGZ, PLGA-PEG and NSs. The X-ray spectrum of PGZ powder showed sharp crystalline peaks, whereas PLGA-PEG and NSs, according to their profiles, were amorphous. These results suggested that when the drug was loaded under the form of NSs, showed a similar polymer profile. This fact can be clearly seen in the detail of Fig. 3a.

FTIR analysis suggests that there is no evidence of new covalent bonds, between the drug and the polymer (Fig. S2. Supplementary data). These results are what can be expected in line with those set forth by other authors [21].

The DSC profiles of PGZ showed an endothermic event between 153.63°C to 209.15°C, which corresponded to solid-liquid transition (T_{max} of 196.54°C and ΔH of 138.00 J/g), followed by another thermic event that corresponded to drug decomposition. The polymer showed an endothermic event attributed to glass transition (T_g) (midpoint ISO of 43.81°C and onset of 43.03°C). PGZ-NSs showed a thermic event that corresponds to glass transition (T_g) of the polymer in the form of NSs (midpoint ISO of 40.98°C and onset of 38.82°C). The T_g parameters decrease in the NSs is probably due to a plastic effect exerted by the drug on the polymer. As there is no endotherm corresponding to the drug fusion this indicates that the PGZ is in the form of either a molecular dispersion or a solid solution (Fig. 3b). These results are similar to those obtained by lipophilic drugs in the form of NSs [19].

In vitro Release Profile

The release profiles of PGZ-NSs and free PGZ (Fig. 4a), performed at 32°C, were the same model for both formulations. However, free drug was released faster than PGZ-NSs. In the first hour, both formulations showed fast release profiles, with 87.35 μg to free solution and 57.80 μg to PGZ-NSs, there being enough quantity to permeate the ocular tissues. This result contrasts with the results of permeations. Since the NSs adhere to the cornea and sclera, and due to the fact that this also happens on the surface of tissues, there is more contact and penetration of the drug [10, 28].

The maximum amounts released (X_{max}) from the drug free solution and PGZ-NSs were 221.70 and 229.60 μg respectively, being significantly different among the formulations (p value = 0.0487). This assay showed a profile Fick's passive diffusion with a constant of dissolution (K) of 0.44 h^{-1} and 0.28 h^{-1} for free drug and NSs, respectively. The free solution has a release rate 1.6 times faster than NSs, this being significantly slower ($p = 0.0001$), although at 30 min the PGZ released was 38.83 *versus* 55.23 μg from free solution. This leads to the conclusion that PGZ release from NSs follows the same course as a concentration gradient pattern, based on the Fick's first law. These results are in line with other studies [8].

In general, the release of the drug from PLGA-PEG particles can occur through diffusion, erosion of the polymer or a combination thereof. If the diffusion of the drug progresses at a higher speed than the degradation of the matrix, the mechanism of drug release makes itself felt mainly by diffusion [29].

After 11 h, a gradual release behavior was shown, where the entrapped PGZ very gradually diffused out of the polymeric matrix into the release medium. According to the AIC and coefficient of determination (r^2) values obtained, the best fitting for all formulations was the one phase exponential association (Table II).

Ex vivo Permeation Studies

The transcorneal and scleral permeation studies (Fig. 4b and c, respectively), carried out for 6 h, showed different profiles for each one. In the statistical analysis of \bar{J}_{ss} and Q_{det} , cornea and sclera expressed significant differences ($p < 0.0001$) when one compares the PGZ-NSs *versus* free PGZ (Table III). The value of \bar{J}_{ss} of the PGZ in cornea and sclera were similar for free drug. The PGZ from NSs permeates less through the cornea than sclera, showing that the cornea has a barrier effect three times higher than the sclera [30].

This is a consequence of the cornea having a regular cellular order, while the cells of the sclera have a more irregular cellular arrangement [31]. Another factor is the physicochemical properties of the molecule, which better interacts with scleral tissue, as well as other molecule properties favoring good scleral permeability, such as Triamcinolone [32]. The permeability from NSs is important because these systems facilitate the permeation of faintly water-soluble drugs, in this case the PGZ.

The K_{ps} is proportional to the \bar{J}_{ss} , therefore this parameter is smaller in the corneal than in scleral tissue. To quantify both tissues, Q_{det} of PGZ from NSs was higher than free drug. In both the Q_{det} of PGZ were similar in the corneal tissue.

Pioglitazone Nanoparticles to Treat Ocular Inflammatory Disorders

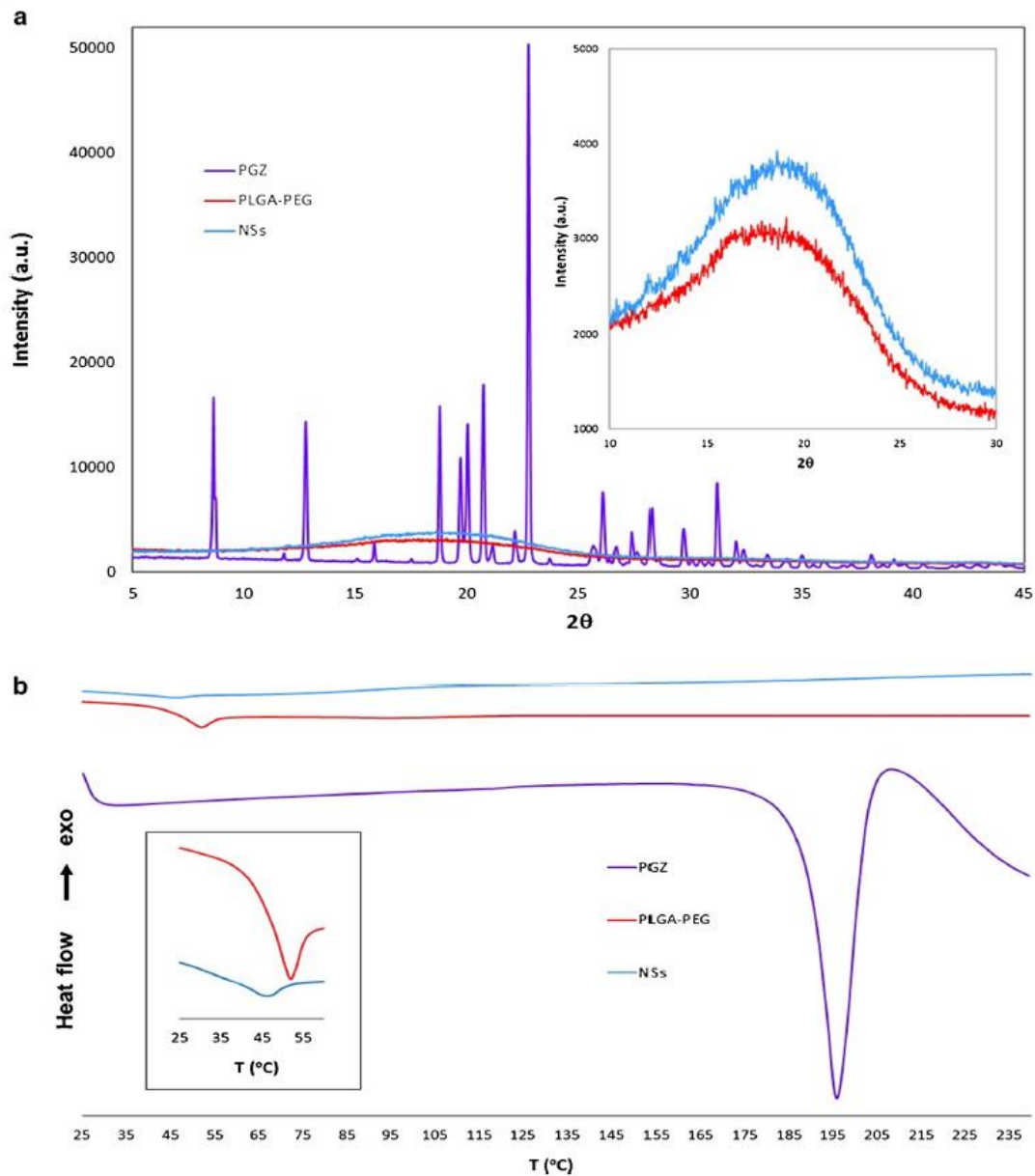


Fig. 3 Interactions studies. (a) X-ray diffraction patterns. (b) Differential scanning calorimetry.

The Q_{ret} in the sclera showed significant differences from PGZ-NSs to free drug 87.9 and 72.47 $\mu\text{g}/(\text{g}\cdot\text{cm}^2)$, respectively. The high permeability and accumulation of PGZ from NSs in the scleral tissue could be attributed to a better activity of these systems for posterior ocular

diseases, as well as uveitis, probably due to high sclera permeability [33]. These findings are in line with those obtained previously, which revealed that the PGZ could be effective for the treatment to endogenous uveitis [3]. In another study, it was shown that PPAR α agonist medical

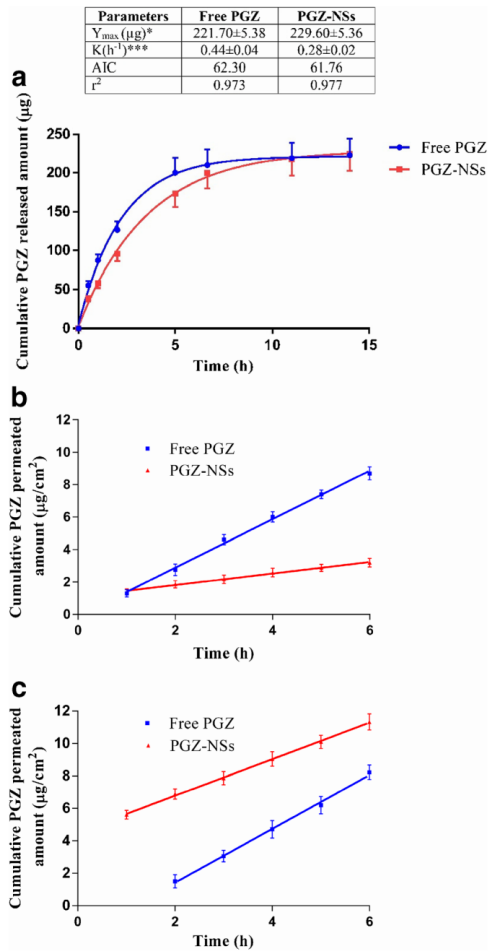


Fig. 4 Biopharmaceutical behavior: **(a)** *In vitro* release profile of PGZ-NSs and Free PGZ. **(b)** Transcorneal permeation. **(c)** Transdermal permeation. Parameters values are expressed as average \pm SD; *** $p < 0.0001$.

care significantly lessens inflammatory cell infiltration, total protein concentration, vessel density, and the development of inflammatory cytokine [34]. After 1 h, the permeated quantify of PGZ from NSs in sclera was 5.6 μg in comparison with 1 μg in the cornea, it being sufficient to cross both tissues.

Ocular Hydration Levels

The HL (%) is frequently taken as a parameter to measure the harm done to the cornea tissue. The normal cornea has a

Table II Parameters of release profile

Kinetics Models	Free PGZ		PGZ-NSs	
	AIC	r^2	AIC	r^2
One exponential association $Q_t = Q_{\infty} \cdot (1 - e^{-K \cdot t})$	62.3	0.974	111.3	0.977
Hyperbola $Q_t = Q_{\infty} \cdot t / (K + t)$	63.0	0.971	113.2	0.974
Zero order $Q_t = K_0 \cdot t + Q_{\infty}$	79.0	0.713	138.5	0.814
Korsmeyer Peppas $Q_t = K \cdot t^n$	69.0	0.931	123.0	0.944

Q_t , cumulative amount of drug release at time t ; Q_{∞} , maximum amount of drug released; K_0 , K_1 , release rate constants; t , time in hours; n is the diffusion release exponent; r^2 , determination coefficient; AIC, Akaike's information criterion

hydration level of 76–80% [35]. A HL level of 3–7% greater than the normal value indicates damage to the epithelium or endothelium. The HL percentage obtained for PGZ-NSs (79.82%) has shown that it can be accepted as being within an adequate range, and does not cause any harm to the corneal tissue (Table S1: Supplementary data). This result is in accordance with that obtained for controlled release systems and transcutol® P [7].

Tolerance Ocular Assays (HET CAM® and Draize Test)

The *in vitro* potential irritation was detected by the HET CAM test. The CAM® is a membrane with such vascularity that it has structure similar to other highly vascularized tissues. Moreover, the conjunctiva is an ideal model for ocular irritation studies. A volume of 0.3 ml of PGZ-NSs was administered to the CAM for 5 min and there was no irritation. Hemorrhage, vascular lysis or coagulation were not seen in any way. An OII of 0.4 was the score, indicating that these systems are safe for application to the eye.

In the *in vivo* studies pigs were used in order to analyze the ocular tolerance level (Draize test) of the PGZ-NSs. No irritations or damaging effects were detected after the PGZ-NSs had been instilled, being the OII = 0 at all the points. This assay indicated an optima ocular tolerance and was reinforced by the results obtained from the Hen's Egg test (HET-CAM®). In accordance with other authors, polymeric NSs are safe for ocular administration, because of their biocompatible material [7, 10, 21, 36] (Table S3: Supplementary data).

In vivo Bioavailability Study

In order to determine the *in vivo* bioavailability studies, the PGZ-NSs were administered topically for 6 h and quantified in different eye tissues. Different levels of PGZ were

Pioglitazone Nanoparticles to Treat Ocular Inflammatory Disorders

Table III Parameters of ocular permeation

	Corneal permeation		Scleral permeation	
	Free PGZ	PGZ-NSs	Free PGZ	PGZ-NSs
J_{ss} ($\mu\text{g}/(\text{cm}^2\cdot\text{h})$)	2.33 \pm 0.04 ^a	0.55 \pm 0.01	2.59 \pm 0.05 ^b	1.75 \pm 0.01
K_p (cm/h)	2.33 \pm 0.02	0.56 \pm 0.03	2.59 \pm 0.03	1.75 \pm 0.01
Q_{ext} ($\mu\text{g}/(\text{g}\cdot\text{cm}^2)$)	22.63 \pm 1.34	23.08 \pm 2.14	16.68 \pm 2.43	20.23 \pm 3.05
Q_{ret} ($\mu\text{g}/(\text{g}\cdot\text{cm}^2)$)	26.64 \pm 0.07 ^a	27.17 \pm 0.05	72.47 \pm 0.12 ^b	87.90 \pm 0.25

J_{ss} , Flux; K_p , permeability coefficient of the drug at the steady state; Q_{ext} , extracted amount; Q_{ret} , retained amount. Parameters values are expressed as average \pm SD; ^{a,b} $p < 0.0001$. ^a = Comparison between Free PGZ vs PGZ NSs with cornea tissue. ^b = Comparison between Free PGZ vs PGZ NSs with sclera tissue

obtained from the PGZ-NSs in the ocular tissues as well as in the retina (30.78 $\mu\text{g}/\text{g}$), cornea (20.52 $\mu\text{g}/\text{g}$), lens (13.45 $\mu\text{g}/\text{g}$), sclera (64.45 $\mu\text{g}/\text{g}$), choroid (159.67 $\mu\text{g}/\text{g}$), iris (117.25 $\mu\text{g}/\text{g}$), aqueous humor (9.60 $\mu\text{g}/\text{ml}$) and vitreous humor (9.20 $\mu\text{g}/\text{ml}$). The values are expressed by mean \pm SD ($n = 6$) (Fig. S4. Supplementary data).

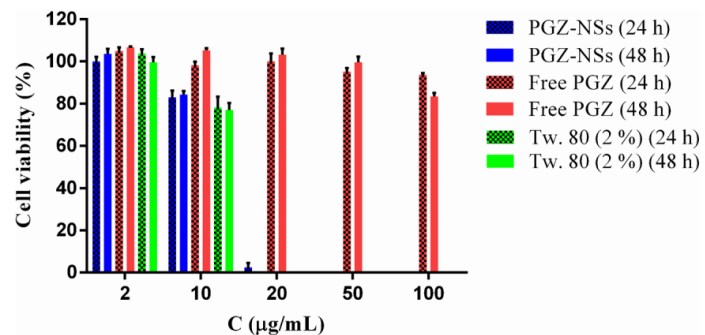
These results are in accordance with those obtained in *ex vivo* corneal and scleral permeation studies. The PGZ exhibited higher levels in the scleral tissue, demonstrating that this drug could be useful to treat diseases affecting the posterior segment of the eye. However, through tests with small amounts of the drug it has been revealed that PGZ encapsulated in NSs achieves a release reaching many parts of the eye, including the retina. Further studies could be carried out to show new routes for the effectiveness of the agonist of PPAR γ against ocular inflammatory diseases. The NSs could be a new strategy for the delivery of PGZ into the eye, also leading to a reduction in the adverse effects.

Toxicity Assay

The cell viability (expressed as % of control) was carried out in human retinoblastoma cell line, Y-79, which were exposed to test the solution of PGZ-NSs, free PGZ and Tw 80 2%, diluted in FBS-free culture media to the final concentrations of 2, 10, 20, 50 and 100 $\mu\text{g}/\text{ml}$. The AB

indicator was used to measure quantitatively the viability and propagation of the cells, rendering measurable the toxicity of tested agents/drugs in relation to non-exposed cells (control). It is possible to observe that the free drug did not produce any toxicity in the concentrations and exposure times analyzed, as the viability is always greater than 80% of control (Fig. 5). The PGZ-NSs, up to 10 $\mu\text{g}/\text{ml}$, shows no toxicity, as cell viability is above 80%, but doubling the concentration to 20 $\mu\text{g}/\text{ml}$ shows a drastic reduction in cell viability with the percentage values being close to zero. Meanwhile, when the effect of Tw 80 (at 2% in the particles) was analyzed, it showed a similar profile of toxicity as that seen in PGZ-NSs up to 10 $\mu\text{g}/\text{ml}$, with 80% of viability. The decrease of the level of cell viability (%) induced by PGZ-NSs leads one to believe in an interaction of Tw 80 (not fully incorporated into the NSs or that leaked from the NSs) with the cell membranes, leading to their lysis. It is worth mentioning that this is an *in vitro* assay in which the living cells are directly exposed to the NSs and their components. The administering of these solutions directly to cells, and the systems used, exposing the cells' membranes to their components, is quite different from the administering of these solutions, with these systems, to the ocular organ. The application of these systems by the ocular route is non-toxic since the NSs are placed on the cornea and not directly on the cells

Fig. 5 Cell viability of Y 79 cells exposed to PGZ-NSs, Free PGZ and Tw 80 2% at different concentrations.



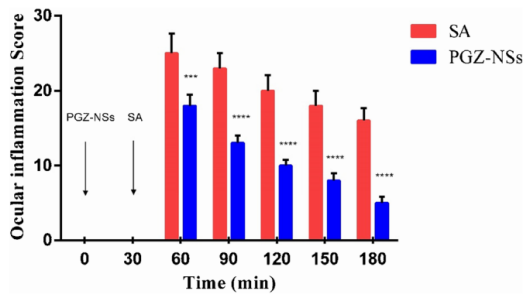


Fig. 6 Comparison of anti-inflammatory efficacy after SA-induced inflammation in the pig's eye. Values are expressed as average \pm SD; *** $p = 0.0008$ **** $p < 0.0001$ significantly lower than the inflammatory effect induced by SA.

(with the exposed cell membranes). According to previous reports, Tw 80, in comparison with other surfactants, showed the lowest cytotoxicity when tested in normal human fibroblast cultures [37].

These *in vitro* results contrast with the *in vivo* assays of ocular tolerance that show that NSs is non-irritant. This comparison corroborates the fact that the cornea works as a barrier, protecting the cells from NSs aggressive components while permitting the permeation of desired drugs.

In vivo Anti-inflammatory Efficacy

With the aim of evaluating the anti-inflammatory efficacy of PGZ-NSs in the prevention of ocular inflammation processes, PGZ-NSs were administered to the pigs 30 min before inducing inflammation with SA. PGZ-NSs showed significant differences regarding the positive control for the first 30 min after SA administration ($p = 0.0008$), reducing the degree of conjunctival inflammation and iris hyperemia significantly, as shown in (Fig. 6). It may be due mainly to the quantity of PGZ provided by NSs in different tissues, resulting in a reservoir effect of the drug and promoting the continuity of the pharmacological action. These results demonstrate that PGZ in reduced doses is an effective therapeutic agent for ocular inflammation, possibly increasing drug effect by encapsulation in polymeric NSs.

It was showed by ocular permeation that free PGZ is distributed and retained in cornea and sclera in smaller proportions whereas PGZ-NSs provide higher drug levels in the sclera and cornea, as well as higher drug penetration in different tissues of the eye. A study showed that PGZ might improve impaired insulin signaling in the diabetic rat retina [38]. Another study provide evidence that TZDs may have the potential to inhibit the progression of diabetic retinopathy [39]. However, it has been

described that an ophthalmic solution containing 0.1% PGZ inhibited inflammation, decreased the fibrotic reaction, and prevented corneal neovascularization in the cornea from the early phase after alkali burn injury in rats [4]. However, in another study, it was shown that the PGZ inhibited intraocular concentrations of TNF- α and IL-6 in the endogenous uveitis model [2]. These results demonstrated that PPAR γ agonists may represent a way of moving forward with a treatment strategy focused on clinical applications in inflammatory processes and better wound healing. This data obtained could also suggest that the dispersion of the drug within the polymer in the form of NSs favors and thus adds to its ocular bioavailability.

CONCLUSIONS

In summary, our study demonstrated that PGZ-NSs developed by the displacement technique were characterized with an Z_{av} appropriate for ocular administration (around 160 nm), suitable ZP, high EE (92%) and a good homogenization characteristic of monodisperse systems. The interaction studies showed that the potential of PGZ-NSs as a drug carrier system in which drug dispersion in the polymer increases the PGZ solubility. This is because the drug has a plastic effect on the polymer.

The release profile corresponds to Fick's passive diffusion, followed by a slower and continuous release. The permeation studies of NSs through the cornea and sclera demonstrated higher Q_{set} of PGZ in the sclera 87.9 $\mu\text{g}/(\text{g}\cdot\text{cm}^2)$, which was corroborated in the bioavailability studies. The percentage of HL for the PGZ-NSs was within the normality parameters (79.82%). No irritation or damaging effects were detected in the HET CAM $^{\text{®}}$ and Draize Test. Cytotoxicity studies of the colloidal systems showed no toxicity up to 10 $\mu\text{g}/\text{ml}$. The *in vivo* assay showed promising effects of the PGZ-NSs with respect to preventing inflammation. Taken together, the results of this study suggest that the PGZ-NSs show anti-inflammatory activity, which could be useful for the prevention of ocular inflammatory processes.

ACKNOWLEDGMENTS AND DISCLOSURES

This work has benefited from the backing of the Spanish Ministry of Science and Innovation (MAT2014-59134R). The authors would like to acknowledge Lidia Gómez Segura for her help with the *in vivo* study. Ms. Marcelle Silva de Abreu acknowledges the positive contribution of the Coordination for the Improvement of Higher Education Personnel (CAPES) - Brazil for the PhD scholarship.

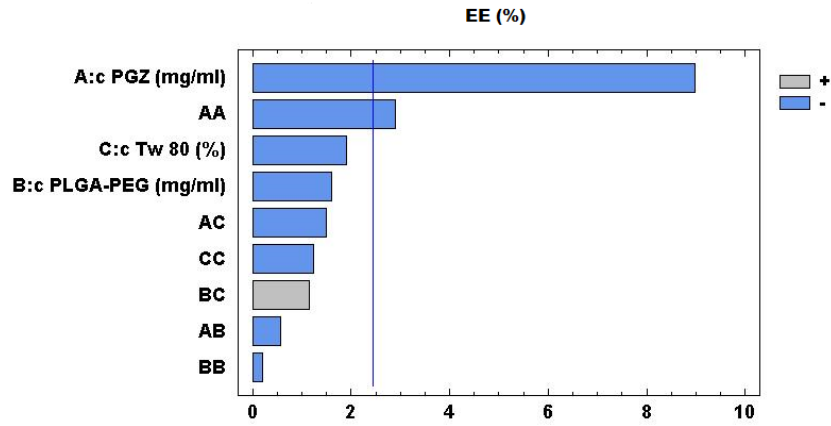
REFERENCES

1. Pan H, Chen J, Xu J, Chen M, Ma R. Antifibrotic effect by activation of peroxisome proliferator-activated receptor- γ in corneal fibroblasts. *Mol Vis*. 2009;15:2279–86.
2. Yamamoto A, Kakuta H, Miyachi H, Sugimoto Y. Involvement of the retinoid X receptor ligand in the anti-inflammatory effect induced by peroxisome proliferator-activated receptor agonist in vivo. *PPAR Res*. 2011;2011:1–8. <https://doi.org/10.1155/2011/840194>
3. Okunuki Y, Usui Y, Nakagawa H, Tajima K, Matsuda R, Ueda S, *et al*. Peroxisome proliferator-activated receptor- γ agonist pioglitazone suppresses experimental autoimmune uveitis. *Exp Eye Res*. 2013;116:291–7.
4. Uchiyama M, Shimizu A, Masuda Y, Nagasaka S, Fukuda Y, Takahashi H. An ophthalmic solution of a peroxisome proliferator-activated receptor gamma agonist prevents corneal inflammation in a rat alkali burn model. *Mol Vis*. 2013;19:2135–50.
5. Calvo P, Vila-Jato JL, Alonso MJ. Evaluation of cationic polymer-coated nanocapsules as ocular drug carriers. *Int J Pharm*. 1997;153(1):41–50.
6. Aratújo J, Vega E, Lopes C, Egea MA, García ML, Souto EB. Effect of polymer viscosity on physicochemical properties and ocular tolerance of FB-loaded PLGA nanospheres. *Colloids Surf B: Biointerfaces*. 2009;72(1):48–56.
7. Alvarado HL, Abrego G, Garduño-Ramírez ML, Clares B, Calpena AC, García ML. Design and optimization of oleonic/ursolic acid-loaded nanoplateforms for ocular anti-inflammatory applications. *Nanomed Nanotech Biol Med*. 2015;11(3):521–30.
8. Parra A, Mallandrich M, Clares B, Egea MA, Espina M, García ML, *et al*. Design and elaboration of freeze-dried PLGA nanoparticles for the transcorneal permeation of carprofen: Ocular anti-inflammatory applications. *Colloids Surf B: Biointerfaces*. 2015;136:935–43.
9. Fangueiro JF, Calpena AC, Clares B, Andreani T, Egea MA, Veiga FJ, *et al*. Biopharmaceutical evaluation of epigallocatechin gallate-loaded cationic lipid nanoparticles (EGCG-LNs): In vivo, in vitro and ex vivo studies. *Int J Pharm*. 2016;502(1–2):161–9.
10. Ramos GR, García ML, Espina M, Parra A, Calpena AC. Influence of freeze-drying and γ -irradiation in preclinical studies of flurbiprofen polymeric nanoparticles for ocular delivery using d-(+)-trehalose and polyethylene glycol. *Int J Nanomedicine*. 2016;11:4093–106.
11. De Campos AM, Sánchez A, Gref R, Calvo P, Alonso MJ. The effect of a PEG versus a chitosan coating on the interaction of drug colloidal carriers with the ocular mucosa. *Eur J Pharm Sci*. 2003;20(1):73–81.
12. Danhier F, Ansoarena E, Silva JM, Coco R, Le Breton A, Pr at V. PLGA-based nanoparticles: An overview of biomedical applications. *J Control Release*. 2012;161(2):505–22.
13. Cañadas C, Alvarado H, Calpena AC, Silva AM, Souto EB, García ML, *et al*. *in vitro*, *ex vivo* and *in vivo* characterization of PLGA nanoparticles loading pranoprofen for ocular administration. *Int J Pharm*. 2016;511(2):719–27.
14. Xu Y, Effect DY. of molecular structure of chitosan on protein delivery properties of chitosan nanoparticles. *Int J Pharm*. 2003;250(1):215–26.
15. Sánchez-López E, Egea MA, Cano A, Espina M, Calpena AC, Etxeto M, *et al*. PEGylated PLGA nanospheres optimized by design of experiments for ocular administration of dexibuprofen-*in vitro*, *ex vivo* and *in vivo* characterization. *Colloids Surf B: Biointerfaces*. 2016;145:241–50.
16. Fessi H, Puisieux F, Devissaguet JP, Ammoury N, Benita S. Nanocapsule formation by interfacial polymer deposition following solvent displacement. *Int J Pharm*. 1989;55(1):R1–4.
17. Satheeshkumar N, Shantikumar S, Srinivas R. 2014. Pioglitazone: A review of analytical methods. *J Pharm Anal*. 2014;4(5):295–302.
18. Clogston JD, Patri AK. Zeta Potential Measurement. In: McNeil SE, editor. *Characterization of nanoparticles intended for drug delivery*. Totowa: Humana Press; 2011. p. 63–70.
19. Vega E, Gamisans F, García ML, Chauvet A, Lacoulonche F, Egea MA. PLGA nanospheres for the ocular delivery of flurbiprofen: drug release and interactions. *J Pharm Sci*. 2008;97:5306–17.
20. Abrego G, Alvarado H, Souto EB, Guevara B, Bellowa LH, Parra A, *et al*. Biopharmaceutical profile of pranoprofen-loaded PLGA nanoparticles containing hydrogels for ocular administration. *Eur J Pharm Biopharm*. 2015;95:261–70.
21. Abrego G, Alvarado HL, Egea MA, Gonzalez-Mira E, Calpena AC, García ML. Design of nanosuspensions and freeze-dried PLGA nanoparticles as a novel approach for ophthalmic delivery of pranoprofen. *J Pharm Sci*. 2014;103(10):3153–64.
22. Yamaoka K, Nakagawa T, Uno T. 1978. Application of Akaike's information Criterion (AIC) in the evaluation of linear pharmacokinetic equations. *J Pharmacokinetic Biopharm*. 1978;6:165–75.
23. Luepke NP. Hen's egg chorioallantoic membrane test for irritation potential. *Food Chem Toxicol*. 1985;23(2):287–91.
24. Draize J, Woodard G, Calvery H. 1944. Methods for the study of irritation and toxicity of substances applied topically to the skin and mucous membranes. *J Pharmacol Exp Ther*. 1944;82(3):377–90.
25. Kay JH, Calandra JC. Interpretation of eye irritation tests. *J Soc Cosmet Chem*. 1962;13:281–9.
26. Andreani T, *et al*. Surface engineering of silica nanoparticles for oral insulin delivery: Characterization and cell toxicity studies. *Colloids Surf B: Biointerfaces*. 2014;123:916–23.
27. Vega E, Egea MA, Calpena AC, Espina M, García ML. Role of hydroxypropyl- β -cyclodextrin on freeze-dried and gamma-irradiated PLGA and PLGA-PEG diblock copolymer nanospheres for ophthalmic flurbiprofen delivery. *Int J Nanomedicine*. 2012;7:1357–71.
28. Prausnitz MR, Noonan JS. Permeability of cornea, sclera, and conjunctiva: a literature analysis for drug delivery to the eye. *J Pharm Sci*. 1998;87(12):1479–88.
29. Niwa T, Takeuchi H, Hino T, Kunou N, Kawashima Y. Preparations of biodegradable nanospheres of water-soluble and insoluble drugs with D,L-lactide/glycolide copolymer by a novel spontaneous emulsification solvent diffusion method, and the drug release behavior. *J Control Release*. 1993;25:89–98.
30. Resende AP, Silva B, Braz BS, Nunes T, Gonçalves L, Delgado E. *Ex vivo* permeation of erythropoietin through porcine conjunctiva, cornea and sclera. *Drug Deliv Transl Res*. 2017;7(5):625–31. <https://doi.org/10.1007/s13346-017-0399-y>
31. Nguyen TD. Biomechanics of the Cornea and Sclera. In: Kassab GS, Sacks MS, editors. *Structure-Based Mechanics of Tissues and Organs* [Internet]. Boston: Springer US; 2016. p. 285–315.
32. Aratújo J, García ML, Mallandrich M, Souto EB, Calpena AC. Release profile and transscleral permeation of triamcinolone acetonide loaded nanostructured lipid carriers (TA-NLC): *In vitro* and *ex vivo* studies. *Nanomed Nanotech Biol Med*. 2012;8(6):1034–41.
33. Wen HE, Hao J, Li SK. Characterization of human sclera barrier properties for transscleral delivery of bevacizumab and ranibizumab. *J Pharm Sci*. 2013;102(3):892–903.
34. Shen W, Gao Y, Lu B, Zhang Q, Hu Y, Chen Y. Negatively regulating TLR4/NF- κ B signaling via PPAR in endotoxin-induced uveitis. *Biochim Biophys Acta Mol Basis Dis*. 2014;1842(7):1109–20.
35. Ronald DS, Huang HS. Corneal Penetration Behavior of β -Blocking Agents I: Physicochemical Factors. *J Pharm Sci*. 1983;72(1):1266–72.

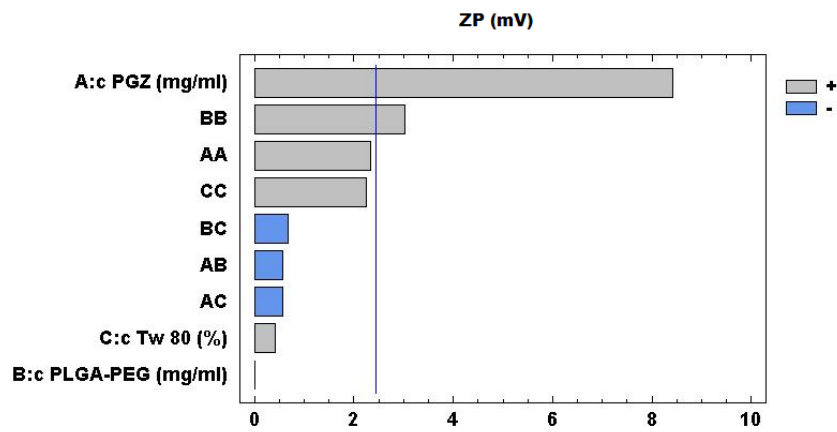
36. Vasconcelos A, Vega E, Pérez Y, Gómara MJ, García ML, Haro I. Conjugation of cell-penetrating peptides with poly(Lactic-co-glycolic acid)-polyethylene glycol nanoparticles improves ocular drug delivery. *Int J Nanomedicine*. 2015;10:609–31.
37. Arechabala B, Coiffard C, Rivalland P, Coiffard IJM, De Roock-Holtzhauer Y. Comparison of cytotoxicity of various surfactants tested on normal human fibroblast cultures using the neutral red test, MTT assay and LDH release. *J Appl Toxicol*. 1999;19(3):163–5.
38. Jiang Y, Thakran S, Bheemreddy R, Ye EA, He H, Walker RJ, *et al.* Pioglitazone normalizes insulin signaling in the diabetic rat retina through reduction in tumor necrosis factor and suppressor of cytokine signaling 3*. *J Biol Chem*. 2014;289(38):26395–405.
39. Murata T, Hata Y, Ishibashi T, Kim S, Hsueh WA, Law RE, *et al.* Response of experimental retinal neovascularization to thiazolidinediones. *Arch Ophthalmol*. 2001;119(5):709–17.

Supplementary data

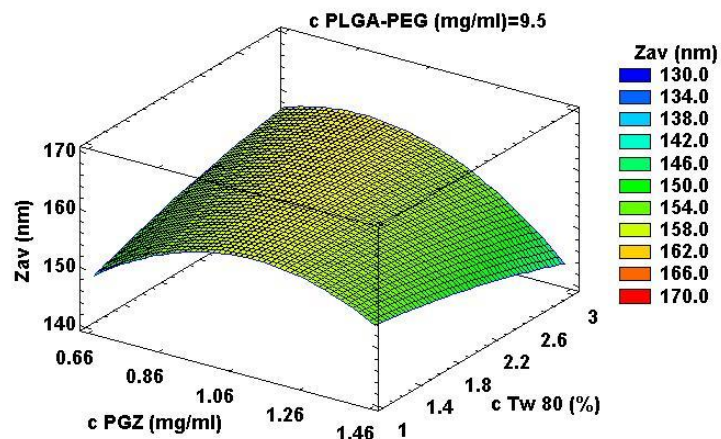
A)



B)



C)



D)

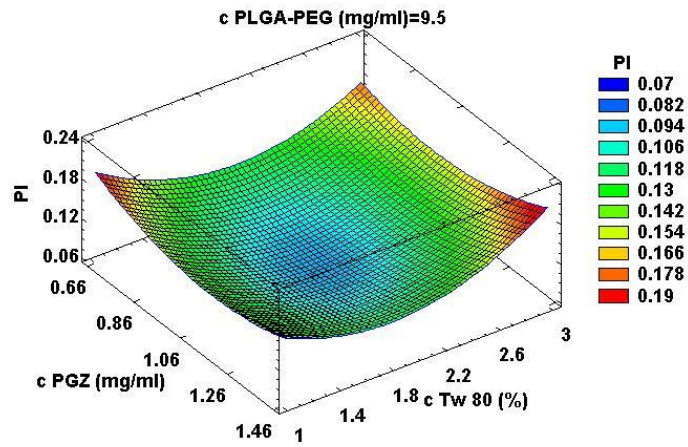


Figure S1: Design of experiments. (A): Pareto's diagram of EE (%). (B): Pareto's diagram of ZP (mV). (C): Response surface of Z_{av} (nm) versus PGZ and Tw 80 concentrations. (D): Response surface of PI versus PGZ and Tw 80 concentrations.

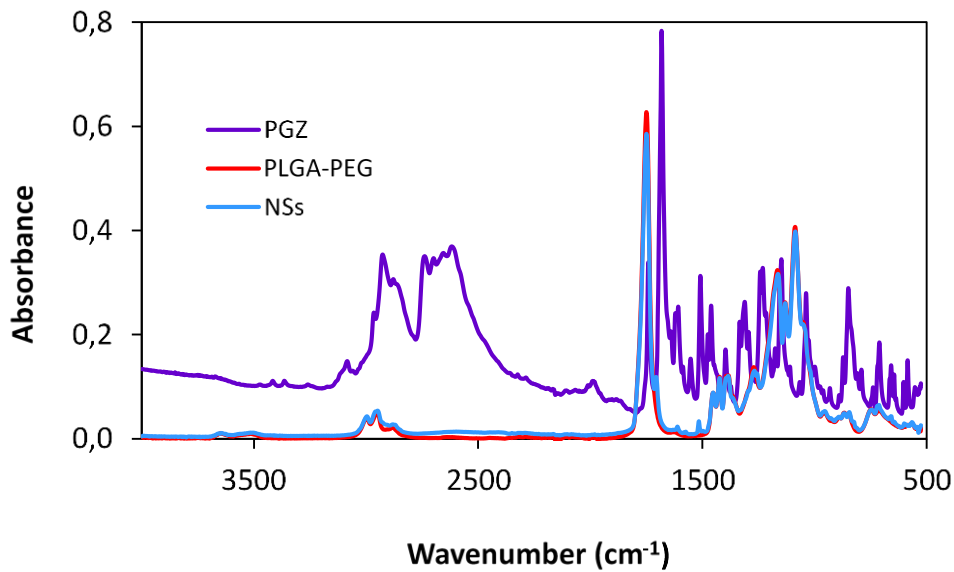


Figure S2: Fourier transformed infrared spectroscopy of PGZ, PLGA-PEG and NSs

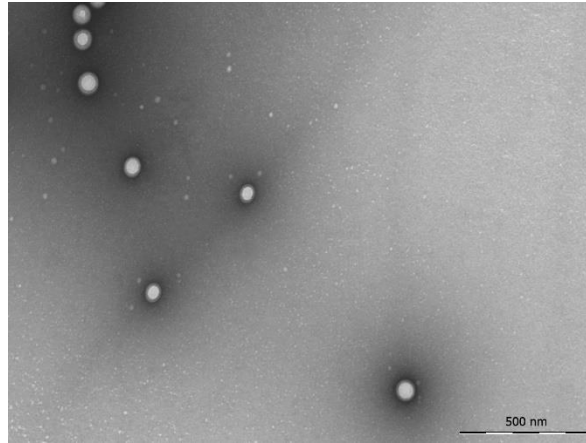


Figure S3: Image of PGZ-NSs by Transmission electron microphotograph

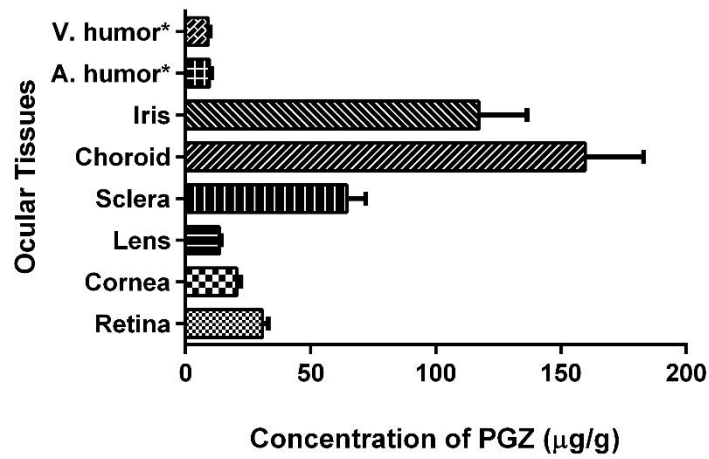


Figure S4: Levels of PGZ in different ocular tissues. Vitreous Humor* and Aqueous Humor* data are expressed as (µg/mL). The values are expressed by mean \pm SD (n=6)

Table S1: Ocular hydration levels

N° of replicates	Wet Cornea (g)	Dried Cornea (g)	Ratio	HL (%)
1	0.33	0.07	0.78	77.84
2	0.43	0.08	0.81	80.64
3	0.45	0.10	0.78	78.13
4	0.35	0.07	0.80	79.94
5	0.37	0.06	0.83	82.56
6	0.45	0.09	0.80	79.78
Mean	0.40	0.08	0.80	79.82
SD	0.05	0.01	0.02	1.73

Table S2: Ocular tolerance levels: a) HET CAM b) *in vivo* DRAIZE TEST c) Scale of Weighted Scores for Grading the Severity of Ocular Lesions.

a)

HET CAM®		
OII	Classification	Calculation
0 - 0.9	Non - irritant	$IIO = \frac{(301-h) \cdot 5}{300} + \frac{(301-v) \cdot 7}{300} + \frac{(301-c) \cdot 9}{300}$ 
1 - 4.9	Weakly irritant	
5 - 8.9	Moderately irritant	
9 - 21	Irritant	

b)

DRAIZE TEST		
OII	Classification	Calculation
0	Non - irritant	$IIO = \text{Corneal } (A \cdot B \cdot 5) + \text{Iris } (A \cdot 5) + \text{Conjunctiva } (A+B+C) \cdot 2$  <p><i>Table c: Injury score</i></p>
0 - 15	Weakly irritant	
> 15 - 30	Moderately irritant	
> 30 - 50	Irritant	
> 50	Very irritant	

c)

Injury	Evaluation	Tissue and score
A) Degree of cloudiness or opacity		CORNEA A·B·5 Maximum = 80
- Absence of ulceration	0	
- Diffuse areas	1	
- Translucents areas	2	
- Opalescent areas	3	
- Full opacity	4	
B) Affected area		
- None	0	
- A quarter or less	1	
- More than a quarter but without means	2	
- More than half but less than three quarters	3	
- More than three quarters up a whole plane	4	
A) Iris injury score		IRIS A·5 Maximum =10
- Normal	0	
- Deep folds, congestion, swelling, moderate circumcorneal injection - No reaction to light, hemorrhage, great destruction	1 2	
A) Redness		CONJUCTIVA (A+B+C)·2 Maximum = 20
- Normal glasses	0	
- Some clearly injected vessels	1	
- Diffuse redness	2	
- Big diffuse redness	3	
B) Chemosis or Inflammation		
- None	0	
- Some	1	
- Marked with partial disorder of the eyelids	2	
- Eyelid more or less closed	3	
- Semi eyelids	4	
C) Sweat		
- None	0	
- Periocular wetting	1	
- Any amount anomalous	2	
- Wetting and eyelid hairs	3	

Table S3: Tolerance assays results.

Formulation	HET CAM®		DRAIZE TEST	
	OII score	classification	OII score	classification
NSs-PGZ (1mg/mL)	0.40 ± 0.21	Non-irritant	0.0 ± 0.0	Non-irritant
Negative Control	0.00 ± 0.00	Non-irritant	0.0 ± 0.0	Non-irritant
Positive Control	10.52 ± 0.12	Irritant	-	-

Data are expressed as mean ± SD (n=6/group)

3.3 Article 3

Comparative Study of Ex Vivo Transmucosal Permeation of Pioglitazone Nanoparticles for the Treatment of Alzheimer's Disease

Marcelle Silva-Abreu, Lupe Carolina Espinoza, Lyda Haubalt, Marta Espina, María Luisa García and Ana Cristina Calpena

Polymers

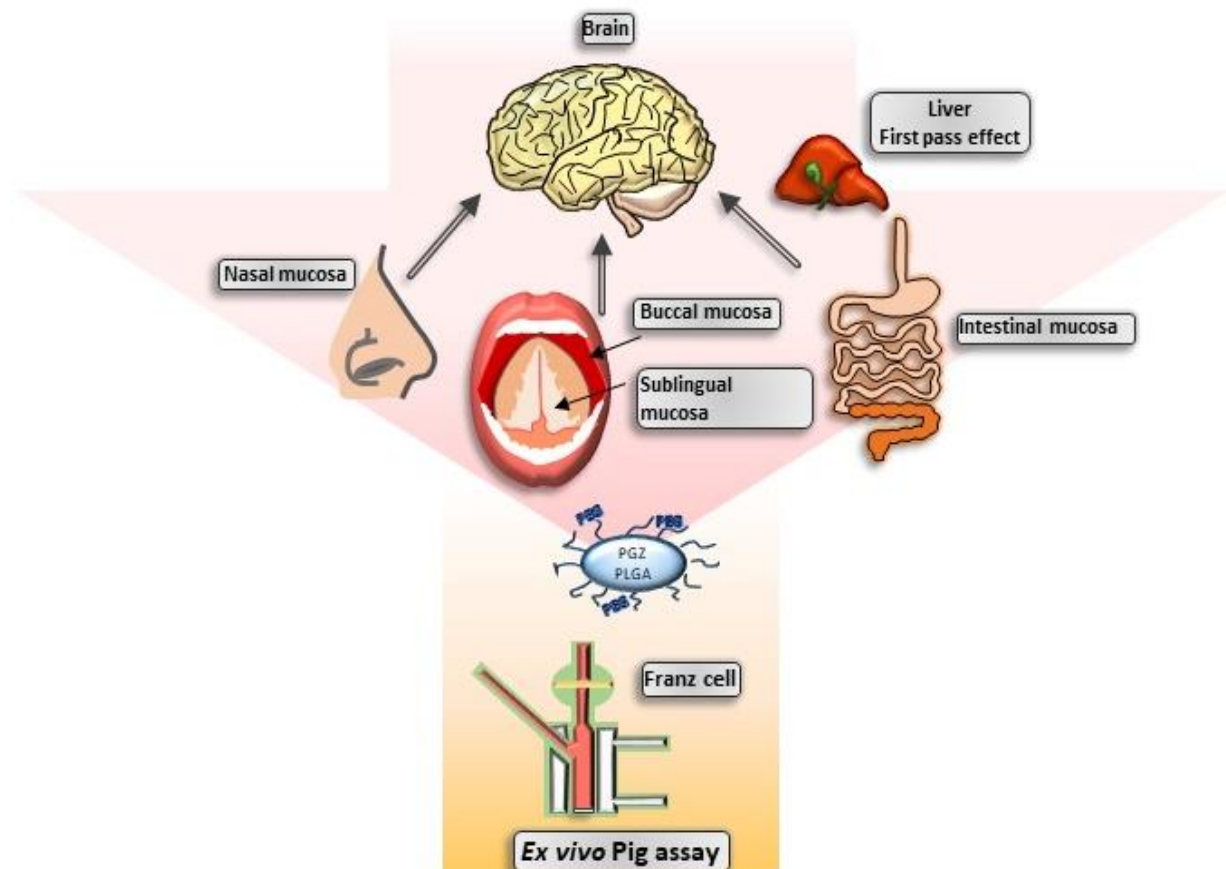
Year: 2018

ISSN: 2073-4370

IF: 2.935

DOI: 10.3390/polym10030316

Graphical abstract





Article

Comparative Study of Ex Vivo Transmucosal Permeation of Pioglitazone Nanoparticles for the Treatment of Alzheimer's Disease

Marcelle Silva-Abreu ^{1,2} , Lupe Carolina Espinoza ^{1,3} , Lyda Halbaut ¹, Marta Espina ^{1,2} ,
María Luisa García ^{1,2} and Ana Cristina Calpena ^{1,2,*}

¹ Department of Pharmacy, Pharmaceutical Technology and Physical Chemistry, Faculty of Pharmacy and Food Sciences, University of Barcelona, 08028 Barcelona, Spain; marcellesabreu@gmail.com (M.S.-A.); lcespinoza@utpl.edu.ec (L.C.E.); halbaut@ub.edu (L.H.); m.espina@ub.edu (M.E.); rdc@ub.edu (M.L.G.)

² Institute of Nanoscience and Nanotechnology (IN2UB), University of Barcelona, 08028 Barcelona, Spain

³ Departamento de Química y Ciencias Exactas, Universidad Técnica Particular de Loja, Loja 1101608, Ecuador

* Correspondence: anacalpena@ub.edu; Tel.: +34-93-402-4560

Received: 27 February 2018; Accepted: 13 March 2018; Published: 14 March 2018

Abstract: Pioglitazone has been reported in the literature to have a substantial role in the improvement of overall cognition in a mouse model. With this in mind, the aim of this study was to determine the most efficacious route for the administration of Pioglitazone nanoparticles (PGZ-NPs) in order to promote drug delivery to the brain for the treatment of Alzheimer's disease. PGZ-loaded NPs were developed by the solvent displacement method. Parameters such as mean size, polydispersity index, zeta potential, encapsulation efficacy, rheological behavior, and short-term stability were evaluated. Ex vivo permeation studies were then carried out using buccal, sublingual, nasal, and intestinal mucosa. PGZ-NPs with a size around of 160 nm showed high permeability in all mucosae. However, the permeation and prediction parameters revealed that lag-time and vehicle/tissue partition coefficient of nasal mucosa were significantly lower than other studied mucosae, while the diffusion coefficient and theoretical steady-state plasma concentration of the drug were higher, providing biopharmaceutical results that reveal more favorable PGZ permeation through the nasal mucosa. The results suggest that nasal mucosa represents an attractive and non-invasive pathway for PGZ-NPs administration to the brain since the drug permeation was demonstrated to be more favorable in this tissue.

Keywords: nanoparticles; pioglitazone; PLGA-PEG; transmucosal permeations; Alzheimer's disease

1. Introduction

Alzheimer's disease (AD) is a progressive neurodegenerative disease that is considered the most common cause of dementia [1,2]. AD is characterized by a gradual decline in cognition and neuropsychiatric disorders that affect the ability to perform activities of daily living [3,4]. Chronic neuroinflammation has been described as a pathological feature which may contribute to amyloid plaque progression and neurodegeneration [5,6].

PPAR- γ is a nuclear receptor whose activation regulates genes involved in glucose homeostasis, lipid metabolism, and inflammation [7–9]. Recent studies have shown that PPAR- γ ligands inhibit proinflammatory gene expression, regulate amyloidogenic pathways, and exhibit neuroprotective effects [10–12]. Pioglitazone (PGZ) is a PPAR- γ activator that increases tissue sensitivity to insulin and is widely used to treat type 2 diabetes mellitus (T2DM) [13]. Other pharmacological effects reported for PGZ include selective suppression of the T-helper 17 (Th17) cells differentiation and improvements in

overall cognition using a mouse model, suggesting that PGZ is a viable treatment option not only for T2DM but also for autoimmune diseases, inflammatory conditions, and neurodegenerative diseases such as multiple sclerosis, rosacea, and AD [14–17].

PGZ is classified as a biopharmaceutical classification system (BCS) Class II drug with low solubility and high permeability which limits its absorption rate [18]. PGZ is available in conventional tablets for oral administration [19]. However, oral delivery of this dosage form has notable disadvantages such as prolonged disintegration time, first-pass metabolism, poor solubility, and low intestinal bioavailability, consequently demonstrating the need to develop new drug delivery systems and their administration by alternative routes [20].

Drugs administered via mucosal surfaces (buccal, sublingual, nasal, and intestinal tissues) provide local and/or systemic pharmacological action [21,22]. Novel mucosal delivery systems have been developed to optimize the efficacy and safety of drugs administered by these routes. Nanostructured systems are considered the most promising strategies [23,24]. Polymeric and solid lipid nanoparticles, nanostructured lipid carriers, and nanoemulsions are examples of nanotechnologies that offer numerous benefits including improved solubility for hydrophobic drugs, controlled drug release, and enhanced stability and bioavailability [25,26]. Polymeric nanoparticles (PNPs) are extensively employed due to their favorable properties, not the least of which include their ease of manufacture, low toxicity, biocompatibility, protection of drug, and biodegradation [27,28]. PNPs are defined as particles with a size ranging from 10 nm to 1000 nm that are composed of either natural polymers (gelatin, albumin, chitosan) or synthetic polymers such as polylactides (PLA), poly(lactic-co-glycolic) acid (PLGA), and polyglycolides (PGA) [28,29]. The incorporation of mucoadhesive polymers that adhere to a mucosal surface prolongs the residence time at the administration site of these drug delivery systems, increasing the local or systemic bioavailability [30]. Polyethylene glycol (PEG) is a hydrophilic polymer that is non-toxic and used in many pharmaceutical formulations. Surface coating with PEG is reported to prevent non-specific interactions of serum proteins with NPs [31]. PLGA-PEG copolymer nanoparticles are composed of a hydrophilic surface of PEG around a hydrophobic core of PLGA [32]. This structure allows the encapsulation of hydrophobic drugs into the core region and prolongs the circulation time while the PEG hydrophilic shield around the particle core augments mucus-penetrating properties [33,34].

The purpose of this study was to determine the best mucosal route for the administration of NPs of PGZ on the basis of their biopharmaceutical parameters in order to provide drug delivery to the brain for optimal treatment of AD. Additionally, rheological behavior and short-term stability were analyzed.

2. Materials and Methods

2.1. Materials

PGZ was purchased from Capot Chemical (Hangzhou, China), and Diblock copolymer PLGA-PEG (Resomer[®] Select 5050 DLG mPEG 5000–5 wt % PEG) was purchased from Evonik Corporation (Birmingham, AL, USA). Tween (Tw) 80 and acetone were obtained from Sigma-Aldrich (Madrid, Spain) and Fisher Scientific (Pittsburgh, PA, USA), respectively. The dialysis membrane MWCO 12,000–14,000 Da was obtained from Mediatech International Ltd. (London, UK) and the Transcutol was obtained from Gattefossé (Barcelona, Spain). Water filtered through a Millipore MilliQ system was used for all the experiments and reagents used were of analytical grade.

2.2. Methods

2.2.1. Preparation of NPs and Physicochemical Characterization

PGZ-loaded PLGA-PEG NPs were developed by the solvent displacement method [35]. The formulation of PGZ-NPs consists of two phases: the first is composed of the drug, dimethyl

sulfoxide (DMSO), and acetone (organic phase) while the second phase consists of Tw 80 (surfactant) and water (aqueous phase). After complete solubilization of both phases, the organic phase was added drop by drop into 10 mL of the aqueous phase. Afterwards, the NPs dispersion was concentrated to 10 mL under reduced pressure (Büchi B-480, Flawil, Switzerland).

The NPs mean size (Z_{av}) and polydispersity index (PI) were determined by photon correlation spectroscopy (PCS) using a ZetaSizer Nano ZS (Malvern Instruments, Madrid, Spain). Measurements were carried out in triplicate at angles of 180° in 10-mm diameter cells at 25°C . The surface charge, or Zeta potential (ZP), was calculated from electrophoretic mobility. This parameter can give information about the possibility of particles aggregation [36]. The encapsulation efficiency (EE) of PGZ in the NPs was determined indirectly following Equation (1). The non-entrapped PGZ was separated using filtration/centrifugation (1:10 dilution) with Ultracell-100 K (Amicon® Ultra; Millipore Corporation, Billerica, MA, USA) centrifugal filter devices at 12,000 rpm for 15 min. PGZ was measured using a previously validated high performance liquid chromatographic (HPLC) method [15].

$$EE(\%) = \frac{\text{Total amount of PGZ} - \text{Free amount of PGZ}}{\text{Total amount of PGZ}} \cdot 100 \quad (1)$$

2.2.2. Tissue Samples

Samples were extracted from pigs (male, weight 30–40 kg, $n = 6$) following a process supervised by veterinary officials in accordance with the Ethics Committee of Animal Experimentation at the University of Barcelona. The pigs were anesthetized with intramuscular administration of ketamine HCl (3 mg/kg), xylazine (2.5 mg/kg) and midazolam (0.17 mg/kg). Once sedated, Propofol (3 mg/kg) was administered through the auricular vein and they were subsequently intubated and maintained under anesthesia by isoflurane inhalation. In order to induce pig euthanasia, sodium pentobarbital (250 mg/kg) was administered through the auricular vein under deep anesthesia.

After the sacrifice, mucosal samples were surgically removed from buccal, sublingual, nasal, and intestinal tissues, preserved in Hank's balanced salt solution and refrigerated until delivery to laboratory for the initiation of experiments.

2.2.3. Transmucosal Ex Vivo Permeations

The study was performed in Franz diffusion cells using buccal and nasal mucosae (0.5 mm thick), sublingual mucosa (0.3 mm thick), and uncut intestinal mucosa. The tissues were used for experiments and placed between the receptor and donor compartments. An aliquot of 0.2 mL of PGZ-NPs at 1 mg/mL were placed in the donor compartment and the same volume of samples was extracted from the receptor compartment at established time intervals of 6 h and replaced with fresh receptor medium (Transcutol/water, 6:4 v/v) at $37 \pm 0.5^\circ\text{C}$ under continuous stirring. The quantitative determination of permeated PGZ per unit area ($\mu\text{g}/\text{cm}^2$) in the different tissues was analyzed six times by the HPLC method [15]. Kinetic parameters were estimated using GraphPad Prism® 6.0 (GraphPad Software Inc., San Diego, CA, USA).

2.2.4. Biopharmaceutical Parameters

- Determination of PGZ extracted and recovered in the tissues

After finishing the experiment, the mucosae were extracted and used to determine the amount of PGZ retained (Q_r , $\mu\text{g PGZ}/\text{g tissue}/\text{cm}^2$). The mucosae were cleaned with sodium lauryl sulphate solution (0.05%) and washed with distilled water. The permeation area was excised and weighed, then the PGZ retained was extracted with methanol (1 mL) under sonication for 20 min in an ultrasound bath. The amount of PGZ was analyzed by HPLC.

To analyze the percentage of PGZ recovered from the mucosae, 1 mL of PGZ solution (110 $\mu\text{g}/\text{mL}$) was added to the different mucosae (six replicates), and kept for 6 h at $37 \pm 1^\circ\text{C}$ using a water bath.

A standard solution of 1 mL PGZ at 110 µg/mL was also kept at 37 ± 1 °C for the same period as a reference.

The PGZ retained from mucosae permeation and recovery samples was quantified using a validated HPLC method [15].

- Data analysis

The cumulative amount of PGZ (µg) permeated through mucosae was plotted as a function of time (h). The slope and intercept of the linear portion of the plot was derived by regression using GraphPad Prism[®], 5.0 version software (GraphPad Software Inc., San Diego, CA, USA).

The flux values (J_{ss} , µg/min/cm²) across the mucosae and the permeability coefficients (K_p) were calculated per unit surface area versus time plot. In this plot, the lag time (T_l , min) is the intercept with the x -axis (time), determined by linear regression analysis of the permeation data using GraphPad Prism[®] 5.01 (GraphPad Software Inc., San Diego, CA, USA). The flux values are demonstrated by Equation (2):

$$J_{ss} = \frac{Qt}{A} \cdot t \quad (2)$$

where Qt is the quantity of PGZ transferred across the mucosae into the receptor compartment (µg), A is the active cross-sectional area accessible for diffusion (cm²), and t is the time of exposure (min).

The permeability coefficients (K_p , cm/min) were obtained by Equation (3):

$$K_p = \frac{J_{ss}}{C_0} \quad (3)$$

where J_{ss} is the flux calculated at the steady state and C_0 is the initial drug concentration in the donor compartment.

Parameters of permeation (cm) and diffusion (min⁻¹), P_1 and P_2 , respectively, were estimated from Equations (4) and (5):

$$K_p = P_1 \cdot P_2 \quad (4)$$

$$T_l = \frac{1}{6} \cdot P_2 \quad (5)$$

The theoretical human steady-state plasma concentration (C_{ss}) of the drug, which predicted the potential systemic concentration achieved after mucosae administration, was obtained using Equation (6):

$$C_{ss} = J_{ss} \cdot \frac{A}{Clp} \quad (6)$$

where C_{ss} is the plasma steady-state concentration, J_{ss} the flux determined in this study, A the hypothetical area of application, and Clp the plasmatic clearance. The calculations were based on a maximum area of application of 20 cm² for buccal, 15 cm² for sublingual, and 150 cm² for nasal [37,38] mucosae, as well as a human Clp value of 2.26 L/h \pm 1.22 [39] in order to ensure the local action of the formulation.

In addition, the mean transit time (MTT, day) of the drug in the mucosae was also obtained using Equation (7):

$$MTT = \left[\frac{V_1}{P_1 \cdot P_2 \cdot A_E} \right] + \left[\frac{1}{2 \cdot P_2} \right] \quad (7)$$

where V_1 (mL) is the volume of the donor compartment and A_E (cm²) is the area of experimental mucosae samples.

2.2.5. Rheological Behavior

The PGZ-NPs were placed in glass vials with rubber tops and aluminum capsules, then stored at room temperature (23 ± 3 °C). Rheological properties were determined at $t_0 = 24$ h after NPs

preparation using a rotational Haake RheoStress 1 rheometer (Thermo Fischer Scientific, Karlsruhe, Germany) connected to a temperature control Thermo Haake Phoenix II + Haake C25P and equipped with cone-plate geometry (0.105 mm gap) including a Haake C60/2Ti mobile cone (60 mm in diameter and 2° angle). The temperature was adjusted to 25 °C. PGZ-NPs were tested in two replicates, each undergoing a program consisting of a Three-Step Shear Profile: firstly, a ramp-up period from 0 s⁻¹ to 50 s⁻¹ over a 3-min span, followed by a constant shear rate period at 50 s⁻¹ for 1 min, and finally the ramp-down period from 50 s⁻¹ to 0 s⁻¹ for 3 min. The data from the flow curves ($\tau = f(\dot{\gamma})$) were fitted to different mathematical models. The equations are summarized in Table 1.

Viscosity mean value at t_0 and 25 °C was determined from the constant shear stretch at 50 s⁻¹ of the viscosity curves ($\eta = f(\dot{\gamma})$). The determination of the disturbance of the microstructure during the test or “apparent thixotropy” (Pa/s) was also evaluated.

Table 1. Mathematical models for regression analysis.

Flow Curve—Models: $\tau = f(\dot{\gamma})$	
Newton	$\tau = \eta \cdot \dot{\gamma}$
Bingham	$\tau = \tau_0 + (\eta_0 \cdot \dot{\gamma})$
Ostwald-de-Waele	$\tau = K \cdot \dot{\gamma}^n$
Herschel-Bulkley	$\tau = \tau_0 + K \cdot \dot{\gamma}^n$
Casson	$\tau = \sqrt[n]{(\tau_0^n + (\eta_0 \cdot \dot{\gamma})^n)}$
Cross	$\tau = \dot{\gamma} \cdot (\eta_\infty + (\eta_0 - \eta_\infty) / (1 + (\dot{\gamma} / \dot{\gamma}_0)^n))$

where τ is the shear stress (Pa), $\dot{\gamma}$ is the shear rate (1/s), η is the dynamic viscosity (Pa·s), τ_0 is the yield shear stress (Pa), η_0 is the zero shear rate viscosity, η_∞ is the infinity shear rate viscosity, n is the flow index, and K is the consistency index [40]. The mathematical model was selected on the basis of the correlation coefficient value (r).

2.2.6. Short-Term Stability

The PGZ-NPs were analyzed for their stability at 4 °C and 25 °C by light backscattering and transmission profiles using Turbiscan[®] Lab Formulation (Toulouse, France). A glass measurement cell was filled with 20 mL of formulation. The radiation source was a pulsed near-infrared light and was received by transmission and backscattering detectors at angles of 90° and 4° from the incident beam, respectively. Data were analyzed once a month for 24 h at 1-h intervals over a period of three months.

2.2.7. Statistical Analysis

The statistical analysis of the permeation studies was made using GraphPad Prism[®] 6.0 (GraphPad Software Inc., San Diego, CA, USA). The values were expressed as averages \pm SEM. The software packages Haake RheoWin[®] Job Manager V.3.3 and RheoWin[®] Data Manager V.3.3 (Thermo Electron Corporation, Karlsruhe, Germany) were used to carry out the testing and analysis of the obtained rheological data, respectively.

3. Results

3.1. Physicochemical Characterization

After previous factorial design, the PGZ-NPs showed a size around 160.0 ± 1.3 nm with PI values in the range of monodisperse systems (PI < 0.1) and high association efficiency ($\approx 92\%$). Moreover, the ZP was -13.9 mV, which is indicative of the stability of these systems [41].

3.2. Ex Vivo Permeation Studies

Figure 1a shows the permeation profile of PGZ (μg) from NPs in buccal, sublingual, nasal, and intestinal mucosae. This revealed that the cumulative permeated amount of PGZ after 6 h of assay was higher in intestinal mucosa with a value of 15.40 μg , while buccal, sublingual, and nasal mucosae

presented values of 5.06, 6.20, and 6.80 μg , respectively. The permeability parameters were calculated for all mucosae studied except intestinal mucosa because it did not show a linear stretch, which is necessary to calculate these parameters (Figure 1b).

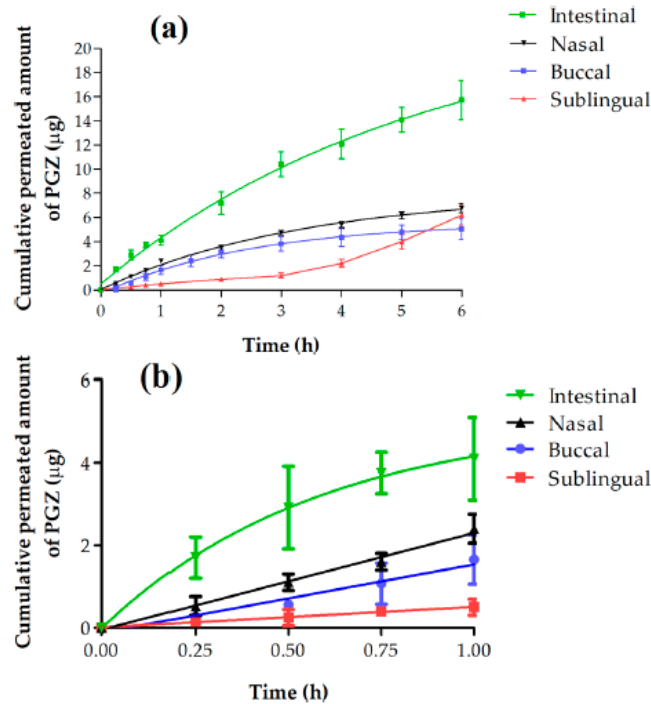


Figure 1. (a) Cumulative permeated amount of Pioglitazone (PGZ) within 6 h; (b) Cumulative permeated amount of PGZ within 1 h.

3.2.1. Retained Amount of PGZ

The NPs showed Significant Statistical Differences (SSD) ($p < 0.05$) in all tissues, except buccal between sublingual mucosa (Figure 2). The highest retained amounts were obtained by sublingual and buccal mucosa with median values of 158.45 and 132.66 ($\mu\text{g PGZ/g tissue/cm}^2$), respectively. The nasal mucosa presented values of 129.81 ($\mu\text{g PGZ/g tissue/cm}^2$). The intestinal mucosa showed a low retained amount of PGZ compared with the other mucosae. The percentage of recovery calculated experimentally for each tissue were: buccal 34.84%; sublingual 32.73%; nasal 37.52%; intestinal 14.87%.

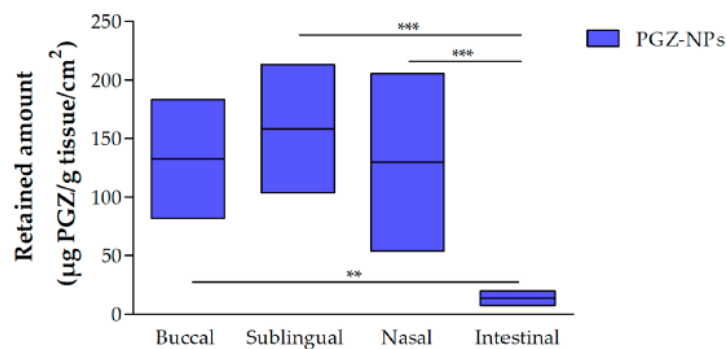


Figure 2. Retained amount of PGZ from nanoparticles (NPs) in different tissues. ($n = 6$). One-way analysis of variance (ANOVA) with Tukey's multiple comparison tests were performed to assess the statistical significance ($p < 0.05$).

3.2.2. Permeation and Predictions Parameters Data

Table 2 shows the permeation and prediction parameters of PGZ from NPs through different mucosae. It was observed that J_{ss} and K_p showed similar values between all studied mucosae without SSD ($p > 0.05$). Concerning Tl, sublingual mucosa showed a value of 175.60 min, followed by buccal and nasal mucosae with values of 41.21 and 3.0 min, respectively. These results revealed an SSD between nasal mucosa with respect to buccal and sublingual mucosa, suggesting that nasal administration makes possible the achievement of state of steady equilibrium in the shortest time. With respect to the other mucosae studied, nasal mucosa also showed an SSD with the lowest values of vehicle/tissue partition coefficient (P1) and the highest values of diffusion coefficient (P2) and C_{ss} .

Table 2. Permeations and prediction parameters of different tissues with PGZ-NPs.

Permeation and Prediction Parameters	Buccal ^a	Sublingual ^b	Nasal ^c
J_{ss} ($\mu\text{g}/(\text{min}/\text{cm}^2)) \times 10^2$	4.28 (2.83–5.72)	5.19 (4.91–5.50)	5.19 (4.91–5.50)
K_p ($\text{cm}/\text{min}) \times 10^5$	4.28 (2.83–5.72)	5.19 (4.91–5.50)	5.20 (4.92–5.50)
Tl (min)	41.21 (27.27–55.15)	175.60 ^a (174.30–179.50)	3.00 ^{a,b} (1.08–5.00)
P_1 (cm) $\times 10^4$	93.74 (93.73–93.74)	547.37 ^a (514.35–592.73)	8.85 ^{a,b} (3.37–16.51)
P_2 (min^{-1})	0.004 (0.003–0.006)	0.0009 (0.0009–0.0009)	0.05 ^{a,b} (0.03–0.15)
Mean Transit Time, MTT (day)	5.80 (3.84–7.77)	4.54 (4.31–4.77)	4.17 ^a (3.95–4.41)
C_{ss} ($\mu\text{g}/\text{mL}$)	0.02 (0.01–0.03)	0.02 (0.02–0.02)	0.20 ^{a,b} (0.19–0.21)

^{a,b,c} Results are expressed by median, minimum, and maximum ($n = 6$). One-way analysis of variance (ANOVA) with Tukey's multiple comparison tests were performed to assess the statistical significance between each mucosa with respect to PGZ-NPs at ($p < 0.05$).

The value of C_{ss} in the nasal mucosa was 10 times greater than the other mucosae studied, signifying that PGZ administered through this route would achieved greater concentrations of PGZ in the bloodstream (relative to the other tissues).

3.3. Rheological Study

Flow and viscosity curves are depicted in Figure 3. Table 3 displays the results obtained from the rheological characterization of PGZ-NPs. The flow curves indicated no thixotropic behavior in the system since the rheograms did not exhibit hysteresis loop. The mathematical model that provided the best overall match of experimental data based on the highest correlation coefficient of regression (r) was the Newton model. PGZ-NPs showed a viscosity of 1.110 mPa·s.

Table 3. Rheological properties of PGZ-NPs.

Rheologic Parameters	PGZ-NPs
Viscosity (mPa·s) at 50 s^{-1} and 25 °C	$1.110 \pm 2.362 \times 10^{-2}$
Flow behavior (best fitting model)	Newtonian Newton * ($r = 0.9993$)

*: After discarding the first and last data.

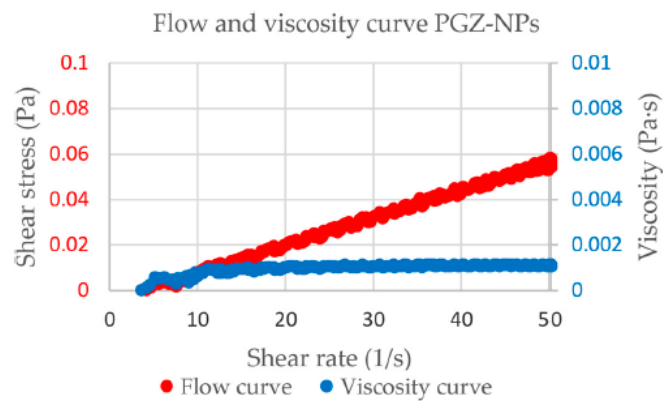


Figure 3. Rheograms obtained for the PGZ-NPs.

3.4. Short-Term Stability

Figure 4a,b show the backscattering profiles of PGZ-NPs at 4 °C and at 25 °C for three months. In both profiles it was observed that after the first month there was an increment of sedimentation and after the second month the samples became unstable with a difference of backscattering above 10%.

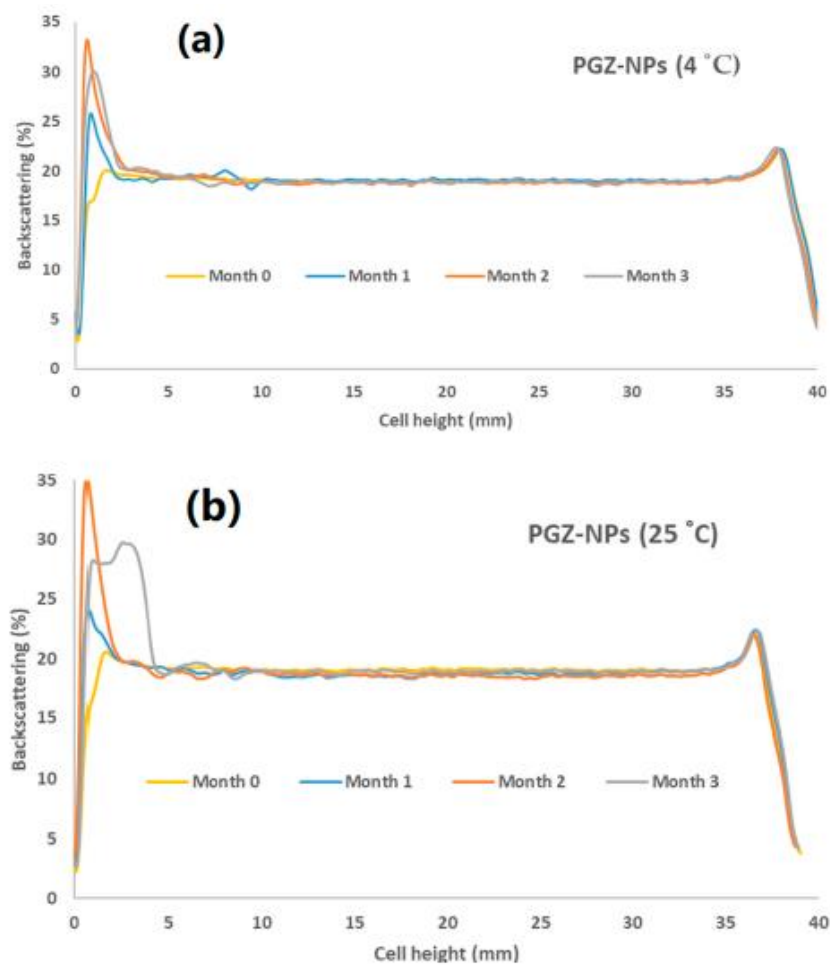


Figure 4. Stability of PGZ-NPs: (a) 4 °C and (b) 25 °C.

4. Discussion

Currently, AD remains incurable and the pharmacological options have notable disadvantages such as conventional dosage forms exclusively for oral administration, which then cause discomfort among geriatric patients who have difficulty swallowing; being limited to only treat the cognitive symptoms; first-pass metabolism; and ineffective ability to cross the blood-brain barrier (BBB) [42,43]. Recently, the anti-inflammatory and neuroprotective effects of PPAR- γ ligands coupled with the advantages of nanotechnology-based drug delivery systems have come to represent a breadth of new possibilities in the treatment of AD [5,44,45]. By taking into account the fact that PGZ metabolizes in the liver and has low solubility, which limits the absorption rate, it can be concluded that it is necessary to optimize the delivery of the therapeutic product to the brain by designing a more appropriate drug delivery system and determining the most effective administration route. The PGZ-loaded PLGA-PEG NPs obtained in this study represent a promising strategy to facilitate the delivery of drugs to the brain. The physicochemical evaluation of this formulation showed favorable properties for the penetration of the drug across the blood-brain barrier (BBB) and the delivery of the drug in a controlled and sustained manner. Such advantages include small size (160.0 ± 1.3 nm), high association efficiency ($\approx 92\%$), and good stability [41,46]. In addition, NPs are generally advantageous because of their good biocompatibility, capacity to adjust drug release, and remarkable enhancement of efficacy and bioavailability [29,47,48]. The surface coating of PNPs with PEG provides an increase in circulation lifetime and an improvement of drug delivery across the BBB [49]. The ability of NPs to cross biological membranes is influenced by size, shape, NP composition, and surface properties. The exact mechanism by which NPs cross lipid bilayers remains unknown because of the complexity of both NPs and cell membranes. Nanotoxicity and cell plasma membrane disruptions are concerns of NP designers [50,51]. Hypotheses such as endocytosis, the formation of nanoscale membrane holes, or membrane translocation have been proposed. Some studies support the idea that NPs cross the cell membrane via adhesive or diffusive mechanisms [51]. Clearly, further studies are required in order to assure the success of biomedical applications of these delivery systems.

The *ex vivo* permeation studies of PGZ-loaded PLGA-PEG NPs through different mucosae (Figure 1a) revealed that intestinal mucosa had the highest amount of drug permeated at 6 h of the assay ($15.40 \mu\text{g}$) followed by nasal ($6.80 \mu\text{g}$), sublingual ($6.20 \mu\text{g}$), and buccal ($5.06 \mu\text{g}$) mucosa. The high permeability of this formulation in all mucosae is likely due to its nano-size structure and lipophilic nature, which confers larger specific surface area and has a permeation-enhancing effect [52]. Although the amount of PGZ permeated through the intestinal mucosa was higher, it is important to consider that this route has notable disadvantages in the drug delivery to the brain, including first-pass metabolism. Gastrointestinal drug degradation constitutes one of the causes of the poor bioavailability of therapeutic agents using this route [53].

The permeation and prediction parameters (Table 2) were calculated for all of the mucosae studied except for intestinal mucosa, because the permeation profile of this mucosa did not show a linear stretch necessary for the calculation of these parameters. The values of J_{ss} and K_p obtained for buccal, sublingual, and nasal mucosa were similar without SSD ($p > 0.05$). However, T_l for nasal mucosa (3 min) was significantly lower with respect to buccal (175.60 min) and sublingual mucosae (41.21 min), which indicates a rapid onset of action using the nasal route [54]. Moreover, the estimated vehicle/tissue partition coefficient (P_1) for nasal mucosa was lower compared with that of other mucosae, whereas the diffusion coefficient (P_2) and C_{ss} were higher, demonstrating that PGZ permeation is more favorable in this tissue and consequently that there is greater probability to deliver effective concentrations of PGZ at the site of action more quickly [55]. These results suggest that nasal mucosa represents an attractive and non-invasive method for drug delivery to the brain [56]. Nasal physiology and histology is characterized by high vascularization, large absorptive surface area, the avoidance of first-pass metabolism, and a porous and endothelial membrane, all of which provide important advantages to deliver drugs to the central nervous system (CNS) [57]. Furthermore, the nasal passage offers direct transport from the nasal cavity to the brain and is painless and uncomplicated for drug

administration [58]. The correct formulation of the dosage form is essential for pharmacological therapy by intranasal administration with the aim of avoiding the elimination of the drug through nasal mucociliary clearance [45]. PGZ-loaded PLGA-PEG NPs as a drug delivery system provide several advantages such as rapid drug permeation, drug protection, and prolonged retention at the site of drug absorption for a suitable period of time [55,59].

The rheogram of PGZ-NPs (Figure 3) shows a linear relationship between the shear stress and the strain rate, which is characteristic of Newtonian behavior [60]. Considering the nasal mucosa as the best mucosa for drug administration, this rheology and the low viscosity obtained (about 1 mPa·s, similar to the water) are ideal for nasal spray application of the formulation [61].

For the stability assay, the PGZ-NPs showed incremental yet stable sedimentation up to the second month, after which the sample became unstable with a difference of backscattering exceeding 10% (Figure 4). This instability of particles is due to the aggregation phenomena and the limited stability of polymeric NPs in aqueous suspension is well known. These results indicate that improved long-term stability could be attained by the removal of water from the solution by lyophilization or a spray-drying technique [62,63].

5. Conclusions

The results obtained showed that PGZ-NPs have appropriate physicochemical characteristics to facilitate their permeability through different types of mucosa. According to the permeations and prediction parameters of these delivery systems, nasal mucosa constitutes the most convenient administration route to treat AD due to the enhanced drug permeation in this tissue, resulting in a greater likelihood of achieving effective concentrations of the drug at the site of action.

Acknowledgments: This work was supported by the Coordination for the Improvement of Higher Education Personnel (CAPES)—Brazil and Spanish Ministry of Science and Innovation (MAT2014-59134R). Marcelle Silva-Abreu also acknowledges her Ph.D. scholarship—CAPES, Brazil. The authors would like to thank the University of Barcelona for the financial support to cover the cost of open access publication. Thanks to María-José Fábrega for the design of the graphical abstract. Additionally, thanks to Jonathan Proctor for his review of the use of the English language.

Author Contributions: Marcelle Silva-Abreu carried out all the experiments, analyzed the data/results and wrote the paper; Lupe Carolina Espinoza analyzed the results and helped write the paper; Lyda Halbaut analyzed the rheological studies; Marta Espina examined the statistical analysis; María Luisa García corrected and analyzed the physicochemical characterization; and Ana Cristina Calpena conceived and designed all the experiments.

Conflicts of Interest: The authors declare no conflict of interest.

References

1. Alzheimer's Association. 2016 Alzheimer's disease facts and figures. *Alzheimer Dement. J. Alzheimer Assoc.* **2016**, *12*, 459–509. [[CrossRef](#)]
2. El Kadmiri, N.; Said, N.; Slassi, I.; El Moutawakil, B.; Nadifi, S. Biomarkers for Alzheimer Disease: Classical and Novel Candidates' Review. *Neuroscience* **2018**, *370*, 181–190. [[CrossRef](#)] [[PubMed](#)]
3. Wilkinson, D.; Schindler, R.; Schwam, E.; Waldemar, G.; Jones, R.W.; Gauthier, S.; Lopez, O.L.; Cummings, J.; Xu, Y.; Feldman, H.H. Effectiveness of donepezil in reducing clinical worsening in patients with mild-to-moderate alzheimer's disease. *Dement. Geriatr. Cogn. Disord.* **2009**, *28*, 244–251. [[CrossRef](#)] [[PubMed](#)]
4. Kumar, K.; Kumar, A.; Keegan, R.M.; Deshmukh, R. Recent advances in the neurobiology and neuropharmacology of Alzheimer's disease. *Biomed. Pharmacother.* **2018**, *98*, 297–307. [[CrossRef](#)] [[PubMed](#)]
5. Yao, L.; Li, K.; Zhang, L.; Yao, S.; Piao, Z.; Song, L. Influence of the Pro12Ala polymorphism of PPAR- γ on age at onset and sRAGE levels in Alzheimer's disease. *Brain Res.* **2009**, *1291*, 133–139. [[CrossRef](#)] [[PubMed](#)]
6. Combarros, O.; Rodriguez-Rodriguez, E.; Mateo, I.; Vazquez-Higuera, J.L.; Infante, J.; Berciano, J.; Sanchez-Juan, P. APOE dependent-association of PPAR- γ genetic variants with Alzheimer's disease risk. *Neurobiol. Aging* **2011**, *32*, 547.e1–547.e6. [[CrossRef](#)] [[PubMed](#)]

7. Radenkovic, M. Pioglitazone and Endothelial Dysfunction: Pleiotropic Effects and Possible Therapeutic Implications. *Sci. Pharm.* **2014**, *82*, 709–721. [[CrossRef](#)] [[PubMed](#)]
8. Suzuki, S.; Mori, Y.; Nagano, A.; Naiki-Ito, A.; Kato, H.; Nagayasu, Y.; Kobayashi, M.; Kuno, T.; Takahashi, S. Pioglitazone, a Peroxisome Proliferator-Activated Receptor γ Agonist, Suppresses Rat Prostate Carcinogenesis. *Int. J. Mol. Sci.* **2016**, *17*, 2071. [[CrossRef](#)] [[PubMed](#)]
9. Jia, C.; Huan, Y.; Liu, S.; Hou, S.; Sun, S.; Li, C.; Liu, Q.; Jiang, Q.; Wang, Y.; Shen, Z. Effect of Chronic Pioglitazone Treatment on Hepatic Gene Expression Profile in Obese C57BL/6J Mice. *Int. J. Mol. Sci.* **2015**, *16*, 12213–12229. [[CrossRef](#)] [[PubMed](#)]
10. Park, H.J.; Park, H.S.; Lee, J.U.; Bothwell, A.L.; Choi, J.M. Sex-Based Selectivity of PPAR γ Regulation in Th1, Th2, and Th17 Differentiation. *Int. J. Mol. Sci.* **2016**, *17*, 1347. [[CrossRef](#)] [[PubMed](#)]
11. Tobiasova, Z.; Zhang, L.; Yi, T.; Qin, L.; Manes, T.D.; Kulkarni, S.; Lorber, M.I.; Rodriguez, F.C.; Choi, J.M.; Tellides, G.; et al. Peroxisome proliferator-activated receptor- γ agonists prevent in vivo remodeling of human artery induced by alloreactive T cells. *Circulation* **2011**, *124*, 196–205. [[CrossRef](#)] [[PubMed](#)]
12. Fakhfour, G.; Ahmadiani, A.; Rahimian, R.; Grolla, A.A.; Moradi, F.; Haeri, A. WIN55212-2 attenuates amyloid-beta-induced neuroinflammation in rats through activation of cannabinoid receptors and PPAR- γ pathway. *Neuropharmacology* **2012**, *63*, 653–666. [[CrossRef](#)] [[PubMed](#)]
13. El-Zaher, A.A.; Elkady, E.F.; Elwy, H.M.; Saleh, M. Simultaneous spectrophotometric determination of glibenclamide and pioglitazone in binary mixture and combined dosage form using chemometric-assisted techniques. *Spectrochim. Acta Part A Mol. Biomol. Spectrosc.* **2017**, *182*, 175–182. [[CrossRef](#)] [[PubMed](#)]
14. Klotz, L.; Burgdorf, S.; Dani, I.; Saijo, K.; Flossdorf, J.; Hucke, S.; Alferink, J.; Novak, N.; Beyer, M.; Mayer, G.; et al. The nuclear receptor PPAR γ selectively inhibits Th17 differentiation in a T cell-intrinsic fashion and suppresses CNS autoimmunity. *J. Exp. Med.* **2009**, *206*, 2079–2089. [[CrossRef](#)] [[PubMed](#)]
15. Silva-Abreu, M.; Espinoza, L.C.; Rodriguez-Lagunas, M.J.; Fabrega, M.J.; Espina, M.; Garcia, M.L.; Calpena, A.C. Human Skin Permeation Studies with PPAR γ Agonist to Improve Its Permeability and Efficacy in Inflammatory Processes. *Int. J. Mol. Sci.* **2017**, *18*, 2548. [[CrossRef](#)] [[PubMed](#)]
16. Heneka, M.T.; Sastre, M.; Dumitrescu-Ozimek, L.; Hanke, A.; Dewachter, I.; Kuiperi, C.; O'Banion, K.; Klockgether, T.; Van Leuven, F.; Landreth, G.E. Acute treatment with the PPAR γ agonist pioglitazone and ibuprofen reduces glial inflammation and A β 1–42 levels in APPV717I transgenic mice. *Brain* **2005**, *128*, 1442–1453. [[CrossRef](#)] [[PubMed](#)]
17. Sato, T.; Hanyu, H.; Hirao, K.; Kanetaka, H.; Sakurai, H.; Iwamoto, T. Efficacy of PPAR- γ agonist pioglitazone in mild Alzheimer disease. *Neurobiol. Aging* **2011**, *32*, 1626–1633. [[CrossRef](#)] [[PubMed](#)]
18. Hyma, P.; Abbulu, K. Formulation and characterisation of self-microemulsifying drug delivery system of pioglitazone. *Biomed. Prev. Nutr.* **2013**, *3*, 345–350. [[CrossRef](#)]
19. He, W.; Li, Y.; Zhang, R.; Wu, Z.; Yin, L. Gastro-floating bilayer tablets for the sustained release of metformin and immediate release of pioglitazone: Preparation and in vitro/in vivo evaluation. *Int. J. Pharm.* **2014**, *476*, 223–231. [[CrossRef](#)] [[PubMed](#)]
20. Ahad, A.; Al-Saleh, A.A.; Akhtar, N.; Al-Mohizea, A.M.; Al-Jenoobi, F.I. Transdermal delivery of antidiabetic drugs: Formulation and delivery strategies. *Drug Discov. Today* **2015**, *20*, 1217–1227. [[CrossRef](#)] [[PubMed](#)]
21. Jug, M.; Hafner, A.; Lovric, J.; Kregar, M.L.; Pepic, I.; Vanic, Z.; Cetina-Cizmek, B.; Filipovic-Grcic, J. An overview of in vitro dissolution/release methods for novel mucosal drug delivery systems. *J. Pharm. Biomed. Anal.* **2018**, *147*, 350–366. [[CrossRef](#)] [[PubMed](#)]
22. Fonseca-Santos, B.; Chorilli, M. An overview of polymeric dosage forms in buccal drug delivery: State of art, design of formulations and their in vivo performance evaluation. *Mater. Sci. Eng. C* **2017**. [[CrossRef](#)] [[PubMed](#)]
23. Fonseca-Santos, B.; Gremiao, M.P.; Chorilli, M. Nanotechnology-based drug delivery systems for the treatment of Alzheimer's disease. *Int. J. Nanomed.* **2015**, *10*, 4981–5003. [[CrossRef](#)] [[PubMed](#)]
24. Sosnik, A.; das Neves, J.; Sarmiento, B. Mucoadhesive polymers in the design of nano-drug delivery systems for administration by non-parenteral routes: A review. *Prog. Polym. Sci.* **2014**, *39*, 2030–2075. [[CrossRef](#)]
25. Lee, G.H.; Lee, S.J.; Jeong, S.W.; Kim, H.C.; Park, G.Y.; Lee, S.G.; Choi, J.H. Antioxidative and antiinflammatory activities of quercetin-loaded silica nanoparticles. *Colloids Surf. B Biointerfaces* **2016**, *143*, 511–517. [[CrossRef](#)] [[PubMed](#)]
26. Desmet, E.; Van Gele, M.; Lambert, J. Topically applied lipid- and surfactant-based nanoparticles in the treatment of skin disorders. *Expert Opin. Drug Deliv.* **2016**, *14*, 109–122. [[CrossRef](#)] [[PubMed](#)]

27. Crucho, C.I.C.; Barros, M.T. Polymeric nanoparticles: A study on the preparation variables and characterization methods. *Mater. Sci. Eng. C Mater. Biol. Appl.* **2017**, *80*, 771–784. [[CrossRef](#)] [[PubMed](#)]
28. Jin, K.; Luo, Z.; Zhang, B.; Pang, Z. Biomimetic nanoparticles for inflammation targeting. *Acta Pharm. Sin. B* **2017**, *8*, 23–33. [[CrossRef](#)]
29. El-Say, K.M.; El-Sawy, H.S. Polymeric nanoparticles: Promising platform for drug delivery. *Int. J. Pharm.* **2017**, *528*, 675–691. [[CrossRef](#)] [[PubMed](#)]
30. Mansuri, S.; Kesharwani, P.; Jain, K.; Tekade, R.K.; Jain, N.K. Mucoadhesion: A promising approach in drug delivery system. *React. Funct. Polym.* **2016**, *100*, 151–172. [[CrossRef](#)]
31. Labarre, D. The Interactions between Blood and Polymeric Nanoparticles Depend on the Nature and Structure of the Hydrogel Covering the Surface. *Polymers* **2012**, *4*, 986–996. [[CrossRef](#)]
32. Shen, Z.; Nieh, M.-P.; Li, Y. Decorating Nanoparticle Surface for Targeted Drug Delivery: Opportunities and Challenges. *Polymers* **2016**, *8*, 83. [[CrossRef](#)]
33. Ozturk-Atar, K.; Eroglu, H.; Calis, S. Novel advances in targeted drug delivery. *J. Drug Target.* **2017**, 1–10. [[CrossRef](#)] [[PubMed](#)]
34. Lautenschlager, C.; Schmidt, C.; Fischer, D.; Stallmach, A. Drug delivery strategies in the therapy of inflammatory bowel disease. *Adv. Drug Deliv. Rev.* **2014**, *71*, 58–76. [[CrossRef](#)] [[PubMed](#)]
35. Fessi, H.; Puisieux, F.; Devissaguet, J.; Ammoury, N.; Benita, S. Nanocapsule formation by interfacial polymer deposition following solvent displacement. *Int. J. Pharm.* **1989**, *55*, R1–R4. [[CrossRef](#)]
36. Clogston, J.; Patri, A. Zeta potential measurement. In *Characterization of Nanoparticles Intended for Drug Delivery*; McNeil, S.E., Ed.; Humana Press: Totowa, NJ, USA, 2011; pp. 63–70.
37. Kapoor, M.; Cloyd, J.C.; Siegel, R.A. A review of intranasal formulations for the treatment of seizure emergencies. *J. Control. Release* **2016**, *237*, 147–159. [[CrossRef](#)] [[PubMed](#)]
38. Christrup, L.; Lundorff, L.; Werner, M. Novel formulations and routes of administration for opioids in the treatment of breakthrough pain. *Therapy* **2009**, *6*, 695–706. [[CrossRef](#)]
39. Wittayalertpanya, S.; Chompootaweep, S.; Thaworn, N. The Pharmacokinetics of Pioglitazone in Thai Healthy Subjects. *J. Med. Assoc. Thail.* **2006**, *89*, 2116–2122.
40. Schramm, G. *A Practical Approach to Rheology and Rheometry*, 2nd ed.; Gebrueder HAAKE: Karlsruhe, Germany, 1994.
41. Silva-Abreu, M.; Calpena, A.C.; Espina, M.; Silva, A.M.; Gimeno, A.; Egea, M.A.; Garcia, M.L. Optimization, Biopharmaceutical Profile and Therapeutic Efficacy of Pioglitazone-loaded PLGA-PEG Nanospheres as a Novel Strategy for Ocular Inflammatory Disorders. *Pharm. Res.* **2018**, *35*, 11. [[CrossRef](#)] [[PubMed](#)]
42. Sozio, P.; Cerasa, L.S.; Marinelli, L.; Di Stefano, A. Transdermal donepezil on the treatment of Alzheimer's disease. *Neuropsychiatr. Dis. Treat.* **2012**, *8*, 361–368. [[CrossRef](#)] [[PubMed](#)]
43. Ulep, M.G.; Saraon, S.K.; McLea, S. Alzheimer Disease. *J. Nurse Pract.* **2017**. [[CrossRef](#)]
44. Saraiva, C.; Praca, C.; Ferreira, R.; Santos, T.; Ferreira, L.; Bernardino, L. Nanoparticle-mediated brain drug delivery: Overcoming blood-brain barrier to treat neurodegenerative diseases. *J. Control. Release* **2016**, *235*, 34–47. [[CrossRef](#)] [[PubMed](#)]
45. Kumar, B.; Jalodia, K.; Kumar, P.; Gautam, H.K. Recent advances in nanoparticle-mediated drug delivery. *J. Drug Deliv. Sci. Technol.* **2017**, *41*, 260–268. [[CrossRef](#)]
46. Tapeinos, C.; Battaglini, M.; Ciofani, G. Advances in the design of solid lipid nanoparticles and nanostructured lipid carriers for targeting brain diseases. *J. Control. Release* **2017**, *264*, 306–332. [[CrossRef](#)] [[PubMed](#)]
47. Kreuter, J. Drug delivery to the central nervous system by polymeric nanoparticles: What do we know? *Adv. Drug Deliv. Rev.* **2014**, *71*, 2–14. [[CrossRef](#)] [[PubMed](#)]
48. Han, J.; Zhao, D.; Li, D.; Wang, X.; Jin, Z.; Zhao, K. Polymer-Based Nanomaterials and Applications for Vaccines and Drugs. *Polymers* **2018**, *10*, 31. [[CrossRef](#)]
49. Wen, M.M.; El-Salamouni, N.S.; El-Refaie, W.M.; Hazzah, H.A.; Ali, M.M.; Tosi, G.; Farid, R.M.; Blanco-Prieto, M.J.; Billa, N.; Hanafy, A.S. Nanotechnology-based drug delivery systems for Alzheimer's disease management: Technical, industrial, and clinical challenges. *J. Control. Release* **2017**, *245*, 95–107. [[CrossRef](#)] [[PubMed](#)]
50. Nakamura, H.; Watano, S. Direct Permeation of Nanoparticles across Cell Membrane: A Review. *KONA Powder Part. J.* **2018**, *35*, 49–65. [[CrossRef](#)]

51. Leroueil, P.R.; Hong, S.; Mecke, A.; Baker, J.R., Jr.; Orr, B.G.; Banaszak Holl, M.M. Nanoparticle interaction with biological membranes: Does nanotechnology present a Janus face? *Acc. Chem. Res.* **2007**, *40*, 335–342. [[CrossRef](#)] [[PubMed](#)]
52. Patel, R.R.; Chaurasia, S.; Khan, G.; Chaubey, P.; Kumar, N.; Mishra, B. Cromolyn sodium encapsulated PLGA nanoparticles: An attempt to improve intestinal permeation. *Int. J. Biol. Macromol.* **2016**, *83*, 249–258. [[CrossRef](#)] [[PubMed](#)]
53. Dunnhaupt, S.; Barthelmes, J.; Hombach, J.; Sakloetsakun, D.; Arkhipova, V.; Bernkop-Schnurch, A. Distribution of thiolated mucoadhesive nanoparticles on intestinal mucosa. *Int. J. Pharm.* **2011**, *408*, 191–199. [[CrossRef](#)] [[PubMed](#)]
54. Fortuna, A.; Alves, G.; Serralheiro, A.; Sousa, J.; Falcao, A. Intranasal delivery of systemic-acting drugs: Small-molecules and biomacromolecules. *Eur. J. Pharm. Biopharm.* **2014**, *88*, 8–27. [[CrossRef](#)] [[PubMed](#)]
55. Khan, A.R.; Liu, M.; Khan, M.W.; Zhai, G. Progress in brain targeting drug delivery system by nasal route. *J. Control. Release* **2017**, *268*, 364–389. [[CrossRef](#)] [[PubMed](#)]
56. Lochhead, J.J.; Thorne, R.G. Intranasal delivery of biologics to the central nervous system. *Adv. Drug Deliv. Rev.* **2012**, *64*, 614–628. [[CrossRef](#)] [[PubMed](#)]
57. Tuitou, E.; Illum, L. Nasal drug delivery. *Drug Deliv. Transl. Res.* **2013**, *3*, 1–3. [[CrossRef](#)] [[PubMed](#)]
58. Pardeshi, C.V.; Belgamwar, V.S. Direct nose to brain drug delivery via integrated nerve pathways bypassing the blood-brain barrier: An excellent platform for brain targeting. *Expert Opin. Drug Deliv.* **2013**, *10*, 957–972. [[CrossRef](#)] [[PubMed](#)]
59. Mogoşanu, G.D.; Grumezescu, A.M.; Bejenaru, C.; Bejenaru, L.E. Polymeric protective agents for nanoparticles in drug delivery and targeting. *Int. J. Pharm.* **2016**, *510*, 419–429. [[CrossRef](#)] [[PubMed](#)]
60. Abdelhalim, M.A. The rheological properties of different GNPs. *Lipids Health Dis.* **2012**, *11*, 14. [[CrossRef](#)] [[PubMed](#)]
61. Fernandez-Campos, F.; Clares Naveros, B.; Lopez Serrano, O.; Alonso Merino, C.; Calpena Campmany, A.C. Evaluation of novel nystatin nanoemulsion for skin candidosis infections. *Mycoses* **2013**, *56*, 70–81. [[CrossRef](#)] [[PubMed](#)]
62. Abrego, G.; Alvarado, H.L.; Egea, M.A.; Gonzalez-Mira, E.; Calpena, A.C.; Garcia, M.L. Design of nanosuspensions and freeze-dried PLGA nanoparticles as a novel approach for ophthalmic delivery of pranoprofen. *J. Pharm. Sci.* **2014**, *103*, 3153–3164. [[CrossRef](#)] [[PubMed](#)]
63. Ramos Yacasi, G.R.; Garcia Lopez, M.L.; Espina Garcia, M.; Parra Coca, A.; Calpena Campmany, A.C. Influence of freeze-drying and γ -irradiation in preclinical studies of flurbiprofen polymeric nanoparticles for ocular delivery using d-(+)-trehalose and polyethylene glycol. *Int. J. Nanomed.* **2016**, *11*, 4093–4106. [[CrossRef](#)] [[PubMed](#)]



© 2018 by the authors. Licensee MDPI, Basel, Switzerland. This article is an open access article distributed under the terms and conditions of the Creative Commons Attribution (CC BY) license (<http://creativecommons.org/licenses/by/4.0/>).

3.4 Article 4

PPAR γ agonist-loaded PLGA-PEG nanocarriers as a potential treatment for Alzheimer's disease: *in vitro* and *in vivo* studies

Marcelle Silva-Abreu^{1,2}, Ana Cristina Calpena^{1,2}, Pol Andrés-Benito^{3,4}, Ester Aso^{3,4}, Ignacio A. Romero⁵, David Roig-Carles⁵, Radka Gromnicova⁵, Marta Espina^{1,2}, Isidre Ferrer^{3,4}, María Luisa García^{1,2} and David Male⁵

International Journal of Nanomedicine

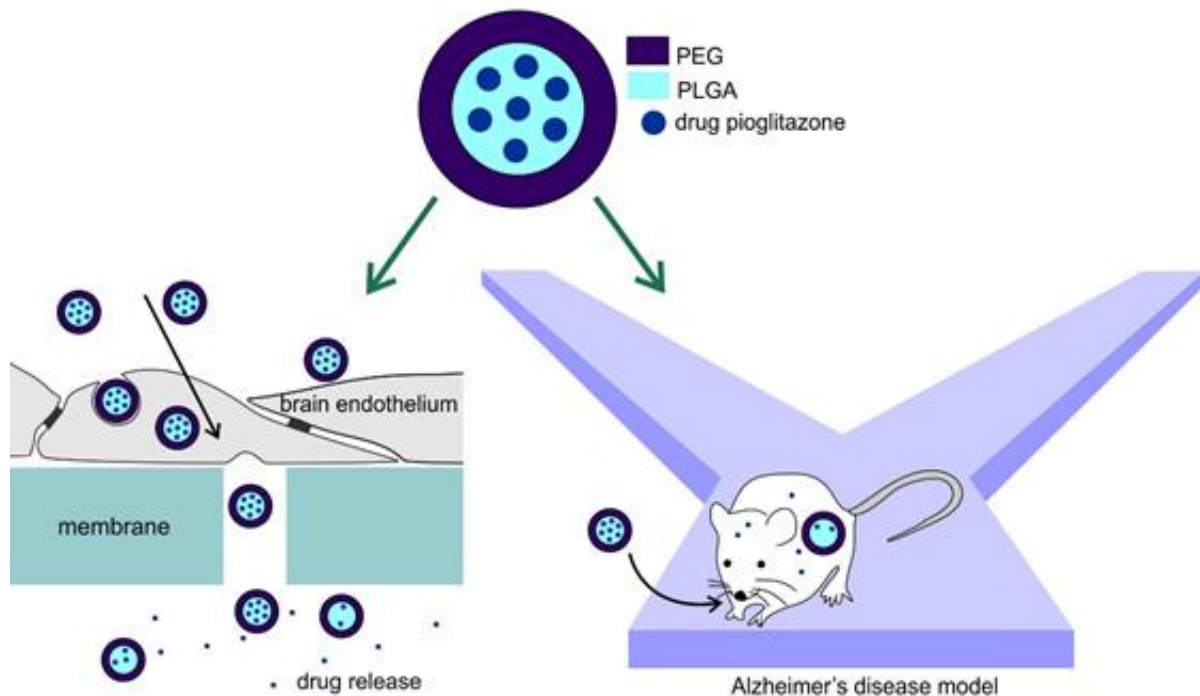
Year: 2018

ISSN: 1178-2013

IF: 4.370

Status: Accepted for publication

Graphical abstract



PPAR γ agonist-loaded PLGA-PEG nanocarriers as a potential treatment for Alzheimer's disease: *in vitro* and *in vivo* studies

Authors: Marcelle Silva-Abreu^{1,2}, Ana Cristina Calpena^{1,2}, Pol Andrés-Benito^{3,4}, Ester Aso^{3,4}, Ignacio A. Romero⁵, David Roig-Carles⁵, Radka Gromnicova⁵, Marta Espina^{1,2}, Isidre Ferrer^{3,4}, María Luisa García^{1,2}, David Male⁵

¹Department of Pharmacy, Pharmaceutical Technology and Physical Chemistry, Faculty of Pharmacy and Food Sciences, University of Barcelona, Barcelona 08028, Spain.

²Institute of Nanoscience and Nanotechnology (IN2UB). University of Barcelona, Barcelona, Spain.

³Servei d'Anatomia Patològica, IDIBELL-Hospital Universitari de Bellvitge, Universitat de Barcelona, L'Hospitalet de Llobregat, Spain.

⁴CIBERNED, Centro de Investigación Biomédica en Red de Enfermedades Neurodegenerativas, Instituto de Salud Carlos III, Spain.

⁵School of Life, Health and Chemical Sciences, Faculty of Science, The Open University, Walton Hall, Milton Keynes, MK7 6AA, United Kingdom.

Corresponding author: David Male. E-mail: David.Male@Open.ac.uk Tel.: +44 (0) 1908 659226

ABSTRACT

Objective: The first aim of this study was to develop a nanocarrier that can transport the PPAR γ agonist, pioglitazone (PGZ) across brain endothelium, and to examine the mechanism of nanoparticle transcytosis. The second aim was to determine whether these nanocarriers could successfully treat a mouse model of Alzheimer's disease.

Methods: PGZ-loaded nanoparticles (PGZ-NPs) were synthesized by the solvent displacement technique, following a factorial design using poly (lactic-co-glycolic acid) polyethylene glycol (PLGA-PEG). Transport of the carriers was assessed *in vitro* using a human brain endothelial cell line, cytotoxicity, fluorescence-tagged nanocarriers, FACS, confocal and transmission electron microscopy. The effectiveness of the treatment was

assessed in APP/PS1 mice, in a behavioural assay and by measuring cortical deposition of β -amyloid.

Results: Incorporation of PGZ into the carriers promoted 50x greater uptake into brain endothelium compared with free drug and the carriers showed a delayed release profile of PGZ *in vitro*. At the doses used the nanocarriers were not toxic for the endothelial cells, nor did they alter permeability of the blood-brain barrier model. Electron microscopy indicated that the nanocarriers were transported from the apical to basal surface of the endothelium by vesicular transcytosis. An efficacy test carried out in APP/PS1 transgenic mice showed a reduction of memory deficit in mice chronically treated with PGZ-NPs. Deposition of β -amyloid in the cerebral cortex, measured by immunohistochemistry and image analysis was correspondingly reduced.

Conclusions: PLGA-PEG nanocarriers cross brain endothelium by transcytosis, and can be loaded with a pharmaceutical agent, to effectively treat a mouse model of Alzheimer's disease.

Keywords: Nanoparticle; Alzheimer's disease; Blood brain barrier; Brain endothelium; Pioglitazone; Drug delivery systems; APP/PS1 transgenic mouse.

Introduction

Alzheimer's disease (AD) is a multifactorial brain disorder prevalent in elderly people.^{1,2} It is characterized by cognitive impairment, synaptic failure, aggregates of amyloid-beta ($A\beta$) and intraneuronal neurofibrillary tangles.³⁻⁵ However, AD is also referred to as a degenerative metabolic disease that is associated with physiological alterations such as hypercholesterolemia, metabolic syndrome, hypertension and diabetes type-2⁶, a condition identified as a risk factor for the development of AD.

Pioglitazone (PGZ) (5-[[4-[2-(5-ethylpyridin-2-yl)ethoxy]phenyl]methyl]-1,3-thiazolidine-2,4-dione), an agonist of the peroxisome proliferator-activated receptor (PPAR γ), is a thiazolidinedione which is used for the treatment of type-2 diabetes. The PPAR γ receptors have various functions including anti-angiogenic, antifibrotic, anti-inflammatory and anti-tumor effects.⁷⁻¹⁰ PGZ is also neuroprotective in models of neurodegenerative disorders¹⁰, highlighting PPAR γ agonists as a promising treatment for AD.¹¹ Thus, PGZ has been reported to reduce oxidative stress, normalize cerebral blood flow and glucose uptake, to increase neuronal activity, and exert positive effects on

cerebrovascular function in an animal model of AD.¹² Furthermore, treatment with PGZ produced a significantly lower risk of dementia over the 5-year follow-up period, in diabetic patients treated with PGZ compared with those who were not treated.¹³

Drug delivery to the brain is a challenge for the treatment of neurological disorders. The blood-brain barrier (BBB) is a physical interface between the central nervous system (CNS) and the peripheral circulation that strictly controls which molecules can enter into the brain parenchyma.¹⁴ Only lipophilic molecules smaller than 400 Da can diffuse through the BBB; the passage of lipid insoluble or larger hydrophilic molecules is very limited.^{15,16} However, different strategies to increase the transport of drugs through the BBB include liposomes, solid lipid nanoparticles (NPs), gold NPs and polymeric NPs.¹⁷⁻¹⁹ These drug-loaded polymeric NPs are a potential alternative to improve drug delivery to the brain.

The properties of polymeric NPs include drug encapsulation, stability, high loading capacity for many agents and controlled drug release kinetics. Moreover, they can be easily modified with a variety of surface-attached ligands.^{20,21} Different polymers have been studied which deliver a variety of molecules through the BBB.²²⁻²⁴ However, poly (lactic-co-glycolic acid) (PLGA) systems have received great scientific interest due to their properties, specifically their biocompatibility and biodegradability. PLGA is an FDA-approved polymer used successfully for delivery to different tissues including the brain.^{19,25-27}

The attachment of specific ligands to the surface of NPs makes the delivery of drugs to CNS more targeted and may enhance the limited BBB penetration of therapeutic compounds. For instance, polyethylene glycol (PEG) can functionalize the NPs to increase their plasma residence time, preventing their removal by mononuclear phagocytes. This allows the NPs to remain longer in the circulation, thus increasing the probability for successful organ-targeted delivery and passage across the BBB.²⁸⁻³⁰

In this study, a formulation of PGZ-PLGA-PEG NPs was synthesized and their suitability for the treatment of AD was demonstrated. Physicochemical characterization, and *in vitro* studies with a human brain microvascular endothelial cell line (hCMEC/D3) were carried out. An *in vivo* study for cognitive evaluation after treatment was performed in male APP/PS1 mice and wild-type-like (WT) littermates.

Materials and Methods

Materials

PGZ was obtained from Capot Chemical (Hangzhou, P.R. China) and Diblock copolymer PLGA-PEG (Evonik Ind., Resomer[®] Select 5050 DLG mPEG 5000 - 5 wt% PEG), was purchased from Evonik Corporation (Birmingham, USA). Rhodamine 6G (Rhod), 70kDA FITC-dextran and 24-well filter inserts (PET membrane, pore 1 μ m) were acquired from Sigma-Aldrich. The dialysis membrane MWCO 12,000–14,000 Da., was obtained from Medicell International Ltd. (London, UK). Trypsin-EDTA was purchased from Thermo Fisher (London, UK). Alamar Blue was obtained from Invitrogen Alfacene[®] (Portugal).

Methods

Optimization and Characterization of Nanoparticles

PGZ-NPs were obtained by the solvent displacement technique.³¹ The organic phase with PGZ (1 mg/ml) was solubilized in DMSO 5%, to which was added a mixture of PLGA-PEG (9.5 mg/ml) and acetone (5 ml). Once completely dissolved, the solution was added dropwise with moderate stirring into 10 ml of an aqueous solution of 1.16% Tw 80. The pH was adjusted to 4.5 with HCl 0.1 M. Then, the solvents were evaporated and the NP dispersion was concentrated to a final volume of 10 ml under reduced pressure.

The conditions for NP production were optimized in a factorial design²⁶ (Supplementary material: Figure S1). Three independent variables (PGZ, PLGA-PEG and tween-80 concentrations) and four dependent variables (average particle size (Z_{av}), polydispersity index (PI), zeta potential (ZP) and EE) were studied. A pH of 4.5 was kept constant for all the assays. A total of 16 experiments (8 factorial points, 6 axial points and 2 replicated centre points) for estimation of the pure error sum of squares were required using Statgraphics Plus 5.1 software.

The experimental responses were the results of the individual influence and interactions of the three independent variables. In the surface of response, a low concentration of PGZ and PLGA-PEG produced smaller NPs and consequently greater homogeneity of the formulation. The formulation with the most appropriate physicochemical characteristics to use in this study was selected.

Transmission Electronic Microscopy (TEM) was used to evaluate the morphology of PGZ-NPs. Before negative staining, copper grids were activated with UV light and samples were positioned on the grid surface, diluted in water (1:3) and negative stained with a 2% (v/v) uranyl acetate solution. After drying at room temperature, the samples were examined by TEM on a Jeol 1010 (Tec-nai Spirit TEM, FEI) at 80 kV.

The morphometric parameters (Z_{av} and PI) of PGZ-NPs were determined by photon correlation spectroscopy (PCS) (after 1:10 dilution in water) with a Zetasizer Nano ZS (Malvern instruments) at 25 °C. The surface charge or ZP, was calculated from electrophoretic mobility. The values are the mean \pm SD of at least three different batches.³²

The EE of PGZ-NPs was determined indirectly by measuring the concentration of the free drug in the dispersion medium. The non-entrapped drug was separated by a filtration/centrifugation technique (1:10 dilution) using Ultracell–100K (Amicon® Ultra; Millipore Corporation, Billerica, Massachusetts) centrifugal filter devices at 12,000 rpm for 15 minutes. The EE was calculated using equation (1):

$$EE(\%) = \frac{\text{Total amount of PGZ} - \text{Free amount of PGZ}}{\text{Total amount of PGZ}} \cdot 100 \quad (1)$$

Samples were evaluated by HPLC, using a validated analytical method.³³ The mobile phase was: acetonitrile, ammonium acetate 0.1 M and glacial acetic acid (75:25:1 v/v), with a flow of 0.7 ml/min and a volume of injection of 10 μ l. The reported values are the mean \pm SD ($n = 6$).

The morphologic and morphometric characteristics of the optimized PGZ-NPs were performed by TEM and dynamic light scattering (Figure S2).

Release profile

In vitro PGZ release studies from NPs were performed in vertical Franz diffusion cells, using membrane dialysis with MW 12 – 14 KDa cutoff under sink conditions²⁷ at $37.0 \pm 0.5^\circ\text{C}$ with moderate and continuous stirring. The PGZ-NPs and free drug at the

same concentration (1 mg/ml) were dissolved in DMSO and phosphate buffered saline (PBS) (60:40), receptor solution (RS) at pH 7.4 for 23 hours. At specific time intervals, a volume of 0.2 ml of the formulations was placed in the donor compartment and the receptor compartment was filled with the same volume of RS. Amounts of PGZ released were measured by HPLC. Values are reported as the mean \pm SD ($n = 3$). PGZ released at each time point was evaluated and data were fitted to different kinetic models³⁴ Akaike's information criterion (AIC) and coefficient of determination (r^2) were determined for each case as an indicator of the model's suitability for each dataset.³⁵

Syntheses of Rhodamine NPs

To evaluate the cellular uptake of NPs by hCMEC/D3, Rhodamine 6G (Rhod) was incorporated into the NPs. Rhod-NPs were synthesized by the same method as PGZ-NPs, but with addition of 100 μ g/ml Rhod in 500 μ l of methanol, mixed with 9.5 mg/ml PLGA-PEG in 5 ml of acetone (organic phase). After the preparation of Rhod-NPs the EE was determined from the amount of the free-Rhod present in the aqueous phase of the formulations, obtained by filtration/centrifugation at 12,000 rpm for 15 minutes. The amount of Rhod was measured by fluorescence spectroscopy (λ_{ex} 528 nm, λ_{em} 547 nm).

Cell culture

An immortalized human cerebral microvascular endothelial cell (hCMEC/D3) line³⁶ was cultured in endothelial basal medium (EBM-2), supplemented with 2.5% fetal bovine serum, hydrocortisone, vascular endothelial growth factor (VEGF), epidermal growth factor (EGF), insulin-like growth factor I (IGF-I), human fibroblast growth factor (FGF), ascorbic acid and gentamicin sulphate according to the manufacturer's formulation (Lonza, Switzerland). Cells were grown to confluence on tissue culture flasks or inserts coated with collagen Type 1 from calf skin (Sigma, USA) and incubated in 5% CO₂ in air at 37 °C.

Alamar blue (AB) was used to test for any cytotoxic effect of NPs on the hCMEC/D3 cell line. Cells were seeded in collagen-coated 96-well plates at $3 \cdot 10^4$ cells/well and maintained for 24 h. Then, cells were incubated with 100 μ l/well of 0.5 - 10 μ g/ml of either PGZ-NPs or Rhod-NPs diluted in endothelial culture medium for 24 h. After the incubation, hCMEC/D3 cells were treated with 10% (v/v) of AB diluted in FBS-free

endothelial culture medium. Absorbance was measured at 570 nm (reduced AB form) and 620 nm (oxidized AB form) between 4-5 hours after AB treatment using a FLUOstar OPTIMA microplate reader (BMG LABTECH). The cell viability was calculated by the percentage of AB reduction, using the manufacturers protocol as described previously.³⁷ All experiments were performed three times.

Cellular uptake of nanoparticles

hCMEC/D3 cells were seeded in 12 well plates (120.000 cells/well) and grown for 2 days. At confluence, hCMEC/D3 cells were incubated with 1 µg/ml of Rhod-NPs for 15, 30 and 60 minutes and compared to untreated cells, analysed by flow cytometry. The Free-Rhod and Free-Rhod-NPs (Rhod not encapsulated during NP production) were also studied to analyze whether the Rhod can internalize without NPs. FACS analysis was performed by collecting cells with trypsin/EDTA and washing twice with Hanks balanced salt solution (HBSS) (Sigma Aldrich, UK). Washed cells were analysed on a Becton-Dickinson, FACScalibur (FL2 detector set at 410V). The experiments were done in triplicate and the values are reported as the mean ± SD ($n = 3$) of the median fluorescence of 10,000 cells.

hCMEC/D3 monolayers were grown to confluence on fibronectin and collagen-coated 8-well Nunc La-Tek Chamber slides (Sigma Aldrich, UK). Confluent cells were treated with 1 µg/ml of Rhod-NPs for 3h at 37 °C. Then, hCMEC/D3 cells were washed with HBSS and fixed in 4% formalin solution for 10 min at room temperature. The nuclei were counterstained with mounting medium with DAPI (blue) (Vector Laboratories, Burlingame, CA). Both nuclei staining and Rhod-NP-internalization were analyzed using confocal laser scanning microscopy (Leica TCS SP5).

Detection of internalization of NPs by Transmission Electronic Microscopy

The internalization of PGZ-NPs and Rhod-NPs in hCMEC/D3 cells was investigated by TEM. The cells were seeded at 120.000 cells per 1 cm² on Transwell® inserts of polyester membrane (Costar, Corning, NY). At confluence, the NPs (1 µg/ml) were applied to the

apical side in endothelial culture medium for 6 h. Then, both chambers were washed three times in HBSS and fixed in 2.5% glutaraldehyde for 1 hour at room temperature. The fixative was removed and chambers were washed three times with 0.1 M Sörenson's phosphate (PB) and stored in this buffer at 4 °C.

In order to process the samples for TEM, all incubations were applied to both sides of the chamber at room temperature. Firstly, the cells were post-fixed in 1% osmium tetroxide diluted in 0.1 M PB for 1 hour. Then, the insert was washed three times in 0.1 M PB and removed from the well. The membrane was cut out of the insert and gradually dehydrated in series of ethanol: 30% for 5 min, 50% for 5 min, 70% for 10 min, 100% for 10 min twice and 100% with a molecular sieve for 10 min. Then, the membranes were incubated in a mixture of 1:1 ratio of 100% ethanol and Epon resin overnight. They were embedded in Epon resin and formed blocks were polymerized at 60 °C for 48 hrs. Resin blocks were microsectioned at 80 nm thickness using a Diatome diamond knife. The sections were mounted onto pioloform-coated copper grids and counter stained in 3.5% uranyl acetate for 35 minutes followed by lead citrate for 10 minutes and finally washed three times before air-drying. The grids were imaged on TEM JEM 1010 (Jeol, Japan) at an acceleration voltage of 80 kV using a magnification of 25,000 - 40,000.

Transport and Permeability assay

Transfer of NPs across brain endothelium was analysed using permeable cell culture inserts and TEM. Briefly, 24-well cell-culture inserts (Millipore Millicell Hanging Cell Culture Insert, PET membrane; 1 µm) were coated with collagen and fibronectin and seeded with 8×10^4 cells per insert. At confluence, cells were washed with HBSS and cultured with endothelial culture medium, but without the growth factors: VEGF, IGF, EGF, and maintained for 48 h. Then, cells were treated with 1 µg/ml of PGZ-NPs or Rhod-NPs diluted in VEGF, IGF and EGF-free endothelial culture medium for 6 hours. The basolateral side-medium was collected and negative stained. NP (as described above) were observed on TEM JEM-1400 operated at an accelerating voltage of 80 kV. The experiments were done in triplicate and the values are reported as the mean \pm SD ($n = 3$).

The effect of the transport of NPs on the hCMEC/D3 cells was measured by a paracellular permeability assay as described previously by Tai et al.³⁸ hCMEC/D3 treated with 10

ng/mL of TNF α and IFN γ for 24h was used as a positive control.³⁹ At the end of these experiments, the apical side-culture medium was removed and 400 μ L of assay buffer (0.1% BSA in DMEM without phenol red) containing 2 mg/mL 70kDa FITC-dextran was added. The fluorescence that crossed to the basolateral side was measured every 10 min for 1h using a BMG plate reader, and the permeability coefficient P $_e$ derived.³⁸

***In vivo* assay with APP/PS1 mice**

The experiments were carried out in 7 month male APP/PS1 mice and wild-type-like (WT) littermates on a C57/B16J genetic background. The generation of mice expressing the human mutated APP^{swe} and PS1^{dE9} has been described elsewhere.⁴⁰ Animals were maintained under standard animal housing conditions in a 12-h dark-light cycle with free access to food and water. Genotypes were confirmed from 1cm tail clips by PCR using conditions recommended by Jackson Laboratory. Mice were randomly assigned to treatment groups and the experiments were analysed blind. The study was carried out following the guidelines of the European Communities Council Directive 2010/63/EU and with the approval of the local ethical committee of the University of Barcelona.

Free-PGZ and PGZ-NPs (10 mg/kg) were dissolved in 5% DMSO and administered orally in a volume of 10 mL/kg body weight. Animals were treated once a day, 5 days per week, during 4 weeks with the compounds or with vehicle alone. The number of animals included in each group was 3-4. After a 3-day wash-out animals were subjected to behavioral evaluation.

Memory performance was evaluated with the two-object recognition test. On day 1, mice were placed for 9 min in a Y-maze, in which two identical objects were situated at the ends of the arms; the time that the mice spent exploring each object was recorded. Then, 24 h after the training session, animals were placed again for 9 min in the V-maze, with one of the two familiar objects replaced by a novel object. The time that the animals spent exploring the two objects was recorded and an object recognition index (RI) was calculated, as the difference between the time spent exploring the novel object (T_N) and the familiar object (T_F) divided by the total time spent exploring the two objects [RI=(T_N-T_F)/(T_N+T_F)]. At the end of the behavioral testing, the animals were killed and their brains

rapidly removed from the skull, fixed in 4% paraformaldehyde and processed for immunohistochemistry.

A β immunohistochemistry

Fixed tissue samples were embedded in paraffin. Consecutive de-waxed 4 μ coronal sections were incubated with 98% formic acid (20M, 3 min) and treated with 10 mM sodium citrate buffer, pH 6.0, for 20 min to enhance antigenicity. Endogenous peroxidases were blocked with 10% methanol-1% H₂O₂ for 15 min and then blocked with 3% normal horse serum in PBS. They were incubated (4°C overnight) with primary antibody against A β (clone 6F/3D 1:50, Dako, Denmark) and a peroxidase-conjugated secondary antibody, visualized with 7mM diaminobenzidine in PBS (5 min). Sections were lightly counterstained with hematoxylin. The cortical total A β burden was calculated as the percentage of the area of amyloid deposition in plaques with respect to the total cortical area (0.6 mm²) in 9 pictures taken from 3 different sections (-0.1 mm, -1.5 mm and -2.0 mm from bregma) of each animal brain (3 pictures per section corresponding to cingular/retrosplenial and motor cortex, somatosensory cortex and piriform/entorhinal cortex). The selected areas were the main regions of the cerebral cortex in which A β is deposited in APP/PS1 mice. A researcher who did not know the treatments performed the quantifications. A β quantification was calculated using the Analysis tool of Adobe[®] Photoshop[®] CS4.

Statistical analysis

The sample size for experimentation was computed using the Power and Precision software (Biostat, Englewood, NJ, USA), assuming a power of 95% and no missing data. Data were analyzed using GraphPad Prism version 6.0 software. Statgraphics Plus 5.1 software was used to analyze the surface of response. Student's t-test or one way ANOVA, followed by Tukey's multiple comparison or Dunnett's multiple comparison test were used to analyze the in vitro assays. Statistical analysis for the in vivo assay was performed with the SPSS[®] Statistics v21.0 software (IBM, New York, NY, USA). Memory data were analyzed with two-way ANOVA (genotype and treatment as between factors), followed by Tukey's *post hoc*. A β area was analyzed with one-way ANOVA (treatment as between factors).

Results

Pioglitazone nanocarrier characterization and release profile

After detailed analysis of the parameters affecting NP synthesis (Figures S1), a single formulation of nanoparticles was chosen for the biological studies (Figure S2). These PGZ-NPs had a mean size of 155.0 ± 1.8 nm, a polydisperse index distribution of 0.1, negative ZP of -13.0 ± 0.5 mV and an EE of 92.5%. Smaller size facilitates passage through the BBB [16], and may improve the delivery of drugs. Moreover, low PGZ concentrations produced NPs with greater negative ZP, that could help prevent particle aggregation, thereby increasing the stability of the dispersion. ⁴¹ Importantly, the lower concentration of Tw also decreased the toxicity for hCMEC/D3 cells, besides facilitating interaction with endothelial surface molecules and hence transport across the BBB. ⁴²

Different kinetic models of drug release were tested with both formulations to select the best fit. The formulations showed dissimilar profiles and the best fits were ‘Phase Exponential Association’ for Free-NPs and ‘Hyperbola’ for PGZ-NPs, with respect to the AIC and coefficient of determination (r^2) values obtained (Figure 1). After 10 hours, the free drug achieved 76.2% transfer whereas NPs released 57.1 % of the initially bound drug. In addition, Free-PGZ showed a faster release than PGZ entrapped in the particles (comparing Y_{\max} to B_{\max}). Free-PGZ had a constant of dissolution (K) of 0.46 h^{-1} whereas NP-entrapped PGZ had a constant of 1.72 h. This result indicates that NPs are still achieving a sustained release of the drug.

Cytotoxicity assay

The *in vitro* cytotoxicity of PGZ-NPs and Rhod-NPs for hCMEC/D3 cells was assessed by determining the cell viability using the Alamar Blue assay (Figure 2). Cells exposed to increasing concentrations of PGZ-NPs for 24h showed a decreased cell viability from $5.1 \text{ nM} = 2 \text{ } \mu\text{g/mL}$ ($76.56 \pm 2.72\%$). Treatment with Rhod-NPs also produced significant toxicity at 5.1 nM and Rhod-NPs were more toxic than PGZ-NPs at concentrations from 5.1 nM ($p < 0.05$). On the basis of the cytotoxicity assays, the dose of $1 \text{ } \mu\text{g/ml}$ was selected to investigate the characteristics of both types of NPs *in vitro*.

Transport of nanoparticles by brain endothelium

Rhodamine-6G was used to track the cellular uptake of NPs by hCMEC/D3 cells. NPs prepared using Rhod showed high EE (around 99%) and remained associated with the cells for extended periods of time. The cellular uptake of Rhod-NPs into hCMEC/D3 was measured at 15, 30 and 60 minutes by FACS. The values of fluorescence of Rhod-NPs increased in a dose- and time-dependent manner ($p < 0.05$) when compared to untreated cells (Figure 3). Uptake was time-dependent with significant uptake of NPs within the first 15 minutes of exposure. The fluorescence in Rhod-NPs treated hCMEC/D3 cells was >50x higher than cells exposed to Free-Rhod (Figure 3C).

Routes of transcytosis

To determine the subcellular localisation of the NPs, hCMEC/D3 cells were treated with Rhod-NPs and examined by confocal microscopy (Figure 4). Red punctate fluorescence was observed in all cells; the size corresponded to individual NPs, localised primarily in the cell body, close to the nucleus. These observations confirm the results obtained by FACS, which demonstrated that all cells take up the Rhod-NPs (Figure 3A) and that the fluorescence signal was much higher when using Rhod-NPs in comparison to Free-Rhod. It has been proposed that internalisation of NPs of this size occurs predominantly by adsorption to the cell surface followed by vesicular endocytosis. The results are consistent with NP-uptake into either caveolae or clathrin-coated vesicles (CCVs).

Confocal microscopy has insufficient resolution to determine exactly where the nanoparticles are localised within the cells. To obtain a better understanding of the mechanism of NPs uptake, the cells were examined by transmission electron microscopy (TEM). The images show individual PGZ-NPs and Rhod-NP (100-150nm) in the cytoplasm (Figure 5); the size corresponds to their initial physical characterisation (Figure S2). No NPs were seen in intercellular junctions. This implies that the NPs have been taken up individually by endothelial cells and have not aggregated inside the cells. It is not possible to see a distinct vesicle membrane or electron-dense coat proteins around the NPs. However, it should be noted that both caveolae and CCVs are normally smaller (50-100nm) than these NPs, hence a caveolus or CCV would contain just one NP and the closely apposed vesicular membrane would be difficult to visualise by TEM. Notably, NPs were not seen in larger pinocytotic vesicles or intercellular junctions. Nor was there

any evidence for disturbance of the plasma membrane. These observations exclude paracellular movement as the route of movement and direct trans-membrane transfer to the cytosol is also unlikely. Hence, the most likely route of uptake across the endothelium is via endocytosis from the apical surface, into a single CCV or caveolus. This accords with the observed clustering of the NPs in the perinuclear region seen by confocal fluorescence microscopy, which is a characteristic of caveolae.

Transport and Permeability assays

To determine whether NPs are released from the basolateral side of the endothelium, hCMEC/D3 cells were grown in confluent monolayers on filters in tissue-culture inserts. PGZ-NPs and Rhod-NPs were applied to the apical surface and the medium harvested from the basolateral side. After 6 hours, NPs had crossed the endothelial monolayer (Figure 6A and S3). The NPs are similar in size (100-200nm) to those initially applied, suggesting they have crossed the endothelium intact.

The integrity of the cell monolayer after exposure to both types of NP was assessed using a paracellular tracer, FITC-dextran (MW 70 kDa). Changes in the permeability coefficient were calculated and the data shows that treatment of hCMEC/D3 cells with PGZ-NPs and Rhod-NPs for 6h does not increase the paracellular permeability of the endothelial monolayer (Figure 6B). This demonstrates that the NPs had not altered paracellular permeability of the endothelial monolayer, and further confirms that the NPs seen in Figure 6A had crossed the endothelium by transcytosis.

Effect of treatment on memory and neuropathology in APP/PS1 mice

In order to test the *in vivo* effect of the PGZ-NPs a comparison was made with Free-PGZ in APP/PS1 mice. Oral administration was chosen as this reflects the route of PGZ administration in humans. Previous work has shown that exposure of these NPs to acid (0,1M HCl) for 15 minutes (reflecting gastric conditions) followed by neutralization, does not affect their size, ZP, PI or EE. Daily administration of Free-PGZ and PGZ-NPs (10 mg/kg) for 4 weeks reduced the memory impairment observed in vehicle-treated APP/PS1 mice, as revealed by the two-object recognition test (Figure 7A). Two-way ANOVA revealed a significant genotype ($F_{(1, 16)} = 5.413, p < 0.05$) and treatment effect

($F_{(2, 16)} = 12.717, p < 0.001$) and interaction between the two factors ($F_{(2, 16)} = 3.551, p = 0.053$). Subsequent Tukey's *post hoc* tests revealed that APP/PS1 mice treated with vehicle exhibited a memory impairment when compared to corresponding WT littermates ($p < 0.01$) and that Free-PGZ ($p < 0.05$) and PGZ-NPs ($p < 0.01$) increased the recognition index in APP/PS1 mice when compared to vehicle. No significant difference in the total exploration time during the memory acquisition session or the memory test was observed between groups, discarding any possible impact of the treatments on the anxiety levels or the activity of the mice.

Chronic treatment with Free-PGZ or PGZ-NPs did not significantly modify ($F_{(2, 8)} = 2.993, p = 0.04$) the total A β burden in the cortex respect vehicle-treated mice (Figure 7B-C). The vehicle employed in this study did not induce any modification in A β burden when compared to untreated mice (data not shown). Notably, the level of A β deposition in mice treated with PGZ-NPs was half of that in mice treated with Free-PGZ (Figure 7), however there was considerable variation between individual animals. These results demonstrate that a PPAR γ agonist improves memory in APP/PS1 mice, and suggest that encapsulation of PGZ in the NPs can reduce the A β burden.

Discussion

In this study, we have demonstrated that PGZ-NPs developed by a displacement technique are appropriate for the treatment of a model of AD. The release profile from NPs was slower than Free-PGZ. Moreover, the NPs were not cytotoxic for human brain endothelium (hCMEC/D3) at the doses used, and produced no alteration in permeability of the endothelial monolayer. These results are in accordance with a previous study using mouse Bend-3 cells, which indicated that PLGA-PEG NPs did not damage the endothelial cells.¹⁹

Theoretically, endocytosis of NPs can occur by passive transfer across the cell membrane into the cytoplasm or by active endocytosis into vesicles, including CCVs and caveolae. NP size affects the principal entry route; the smallest NPs (<10nm) can directly cross the plasma membrane whereas endocytosis is the principal entry route for larger NPs.⁴³

The route of endocytosis depends greatly on how the NPs interact with different domains on the plasma membrane which is affected by size, coating, surfactant and surface charge,

as well as any specific targeting molecule on the NPs. These factors may also affect the ability of the NPs to cross the BBB *in vivo*.⁴⁴ The subcellular localization of NPs in this study, determined by confocal and electron microscopy indicated that they cross the endothelium intact, by vesicular transcytosis.

Most endothelial cells have large numbers of caveolae, which mediate transport of nutrients to the tissue.⁴⁵ However, brain endothelium *in vivo* has relatively few caveolae compared with endothelium in other tissues and consequently there is less internalization by this route. However, PEG on the surface of NPs can improve their internalization by brain endothelium⁴⁶ and it has been suggested that PEGylated PLGA NPs could enter these cells in CCVs⁴⁷ as an alternative to caveolar transcytosis. CCVs have previously been shown to play a key role in the transportation of pegylated NPs in which energy-dependent endocytosis is involved.⁴⁸ Moreover, particles up to 200 nm in diameter can be efficiently taken up into CCVs.⁴⁹ The 50-fold higher rate of uptake of Rhod-NPs compared with free rhodamine also implies that the NPs are taken up by a different mechanism than the free tracer.

These observations indicate that the PGZ-NPs enter and can potentially cross brain endothelium directly. Transcytosis of NPs within vesicles shields any cargo molecule such as PGZ or rhodamine from ABC-transporters (eg pgp/ABCB1) located in the apical plasma membrane which act on substrates in the cytoplasm and/or the membrane. Even if the NPs enter the cytoplasm the delayed release of cargo means that less drug can be removed by multi-drug transporters.

The experiments *in vivo* demonstrated the potential for PGZ and particularly PGZ-NPs to reduce memory deficit and neuropathology in APP/PS1 mice. These results are in accordance with Searcy et al⁵⁰ who demonstrated that Free-PGZ improved reversal learning in a triple transgenic mouse model of AD mice. Moreover, other studies showed that APP/PS1 mice treated for nine days with PGZ reversed non-cognitive behavioural deficits and restored distance and speed travelled in an open field⁵¹ and improved partially the cognitive impairments in the Morris water maze test.⁵² A number of other studies have reported neuroprotective properties of PGZ.^{9,10,50,52,53} Moreover, a phase III clinical trial also demonstrated a role for PGZ in slowing cognitive decline in people with mild cognitive impairment due to Alzheimer's Disease.⁵⁴

In this study, the overall reduction in A β burden in PGZ-NPs treated mice was striking although individual results were variable. Previous work has also produced divergent results. In one other study, the amyloidogenic APP processing and A β production were not affected by treatment with pioglitazone.⁵¹ In contrast, an acute 2-week treatment with combined leptin and PGZ resulted in a reduction of spatial memory deficits (Y maze) and brain β -amyloid levels (soluble β -amyloid and amyloid plaque burden) relative to vehicle-treated animals.⁵⁵

Conclusion

The overall conclusion from our study is that PGZ-NPs reduce the memory impairment and neuropathology, in APP/PS1 mice. However, it is not certain whether the release of PGZ from NPs *in vivo* occurs inside the CNS or outside the CNS. The results indicate that any difference between the effect of Free-PGZ and PGZ-NPs is most likely due to either the slower release profile from PGZ-NPs (Figure 1) or the improved rate of transcytosis across brain endothelium (Figures 3-6) with the potential for evading the action of multi-drug transporters at the blood-brain barrier.

The data all confirm that NPs cross endothelial cells *in vitro* without affecting cellular integrity. Moreover, PGZ encapsulated into polymeric NPs (PLGA-PEG) improved the cognitive deficit in APP/PS1 male mice in a similar way to Free-PGZ, and showed a clear tendency to reduce beta amyloid deposition in the cerebral cortex, suggesting PGZ-NPs are a new alternative to treat AD, both improving drug delivery into the brain and providing for a more sustained drug release.

Acknowledgements

This work was supported by the Coordination for the Improvement of Higher Education Personnel (CAPES) – Brazil; the Spanish Ministry of Science and Innovation (MAT2014-59134R). Studies at the Open University were supported by the Santander Research Foundation and the BBSRC (BB/K009184/1). The authors would like to thank Ms. Shereen Nizari for her help with confocal microscopy.

Author contributions

M Silva-Abreu, carried out the experiments, analysed the data/results and wrote the paper. AC Calpena, helped analyse the results of the release profile and statistics. P Andrés-

Benito and E Aso carried out in vivo experiments and analysed in vivo results. I A Romero designed the in vitro permeability assay. D Roig-Carles helped with uptake assays and analysis of the permeability assay. R Gromnicova carried out localization of nanoparticles by transmission electronic microscopy. M Espina analysed the design factorial. I Ferrer provided the APP-PS1 mice and facilities to carry out the behavioural experiments. ML García helped with physicochemical characterization of nanoparticles, D Male conceived and designed all the in vitro experiments with hCMEC/D3 cells and edited the paper.

Conflict of interest

All authors declare no conflict of interest.

References

1. Anand R, Gill KD, Mahdi AA. Therapeutics of Alzheimer's disease: Past, present and future. *Neuropharmacology*. 2014;76:27–50.
2. Toba J, Nikkuni M, Ishizeki M, Yoshii A, Watamura N, Inoue T, et al. PPAR γ agonist pioglitazone improves cerebellar dysfunction at pre-A β deposition stage in APP^{swe}/PS1^{dE9} Alzheimer's disease model mice. *Biochem Biophys Res Commun*. 2016;473(4):1039–44.
3. Md S, Bhattmisra SK, Zeeshan F, et al. Nano-carrier enabled drug delivery systems for nose to brain targeting for the treatment of neurodegenerative disorders. *J Drug Deliv Sci Technol*. 2018;43:295–310.
4. Anand A, Patience AA, Sharma N, Khurana N. The present and future of pharmacotherapy of Alzheimer's disease: A comprehensive review. *Eur J Pharmacol*. 2017;815:364–75.
5. Sun D, Li N, Zhang W, et al. Design of PLGA-functionalized quercetin nanoparticles for potential use in Alzheimer's disease. *Colloids Surf B Biointerfaces*. 2016;148:116–29.
6. Calvo-Ochoa E, Arias C. Cellular and metabolic alterations in the hippocampus caused by insulin signalling dysfunction and its association with cognitive

- impairment during aging and Alzheimer's disease: studies in animal models. *Diabetes Metab Res Ver.* 2015;31:1–13.
7. Pan H, Chen J, Xu J, Chen M, Ma R. Antifibrotic effect by activation of peroxisome proliferator- activated receptor – γ in corneal fibroblasts. *Mol Vis.* 2009;15:2279–86.
 8. Yamamoto A, Kakuta H, Miyachi H, Sugimoto Y. Involvement of the retinoid X receptor ligand in the anti-inflammatory effect induced by peroxisome proliferator-activated receptor agonist in vivo. *PPAR Res.* 2011;2011:1-8.
 9. Chen J, Li S, Sun W, Li J. Anti-diabetes drug pioglitazone ameliorates synaptic defects in AD transgenic mice by inhibiting cyclin-dependent kinase5 activity. *PLoS One.* 2015;10(4):1–12.
 10. El-Sahar AE, Safar MM, Zaki HF, Attia AS, Ain-Shoka AA. Neuroprotective effects of pioglitazone against transient cerebral ischemic reperfusion injury in diabetic rats: Modulation of antioxidant, anti-inflammatory, and anti-apoptotic biomarkers. *Pharmacol Reports.* 2015;67(5):901–6.
 11. Zolezzi JM, Inestrosa NC. Peroxisome proliferator-activated receptors and alzheimer's disease: Hitting the blood-brain barrier. *Mol Neurobiol.* 2013;48(3):438–51.
 12. Nicolakakis N, Aboukassim T, Ongali B, et al. Complete Rescue of Cerebrovascular Function in Aged Alzheimer's Disease Transgenic Mice by Antioxidants and Pioglitazone, a Peroxisome Proliferator-Activated Receptor γ Agonist. *J Neurosci.* 2008;28(37):9287–96.
 13. Chou PS, Ho BL, Yang YH. Effects of pioglitazone on the incidence of dementia in patients with diabetes. *J Diabetes Complications.* 2017;31(6):1053–7.
 14. Liu D, Lin B, Shao W, Zhu Z, Ji T, Yang C. In Vitro and in Vivo Studies on the Transport of PEGylated Silica Nanoparticles across the Blood – Brain Barrier. *CS Appl Mater Interfaces.* 2014; 6: 2131-36.
 15. Masserini M. Nanoparticles for Brain Drug Delivery. *ISRN Biochem.* 2013;2013:1–18.
 16. Mikitsh JL, Chacko AM. Pathways for small molecule delivery to the central nervous system across the blood-brain barrier. *Perspect Medicin Chem.* 2014;(6):11–24.
 17. Al Asmari AK, Ullah Z, Tariq M, Fatani A. Preparation, characterization, and in vivo evaluation of intranasally administered liposomal formulation of donepezil.

- Drug Des Devel Ther.* 2016;10:205–15.
18. Gromnicova R, Yilmaz CU, Orhan N, et al. Localization and mobility of glucose-coated gold nanoparticles within the brain. *Nanomedicine.* 2016;11(6):617–25.
 19. Sánchez-López E, Ettcheto M, Egea MA, et al. New potential strategies for Alzheimer's disease prevention: pegylated biodegradable dexibuprofen nanospheres administration to APP^{swe}/PS1^{dE9}. *Nanomedicine Nanotechnology, Biol Med.* 2017;13(3):1171–82.
 20. Patel T, Zhou J, Piepmeier JM, Saltzman WM. Polymeric nanoparticles for drug delivery to the central nervous system. *Adv Drug Deliv Ver.* 2012;64(7):701–5.
 21. Tosi G, Bortot B, Ruozi B, et al. Potential Use of Polymeric Nanoparticles for Drug Delivery Across the Blood-Brain Barrier. *Curr Med Chem.* 2013;20(17):2212–25.
 22. Salvalaio M, Rigon L, Belletti D, et al. Targeted Polymeric Nanoparticles for Brain Delivery of High Molecular Weight Molecules in Lysosomal Storage Disorders. *PLoS One.* 2016;11(5):e0156452.
 23. Guccione C, Oufir M, Piazzini V, et al. Corrigendum to Andrographolide-loaded nanoparticles for brain delivery: Formulation, characterisation and in vitro permeability using hCMEC/D3 cell line. *Eur. J. Pharm. Biopharm.* 2017;119:253–263.
 24. Bhavna K, Md S, Ali M, et al. Design, Development, Optimization and Characterization of Donepezil Loaded Chitosan Nanoparticles for Brain Targeting to Treat Alzheimer's Disease. *Sci Adv Mater.* 2014;6(4):720–35.
 25. Araújo J, Vega E, Lopes C, Egea MA, Garcia ML, Souto EB. Effect of polymer viscosity on physicochemical properties and ocular tolerance of FB-loaded PLGA nanospheres. *Colloids Surf B Biointerfaces.* 2009;72(1):48–56.
 26. Silva-Abreu M, Calpena AC, Espina M, et al. Optimization, Biopharmaceutical Profile and Therapeutic Efficacy of Pioglitazone-loaded PLGA-PEG Nanospheres as a Novel Strategy for Ocular Inflammatory Disorders. *Pharm Res.* 2018;35(1):11.
 27. Abrego G, Alvarado H, Souto EB, et al. Biopharmaceutical profile of pranoprofen-loaded PLGA nanoparticles containing hydrogels for ocular administration. *Eur J Pharm Biopharm.* 2015;95:261–70.
 28. Xu Y, Du Y. Effect of molecular structure of chitosan on protein delivery properties of chitosan nanoparticles. *Int J Pharm.* 2003;250(1):215–26.
 29. Resende AP, Silva B, Braz BS, Nunes T, Gonçalves L, Delgado E. Ex vivo

- permeation of erythropoietin through porcine conjunctiva, cornea, and sclera. *Drug Deliv Transl Res.* 2017;7(5):625–31.
30. Grabrucker AM, Ruozi B, Belletti D, et al. Nanoparticle transport across the blood brain barrier. *Tissue Barriers.* 2016;4(1).
 31. Fessi H, Puisieux F, Devissaguet JP, Ammoury N, Benita S. Nanocapsule formation by interfacial polymer deposition following solvent displacement. *Int J Pharm.* 1989;55(1):R1–4.
 32. Vega E, Gamisans F, García ML, Chauvet A, Lacoulonche F, Egea MA. PLGA Nanospheres for the Ocular Delivery of Flurbiprofen: Drug Release and Interactions. *J Pharm Sci.* 2008;97:5306–17.
 33. Silva-Abreu M, Espinoza LC, Rodríguez-Lagunas MJ, et al. Human skin permeation studies with PPAR γ agonist to improve its permeability and efficacy in inflammatory processes. *Int J Mol Sci.* 2017;18(12).
 34. Mallandrich M, Fernández-Campos F, Clares B, et al. Developing Transdermal Applications of Ketorolac Tromethamine Entrapped in Stimuli Sensitive Block Copolymer Hydrogels. *Pharm Res.* 2017;34(8):1728–40.
 35. Yamaoka K, Nakagawa T. Application of Akaike's information Criterion (AIC) in the evaluation of linear pharmacokinetic equations. *J Pharmacokinet Biopharm* 1978;6:165–75.
 36. Weksler BB, Subileau EA, Perrie N, et al. Blood-brain barrier-specific properties of a human adult brain endothelial cell line. *FASEB J.* 2005;19(13):1872–4.
 37. Andreani T, Kiill CP, Souza AL, et al. Surface engineering of silica nanoparticles for oral insulin delivery: Characterization and cell toxicity studies. *Colloids Surf B.* 2014;123:916–923.
 38. Tai LM, Holloway KA, Male DK, Loughlin AJ, Romero IA. Amyloid- β -induced occludin down-regulation and increased permeability in human brain endothelial cells is mediated by MAPK activation. *J Cell Mol Med.* 2010;14(5):1101–12.
 39. Lopez-Ramirez MA, Wu D, Pryce G, et al. MicroRNA-155 negatively affects blood–brain barrier function during neuroinflammation. *FASEB J.* 2014;28(6):2551–65.
 40. Borchelt DR, Ratovitski T, van Lare J, et al. Accelerated Amyloid Deposition in the Brains of Transgenic Mice Coexpressing Mutant Presenilin 1 and Amyloid Precursor Proteins. *Neuron.* 1997;19(4):939–45.
 41. Dal Magro R, Ornaghi F, Cambianica I, et al. ApoE-modified solid lipid

- nanoparticles: A feasible strategy to cross the blood-brain barrier. *J Control Release*. 2017;249(2016):103–10.
42. Kreuter J, Ränge P, Petrov V, et al. Direct evidence that polysorbate-80-coated poly(butylcyanoacrylate) nanoparticles deliver drugs to the CNS via specific mechanisms requiring prior binding of drug to the nanoparticles. *Pharm Res*. 2003;20(3):409–16.
 43. Gromnicova R, Kaya M, Romero IA, et al. Transport of Gold Nanoparticles by Vascular Endothelium from Different Human Tissues. *PLoS One*. 2016;11(8):e0161610.
 44. Shilo M, Sharon A, Baranes K, Motiei M, Lellouche JM, Popovtzer R. The effect of nanoparticle size on the probability to cross the blood-brain barrier: an in-vitro endothelial cell model. *J Nanobiotechnology*. 2015;13(1):19.
 45. Fröhlich E. The role of surface charge in cellular uptake and cytotoxicity of medical nanoparticles. *Int J Nanomedicine*. 2012;5577-91.
 46. Neves AR, Queiroz JF, Weksler B, Romero IA, Couraud P-O, Reis S. Solid lipid nanoparticles as a vehicle for brain-targeted drug delivery: two new strategies of functionalization with apolipoprotein E. *Nanotechnology*. 2015;26(49):495103.
 47. Wohlfart S, Gelperina S, Kreuter J. Transport of drugs across the blood–brain barrier by nanoparticles. *J Control Release*. 2012;161(2):264–73.
 48. Smith MW, Gumbleton M. Endocytosis at the blood–brain barrier: From basic understanding to drug delivery strategies. *J Drug Target*. 2006;14(4):191–214.
 49. Rejman J, Oberle V, Zuhorn IS, Hoekstra D. Size-dependent internalization of particles via the pathways of clathrin- and caveolae-mediated endocytosis. *Biochem J*. 2004;377(1):159–69.
 50. Searcy JL, Phelps JT, Pancani T, et al. Long-Term Pioglitazone Treatment Improves Learning and Attenuates Pathological Markers in a Mouse Model of Alzheimer’s Disease. *J Alzheimer’s Dis*. 2012;30:943–61.
 51. Mandrekar-Colucci S, Karlo JC, Landreth GE. Mechanisms Underlying the Rapid Peroxisome Proliferator-Activated Receptor- γ -Mediated Amyloid Clearance and Reversal of Cognitive Deficits in a Murine Model of Alzheimer’s Disease. *J Neurosci*. 2012;32(30):10117–28.
 52. Yin Q-Q, Pei J-J, Xu S, et al. Pioglitazone Improves Cognitive Function via Increasing Insulin Sensitivity and Strengthening Antioxidant Defense System in Fructose-Drinking Insulin Resistance Rats. *PLoS One*. 2013;8(3):e59313.

53. Papadopoulos P, Rosa-Neto P, Rochford J, Hamel E. Pioglitazone Improves Reversal Learning and Exerts Mixed Cerebrovascular Effects in a Mouse Model of Alzheimer's Disease with Combined Amyloid- β and Cerebrovascular Pathology. *PLoS One*. 2013;8(7):e68612.
54. Takeda. Extension Study of the Safety and Efficacy of Pioglitazone to Slow Cognitive Decline in Participants With Mild Cognitive Impairment Due to Alzheimer Disease. Available from: <https://clinicaltrials.gov/ct2/show/NCT02284906?term=pioglitazone&cond=Alzheimer+Disease&rank=3>. NLM Identifier: NCT022849062014. Accessed February 15, 2018.
55. Fernandez-Martos CM, Atkinson RAK, Chuah MI, King AE, Vickers JC. Combination treatment with leptin and pioglitazone in a mouse model of Alzheimer's disease. *Alzheimer's Dement Transl Res Clin Interv*. 2017;3(1):92–106.

Figure set article

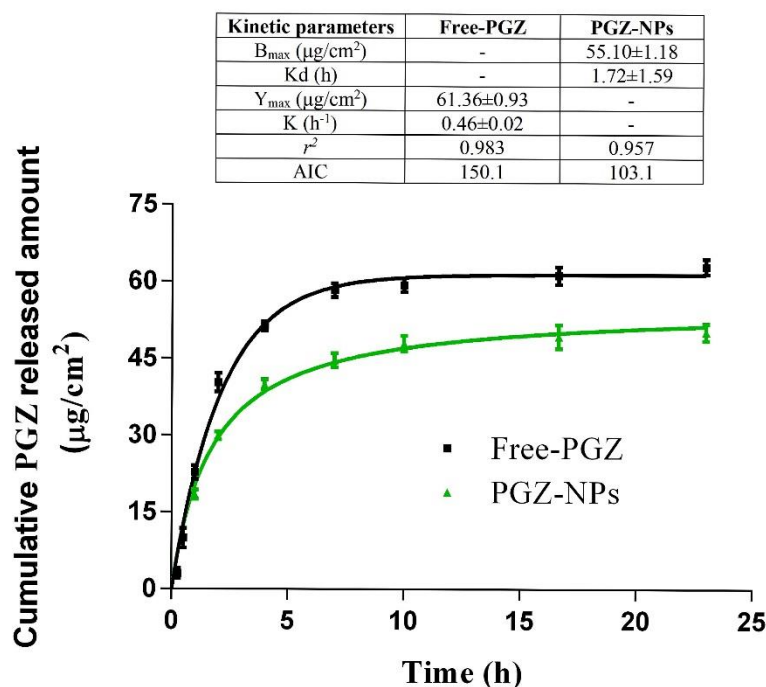


Figure 1. Release profile of PGZ from NPs and Free-PGZ

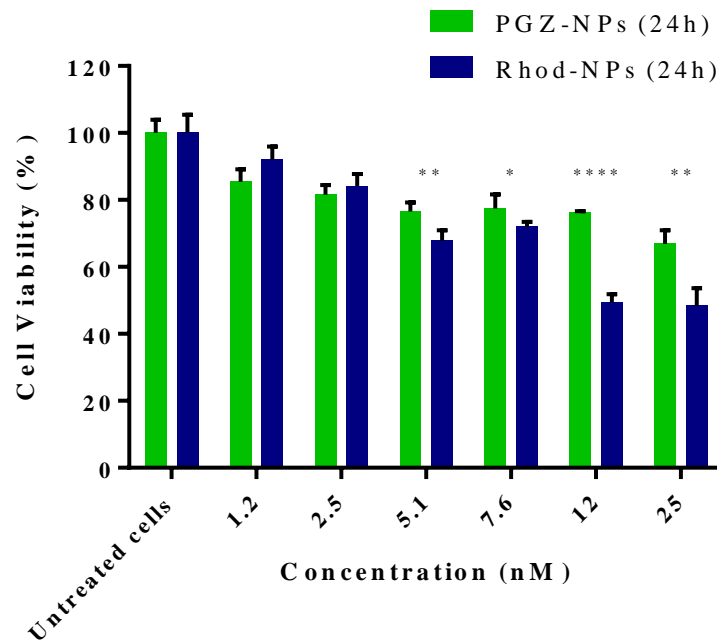


Figure 2. hCMEC/D3 cell viability measured by Alamar blue assay when exposed to 1.2 to 25nM of PGZ-NPs and Rhod-NPs for 24h. Data are shown as percentage of control (cell culture medium), which represents the maximum cell viability. Data are compared for each concentration of Rhod-NPs versus PGZ-NPs * $p < 0.05$, ** $p < 0.01$, **** $p < 0.0001$ by Student t-test ($n = 3$).

Figure 3a

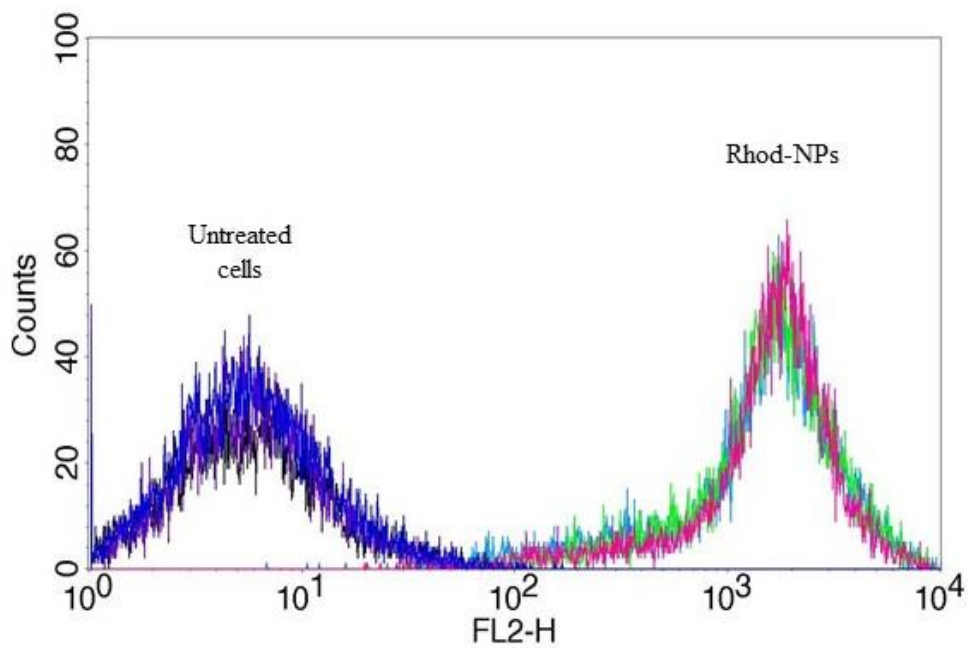


Figure 3b

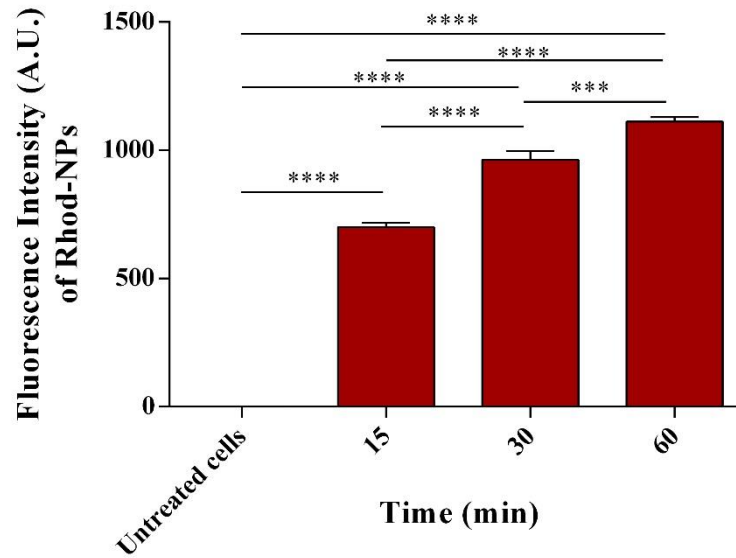


Figure 3c

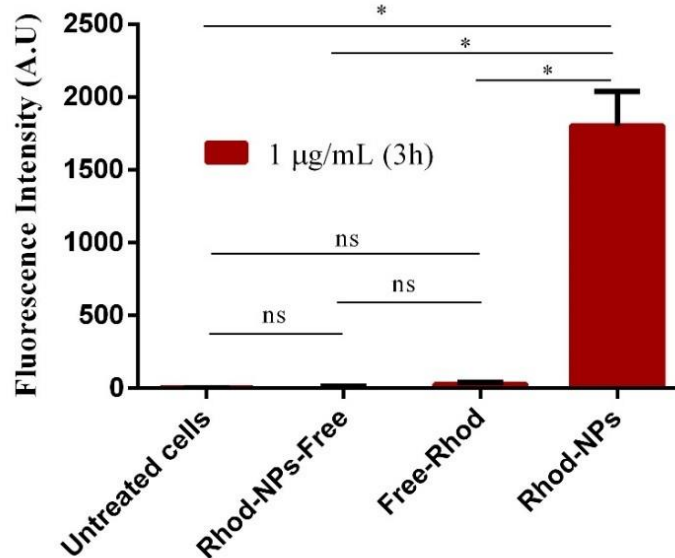


Figure 3. a) FACS histograms of 10,000 hCMEC/D3 cells treated for 3 hours with Rhod-NPs or untreated cells. b) Time-dependent interaction of Rhod-NPs with hCMEC/D3. Each value is the mean of the median fluorescence of 10,000 cells from three independent experiments. *** $p < 0.001$, **** $p < 0.0001$ by one way ANOVA followed by Tukey's multiple comparison ($n = 3$). c) Uptake of Rhod-NPs; Rhod-NPs-Free (not incorporated into the NPs) and Free-Rhod in comparison with untreated cells at 3 hours. Each value is the mean of three independent experiments. * $p < 0.05$ by one way ANOVA and Tukey's multiple comparison ($n = 3$).

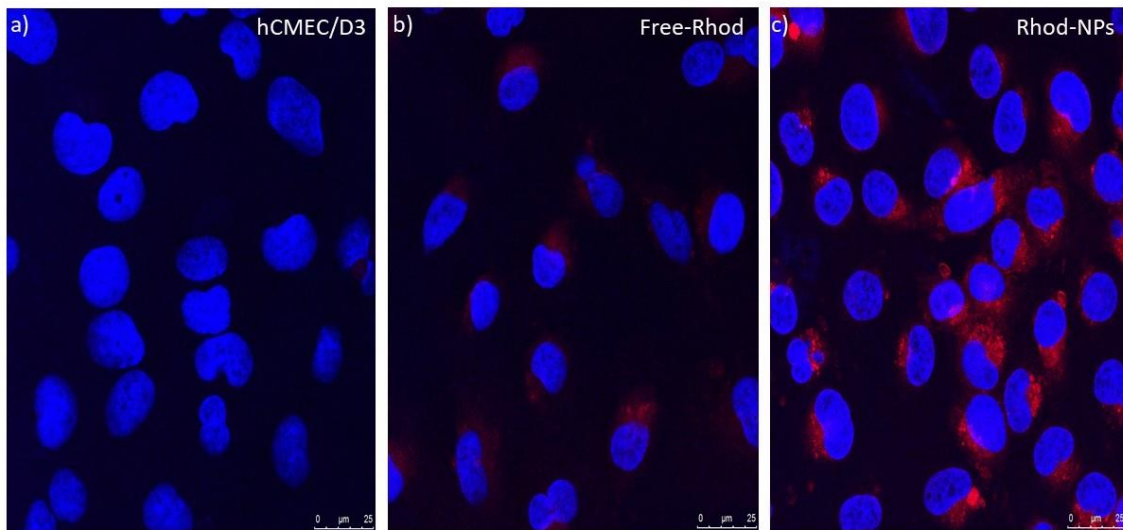


Figure 4. Cellular uptake and intracellular distribution of Rhod-NPs in hCMEC/D3. a) hCMEC/D3 untreated (control); b) hCMEC/D3 exposed to Free-Rhod and c) hCMEC/D3 exposed to Rhod-NPs. Cells were incubated for 3 hours with 1 µg/ml of NPs. Nuclei were counterstained with DAPI (blue).

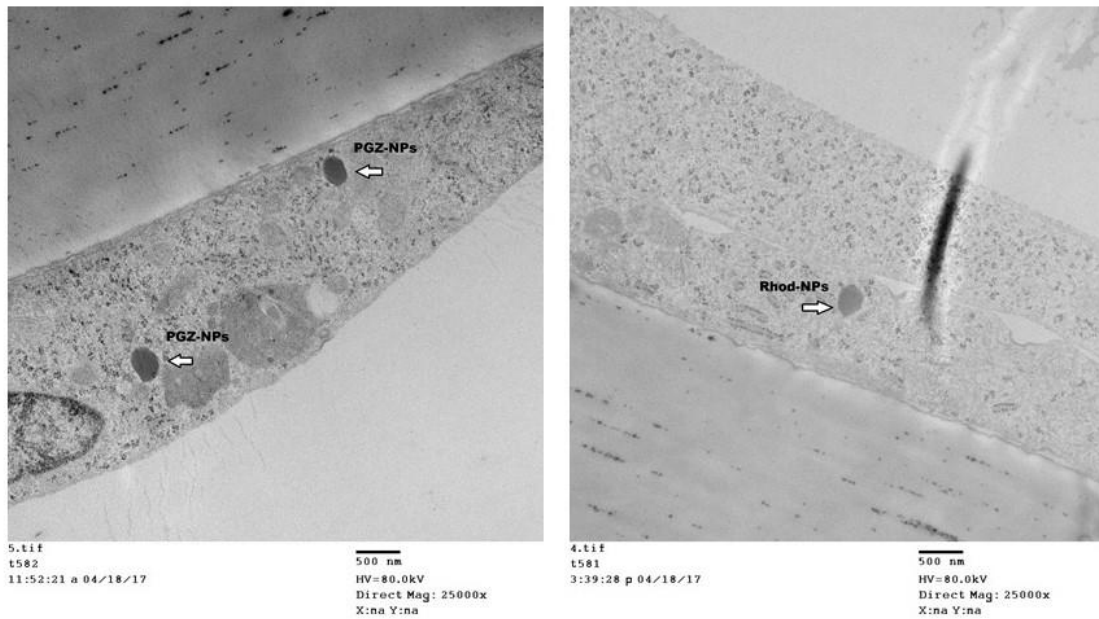


Figure 5. Localization of PGZ-NPs and Rhod-NPs in hCMEC/D3 by TEM. Cells exposed to 1 µg/ml for 6 hours.

Figure 6A

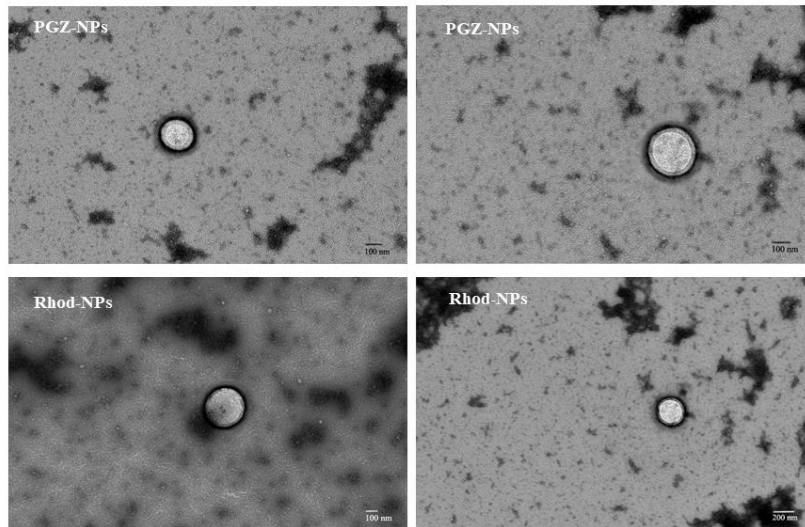


Figure 6B

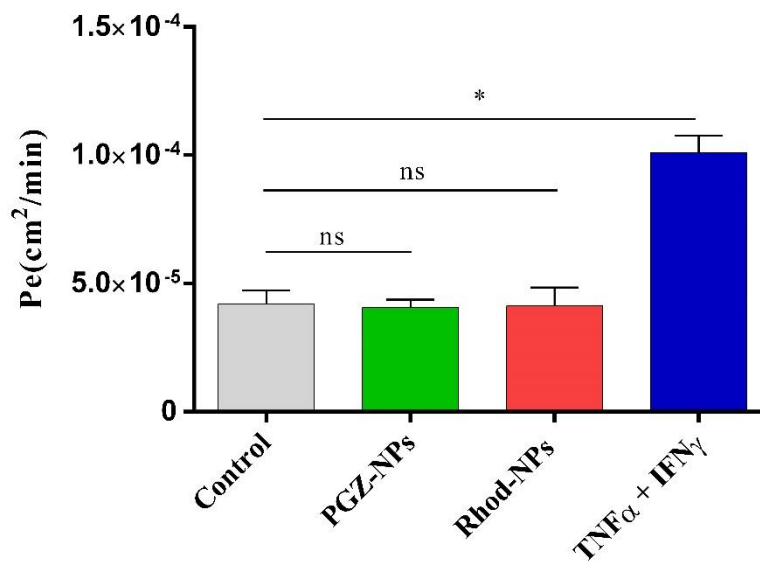


Figure 6. A) Images of PGZ-NPs and Rhod-NPs by TEM after 6 hours in the basolateral compartment. B) Permeability of hCMEC/D3, following exposure to 1 μ g/ml of NPs for 6 hours. TNF α + IFN γ (10ng/ml, for 24 hours) was used as a positive control, increasing endothelial permeability. Each value is the mean of three independent experiments. ns = nonsignificant, * $p < 0.05$ by One way ANOVA and Dunnett's multiple comparison test ($n = 3$).

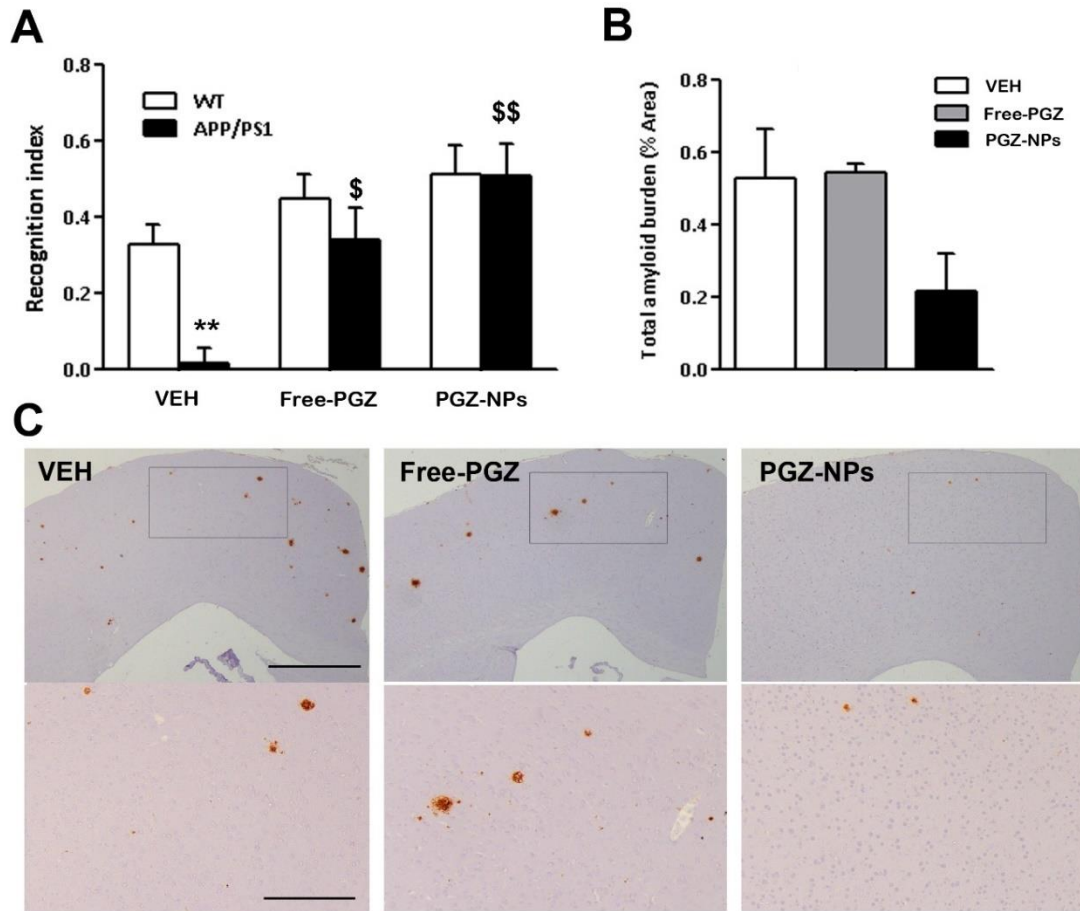
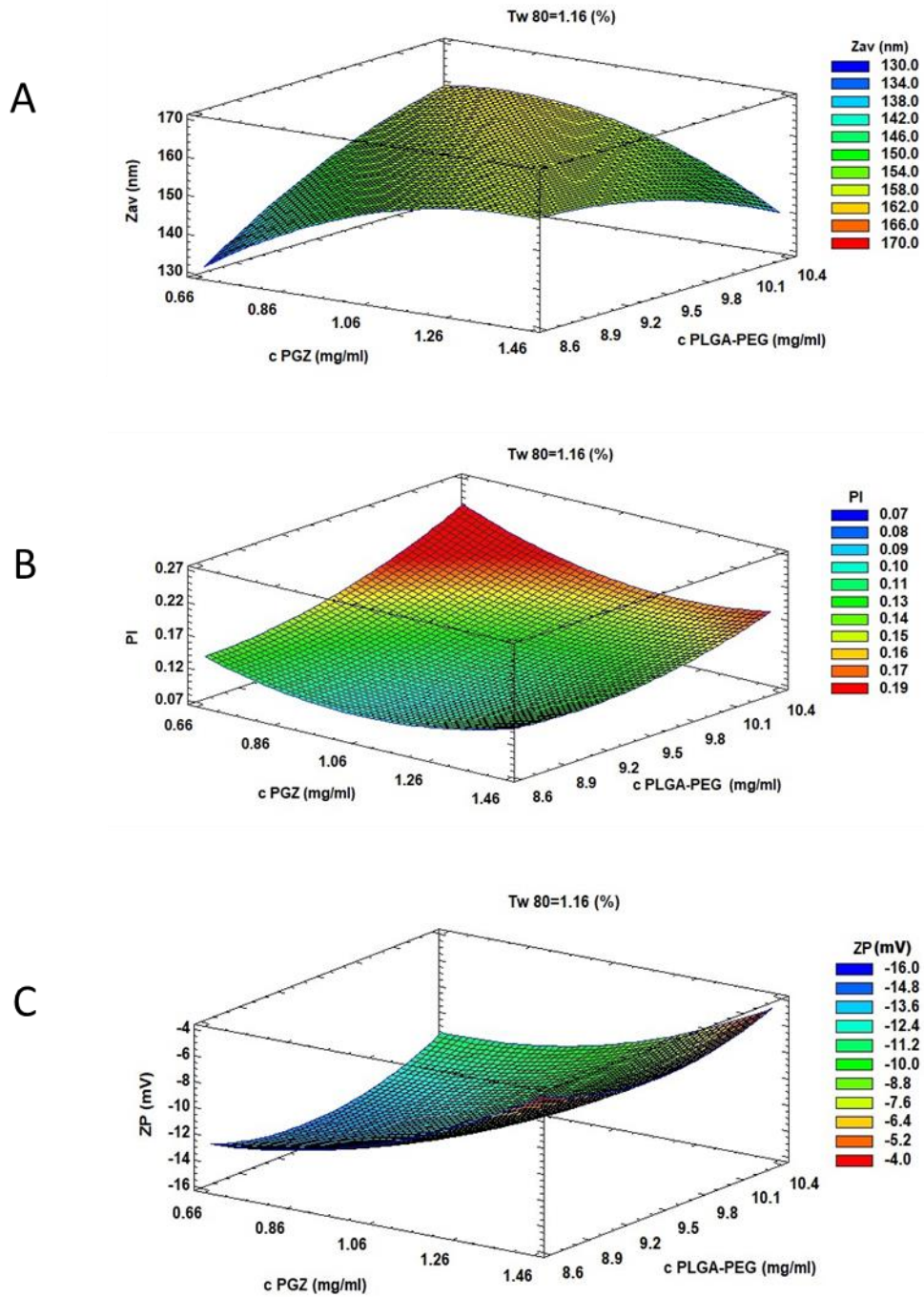


Figure 7. *In vivo* evaluation of PGZ-NPs. A) Memory performance of treated animals in the two-object recognition test. APP/PS1 animals treated with vehicle showed cognitive impairment when compared with wild-type littermates. In contrast, Free-PGZ and PGZ-NPs treatment reduced the memory impairment in APP/PS1 mice. B) Cortical A β burden is not significantly modified in treated APP/PS1 mice, in spite of the tendency to decreased deposition in NP-PGZ-treated animals. C) Representative images of A β immunoreactivity in cortical sections of APP/PS1 mice chronically treated with Free-PGZ, PGZ-NPs or vehicle. Upper panels correspond to low magnification images (scale bar = 500 μ m). Bottom panels correspond to high magnification of brain areas indicated by squares (scale bar = 200 μ m). Data are expressed as the mean \pm SEM. ** $p < 0.01$ compared to WT animals. \$ $p < 0.05$, \$\$ $p < 0.01$, compared to vehicle group.

Supplementary material



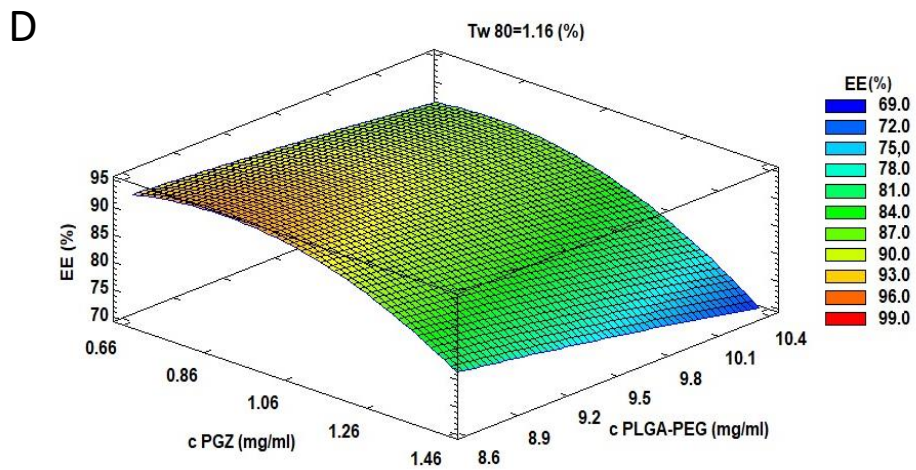
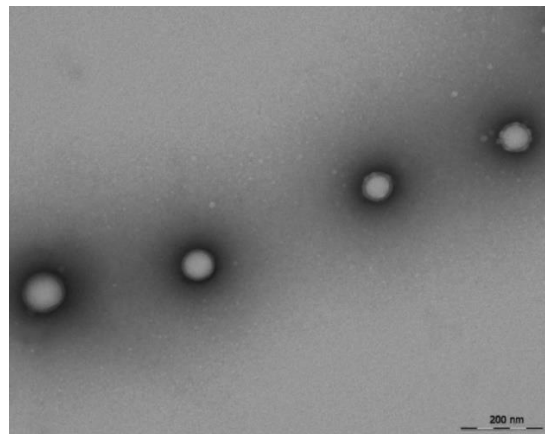


Figure S1: Design of experiments. Response surfaces of PGZ-NPs at Tw 80 1.16%, with different concentrations of PGZ and PLGA-PEG: A) Z_{av} , B) PI, C) ZP and D) EE.

A)



B)

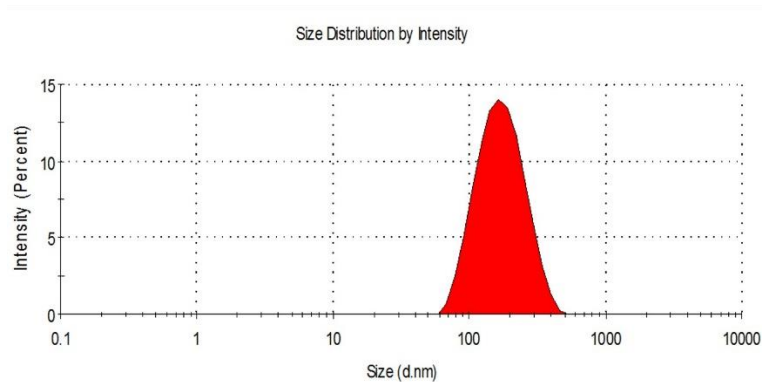


Figure S2: A) Image of PGZ-NPs by TEM and B) Size of PGZ-NPs by dynamic light scattering.

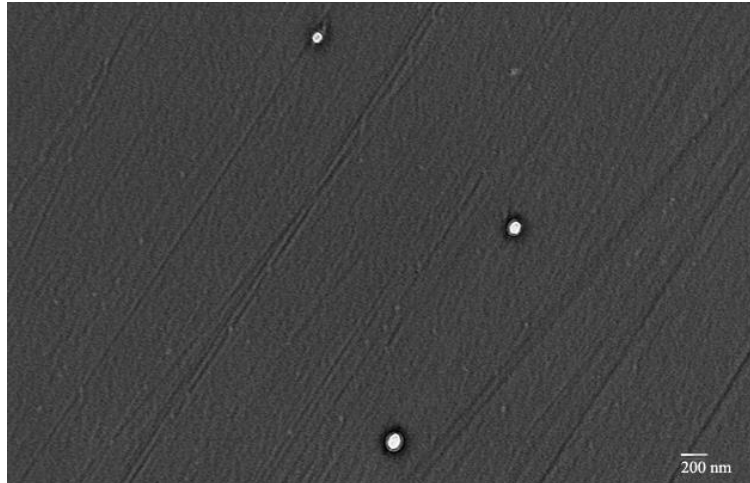


Figure S3: Transport in vitro assay in hCMEC/D3. PGZ-NPs on the basolateral surface (filter side) of the endothelium after 6 hours.

Table 1. Analytical measurement of HPLC for release profile.

Time (h)	Free-PGZ			PGZ-NPs		
	Area 1	Area 2	Area 3	Area 1	Area 2	Area 3
0,25	17090,4	13038,0	15064,2			
0,5	29912,1	21861,8	25886,9			
1	49411,6	42701,1	46056,3	37265,2	39596,5	38430,9
2	78268,6	68649,6	73459,1	58224,4	53518,4	55871,4
4	93584,9	86809,1	90197,0	69945,9	71449,2	70697,6
7	104859,8	96046,9	100453,3	76024,5	78595,4	77310,0
10	105938,2	100491,4	103214,8	80120,5	83083,5	81602,0
16,6	111385,0	110295,6	110840,3	83061,7	88508,5	85785,1
23	119010,5	113563,7	116287,1	91776,6	89597,9	90687,2

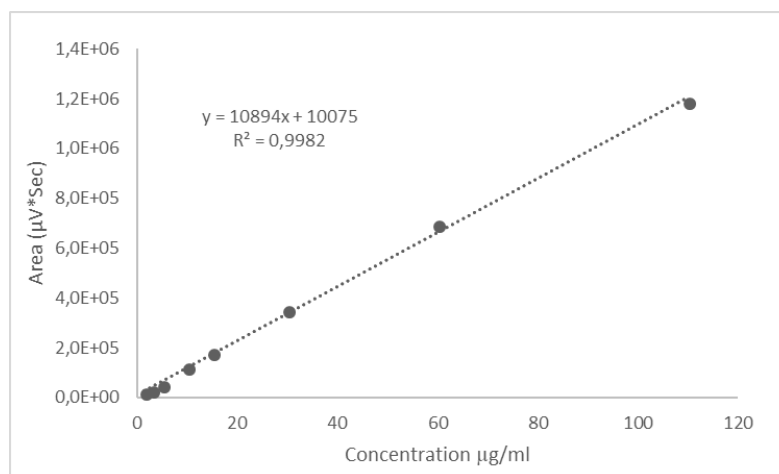


Figure S4: Calibrate curve of Pioglitazone.

3.5 Article 5

Thiazolidinedione as alternative to facilitate oral administration in geriatric patients with Alzheimer's Disease

Marcelle Silva-Abreu, Roberto Gonzalez-Pizarro, Lupe Carolina Espinoza, María José Rodríguez-Lagunas, Marta Espina, María Luisa García and Ana Cristina Calpena

European Journal of Pharmaceutical Science

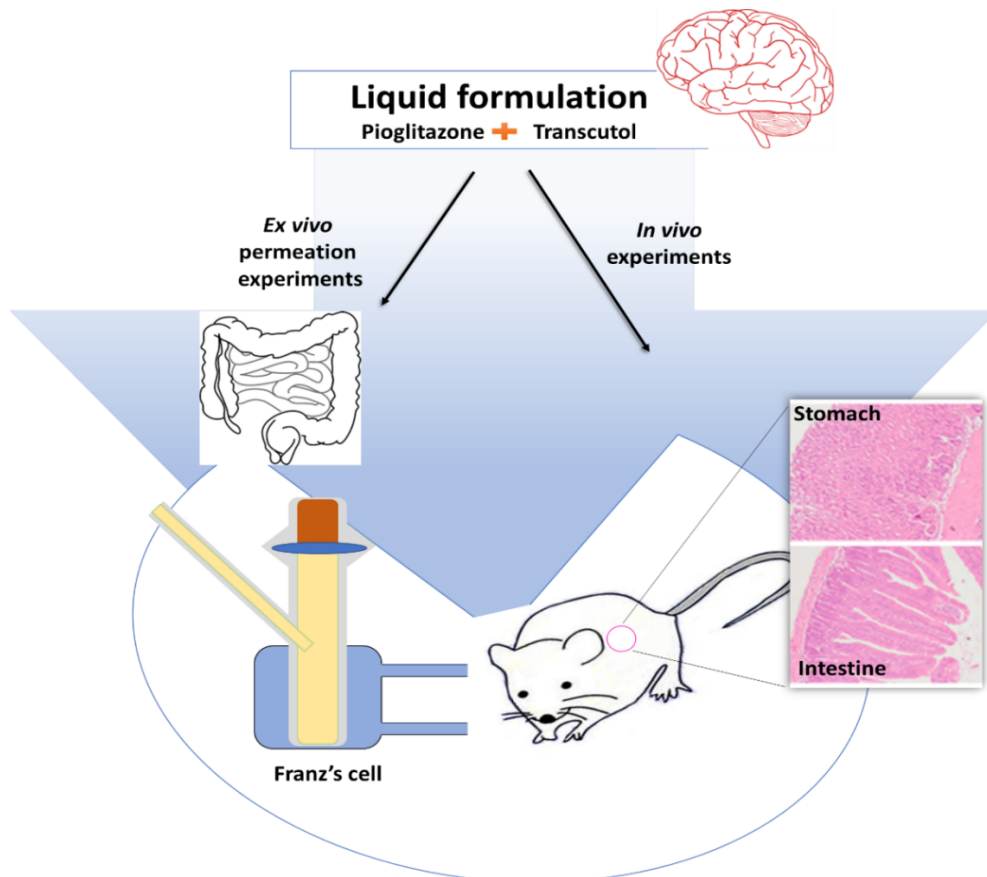
Year: 2018

ISSN: 0928-0987

IF: 3.773

Status: Submitted

Graphical abstract



Thiazolidinedione as alternative to facilitate oral administration in geriatric patients with Alzheimer's Disease

Marcelle Silva-Abreu^{1,2}, Roberto Gonzalez-Pizarro^{1,2}, Lupe Carolina Espinoza^{1,3}, María José Rodríguez-Lagunas^{4,5}, Marta Espina^{1,2}, María Luisa García^{1,2}, Ana Cristina Calpena^{1,2*}

¹ Department of Pharmacy, Pharmaceutical Technology and Physical Chemistry, Faculty of Pharmacy and Food Sciences, University of Barcelona, 08028 Barcelona, Spain

² Institute of Nanoscience and Nanotechnology (IN2UB), University of Barcelona, 08028 Barcelona, Spain

³ Departamento de Química y Ciencias Exactas, Universidad Técnica Particular de Loja, Loja 1101608, Ecuador

⁴ Department of Biochemistry and Physiology, Faculty of Pharmacy and Food Sciences, University of Barcelona, 08028 Barcelona, Spain

⁵ Institut de Recerca en Nutrició i Seguretat Alimentària (INSA), Universitat de Barcelona (UB), 08028 Barcelona, Spain

Correspondence: Dra Ana Cristina Calpena. Email: anacalpena@ub.edu; Tel.: +34 934024560

Abstract

Pioglitazone (PGZ) is a member of the thiazolidinedione (TZDs) family of drugs used to treat type 2 diabetes. Previous studies have reported anti-inflammatory and neuroprotective effects in the central nervous system. Based on this, the aim of this study was to develop an oral solution of PGZ (PGZ-SOL) as an alternative treatment for geriatric patients with Alzheimer's disease (AD). Solubility of PGZ was evaluated to establish the solution composition. Parameters including pH, rheology, extensibility and retention time were determined. *In vitro* release and *ex vivo* permeation studies were carried out using buccal, sublingual, nasal and intestinal mucosae. The toxicity of PGZ-SOL was evaluated by *in vivo* model using BALB/c mice. PGZ-SOL showed a Newtonian behaviour and physical stability during a period of three months. The release profile of PGZ from formulation followed a first-order kinetic model. The biopharmaceutical parameters revealed the high permeability of PGZ through intestinal mucosa. Finally, the oral administration of PGZ-SOL did not cause damage of buccal, sublingual and intestinal mucosae. Therefore, these results suggest that this formulation constitutes a viable alternative for AD treatment in geriatric populations with difficulty swallowing conventional solid dosage forms.

Keywords: Pioglitazone; thiazolidinediones; geriatric patients; oral administration; mucosal permeation; Alzheimer's disease.

1. Introduction

Alzheimer's disease (AD) is a neurodegenerative disorder characterized by synapse loss, accumulation of senile plaques and a consequent decline in cognition (El Kadmiri et al., 2018). According to the World Health Organization, 50 million people suffer dementia worldwide and this figure is increasing by about 10 million new cases every year. AD represents the most common form of dementia, constituting 60 – 70% of cases and predominantly affecting people aged 65 or older (2016, Alzheimer's Association; Spuch and Navarro, 2011). Pharmacological options currently available for the treatment of the disease include cholinesterase inhibitors (rivastigmine, donepezil and galantamine) and N-methyl-D-aspartate (NMDA) receptor antagonists (memantine) (Coman and Nemeş, 2017; Ulep et al., 2018). However, AD remains incurable because these treatments stop short of reversing, preventing or significantly delaying the progress of the disease (Hajipour et al., 2017). Due to this fact, AD is one of the great medical challenges of the 21st century (Scheltens et al., 2016). Several new therapeutic approaches based on evidence that link this disease to diabetes, inflammation, dyslipidemia and stress are currently being investigated (Caruso et al., 2018; Oliveira et al., 2018; Vieira et al., 2017). Interestingly, chronic neuroinflammation has been related with amyloid plaque progression and neurodegeneration. This development has led to the exploration of new therapeutic targets (Combarros et al., 2011; Yao et al., 2009).

Peroxisome proliferator-activated receptor gamma (PPAR- γ) is a nuclear receptor that regulates glucose hemostasis, lipid metabolism and inflammation (Park et al., 2016). Thiazolidinediones (TZDs) are a class of drugs that act as PPAR- γ agonists and are used to treat type 2 diabetes mellitus since they enhance insulin sensitivity. Several studies have reported additional pharmacological activities of TZDs, including anti-inflammatory effects in the central nervous system (CNS), neuroprotective effects and inhibition of neurotoxicity (Chou et al., 2017; El-Sahar et al., 2015). Pioglitazone (PGZ) is a member of the TZDs and is classified as a class II drug due to its low solubility and high permeability, according to the Biopharmaceutical Classification System. Currently, PGZ is available in tablet form for oral administration (He et al., 2014; Taupitz et al., 2013). However, this type of formulation presents inconveniences among geriatric patients since they frequently have difficulty swallowing solid dosage forms (Mc Gillicuddy et al., 2016).

Difficulty in swallowing medicines is common among elderly patients, especially in those who suffer from cerebrovascular or neurological conditions such as strokes, Parkinson's disease and

AD (Schiele et al., 2013). People's ability to take oral dosage forms is a parameter that must be considered during the development and design of therapeutic products in order to select the most convenient dosage form in accordance to patient needs (Lau et al., 2018; Notenboom et al., 2017).

Oral liquid formulations offer the advantage of dosing flexibility in relation to the corporal weight along with the added benefit of decreased risk of choking. These dosage forms can be administered to patients who are geriatric, pediatric, or in palliative conditions, and can also be used for individual (pharmaceutical compounding) or batch scale (van der Vossen et al., 2017). Oral solutions constitute an appropriate alternative to drug administration for people with individualized needs, such as patients with AD, and therefore is the ideal form of administration because of their non-complex development process, low relative cost of production and ease of swallowing (Walsh et al., 2018).

Considering the therapeutic potential of PGZ on neuroinflammation and the clinical state of patients with AD, the aim of this study was to develop and evaluate the permeability through different transmucosal tissues of an oral solution of PGZ using solubilizing excipients as an alternative treatment for geriatric patients with AD who have difficulty swallowing conventional solid dosage forms.

2. Materials and methods

2.1 Materials

PGZ was purchased from Capot Chemical (Hangzhou, China) and Transcutol-HP (T-HP) was obtained from Gattefossé (Barcelona, Spain). Phosphate buffer saline (PBS) solution, propylene glycol (PG), polyethylene glycol (PEG) and reagents for histological analysis were obtained from Sigma-Aldrich (Madrid, Spain). Double distilled water was obtained from a MilliQ System lab supplied and used for all the experiments. All other chemicals were of analytical grade and used without further purification.

2.2 Methods

2.2.1 Solubility study and preparation of PGZ-SOL

The solubility of PGZ was determined in several solubilizing excipients such as propylene glycol (PG), Transcutol-HP (oral route) and polyethylene glycol (PEG). An excess of drug was added to 2 g of these excipients and then mixed under stirring for 6 h. Samples were centrifuged at 8000 rpm for 20 min. The supernatant was diluted with methanol and PGZ was determined

using Thermo Spectronic Helios Beta UV-Visible Spectrophotometer (Satheeshkumar et al., 2014). PGZ-SOL was prepared using the excipient that showed the greatest solubilizing potential for PGZ in order to improve its aqueous solubility. Different ratios of solubilizing excipient - water (20:80, 40:60, 50:50 and 60:40; v/v) were assayed, and the final formulation was selected based on physical and chemical stability properties analysis during a period of three months. The pH of PGZ-SOL was evaluated using a digital pH meter GLP 22 (Crisson Instruments, Barcelona, Spain). Final formulation was filtered through using a filter of 0.22 μm to ensure microbiological stability.

2.2.2 Release profile

The release profile of the PGZ-SOL was carried out using Franz diffusion cells (FDC 400, Crown Glass, Somerville, NY, USA) with a membrane dialysis of MW 12 – 14 KDa. A volume of 0.3 ml of PGZ-SOL at 1 mg/ml concentration was placed in the donor compartment. Aliquots of 0.3 ml were withdrawn from the receptor compartment via syringe at predefined time points over 24 h. The extracted volume was immediately replaced by an equivalent volume of receptor solution (transcutol and water (60:40), stirred by a small magnetic bar (700 rpm) and thermostated at 37 ± 2 °C guaranteeing sink conditions. The experiment was performed with three cells and the amount of PGZ released was measured by HPLC (Silva-Abreu et al., 2017). The data of PGZ released at each time point was evaluated and fitted to the best kinetic model. Akaike's information criterion (AIC) and coefficient of determination (r^2) were determined for each case as an indicator of the model's suitability for each dataset (Yamaoka et al., 1978).

2.2.3 Rheological compartment

The rheological behavior was conducted with PGZ-SOL in duplicate in a rotational rheometer HAAKE Rheostress 1 (Thermo Fisher Scientific, Karlsruhe, Germany) at 25 ± 0.2 °C, 24 h after preparation sample. For measurements, the device was connected to a thermostatic circulator Thermo Haake Phoenix II + Haake C25P and equipped with cone-plate geometry (0.105 mm gap) including a Haake C60/2Ti mobile cone (60 mm diameter and 2° angle). The shear stress (s) was measured as a function of the shear rate (c). Viscosity curves ($\eta = (\dot{\gamma})$) and flow curves ($\tau = (\dot{\gamma})$) were determined at three steps shear rates; firstly, a ramp-up period from 0 to 50 s^{-1} for 3 min, followed by a constant shear rate period at 50 s^{-1} for 1 min and finally the ramp-down period from 50 to 0 s^{-1} for 3 min. Viscosity mean value at t_0 and 25°C was determined from the constant shear stretch at 50 s^{-1} of the viscosity curves ($\eta = (\dot{\gamma})$). The determination of the disturbance of the microstructure during the test or “apparent thixotropy” (Pa/s) was also

evaluated. The data from the flow curves ($\tau = (\gamma)$) were fitted to different mathematical models (Silva-Abreu et al., 2018) and the best fitting model was based on the correlation coefficient value (r).

2.2.4 Extensibility and Retention Measurement

The extensibility assay was carried out based on the method described previously (Campana-Seoane et al., 2014). A sample of 30 μ l was immediately placed as centered as possible between 2 glass slides of 5 cm². Force was generated onto the upper plate by adding known weights of 8.65, 9.65, 11.65 and 16.65 g. After that, the sample was compressed to uniform thickness. After 60 s, the weights were removed and the area of the sample was recorded. PGZ-SOL was evaluated in triplicate and the values are reported as the mean \pm SD ($n = 3$).

The retention time of the formulation was analyzed by modifying a previously reported method (Vermani et al., 2002). The tubular intestine immediately extracted from the pig was cut into sections of 15 cm of diameter and suspended vertically with the help of some supports. The intestine was previously covered with wet cotton using Hanks solution and aluminium foil to keep the mucosa in ideal condition. An analytical balance was placed under the suspended intestine to weigh the quantity of PGZ formulation that falls at certain times. 1 mL sample was applied to the upper part of the intestine with the help of a syringe of 2 mL and the weights were determined for 10 min. The experiments were done in triplicate and the values are reported as the mean \pm SD ($n = 3$).

2.2.5 Mucosa samples

Porcine mucosa was obtained from the Animal Facility at Bellvitge Campus of Barcelona University (Barcelona, Spain) ($n=6$), approved by the Animal Experimentation Ethical Committee of the University of Barcelona, Spain (CEEAA-UB). Fresh mucosa was obtained immediately after pig's sacrifice (male, weight 30–40 kg). Firstly, the animals were anesthetized with ketamine HCl (3 mg/kg), xylazine (2.5 mg/kg) and midazolam (0.17 mg/kg). To induce the sacrificed an overdose of sodium pentobarbital under deep anaesthesia was used. Then buccal, sublingual, nasal and intestinal mucosa was surgically removed and placed in Hanks balanced salt solution and refrigerated until the start of the experiments (not more than 24 h).

2.2.6 *Ex vivo* permeation studies

Each porcine mucosa was mounted using a membrane holder between the donor and the receptor compartments of Franz-type diffusion cells (Vidra Foc, Barcelona, Spain). Buccal and nasal tissue thickness was of 0.5 mm, sublingual of 0.3 mm and whole intestine. A volume of 200 μ l of PGZ at 1 mg/ml (dissolved in transcutol/water, 6:4 v/v) was placed in the donor compartment and the same volume was withdrawn via syringe from the receptor compartment at predefined time intervals up to a maximum of 6 h and replaced with an equivalent volume of fresh receptor medium of transcutol/water (6:4 v/v). The condition temperature was controlled at 37 ± 0.5 °C by a circulating water bath and magnetic stir bar at 700 rpm to guarantee homogeneity of the fluid in the receptor compartment during the experiments. The amount of permeated PGZ per unit area (μ g/cm²) in the different mucosa was analyzed in triplicates using a previously validated analytical method (Silva-Abreu et al., 2017). The parameters were assessed using GraphPad Prism® 6.0 (GraphPad Software Inc., San Diego, California, USA). The integrity rated of mucosae was assessed by measuring transepidermal water loss (TEWL) (TEWL-meter TM210 Courage & Khazaka, Koln, Germany) and transepithelial electrical resistance (TEER), exhibiting values below 10 g/m²h and around 3.0 K Ω , respectively. Additionally, buccal, sublingual and intestine tissue structure were histologically analyzed after finishing the permeation assay.

2.2.7 *In vivo* assay and histology analysis

According to the previous permeation results, an *in vivo* model study was carried out using four months old male BALB/c mice. Animals were maintained under standard animal housing conditions in a 12-h dark-light cycle with free access to food and water. The experiment followed the guidelines of Ethical Committee for Animal Experimentation of the University of Barcelona and the Catalonia Government. For one week, a dose of 10 mg/kg per day of PGZ-SOL, vehicle of transcutol/water, negative control with PBS solution and positive control with ketorolac tromethamine (NSAID) were orally administrated ($n = 5$). After the supplementation period, the mice were sacrificed by cervical dislocation and the intestine and stomach were removed to be analyzed histomorphologically.

To carry out the histological analysis, the mucosa samples were fixed in 4% buffered formaldehyde at room temperature for 24 h, then washed in PBS for 3 h, dehydrated in graded ethanol (70%, 90%, and 100%), and after permeation in xylene, embedded in paraffin. The paraffin embedded samples were cut into 5 μ m-sections and stained with hematoxylin and

eosin. After that, the samples were analyzed under a microscope (Olympus BX41 and camera Olympus XC50) with 100 or 200 times magnification for the evaluation of the tissue structure.

2.2.8 Biopharmaceutical parameters

2.2.8.1 Pioglitazone remaining in the tissue and data analysis

After the *ex vivo* experiments, the amount of PGZ retained in the tissues was measured as previously described Q_r , ($\mu\text{g PGZ/g tissue/cm}^2$) (Silva-Abreu et al., 2017). The tissue was rinsed with sodium lauryl sulphate solution 0.05% and washed with distilled water. The permeation area was excised and weighed, then the PGZ retained was extracted with methanol (1 ml) under sonication for 20 min in ultrasound bath. The amount of PGZ was analysed by HPLC. The cumulative amount of PGZ (μg) permeated through mucosa was plotted as a function of time (h). The slope and intercept of the linear portion of the plot was derived by regression.

The flux values J_{ss} , ($\mu\text{g/min/cm}^2$) across the mucosa and the permeability coefficients (Kp) were determined per unit surface area versus time plot. In this plot the lag time (T_l , min) is the intercept with the X-axis (time) by linear regression analysis of permeation. The flux values were demonstrated by the following equation (2) and all these parameters were estimated using the Prism®, version 6.0 software (GraphPad Software Inc., San Diego, CA, USA).

$$J_{ss} = \frac{Qt}{A} \cdot t \quad (2)$$

Where Qt is the quantity of PGZ across the mucosa into the receptor compartment (μg), A is the active cross-sectional area accessible for diffusion (cm^2) and t is the time of exposure (min).

The permeability coefficient (Kp , cm/min) and the parameters of permeation (cm) and diffusion (min^{-1}) P_1 and P_2 , were estimated (Sanz et al., 2017). Moreover, the mean transit time (MTT, day) of the drug in the mucosa was stipulate (Parra et al., 2016).

The theoretical human steady-state plasma concentration (C_{ss}) of drug, which would predict the potential systemic concentration achieved after mucosa administration, was obtained using the following equation (3):

$$C_{ss} = J_{ss} \cdot \frac{A}{Cl_p} \quad (3)$$

Where C_{ss} , is the plasma steady-state concentration, J_{ss} the flux determined in this study, A the hypothetical area of application and Clp the plasmatic clearance. The calculations are based on a maximum area of application of 20 cm² for buccal, 15 cm² for sublingual, 150 cm² for nasal and 126.5 cm² for intestinal duodenal part (Christrup et al., 2009; Kapoor et al., 2016). The human Clp value of PGZ was 2.26 L/h \pm 1.22 in order to estimate the blood concentration (Wittayalerpanya, 2006).

2.2.9 Statistical analysis

All the data were presented as mean \pm SD. One-way ANOVA followed by Tukey's test were used for multi-group comparison. Statistical significance was set at $p < 0.05$. The software Haake RheoWin[®] Job Manager V.3.3 and RheoWin[®] Data Manager V.3.3 (Thermo Electron Corporation, Karlsruhe, Germany) were also used to carry out the test and analysis of the results of rheological data, respectively. GraphPad Prism[®] software version 6.0 (GraphPad Software Inc.) was used to carry out the analysis of all experiments.

3. Results and discussion

3.1 Solubility and preparation of PGZ-SOL

The water-soluble organic solvent with the highest solubilizing potential for PGZ was Transcutol-HP (Figure 1) and was consequently selected for the formulation. PGZ-SOL with ratios of Transcutol-HP-water of 20:80, 40:60 and 50:50 (v/v) showed physical instability, which was evident by the presence of visible precipitation of the drug. The formulation with the ratio of Transcutol-HP-water of 60:40 (v/v) was physically stable during the study period, and therefore, was chosen as final formulation. The pH value of PGZ-SOL was 4.5, which is compatible for oral administration. Transcutol is an ethylene oxide derivative that is widely used as a strong solubilizer in pharmaceutical, cosmetic, nutraceutical and food products due to its low toxicity and high biocompatibility (Sullivan et al., 2014).

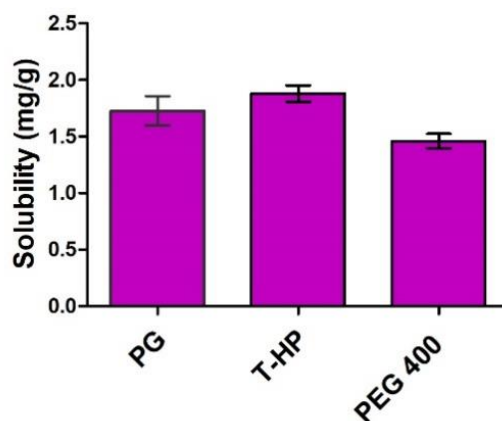


Figure 1: Solubility of PGZ at 25 °C in different water-soluble organic solvents ($n = 3$)

3.2 Release profile

The drug release studies demonstrate that release kinetics is not a limiting factor of the drug permeation. The data showed that at 4 h, 38.13 % of PGZ was released. Figure 2 shows the results fitted to “one-phase exponential association” reaching levels of Y_{\max} of 52.19 ($\mu\text{g}/\text{cm}^2$) with a constant of dissolution (h^{-1}) of 0.53 during 24 h of experiment. The lower AIC (162.7) indicates that the release kinetics from the drug release was the best model assayed. This fact is due to PGZ being released from formulation following the concentration gradient pattern, based on Fick’s first law (Parra et al., 2015). This model showed a coefficient of determination (r) of 0.987 with a fast release.

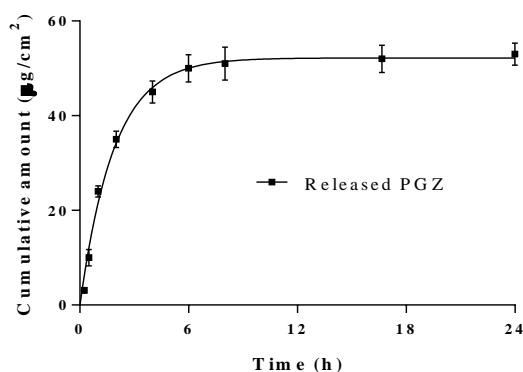


Figure 2: Released cumulative amount of PGZ-SOL and its kinetic approach (One phase exponential association). Results are given as mean \pm SD ($n = 3$).

3.3 Rheological study

The rheological behavior of PGZ solution showed the flow curves and indicated no thixotropic behavior in the system as the rheograms did not display any hysteresis loop (Figure 3).

Newton model was the best overall match fitted for rheological behavior, based on the correlation coefficient of regression ($r = 0.9996$). The value of viscosity (mPa·s) at 50 s^{-1} and 25°C was of $(5.66 \pm 4.96) 10^{-2}$, confirming that viscosity is not affected by changes in shear rate. On the other hand, rheology is a useful technique to characterize the structure of different formulations. However, viscosity of vehicles may play an important role in controlling the release and permeation of drugs. In this case, the formulation was found to be easily spreadable. Moreover, the Newtonian behavior of the PGZ solution at room temperature makes it suitable for application as an oral spray for geriatric patients, who have difficulty swallowing medicines such as tablets, capsules or pills (van der Vossen et al., 2017).

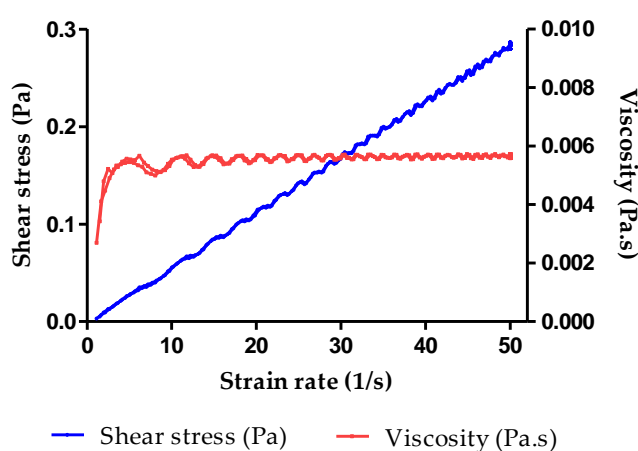


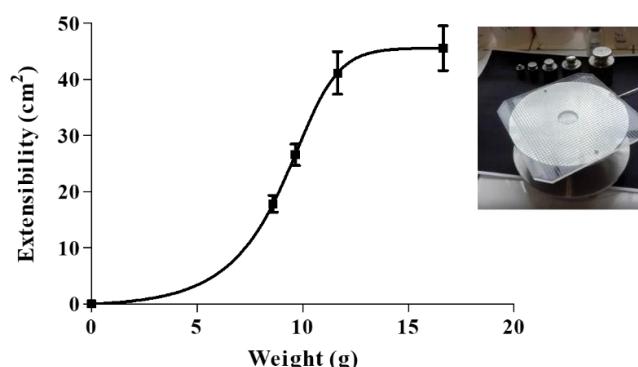
Figure 3: Rheogram profile obtained from PGZ-SOL.

3.4 Extensibility and Retention Measurement

The extensibility showed an asymmetric sigmoidal profile, with a coefficient of determination (r^2) = 0.980 (Figure 4). According to this result, the formulation presents easy extensibility, being able to spread over the surface of the application without difficulty in contrast to other formulations such as cream, gel and ointments (Abrego et al., 2016; Abrego et al., 2015; Mallandrich et al., 2017; Sanz et al., 2018).

Retention of PGZ-SOL in the intestinal mucosa was assessed as described before (section 2.2.4). The total weight of PGZ-SOL expelled from the vertically suspended pig's intestinal was considered to be 100%, and the percentage of weight fallen with time was recorded (Fig. 4b). PGZ-SOL was retained in the pig intestine suspended in the assembly for the entire period of observation (10 min). From the results obtained, it can be concluded that PGZ-SOL possesses lower bioadhesive strength under the conditions established in contrast to others studies of different formulation (Abrego et al., 2016; Mallandrich et al., 2017).

a)



b)

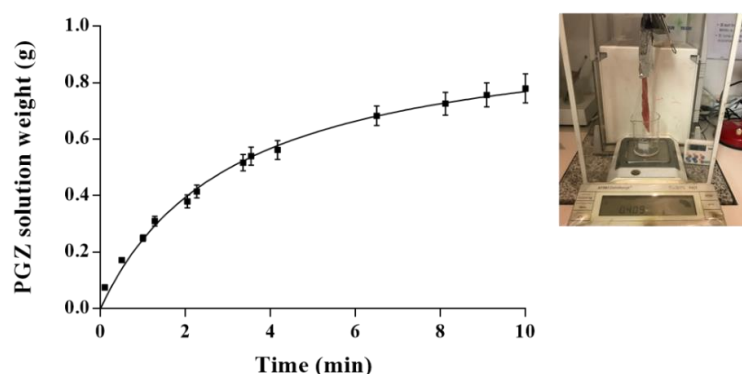


Figure 4: a) Profile of extensibility of PGZ solution; b) Retention of PGZ solution in vertically suspended isolated sheep intestinal tube. (The formulation fell down in 10 min) ($n = 3$).

3.5 *Ex vivo* permeation assays

Figure 5 shows the permeation profile of PGZ (μg) in nasal, sublingual, buccal and intestinal mucosa. The permeation of PGZ through the nasal mucosa showed high values in the different parameters analyzed (Table 1). In accordance with previous studies, the C_{max} of orally administered PGZ in healthy people showed values from 0.1 $\mu\text{g}/\text{ml}$ to 3.5 $\mu\text{g}/\text{ml}$ at the doses of 2 mg and 60 mg, respectively (Eckland and Danhof, 2000). The nasal passage is not a safe route due to its high levels of steady-state of PGZ in this study (C_{ss} : $4.20 \pm 0.32 \mu\text{g}/\text{ml}$, Table 1), therefore it could be a toxic route for administration of this formulation in geriatric patients with AD. Since it exceeds the allowed levels administered clinically in diabetes patients (45mg/day), it could cause hypoglycemic shock. Moreover, in Phase III clinical trials, PGZ has been used at 0.8 mg per day in people with mild cognitive impairment due to AD (Takeda). Based on this result, the nasal route has been excluded from the next analysis, instead focusing on the sublingual, buccal and intestinal routes.

According to the prediction and permeation parameters (Table 1), the intestinal mucosa showed statistically significant difference (SSD) in comparison with the other mucosae (sublingual and buccal). The intestinal mucosa showed lower T_l values than in the other mucosae, reaching plasma levels of steady-state equilibrium in less time ($p < 0.05$). Moreover, the P₁ (partition coefficient vehicle/mucosa) has greater affinity in leaving the vehicle to penetrate the mucosa and the P₂ (diffusion coefficient) in relation to the diffusion of drug through the mucosa, showing higher values compared to the other mucosae. In addition, the values of MTT showed that intestinal mucosa had a shorter residence time.

When compared to sublingual and buccal mucosa, the intestinal mucosa showed the best values to the C_{ss} of 0.09 µg/ml ($p < 0.05$) and has safe plasma levels because the sublingual and buccal mucosa presented very low values for C_{ss} of 0.01 µg/ml and 0.02 µg/ml, respectively. Even in the early stages of the disease this could be useful for geriatric patients with AD, due to the absence of a first pass effect.

Considering that the AD overwhelmingly affects the elderly, the drug administration ought to be as uncomplicated as possible. Solid dosage forms would be complicated medicines for them, especially in advanced stages of the disease when many do not have complete control of their faculties in order to keep the formulation in the buccal mucosa or under the tongue. Although the intestinal mucosa has a first-pass effect, it is important to mention that PGZ has active metabolites and will continue to be effective through oral route (Eckland and Danhof, 2000).

The values of PGZ retained in the mucosa were different in all the tissue studied showing SSD ($p < 0.05$) (Figure 6). High values were found in the case of sublingual and nasal with an average amount of 977.46 and 478.91 (µg PGZ/ g tissue/ cm²), respectively. The intestine showed very low retained amount of PGZ, which indicates that the drug had crossed the intestinal wall and accessed the systemic circulation.

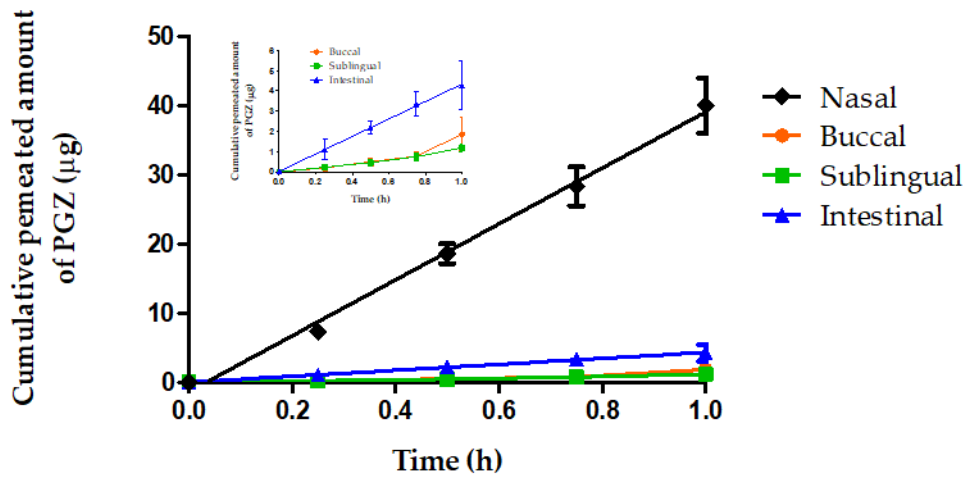


Figure 5: Cumulative permeated amount of PGZ through different mucosae ($n = 6$).

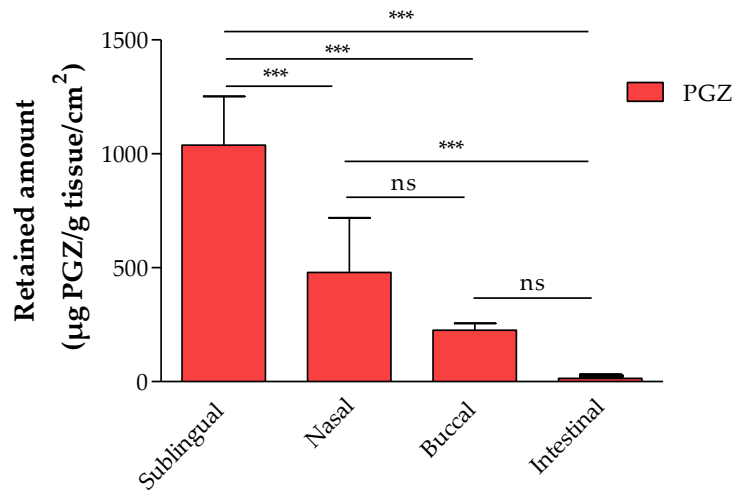


Figure 6: Retained amount of PGZ in different tissues ($n = 6$). One-way Analysis of Variance (ANOVA) with Tukey's Multiple Comparison Tests were performed to assess the statistical significance with respect to PGZ solution at ($p < 0.05$).

Table 1: Permeation and prediction parameters of PGZ expressed in different mucosae.

Permeation and Prediction Parameters	Nasal	Sublingual ^a	Buccal ^b	Intestinal
J_{ss} ($\mu\text{g}/(\text{h}/\text{cm}^2)$)	63.12 ± 6.29	1.82 ± 0.19	2.74 ± 0.24^a	1.71 ± 0.16^b
K_p ($\text{cm}/\text{h}) \cdot 10^3$	63.12 ± 5.50	1.82 ± 0.15	2.74 ± 0.25^a	1.71 ± 0.15^b
Tl (min)	2.01 ± 0.15	2.76 ± 0.21	11.17 ± 0.01^a	$0.19 \pm 0.01^{a,b}$
P1 (cm) $\cdot 10^5$	1274.87 ± 112.50	50.37 ± 4.50	307.05 ± 31.02^a	$3.30 \pm 0.29^{a,b}$
P2 (h^{-1})	4.95 ± 0.41	3.62 ± 0.32	0.89 ± 0.07^a	$51.85 \pm 0.49^{a,b}$
MTT (day)	0.21 ± 0.01	7.14 ± 0.65	4.76 ± 0.35^a	$2.87 \pm 0.18^{a,b}$
C_{ss} ($\mu\text{g}/\text{ml}$)	4.20 ± 0.32	0.01 ± 0.00	0.02 ± 0.00^a	$0.09 \pm 0.00^{a,b}$

^{a,b} Results are expressed by mean \pm SD ($n = 6$). One-way Analysis of Variance (ANOVA) with Tukey's Multiple Comparison Tests were performed to assess the statistical significance between each mucosae with respect to PGZ at ($p < 0.05$).

3.6 Histomorphological assay

Ex vivo assay

After the *ex vivo* permeation assay histological architecture of buccal, sublingual or intestinal, tissues were analyzed.

Treatment of the different tissues with PGZ did not induce important changes at the histological level. In Figure 7, histological sections from buccal, sublingual and intestine tissues stained with hematoxylin and eosin show normal morphology after exposure to control conditions and vehicle (A and C, respectively), and altered tissues induced by isopentaine alcohol application (B). Treatment of buccal mucosa and intestine with PGZ-SOL showed a similar pattern of the normal conditions or the vehicle. In the case of sublingual tissue, isopentaine alcohol showed loss of cornified layer and alteration of the stratum granulosum. The exposure to PGZ did not alter the different layers of the sublingual tissue, however some retraction can be observed. Altogether, these results suggest that PGZ does not damage the tissue, which corroborates with previous findings (Kandeel and Balaha, 2015).

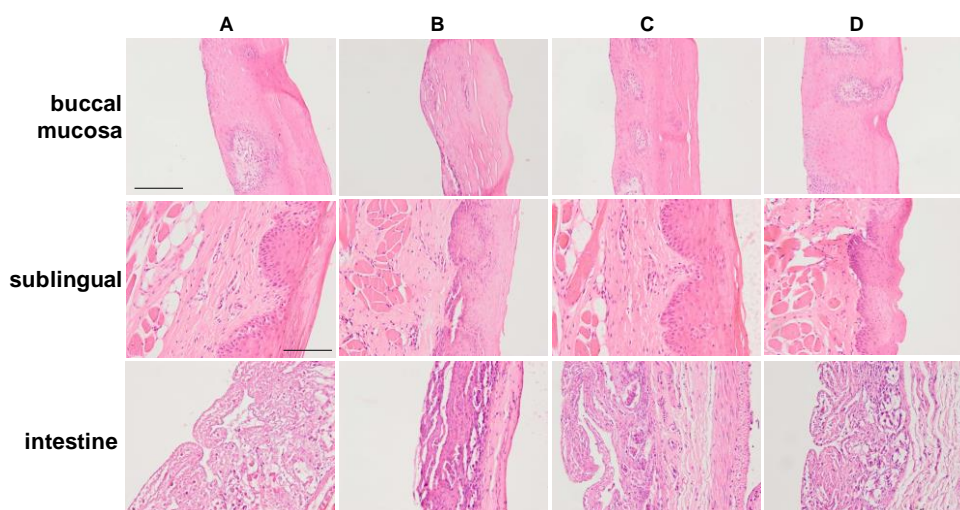


Figure 7. Histological sections of freshly excised normal buccal, sublingual or intestinal mucosae exposed to PBS (A), isopentaine alcohol (B), vehicle (C) or PGZ (D). Micrographs showing hematoxylin and eosin staining of buccal mucosa (x100, scale bar = 200 μ m), sublingual and intestinal mucosae (x200, scale bar = 100 μ m).

In vivo assay

Moreover, in the *in vivo* results (Figure 8) normal stomach and intestinal architecture could be observed in control conditions. In the case of the positive condition (ketorolac tromethamine, an NSAID) a leukocyte infiltrate was present in both tissues, being more noticeable in the case of the stomach. Treatment with PGZ did not show alterations of the tissue structure or signs of inflammation in any of the tissues analyzed.

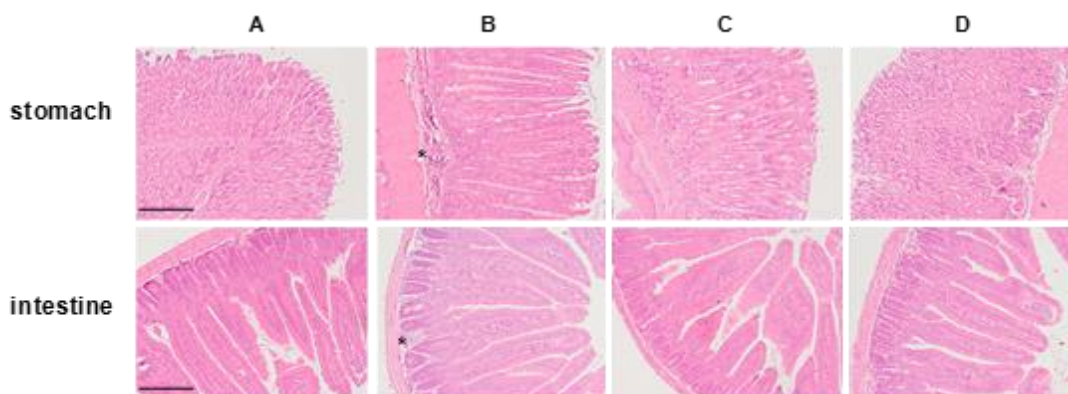


Figure 8. Histological sections of mice stomach and intestinal tissue. Hematoxylin and eosin staining of the tissues after administration of PBS (A), ketorolac tromethamine (B), vehicle (C) or PGZ (D). (x100, scale bar = 200 μ m, * indicates leukocyte infiltrate).

4. Conclusion

In summary, an oral solution of a poorly water-soluble drug was developed. PGZ-SOL showed Newtonian behavior, which is typical of a solution, and was physically stable during the study period. The formulation exhibited a fast release following a first-order kinetic model. The biopharmaceutical parameters revealed the ability of formulation to permeate through intestinal mucosa, thus favouring the likelihood of achieving adequate bioavailability of the drug at the site of action. Moreover, PGZ-SOL administered orally *in vivo* results in no damage of the mucosa, as demonstrated by histological results, and therefore suggests that this formulation is safe for oral administration. In conclusion, PGZ-SOL constitutes a suitable alternative for the geriatric population with AD who have difficulty swallowing solid dosage forms and can be developed for large-scale production or for pharmaceutical compounding.

Acknowledgements

This work was supported by the Coordination for the Improvement of Higher Education Personnel (CAPES) – Brazil. Marcelle Silva-Abreu also acknowledges her Ph.D. scholarship - CAPES, Brazil. The authors thank Jonathan Proctor for reviewing English.

REFERENCES

- Alzheimer's Association. 2016 Alzheimer's disease facts and figures. *Alzheimer's & Dementia* 12, 459-509.
- Abrego, G., Alvarado, H., Souto, E.B., Guevara, B., Bellowa, L.H., Garduno, M.L., Garcia, M.L., Calpena, A.C., 2016. Biopharmaceutical profile of hydrogels containing pranoprofen-loaded PLGA nanoparticles for skin administration: In vitro, ex vivo and in vivo characterization. *International journal of pharmaceutics* 501, 350-361.

- Abrego, G., Alvarado, H., Souto, E.B., Guevara, B., Bellowa, L.H., Parra, A., Calpena, A., Garcia, M.L., 2015. Biopharmaceutical profile of pranoprofen-loaded PLGA nanoparticles containing hydrogels for ocular administration. *European journal of pharmaceutics and biopharmaceutics* 95, 261-270.
- Campana-Seoane, M., Peleteiro, A., Laguna, R., Otero-Espinar, F.J., 2014. Bioadhesive emulsions for control release of progesterone resistant to vaginal fluids clearance. *International journal of pharmaceutics* 477, 495-505.
- Caruso, A., Nicoletti, F., Mango, D., Saidi, A., Orlando, R., Scaccianoce, S., 2018. Stress as risk factor for Alzheimer's disease. *Pharmacological research* 132, 130-134.
- Coman, H., Nemeş, B., 2017. New Therapeutic Targets in Alzheimer's Disease. *International Journal of Gerontology* 11, 2-6.
- Combarros, O., Rodriguez-Rodriguez, E., Mateo, I., Vazquez-Higuera, J.L., Infante, J., Berciano, J., Sanchez-Juan, P., 2011. APOE dependent-association of PPAR-gamma genetic variants with Alzheimer's disease risk. *Neurobiology of aging* 32, 547 e541-546.
- Chou, P.S., Ho, B.L., Yang, Y.H., 2017. Effects of pioglitazone on the incidence of dementia in patients with diabetes. *Journal of diabetes and its complications* 31, 1053-1057.
- Christrup, L., Lundorff, L., Werner, M., 2009. Novel formulations and routes of administration for opioids in the treatment of breakthrough pain. *Therapy* 6, 695-706.
- Eckland, D., Danhof, D., 2000. Clinical pharmacokinetics of pioglitazone. *Endocrinology & Diabetes* 108, S234-S242.
- El-Sahar, A.E., Safar, M.M., Zaki, H.F., Attia, A.S., Ain-Shoka, A.A., 2015. Neuroprotective effects of pioglitazone against transient cerebral ischemic reperfusion injury in diabetic rats: Modulation of antioxidant, anti-inflammatory, and anti-apoptotic biomarkers. *Pharmacological reports : PR* 67, 901-906.
- El Kadmiri, N., Said, N., Slassi, I., El Moutawakil, B., Nadifi, S., 2018. Biomarkers for Alzheimer Disease: Classical and Novel Candidates' Review. *Neuroscience* 370, 181-190.
- Hajipour, M.J., Santoso, M.R., Rezaee, F., Aghaverdi, H., Mahmoudi, M., Perry, G., 2017. Advances in Alzheimer's Diagnosis and Therapy: The Implications of Nanotechnology. *Trends in biotechnology* 35, 937-953.
- He, W., Li, Y., Zhang, R., Wu, Z., Yin, L., 2014. Gastro-floating bilayer tablets for the sustained release of metformin and immediate release of pioglitazone: preparation and in vitro/in vivo evaluation. *International journal of pharmaceutics* 476, 223-231.
- Kandeel, S., Balaha, M., 2015. The possible protective effect of simvastatin and pioglitazone separately and in combination on bleomycin-induced changes in mice thin skin. *Tissue & cell* 47, 159-170.
- Kapoor, M., Cloyd, J.C., Siegel, R.A., 2016. A review of intranasal formulations for the treatment of seizure emergencies. *Journal of controlled release* 237, 147-159.
- Lau, E.T.L., Steadman, K.J., Cichero, J.A.Y., Nissen, L.M., 2018. Dosage form modification and oral drug delivery in older people. *Advanced drug delivery reviews*.
- Mallandrich, M., Fernández-Campos, F., Clares, B., Halbaut, L., Alonso, C., Coderch, L., Garduño-Ramírez, M.L., Andrade, B., del Pozo, A., Lane, M.E., Calpena, A.C., 2017. Developing Transdermal Applications of Ketorolac Tromethamine Entrapped in Stimuli Sensitive Block Copolymer Hydrogels. *Pharmaceutical Research* 34, 1728-1740.
- Mc Gillicuddy, A., Kelly, M., Sweeney, C., Carmichael, A., Crean, A.M., Sahn, L.J., 2016. Modification of oral dosage forms for the older adult: An Irish prevalence study. *International journal of pharmaceutics* 510, 386-393.
- Notenboom, K., Leufkens, H.G., Vromans, H., Bouvy, M.L., 2017. Learning from patients: Identifying design features of medicines that cause medication use problems. *International journal of pharmaceutics* 517, 128-134.
- Oliveira, B.C.L., Bellozi, P.M.Q., Reis, H.J., de Oliveira, A.C.P., 2018. Inflammation as a Possible Link Between Dyslipidemia and Alzheimer's Disease. *Neuroscience* 376, 127-141.
- Park, H.J., Park, H.S., Lee, J.U., Bothwell, A.L., Choi, J.M., 2016. Sex-Based Selectivity of PPARgamma Regulation in Th1, Th2, and Th17 Differentiation. *International journal of molecular sciences* 17.

- Parra, A., Clares, B., Rossello, A., Garduno-Ramirez, M.L., Abrego, G., Garcia, M.L., Calpena, A.C., 2016. Ex vivo permeation of carprofen from nanoparticles: A comprehensive study through human, porcine and bovine skin as anti-inflammatory agent. *International journal of pharmaceutics* 501, 10-17.
- Parra, A., Mallandrich, M., Clares, B., Egea, M.A., Espina, M., Garcia, M.L., Calpena, A.C., 2015. Design and elaboration of freeze-dried PLGA nanoparticles for the transcorneal permeation of carprofen: Ocular anti-inflammatory applications. *Colloids and surfaces. B, Biointerfaces* 136, 935-943.
- Sanz, R., Calpena, A.C., Mallandrich, M., Gimeno, A., Halbaut, L., Clares, B., 2017. Development of a buccal doxepin platform for pain in oral mucositis derived from head and neck cancer treatment. *European journal of pharmaceutics and biopharmaceutics* 117, 203-211.
- Sanz, R., Clares, B., Mallandrich, M., Suner-Carbo, J., Montes, M.J., Calpena, A.C., 2018. Development of a mucoadhesive delivery system for control release of doxepin with application in vaginal pain relief associated with gynecological surgery. *International journal of pharmaceutics* 535, 393-401.
- Satheeshkumar, N., Shantikumar, S., Srinivas, R., 2014. Pioglitazone: A review of analytical methods. *Journal of pharmaceutical analysis* 4, 295-302.
- Scheltens, P., Blennow, K., Breteler, M.M.B., de Strooper, B., Frisoni, G.B., Salloway, S., Van der Flier, W.M., 2016. Alzheimer's disease. *The Lancet* 388, 505-517.
- Schiele, J.T., Quinzler, R., Klimm, H.D., Pruszydlo, M.G., Haefeli, W.E., 2013. Difficulties swallowing solid oral dosage forms in a general practice population: prevalence, causes, and relationship to dosage forms. *European journal of clinical pharmacology* 69, 937-948.
- Silva-Abreu, M., Espinoza, L., Halbaut, L., Espina, M., García, M., Calpena, A., 2018. Comparative Study of Ex Vivo Transmucosal Permeation of Pioglitazone Nanoparticles for the Treatment of Alzheimer's Disease. *Polymers* 10, 316.
- Silva-Abreu, M., Espinoza, L.C., Rodriguez-Lagunas, M.J., Fabrega, M.J., Espina, M., Garcia, M.L., Calpena, A.C., 2017. Human Skin Permeation Studies with PPARgamma Agonist to Improve Its Permeability and Efficacy in Inflammatory Processes. *International journal of molecular sciences* 18.
- Spuch, C., Navarro, C., 2011. Liposomes for Targeted Delivery of Active Agents against Neurodegenerative Diseases (Alzheimer's Disease and Parkinson's Disease). *Journal of drug delivery* 2011, 469679.
- Sullivan, D.W., Jr., Gad, S.C., Julien, M., 2014. A review of the nonclinical safety of Transcutol(R), a highly purified form of diethylene glycol monoethyl ether (DEGEE) used as a pharmaceutical excipient. *Food and chemical toxicology : an international journal published for the British Industrial Biological Research Association* 72, 40-50.
- Takeda, Extension Study of the Safety and Efficacy of Pioglitazone to Slow Cognitive Decline in Participants With Mild Cognitive Impairment Due to Alzheimer Disease.
- Taupitz, T., Dressman, J.B., Klein, S., 2013. New formulation approaches to improve solubility and drug release from fixed dose combinations: case examples pioglitazone/glimepiride and ezetimibe/simvastatin. *European journal of pharmaceutics and biopharmaceutics* 84, 208-218.
- Ulep, M.G., Saraon, S.K., McLea, S., 2018. Alzheimer Disease. *The Journal for Nurse Practitioners* 14, 129-135.
- van der Vossen, A.C., van der Velde, I., Smeets, O.S., Postma, D.J., Eckhardt, M., Vermes, A., Koch, B.C., Vulto, A.G., Hanff, L.M., 2017. Formulating a poorly water soluble drug into an oral solution suitable for paediatric patients; lorazepam as a model drug. *European journal of pharmaceutical sciences* 100, 205-210.
- Vermani, K., Garg, S., Zaneveld, L.J., 2002. Assemblies for in vitro measurement of bioadhesive strength and retention characteristics in simulated vaginal environment. *Drug development and industrial pharmacy* 28, 1133-1146.
- Vieira, M.N.N., Lima-Filho, R.A.S., De Felice, F.G., 2017. Connecting Alzheimer's disease to diabetes: Underlying mechanisms and potential therapeutic targets. *Neuropharmacology*.
- Walsh, J., Ranmal, S.R., Ernest, T.B., Liu, F., 2018. Patient acceptability, safety and access: A balancing act for selecting age-appropriate oral dosage forms for paediatric and geriatric populations. *International journal of pharmaceutics* 536, 547-562.

Wittayalertranya, S., 2006. The Pharmacokinetics of Pioglitazone in Thai Healthy Subjects. *J Med Assoc Thai* 89, 2116-2122.

Yamaoka, K., Nakagawa, T., Uno, T., 1978. Application of Akaike's Information Criterion (AIC) in the Evaluation of Linear Pharmacokinetic Equations. *Journal of Pharmacokinetics and Biopharmaceutics* 6, 165-175.

Yao, L., Li, K., Zhang, L., Yao, S., Piao, Z., Song, L., 2009. Influence of the Pro12Ala polymorphism of PPAR-gamma on age at onset and sRAGE levels in Alzheimer's disease. *Brain research* 1291, 133-139.

CHAPTER 4

DISCUSSION

4. DISCUSSION

This research focused on the development and characterization dosage forms of PGZ able to reduce inflammation associated with rosacea, uveitis and Alzheimer disease's.

In recent years PPAR- γ agonists have been receiving considerable attention due to their capacity to act in different diseases, where the inflammation is of relevant importance (58,63). PGZ is an antidiabetic oral agent, agonist of PPAR- γ . It belongs to the TDZ class and is used to treat type 2 diabetes. This drug has been investigated due to its ability to reduce inflammation responses by different mechanisms (146).

4.1 DEVELOPMENT, OPTIMIZATION AND CHARACTERIZATION OF DOSAGE FORMS

PGZ dosage forms were optimized and characterized by different techniques. Liquid formulation is excellent to dermal and orally administration. It is easy to prepare, being suitable for compounding formulation. Moreover, it allows an individualized dosage according to the patient's age and the stage to which the disease has developed. It enables dosing flexibility and offers a reduced risk of choking. Furthermore, they are very appropriate for geriatric patients who find it hard to swallow or in palliative conditions (182,183).

PGZ solution with transcutool and water showed a transparent colour, a pH of 4.5 and good stability at 25°C and 40°C for 3 months. Moreover, extensibility and gravimetric assays for PGZ solution showed asymmetric sigmoidal and hyperbola profiles, respectively (Article 5, figure 4 a,b). It is able to spread over the surface of the application without difficulty, in contrast to other formulations such as cream, gel and ointments (184–187).

The PGZ-NPs was produced by solvent displacement technique (178). This is an easy and fast method which can produce particles in the range of around 50-300 nm (188). To select the better formulation a factorial design was carried out studying the effects of the independent variables such as: concentration of polymer, surfactant and drug, on the dependent variable (Size, polydispersity index (PI), ZP, encapsulation efficiency (EE)) (Article 2, Table 1). PLGA was selected to encapsulate NPs because of its characteristics of being biocompatible, biodegradable and easy to metabolize by the body via Krebs cycle. It is a polymer approved by the EMA and FDA for use in humans (170–173). In

addition, PEG was added to the surface of PLGA to increase selective cellular binding, internalization and to avoid the RES uptake (171). In general, NPs are advantageous systems of drug delivery as they offer good biocompatibility, the capacity to adjust drug release, remarkably enhance the efficacy and bioavailability (189–191). PGZ-NPs showed an average size of less than 200 nm with an PI range of monodisperse systems of 0.1, a negative ZP (– 13.6) and EE of around 92 %. This system is a promising strategy to facilitate the delivery of PGZ across different tissues (Article 2 and 4, Figure 2 and S2, respectively). The ability of the NPs to cross biological membranes is influenced by their size, shape, NP composition, and surface properties (192). The analysis of PGZ was carried out by a reverse phase HPLC. The analytical method to PGZ determination was validated following the ICH guidelines Q2A and ICH Q2B in terms of linearity, precision, accuracy, robustness, sensitivity and specificity (Article 1).

The **interactions studies** between drug and polymer were determined by thermal (DSC) and spectroscopic (Fourier transform infrared spectroscopy (FTIR) and X-Ray) methods. DSC profiles (Article 2, Figure 3 b) showed that PGZ-NPs had a thermic event that corresponds to glass transition (T_g) of the polymer in the form of NPs (midpoint ISO of 40.98°C and onset of 38.82°C). The decrease in the T_g parameters in the NPs is probably due to a plastic effect exerted by the drug on the polymer. It showed how in the formulation the drug remained linked with the polymer. Furthermore, it showed no fusion of the drug, indicating that it is in a molecular dispersion or solid solution. These results are similar to those obtained by loaded NPs lipophilic drugs (193). As would be expected, FTIR analysis suggests that there is no evidence of new covalent bonds between the drug and the polymer (Article 2, Figure S2. Supplementary data) (194). The X-ray spectrum of PGZ powder showed sharp crystalline peaks, whereas PLGA-PEG and NPs, according to their profiles, were amorphous. These results suggested that when the drug was loaded in the form of NSs, it showed a similar polymer profile (Article 2, Figure 3 a).

The **short-time stability** of PGZ-NPs showed a slight increase in sedimentation after the second month (Article 3, figure 4). The limited stability of NPs in aqueous suspension is well known. These results indicate that improved long-term stability could be attained by the removing of water from the solution by lyophilization or a spray-drying technique (194,195).

In accordance with **rheological behaviour**, both formulations showed flow curves which do not indicate any thixotropic behaviour in the system. This was because the rheograms did not display any hysteresis loop (Article 3 and 5, Figure 3 and 3, respectively). Moreover, the rheograms show a linear relationship between the shear stress and the strain rate, which is characteristic of Newtonian behaviour (196). In this case, the formulations were found to be easily spreadable, and they could be applied orally or via nasal route.

4.2 BIOPHARMACEUTICAL BEHAVIOUR

The **drug release studies** demonstrate that release kinetics is not a limiting factor of the drug permeation. To achieve sustained drug release and prolonged therapeutic activity, the particles need to be retained in the tissue after administration, and the consequent release of the drug from the particles must then be at an appropriate rate (172). The release profile of the PGZ-NPs and PGZ solution showed the same kinetic model for both formulations (one exponential association) (Article 2 and 5, Figure 4a and 2, respectively). This fact is due to PGZ being released from both formulations following the concentration gradient pattern, based on Fick's first law (197). This is common of PLGA-NPs (184,185,194). Another consideration is that decreasing the surfactant concentration of the PGZ-NPs to 1.16 % the proportion of excipients leads to variations in the model, changing the fit model to hyperbola (Article 4, Figure 1), according to previous studies (198,199). This model at low concentrations behaves like a kinetic first order, similar to the results in articles 2 and 5. In addition, the fit models depend on the physicochemical characteristics of the molecules, excipients and the technology used in the preparation of the sample. However, the release of the drug from PLGA-PEG particles can occur through diffusion, erosion of the polymer or a combination thereof. If the diffusion of the drug progresses at a higher speed than the degradation of the matrix, the drug release mechanism makes itself felt mainly by diffusion (200).

The **ex vivo permeation** of PGZ dosage forms were tested in different tissues, such as skin, eye and different types mucosae (buccal, sublingual, nasal and intestinal).

PGZ solution was tested with different enhancers to improve its permeability through human skin and to see how it treated the rosacea (Article 1, Figure 1). This led to the conclusion that limonene was the most effective penetration enhancer that promoted the permeation of PGZ through human skin. Moreover, as shown in (Article 1, Table 1), limonene presents the highest values for flux (J_{ss}), permeability coefficient (k_p), retained

drug (Q_{ret}) and steady-state plasma concentration (C_{ss}). These results are in accordance with those obtained by others authors (201,202), suggesting that hydrocarbon terpenes like limonene are more effective to enhance skin penetration of lipophilic drugs like PGZ. The amount of PGZ retained in the skin was higher in the presence of limonene (207.65 $\mu\text{g/g}$ of tissue) in comparison with other enhancers. This indicates that it can prolong the duration of drug action and increase efficacy in the treatment of rosacea, favouring the likelihood of a reduction in the dosing frequency in clinical practice.

The results of the ocular permeation showed that PGZ from NPs permeates the sclera more than the cornea, indicating that the latter has a barrier effect three times higher than the sclera (203). This could be due to the physicochemical properties of the molecule, which interact better with scleral tissue, as well as another molecule favouring good scleral permeability, such as Triamcinolone (204). The permeability of the NPs is important because these systems facilitate the permeation of faintly water-soluble drugs, as PGZ. The permeability values (J_{ss} , K_p and Q_{ret}), were higher in scleral tissue over corneal (Article 2, Figure 4 b,c). The high permeability and accumulation of PGZ from NPs in the scleral tissue could be attributed to these systems being more active against posterior ocular diseases, as well as posterior uveitis. This is probably due to high sclera permeability (205). These findings are in line with those obtained previously, which revealed that the PGZ could be effective in the treatment of endogenous uveitis (58).

The PGZ-NPs and PGZ solution permeations through different mucosae (buccal, sublingual, nasal and intestinal) were also studied. PGZ-NPs showed a high retained amount in buccal, sublingual and nasal mucosae, with medium values of 158.45, 132.66 and 129.81 ($\mu\text{g PGZ/g tissue /cm}^2$), respectively. Moreover, based on the permeation parameters, the P_2 and C_{ss} were higher for nasal mucosa, demonstrating that PGZ permeation is more favourable in this tissue and consequently that there is greater probability of delivering effective PGZ concentrations the site of action more quickly (206). The nasal mucosa showed values of C_{ss} 10 times greater than the other tissues, signifying that PGZ administered through this route would achieve greater PGZ concentrations in the bloodstream (Article 3, Table 2) (207).

In a similar vein, the PGZ solution was tested in the same mucosae, and different results were given depending on the PGZ dosage forms (Article 5, Table 1). The intestinal mucosa showed significant statistical difference compared with other mucosae.

Moreover, the intestinal mucosa showed lower lag time (min) values compared to other mucosae, reaching plasma levels of steady-state equilibrium in less time ($p < 0.05$).

The intestinal mucosa in comparison to sublingual and buccal mucosa showed best values of the C_{ss} of $0.09 \mu\text{g/ml}$ ($p < 0.05$). This mucosa showed a very low amount of PGZ retained, indicating that the PGZ had crossed the intestinal wall and accessed the systemic circulation.

4.3 TOLERANCE AND CYTOTOXICITY

Tests on **skin and ocular tolerance** of PGZ dosage forms were carried out *in vitro* or *in vivo*. The possibility of causing skin damage, a crucial factor to be reduced in the development of topical treatments, was assayed in the “*in vivo* Draize test” (208). PGZ solution was tested on a rabbit during 72 hours and the skin was evaluated in accordance with the guidelines (209). The data showed a primary irritation index below 0.5 in all cases, in accordance with others results (185,208) (Article 1). The ocular tolerances of the PGZ dosage forms were determined the *in vivo* (Draize) and *in vitro* (HET-CAM) test. In both assays PGZ-NPs showed an ocular irritation index less than 0.4, indicating that these systems are safe for application to the eye (Article 2). Moreover, in accordance with others studies they showed that NPs are safe for ocular administration (194,195,210).

***In vitro* cytotoxicity** assays in cell culture from skin (HaCat), ocular (Y-79) and in the brain (hCMEC/D3) have been studied.

Toxicology of nanomaterials is becoming an important issue nowadays, especially with regard to nanomaterials present in the environment and nanomaterials intended for medical use (211). PGZ solution exposed to HaCat cell line showed greater than 80 % in cellular viability in almost all the dilutions assayed (Article 1, Figure 2). In the case of Y-79 cell line PGZ-NPs up to $10 \mu\text{g/ml}$ showed no toxicity with a viability above 80 % (Article 2, Figure 5). Moreover, for hCMEC/D3 PGZ-NPs up to $2 \mu\text{g/ml} = 5.1\text{nM}$ also showed 80% of cellular viability (Article 4 Figure 2). These results are in accordance with a previous study using HaCat, Y-79 and mouse Bend-3 cells, which indicated that NPs did not damage the cells line (179,212,213). Additionally, the uptake of NPs can vary depending on the cell types into which they induce cytotoxicity, which can be by a number of means (182). Moreover, characteristics such as material, surfactants, size and

surface of the particle are decisive in the internalizing in the cell and whether or not they consequently produce toxicity.

4.4 INTERNALIZATION, TRANSPORT AND PERMEABILITY STUDIES

Internalization, transport and permeability studies of PGZ-NPs in hCMEC/D3 cell line have been carried out.

The subcellular localization of NPs was determined by confocal and electron microscopy indicating that they crossed the endothelium by vesicular transcytosis intact. In addition, images of TEM show individual PGZ-NPs (100-150 nm) in the cytoplasm (Article 4, Figure 5), and no NPs were seen in the intercellular junctions. This implies that the NPs were taken up individually by endothelial cells and had not aggregated inside the cells.

Moreover, the PEG on the surface of NPs can improve their internalization by brain endothelium (214) and it has been suggested that PEGylated PLGA NPs can enter these cells in CCVs (215) as an alternative to caveolar transcytosis.

Over the last decade, drug access directly into the brain has been extensively investigated. It has made marked progress recently with different mechanisms and techniques to transport therapeutics through the BBB (85). It is believed that only small and soluble lipid (lipophilic) molecules with a molecular mass under 400 Da can go through the BBB (80,81) and due to their structure make it difficult for the development of new treatments for brain diseases (216).

The assay showed that PGZ-NPs were able to across the BBB the *in vitro* model without changing the permeability of the barrier (Article 4, Figure 6 a,b). Due to the small particle size, negative charge and appropriate surfactant (Tween 80) this meant that these systems were able to across the BBB. On the same subject, NPs are efficient nanocarriers for CNS drug delivery because they protect the drug from the first pass metabolism and facilitate the drug delivery across the BBB model without damaging the BBB.

4.5 THERAPEUTIC EFFICACY OF DOSAGE FORMS

The efficacy of the PGZ solution for the treatment of rosacea was determined by a colorimetric assay on an inflammatory model on the back skin of mice (BALB/c), analysing the possible reduction (%) of erythema and vasodilation, which are the main clinical features of rosacea. PGZ decreased the level of erythema in all the time intervals

tested ($p < 0.0001$), and at 20 minutes the differences intensified, decreasing below the basal value with a notably reduction in erythema (Article 1, Figures 3 and 4 b). In the same area, histological analysis from back skin of mice stained with haematoxylin and eosin showed that this had significantly attenuated the inflammatory response with less leukocyte infiltration compared to the positive skin control (Article 1, Figure 5 c). Therefore, the results of histological and colorimetric studies suggested that PGZ might be considered as a promising therapeutic treatment for rosacea. Another study using animal models of inflammatory skin diseases has confirmed that dermal administration of PPAR-ligands, like PGZ, decreases epidermal hyperplasia, enhances the permeability barrier function, and reduces the inflammation mediated by T lymphocytes (217). Consequently, the PGZ could constitute a new therapeutic strategy to reduce the inflammation usually associated to rosacea.

The efficacy of PGZ-NPs to prevent ocular inflammatory process, was tested in the eyes of six male pigs in a model of eye inflammation induced by topical administration of sodium arachidonate (SA). PGZ-NPs showed significant differences regarding the positive control for the first 30 min after SA administration ($p = 0.0008$), reducing the degree of conjunctival inflammation and iris hyperaemia significantly, as shown in Article 2, Figure 6. These results demonstrate that PGZ-NPs constitute an effective therapeutic agent for ocular inflammation, and are in accordance with the permeation studies, in which PGZ-NPs provided higher drug levels in the sclera and cornea, as well as higher drug penetration in different eye tissues (Article 2, Figure S4. Supplementary data). Some studies corroborate that PGZ might improve impaired insulin signalling in the retinas of diabetic rats (218) and that TZDs may have the potential to inhibit the progression of diabetic retinopathy (64). However, in another study it was demonstrated that PGZ inhibited intraocular concentrations of TNF α and IL-6 in the endogenous uveitis model (147). Taking into account these results, it means that PGZ-NPs may constitute a new and promising therapeutic approach focused on clinical applications for the treatment of ocular disorders, such as uveitis, in which inflammatory process could be considered a crucial factor.

The efficacy of PGZ-NPs in AD was evaluated in a transgenic model on mice of APP/PS1 by orally administration or PGZ-NPs (10 mg/Kg) during 30 days. Memory performance was evaluated with the two-object recognition test and after that the mice were killed and

their brains rapidly removed and analyzed by immunohistochemistry. The results showed that PGZ-NPs ($p < 0.01$) reduce memory deficit in APP/PS1 when compare to the vehicle (Article 4, Figure 7 a). These results are in agreement with those obtained by Searcy *et al.* (219), which had demonstrated that PGZ improved reversal learning in a triple transgenic mouse model of AD mice. However, others studies showed that APP/PS1 mice treated for nine days with PGZ reversed non-cognitive behavioural deficits and restored distance and speed travelled in an open field (220). In addition, several studies have reported neuroprotective effects of PGZ (127,219,221–223). Moreover, PGZ-NPs showed a clear tendency to reduce beta amyloid deposition in the cerebral cortex (Article 4, Figure 7 b,c), in agreement with another study (224). These results suggest that PGZ-NPs represent a new alternative to pharmacological treatment for AD, both improving drug delivery into the brain and providing for a more sustained drug release.

CHAPTER 5

CONCLUSIONS

5. CONCLUSIONS

In this work Pioglitazone dosage forms were designed to reduce the inflammation associated with skin, ocular and neurodegenerative diseases.

5.1 Pioglitazone solution has been developed to treat the inflammation associated with rosacea and AD.

- The *in vitro* release of drug from the dosage form follows a first order kinetic model according to Fick's law, being effective and safe in accordance with the results of calorimetric, histological and cytotoxicity assays, for rosacea indication.
- PGZ solution: there was no damage to the intestinal mucosa, reaching in prediction in terms of *ex vivo* permeation, plasmatic concentrations in a steady state effective to treat AD.

5.2 PGZ-NPs prepared by solvent displacement technique and optimized by factorial design, were confirmed to be suitable for inflammation associated with uveitis and AD.

- NPs were characterised by spectroscopic (FTIR, X-Ray) and thermal (DSC) methods confirming that the drug was encapsulated in the polymeric matrix.
- These nanostructured systems demonstrated a sustained release of the drug from the polymer, which can be adjusted to first order and hyperbola kinetic model.
- The optimized NPs demonstrated to be non-cytotoxic at concentration studied in ocular (Y-79) and brain (hCMEC/D3) cells line.
- PGZ-NPs assessed *in vivo* demonstrated to efficiently prevent ocular inflammation, with optima ocular tolerance.
- These systems were internalized and transported in hCMEC/D3 cells line and they were able to pass across the BBB *in vitro* model without alteration in the permeability of the barrier.
- PGZ-NPs were assessed for AD in an *in vivo* model (APP/PS1 mice). These NPs proved to efficiently treat AD improving the cognitive deficit and showing a clear tendency to reduce beta-amyloid depositions in cerebral cortex.
- PGZ dosage forms developed could constitute, after clinical assays, a new therapeutic indication of this drug to provide an approach to the inflammation associated to different local and systemic diseases.

CHAPTER 6 REFERENCES

6. REFERENCES

1. Barreiro LB, Marioni JC, Blekhman R, Stephens M, Gilad Y. Functional comparison of innate immune signaling pathways in primates. *PLoS Genet.* 2010;6(12):1–13.
2. Gallo J, Raska M, Kriegova E, Goodman SB. Inflammation and its resolution and the musculoskeletal system. *J Orthop Transl.* 2017;10:52–67.
3. White M. Mediators of inflammation and the inflammatory process. *J Allergy Clin Immunol.* 1999;103:S378-381.
4. Begley LA, Kasina S, MacDonald J, Macoska JA. The inflammatory microenvironment of the aging prostate facilitates cellular proliferation and hypertrophy. *Cytokine.* 2008;43(2):194–9.
5. Vane JR, Bakhle YS, Botting RM. Cyclooxygenases 1 and 2. *Annu Rev Pharmacol Toxicol.* 1998;38(1):97–120.
6. Kwiecien S, Jasnos K, Magierowski M, Sliwowski Z, Pajdo R, Brzozowski B, et al. Lipid peroxidation, reactive oxygen species and antioxidative factors in the pathogenesis of gastric mucosal lesions and mechanism of protection against oxidative stress - induced gastric injury. *J Physiol Pharmacol.* 2014;65(5):613–22.
7. Bederska-Łojewska D, Orczewska-Dudek S, Pieszka M. Metabolism of arachidonic acid, its concentration in animal products and influence on inflammatory processes in the human body: a review. *Ann Anim Sci.* 2013;13(2):177–94.
8. Ricciotti, Emanuela and FitzGerald GA. NIH Public Access. NIH Public Access. 2012;31(5):986–1000.
9. Harizi H, Corcuff JB, Gualde N. Arachidonic-acid-derived eicosanoids: roles in biology and immunopathology. *Trends Mol Med.* 2008;14(10):461–9.
10. Urade M. Cyclooxygenase (COX)-2 as a potent molecular target for prevention and therapy of oral cancer. *Jpn Dent Sci Rev.* 2008;44(1):57–65.
11. Fosslien E. Review: Molecular pathology of cyclooxygenase-2 in cancer-induced angiogenesis. *Ann Clin Lab Sci.* 2001;31(4):325–48.
12. Proksch E, Brandner JM, Jensen JM. The skin: An indispensable barrier. *Exp Dermatol.* 2008;17(12):1063–72.
13. Madison KC. Barrier function of the skin: “La Raison d’Être” of the epidermis. *J Invest Dermatol.* 2003;121(2):231–41.
14. Fore J. A Review of Skin and the Effects of Aging on Skin Structure and Function. *Ostomy Wound Manag.* 2006;52(9):24–35.
15. Hendriks F. Mechanical Behaviour of Human Skin in Vivo. *Bio-medical Eng.* 1969;4:322–327.
16. Bolzinger MA, Briançon S, Pelletier J, Chevalier Y. Penetration of drugs through skin, a complex rate-controlling membrane. *Curr Opin Colloid Interface Sci.* 2012;17(3):156–65.
17. Yamasaki K, Di Nardo A, Bardan A, Murakami M, Ohtake T, Coda A, et al. Increased serine protease activity and cathelicidin promotes skin inflammation in rosacea. *Nat Med.* 2007;13(8):975–80.
18. Igarashi T, Nishino K, Nayar SK. The Appearance of Human Skin: A Survey. *Found*

- Trends® Comput Graph Vis. 2007;3(1):1–95.
19. Mbah CJ, Uzor PF, Omeje EO. Perspectives on transdermal drug delivery. *J Chem Pharm Res.* 2011;3(3):680–700.
 20. Lane ME. Skin penetration enhancers. *Int J Pharm.* 2013;447(1–2):12–21.
 21. Akhtar N. Vesicles: a recently developed novel carrier for enhanced topical drug delivery. *Curr Drug Deliv.* 2014;11(1):87–97.
 22. Menczel, E.; Goldberg S. pH Effect on the Percutaneous Penetration of Lignocaine Hydrochloride. *Dermatologica.* 1978;156(1):8–14.
 23. Hadgraft J, Lane ME. Skin permeation: The years of enlightenment. *Int J Pharm.* 2005;305(1–2):2–12.
 24. Clendenning WE, Stoughton RB. Importance of the Aqueous/Lipid Partition Coefficient for Percutaneous Absorption of Weak Electrolytes. *J Invest Dermatol.* 1962;39(1):47–9.
 25. Magnusson BM, Anissimov YG, Cross SE, Roberts MS. Molecular size as the main determinant of solute maximum flux across the skin. *J Invest Dermatol.* 2004;122(4):993–9.
 26. Bos JD, Meinardi MMHM. The 500 Dalton rule for the skin penetration of chemical compounds and drugs. *Exp Dermatol.* 2000;9(3):165–9.
 27. Hadgraft J. Passive enhancement strategies in topical and transdermal drug delivery. *Int J Pharm.* 1999;184(1):1–6.
 28. Mujtaba A. Viscoelasticity of Filled Elastomers: Determination of Surface-Immobilized Components and their Role in the Reinforcement of SBR-Silica Nanocomposites. 2014;129.
 29. Prausnitz MR, Langer R. Transdermal drug delivery. *Nat Biotechnol.* 2009;26(11):1261–8.
 30. Awais M, Anwar MI, Iftikhar R, Iqbal Z, Shehzad N, Akbar B. Rosacea - The ophthalmic perspective. *Cutan Ocul Toxicol.* 2015;34(2):161–6.
 31. Steinhoff M, Schaubert J, Leyden JJ. New insights into rosacea pathophysiology: A review of recent findings. *J Am Acad Dermatol.* 2013;69(6):15–26.
 32. Wilkin J, Dahl M, Detmar M, Drake L, Liang MH, Odom R, et al. Standard grading system for rosacea: Report of the National Rosacea Society Expert Committee on the Classification and Staging of Rosacea. *J Am Acad Dermatol.* 2004;50(6):907–12.
 33. Micali G, Dall'Oglio F, Verzi AE, Luppino I, Bhatt K, Lacarrubba F. Treatment of erythematotelangiectatic rosacea with brimonidine alone or combined with vascular laser based on preliminary instrumental evaluation of the vascular component. *Lasers Med Sci.* 2017;1–4.
 34. Wollina U. Recent advances in the understanding and management of rosacea. *F1000Prime Rep.* 2014;6.
 35. Holmes AD, Steinhoff M. Integrative concepts of rosacea pathophysiology, clinical presentation and new therapeutics. *Exp Dermatol.* 2017;26(8):659–67.
 36. Vieira AC, Mannis MJ. Ocular rosacea: Common and commonly missed. *J Am Acad Dermatol.* 2013;69 (6): S36–41.
 37. Woo YR, Lim JH, Cho DH, Park HJ. Rosacea: Molecular mechanisms and management

- of a chronic cutaneous inflammatory condition. *Int J Mol Sci.* 2016;17(9):1–23.
38. Sertznig P, Reichrath J. Peroxisome proliferator-activated receptors (PPARs) in dermatology: Challenge and promise. *Dermatoendocrinol.* 2011;3(3):130–5.
 39. Suzuki S, Mori Y, Nagano A, Naiki-Ito A, Kato H, Nagayasu Y, et al. Pioglitazone, a peroxisome proliferator-activated receptor γ agonist, suppresses rat prostate carcinogenesis. *Int J Mol Sci.* 2016;17(12).
 40. El-Zaher AA, Elkady EF, Elwy HM, Saleh MAEM. Simultaneous spectrophotometric determination of glimepiride and pioglitazone in binary mixture and combined dosage form using chemometric-assisted techniques. *Spectrochim Acta - Part A Mol Biomol Spectrosc.* 2017;182:175–82.
 41. Newell FW. *Ophthalmology: Principles And Concepts* By Frank W . 1996; 8th Ed. St.Louis.
 42. Presland A. Applied ocular physiology and anatomy. *Anaesth Intensive Care Med.* 2007;8(9):379–82.
 43. Sheybani ND, Yang H. Pediatric ocular nanomedicines: Challenges and opportunities. *Chinese Chem Lett.* 2017;28(9):1817–21.
 44. Krishnaswami V, Kandasamy R, Alagarsamy S, Palanisamy R, Natesan S. Biological macromolecules for ophthalmic drug delivery to treat ocular diseases. *Int J Biol Macromol.* 2018;110:7–16.
 45. Reimondez-Troitiño S, Csaba N, Alonso MJ, De La Fuente M. Nanotherapies for the treatment of ocular diseases. *Eur J Pharm Biopharm.* 2015;95:279–93.
 46. Cross AG. Uveitis in Childhood. *Journal of the Royal Society of Medicine.* 1954; 47: 971-974.
 47. Rémond AL, Barreau E, Le Hoang P, Bodaghi B. Bilateral uveitis associated with nivolumab therapy. *J Fr Ophtalmol.* 2018;41(3):91–4.
 48. Dawson DG, Ubels JL, Edelhauser HF. *Cornea and Sclera. Science. Physiology of optical media.* Elsevier. 2001;9394(00).
 49. Forrester JV, Kuffova L, Dick AD. Autoimmunity, Autoinflammation, and Infection in Uveitis. *Am J Ophthalmol.* 2018;189:77–85.
 50. Hadjadj J, Dechartres A, Chapron T, Assala M, Salah S, Dunogué B, et al. Relevance of diagnostic investigations in patients with uveitis: Retrospective cohort study on 300 patients. *Autoimmun Rev.* 2017;16(5):504–11.
 51. Teoh SC, Dick AD. Diagnostic techniques for inflammatory eye disease : past , present and future : a review. 2013;1–10.
 52. Gueudry J, Muraine M. Anterior uveitis. *J Fr Ophtalmol.* 2017;41(1):11–21.
 53. Smith JR, Rosenbaum JT. Management of uveitis: A rheumatologic perspective. *Arthritis Rheum.* 2002;46(2):309–18.
 54. Mérida S, Palacios E, Navea A, Bosch-Morell F. New immunosuppressive therapies in uveitis treatment. *Int J Mol Sci.* 2015;16(8):18778–95.
 55. Lee RW, Nicholson LB, Sen HN, Chan CC, Wei L, Nussenblatt RB, et al. Autoimmune and autoinflammatory mechanisms in uveitis. *Semin Immunopathol.* 2014;36(5):581–94.
 56. Takase H, Futagami Y, Yoshida T, Kamoi K, Sugita S, Imai Y, et al. Cytokine profile in

- aqueous humor and sera of patients with infectious or noninfectious uveitis. *Investig Ophthalmol Vis Sci.* 2006;47(4):1557–61.
57. Ooi KG-J, Galatowicz G, Calder VL, Lightman SL. Cytokines and chemokines in uveitis: is there a correlation with clinical phenotype?. *Clin Med Res.* 2006;4(4):294–309.
 58. Okunuki Y, Usui Y, Nakagawa H, Tajima K, Matsuda R, Ueda S, et al. Peroxisome proliferator-activated receptor- γ agonist pioglitazone suppresses experimental autoimmune uveitis. *Exp Eye Res.* 2013;116:291–7.
 59. Clark RB, Bishop-Bailey D, Estrada-Hernandez T, Hla T, Puddington L, Padula SJ. The Nuclear Receptor PPAR and Immunoregulation: PPAR Mediates Inhibition of Helper T Cell Responses. *J Immunol.* 2000;164(3):1364–71.
 60. Ohshima K, Mogi M, Horiuchi M. Role of peroxisome proliferator-activated receptor- γ in vascular inflammation. *Int J Vasc Med.* 2012;2012:1–9.
 61. Harris SG, Phipps RP. The nuclear receptor PPAR gamma is expressed by mouse T lymphocytes and PPAR gamma agonists induce apoptosis. *Eur J Immunol.* 2001;31(4):1098–105.
 62. Croasdell A, Duffney PF, Kim N, Lacy SH, Sime PJ, Phipps RP. PPAR γ and the Innate Immune System Mediate the Resolution of Inflammation. *PPAR Res.* 2015; ID:549691.
 63. Zhang S, Gu H, Hu N. Role of Peroxisome Proliferator-Activated Receptor- γ in Ocular Diseases. 2015;2015:17–20.
 64. Murata T, Hata Y, Ishibashi T, Kim S, Hsueh WA, Law RE, et al. Response of experimental retinal neovascularization to thiazolidinediones. *Arch Ophthalmol.* 2001;119(5):709–17.
 65. Liu YH, Tsai YS, Lin SC, Liao NS, Jan MS, Liang CT, et al. Quantitative PPAR γ expression affects the balance between tolerance and immunity. *Sci Rep.* 2016;6:1–13.
 66. Uchiyama M, Shimizu A, Masuda Y, Nagasaka S, Fukuda Y, Takahashi H. An ophthalmic solution of a peroxisome proliferator-activated receptor gamma agonist prevents corneal inflammation in a rat alkali burn model. *Mol Vis.* 2013;19:2135–50.
 67. Pan H, Chen J, Xu J, Chen M, Ma R. Antifibrotic effect by activation of peroxisome proliferator- activated receptor – γ in corneal fibroblasts. *Mol Vis.* 2009;2279–86.
 68. Ge S, Song L, Pachter JS. Where is the blood-brain barrier ... Really? *J Neurosci Res.* 2005;79(4):421–7.
 69. Bechmann I, Galea I, Perry VH. What is the blood-brain barrier (not)?. *Trends Immunol.* 2007;28(1):5–11.
 70. Purves D, Augustine GJ FD. The Blood Supply of the Brain and Spinal Cord. In: *Neuroscience [Internet].* 2nd ed. Sunderland (MA): Sinauer Associates; 2001. Available from: <https://www.ncbi.nlm.nih.gov/books/NBK11042/>.
 71. Abbott NJ, Rönnbäck L, Hansson E. Astrocyte-endothelial interactions at the blood-brain barrier. *Nat Rev Neurosci.* 2006;7(1):41–53.
 72. Vries HEDE, Kuiper J, Boer AGDE, Berkel TJC VAN, Breimer DD. The Blood-Brain Barrier in Neuroinflammatory. *Pharmacol Rev.* 1997;49(2).
 73. Abbott NJ. Astrocyte-endothelial interactions and blood-brain barrier permeability. *J Anat.* 2002;200(6):629–38.
 74. Saunders NR, Dreifuss JJ, Dziegielewska KM, Johansson PA, Habgood MD, Møllgård K,

- et al. The rights and wrongs of blood-brain barrier permeability studies: A walk through 100 years of history. *Front Neurosci.* 2014;8:1–26.
75. Wolburg H, Noell S, Mack A, Wolburg-Buchholz K, Fallier-Becker P. Brain endothelial cells and the glio-vascular complex. *Cell Tissue Res.* 2009;335(1):75–96.
76. Reese TS, Karnovsky MJ. Fine structural localizatin of blood-brain barrier to exogenous peroxidase. *J Cell Biol.* 1967;34(1):207–17.
77. Brightman MW, Reese TS. Junctions between intimately apposed cell membranes in the vertebrate brain. *J Cell Biol.* 1969;40(3):648–77.
78. Abbott NJ. Prediction of blood-brain barrier permeation in drug discovery from in vivo, in vitro and in silico models. *Drug Discov Today Technol.* 2004;1(4):407–16.
79. Abbott NJ, Patabendige AA, Dolman DE, Yusof SR, Begley DJ. Structure and function of the blood-brain barrier. *Neurobiol Dis.* 2010;37(1):13-25.
80. Grabrucker AM, Ruozi B, Belletti D, Pederzoli F, Forni F, Vandelli MA, et al. Nanoparticle transport across the blood brain barrier. *Tissue Barriers.* 2016; 4.
81. Banks WA. Characteristics of compounds that cross the blood-brain barrier. *BMC Neurol.* 2009;9(1):5–9.
82. Clark L. A FORMIDABLE BARRIER [Internet]. The scientist. 2017 [cited 2018 Apr 5]. Available from: <https://www.the-scientist.com/?articles.view/articleNo/50698/title/Getting-Drugs-Past-the-Blood-Brain-Barrier/>.
83. Upadhyay RK. Drug delivery systems, CNS protection, and the blood brain barrier. *Biomed Res Int.* 2014;2014.
84. Groothuis DR, Benalcazar H, Allen C V., Wise RM, Dills C, Dobrescu C, et al. Comparison of cytosine arabinoside delivery to rat brain by intravenous, intrathecal, intraventricular and intraparenchymal routes of administration. *Brain Res.* 2000;856(1–2):281–90.
85. Lu C-T, Zhao Y-Z, Wong HL, Cai J, Peng L, Tian X-Q. Current approaches to enhance CNS delivery of drugs across the brain barriers. *Int J Nanomedicine.* 2014;9:2241–57.
86. Hearnden V, Sankar V, Hull K, Juras DV, Greenberg M, Kerr AR, et al. New developments and opportunities in oral mucosal drug delivery for local and systemic disease. *Adv Drug Deliv Rev.* 2012;64(1):16–28.
87. Yamahara H, Vincent H.L L. Drug metabolism in the oral cavity. *Adv Drug Deliv Rev.* 1993;12(1–2):25–39.
88. Sankar V, Hearnden V, Hull K, Juras DV, Greenberg M, Kerr A, et al. Local drug delivery for oral mucosal diseases: Challenges and opportunities. *Oral Dis.* 2011;17(1):73–84.
89. Qin R, Steel A, Fazel N. Oral mucosa biology and salivary biomarkers. *Clin Dermatol.* 2017;35(5):477–83.
90. Squier C, Brogden KA. *Human Oral Mucosa.* Oxford, UK. 2011 Ed.1st. Wiley-Blackwell.
91. Sudhakar Y, Kuotsu K, Bandyopadhyay AK. Buccal bioadhesive drug delivery - A promising option for orally less efficient drugs. *J Control Release.* 2006;114(1):15–40.
92. Patel VF, Liu F, Brown MB. Advances in oral transmucosal drug delivery. *J Control Release.* 2011;153(2):106–16.

93. Galey WR, Lonsdale HK, Nacht S. The in vitro permeability of skin and buccal mucosa to selected drugs and tritiated water. *J Invest Dermatol.* 1976;67(6):713–7.
94. Tralau T, Sowada J, Luch A. Insights on the human microbiome and its xenobiotic metabolism: what is known about its effects on human physiology? *Expert Opin Drug Metab Toxicol.* 2015;11(3):411–25.
95. Helander HF, Fändriks L. Surface area of the digestive tract-revisited. *Scand J Gastroenterol.* 2014;49(6):681–9.
96. Turner JR. Intestinal mucosal barrier function in health and disease. *Nat Rev Immunol.* 2009;9(11):799–809.
97. Lee SH. Intestinal Permeability Regulation by Tight Junction: Implication on Inflammatory Bowel Diseases. *Intest Res.* 2015;13(1):11.
98. Sánchez de Medina F, Romero-Calvo I, Mascaraque C, Martínez-Augustin O. Intestinal Inflammation and Mucosal Barrier Function. In: *Inflammatory Bowel Diseases.* Crohn's & Colitis Foundation of America; 2014;2394–404.
99. Mygind N, Änggård A. Anatomy and physiology of the nose-pathophysiologic alterations in allergic rhinitis. *Clin Rev Allergy.* 1984;2(3):173–88.
100. Mygind N, Dahl R. Anatomy, physiology and function of the nasal cavities in health and disease. *Adv Drug Deliv Rev.* 1998;29(1–2):3–12.
101. Watelet J-B, Cauwenberge P Van. Applied anatomy and physiology of the nose and paranasal sinuses. *Allergy.* 1999;54(1):14–25.
102. Vyas T, Shahiwala A, Marathe S, Misra A. Intranasal Drug Delivery for Brain Targeting. *Curr Drug Deliv.* 2005;1;2(2):165–75.
103. Pires A, Fortuna A, Alves G, Falcão A. Intranasal drug delivery: How, why and what for?. *J Pharm Pharm Sci.* 2009;12(3):288–311.
104. Rasso G, Soddu E, Cossu M, Gavini E, Giunchedi P, Dalpiaz A. Particulate formulations based on chitosan for nose-to-brain delivery of drugs. A review. *J Drug Deliv Sci Technol.* 2016;32:77–87.
105. Murman D. The Impact of Age on Cognition. *Semin Hear.* 2015; 36(3):111–21.
106. Murphy MP, Iii HL. Alzheimer`s Disease and the β -Amyloid Peptide. *J Alzheimer`s Dis.* 2010;19(1):1–17.
107. Harizi H, Corcuff JB, Gualde N, Ricciotti, Emanuela and FitzGerald GA, Pascual G, Fong AL, et al. NIH Public Access. *PPAR Res.* 2015;17(1):1–10.
108. Nalivaeva NN, Turner AJ. The amyloid precursor protein: A biochemical enigma in brain development, function and disease. *FEBS Lett.* 2013;587(13):2046–54.
109. O'Brien RJ, Wong PC. Amyloid Precursor Protein Processing and Alzheimer's Disease. *Annu Rev Neurosci.* 2011 Jul 21;34(1):185–204.
110. Hardy J. The Amyloid Hypothesis of Alzheimer's Disease: Progress and Problems on the Road to Therapeutics. *Science's compass.* 2002;19;297(5580):353–6.
111. Avila J, Lucas JJ, Pérez Mar, Hernández F. Role of Tau Protein in Both Physiological and Pathological Conditions. *Physiol Rev.* 2004;84(2):361–84.
112. Hernández F, Avila J. Tauopathies. *Cell Mol Life Sci.* 2007;64(17):2219–33.

113. Brion J-P. Neurofibrillary Tangles and Alzheimer's Disease. *Eur Neurol.* 1998;40(3):130–40.
114. Crane PK, Walker R, Hubbard RA, Li G, Nathan DM, Zheng H, et al. Glucose Levels and Risk of Dementia. *N Engl J Med.* 2013;369(6):540–8.
115. Logue J, Walker JJ, Colhoun HM, Leese GP, Lindsay RS, McKnight JA, et al. Do men develop type 2 diabetes at lower body mass indices than women? *Diabetologia.* 2011;54(12):3003–6.
116. Karlamangla AS, Miller-Martinez D, Lachman ME, Tun PA, Koretz BK, Seeman TE. Biological correlates of adult cognition: Midlife in the United States (MIDUS). *Neurobiol Aging.* 2014;35(2):387–94.
117. de Felice FG, Lourenco M V. Brain metabolic stress and neuroinflammation at the basis of cognitive impairment in Alzheimer's disease. *Front Aging Neurosci.* 2015;7:1–8.
118. Sy M, Kitazawa M, Medeiros R, Whitman L, Cheng D, Lane TE, et al. Inflammation induced by infection potentiates tau pathological features in transgenic mice. *Am J Pathol.* 2011;178(6):2811–22.
119. Chen Y-C, Wu J-S, Tsai H-D, Huang C-Y, Chen J-J, Sun GY, et al. Peroxisome Proliferator-Activated Receptor Gamma (PPAR- γ) and Neurodegenerative Disorders. *Mol Neurobiol.* 2012;46(1):114–24.
120. Polvani S, Tarocchi M, Galli A. PPAR and oxidative stress: Con(β) catenating NRF2 and FOXO. *PPAR Res.* 2012;2012.
121. Fuenzalida K, Quintanilla R, Ramos P, Piderit D, Fuentealba RA, Martinez G, et al. Peroxisome proliferator-activated receptor γ up-regulates the Bcl-2 anti-apoptotic protein in neurons and induces mitochondrial stabilization and protection against oxidative stress and apoptosis. *J Biol Chem.* 2007;282(51):37006–15.
122. Santos MJ, Quintanilla RA, Toro A, Grandy R, Dinamarca MC, Godoy JA, et al. Peroxisomal proliferation protects from β -amyloid neurodegeneration. *J Biol Chem.* 2005;280(49):41057–68.
123. Martín A, Pérez-Girón J V., Hernanz R, Palacios R, Briones AM, Fortuño A, et al. Peroxisome proliferator-activated receptor- γ activation reduces cyclooxygenase-2 expression in vascular smooth muscle cells from hypertensive rats by interfering with oxidative stress. *J Hypertens.* 2012;30(2):315–26.
124. Hernanz R, Martín Á, Pérez-Girón J V., Palacios R, Briones AM, Miguel M, et al. Pioglitazone treatment increases COX-2-derived prostacyclin production and reduces oxidative stress in hypertensive rats: Role in vascular function. *Br J Pharmacol.* 2012;166(4):1303–19.
125. Landreth G, Jiang Q, Mandrekar S, Heneka M, G. L, Q. J, et al. PPARgamma agonists as therapeutics for the treatment of Alzheimer's disease. *Neurotherapeutics.* 2008;5(3):481–9.
126. Sato T, Hanyu H, Hirao K, Kanetaka H, Sakurai H, Iwamoto T. Efficacy of PPAR- γ agonist pioglitazone in mild Alzheimer disease. *Neurobiol Aging.* 2011;32(9):1626–33.
127. El-Sahar AE, Safar MM, Zaki HF, Attia AS, Ain-Shoka AA. Neuroprotective effects of pioglitazone against transient cerebral ischemic reperfusion injury in diabetic rats: Modulation of antioxidant, anti-inflammatory, and anti-apoptotic biomarkers. *Pharmacol Reports.* 2015;67(5):901–6.

128. Upadhyaya P, Seth V, Ahmad M. Therapy of Alzheimer's disease: An update. 2010;4:408–21.
129. Nielsen R, Grontved L, Stunnenberg HG, Mandrup S. Peroxisome Proliferator-Activated Receptor Subtype- and Cell-Type-Specific Activation of Genomic Target Genes upon Adenoviral Transgene Delivery. *Mol Cell Biol*. 2006;26(15):5698–714.
130. Pascual G, Fong AL, Ogawa S, Gamliel A, Li AC, Perissi V, et al. A SUMOylation-dependent pathway mediates transrepression of inflammatory response genes by PPAR- γ . *Nature*. 2005;437(7059):759–63.
131. Kapadia R, Yi JH, Vemuganti R. Mechanisms of anti-inflammatory and neuroprotective actions of PPAR-gamma agonists. *Front Biosci*. 2008;13(3):1813–26.
132. Spinelli SL, O'Brien JJ, Bancos S, Lehmann GM, Springer DL, Blumberg N, et al. The PPAR-platelet connection: Modulators of inflammation and potential cardiovascular effects. *PPAR Res*. 2008;2008.
133. Asada K, Sasaki S, Suda T, Chida K, Nakamura H. Antiinflammatory Roles of Peroxisome Proliferator-activated Receptor γ in Human Alveolar Macrophages. *Am J Respir Crit Care Med*. 2004;169(2):195–200.
134. Padilla J, Leung E, Phipps RP. Human B lymphocytes and B lymphomas express PPAR- γ and are killed by PPAR- γ agonists. *Clin Immunol*. 2002;103(1):22–33.
135. Clark RB. The role of PPARs in inflammation and immunity. *J Leukoc Biol*. 2002;71(3):388–400.
136. Ahmadian M, Suh JM, Hah N, Liddle C, Atkins AR, Downes M, et al. PPAR γ signaling and metabolism: The good, the bad and the future. *Nat Med*. 2013;19(5):557–66.
137. Maeda N, Takahashi M, Funahashi T, Kihara S, Nishizawa H, Kishida K, et al. PPAR γ Ligands Increase Expression and Plasma Concentrations of Adiponectin, an Adipose-Derived Protein. *Diabetes*. 2001;50(9):2094–9.
138. Krönke G, Kadl A, Ikonomu E, Blüml S, Fürnkranz A, Sarembock IJ, et al. Expression of heme oxygenase-1 in human vascular cells is regulated by peroxisome proliferator-activated receptors. *Arterioscler Thromb Vasc Biol*. 2007;27(6):1276–82.
139. Thompson PW, Bayliffe AI, Warren AP, Lamb JR. Interleukin-10 is upregulated by nanomolar rosiglitazone treatment of mature dendritic cells and human CD4⁺ T cells. *Cytokine*. 2007;39(3):184–91.
140. Haffner SM, Greenberg AS, Weston WM, Chen H, Williams K, Freed MI. Effect of rosiglitazone treatment on nontraditional markers of cardiovascular disease in patients with type 2 diabetes mellitus. *Circulation*. 2002;106(6):679–84.
141. Narala VR, Ranga R, Smith MR, Berlin AA, Standiford TJ, Lukacs NW, et al. Pioglitazone is as effective as dexamethasone in a cockroach allergen-induced murine model of asthma. *Respir Res*. 2007;8:1–10.
142. Ko GJ, Kang YS, Han SY, Lee MH, Song HK, Han KH, et al. Pioglitazone attenuates diabetic nephropathy through an anti-inflammatory mechanism in type 2 diabetic rats. *Nephrol Dial Transplant*. 2008;23(9):2750–60.
143. National Institutes of Health Clinical Center. Pioglitazone Hydrochloride (Actos) to Treat Asthma [Internet]. *ClinicalTrials.gov* Identifier: NCT00604578. 2008 [cited 2018 Apr 10]. Available from: <https://clinicaltrials.gov/ct2/show/NCT00604578?term=pioglitazone&cond=Inflammatio>

- n&draw=2&rank=9.
144. VA Office of Research and Development. Effects of PPAR Ligands on Ectopic Fat Accumulation and Inflammation [Internet]. Clinical Trials.gov Identifier: NCT00470262. 2007 [cited 2018 Apr 15]. Available from: <https://clinicaltrials.gov/ct2/show/study/NCT00470262?term=pioglitazone&cond=Inflammation&rank=4>.
 145. Takeda America Research and Development Center I. ACTOS (pioglitazone hydrochloride) Tablets [Internet]. NDA No.21-073. 1999 [cited 2018 May 2]. Available from: https://www.accessdata.fda.gov/drugsatfda_docs/label/1999/21073lbl.pdf.
 146. Shen W, Gao Y, Lu B, Zhang Q, Hu Y, Chen Y. Negatively regulating TLR4/NF- κ B signaling via PPAR α in endotoxin-induced uveitis. *Biochim Biophys Acta - Mol Basis Dis*. 2014;1842(7):1109–20.
 147. Yamamoto A, Kakuta H, Miyachi H, Sugimoto Y. Involvement of the retinoid X receptor ligand in the anti-inflammatory effect induced by peroxisome proliferator-activated receptor agonist *in vivo*. *PPAR Res*. 2011;2011.
 148. Murdan S. Dosage form design and manufacture. In: Aulton ME, Taylor KMG, editors. *Aulton's Pharmaceutics E-Book*. 4th ed. London: Elsevier; 2013. p. 728.
 149. Richards RME, Winfield AJ. *Pharmaceutical Products* [Internet]. 3rd ed. Richards RME, Winfield AJ, editors. Pharmaceutical practice. Edinburgh: Edinburgh: Churchill Livingstone; 2004.
 150. United States Pharmacopeia Convention. *The United States Pharmacopeia. USP 30. NF*. Rockville: The National Formulary; 2007.
 151. Jones D. *pharmaceutics - dosage form and design*. 2nd ed. Devon: Pharmaceutical Press; 2016.
 152. Lund W. *The Pharmaceutical CODEX: Principles & Practice of Pharmaceutics*. 12th ed. Lund W, editor. CBS Publishers & Distributors; 1994.
 153. Sullivan DW, Gad SC, Julien M. A review of the nonclinical safety of Transcutol®, a highly purified form of diethylene glycol monoethyl ether (DEGEE) used as a pharmaceutical excipient. *Food Chem Toxicol*. 2014;72:40–50.
 154. Rowe RC, Sheskey PJ, Cook WG, Fenton ME. Diethylene glycol monoethyl ether. In: Pharmaceutical Press and the American Pharmacists Association. In: *Handbook of Pharmaceutical Excipients*. 7th ed. Washington: Pharmaceutical Press; 2012.
 155. Osborne DW. Diethylene glycol monoethyl ether: An emerging solvent in topical dermatology products. *J Cosmet Dermatol*. 2011;10(4):324–9.
 156. Pandey PK, Sharma AK, Gupta U, Pandey PK, Sharma AK, Gupta U. Blood brain barrier : An overview on strategies in drug delivery , realistic *in vitro* modeling and *in vivo* live tracking Blood brain barrier : An overview on strategies in drug delivery , realistic *in vitro* modeling and *in vivo* live tracking. 2016;8370:1–14.
 157. Anselmo AC, Mitragotri S. An Overview of Clinical and Commercial Impact of Drug Delivery Systems. *J Control Release*. 2015;190:15–28.
 158. Bertrand N, Leroux JC. The journey of a drug-carrier in the body: An anatomophysiological perspective. *J Control Release*. 2012;161(2):152–63.
 159. Wen H, Jung H, Li X. Drug Delivery Approaches in Addressing Clinical Pharmacology-Related Issues: Opportunities and Challenges. *AAPS J*. 2015;17(6):1327–40.

160. Boisseau P, Loubaton B, Nanomedicine , Nanotechnology in medicine. Comptes rendus hebdomadaires des séances de l'Académie des sciences. Elsevier, 2011;2–28.
161. Moghimi SM. Nanomedicine: current status and future prospects. *FASEB J.* 2005;19(3):311–30.
162. Richards DA, Maruani A, Chudasama V. Antibody fragments as nanoparticle targeting ligands: a step in the right direction. *Chem Sci.* 2017;8(1):63–77.
163. Crucho CIC, Barros MT. Polymeric nanoparticles: A study on the preparation variables and characterization methods. *Mater Sci Eng C.* 2017;80:771–84.
164. Patel T, Zhou J, Piepmeier JM, Saltzman WM. Polymeric nanoparticles for drug delivery to the central nervous system. *Adv Drug Deliv Rev.* 2012;64(7):701–5.
165. Lin G, Zhang H, Huang L. Smart polymeric nanoparticles for cancer gene delivery. *Mol Pharm.* 2015;12(2):314–21.
166. Mangraviti A, Tzeng SY, Kozielski KL, Wang Y, Jin Y, Gullotti D, et al. Polymeric nanoparticles for nonviral gene therapy extend brain tumor survival in vivo. *ACS Nano.* 2015;9(2):1236–49.
167. Rao JP, Geckeler KE. Polymer nanoparticles: Preparation techniques and size-control parameters. *Prog Polym Sci.* 2011;36(7):887–913.
168. Garg NK, Mangal S, Khambete H, Sharma PK, Tyagi RK. Mucosal delivery of vaccines: role of mucoadhesive/biodegradable polymers. *Recent Pat Drug Deliv Formul.* 2010;4(2):114–28.
169. Kamaly N, Yameen B, Wu J, Farokhzad OC. Degradable Controlled-Release Polymers and Polymeric Nanoparticles: Mechanisms of Controlling Drug Release. *Chem Rev.* 2016;24;116(4):2602–63.
170. Han FY, Thurecht KJ, Whittaker AK, Smith MT. Bioerodable PLGA-based microparticles for producing sustained-release drug formulations and strategies for improving drug loading. *Front Pharmacol.* 2016;7:1–11.
171. Danhier F, Ansorena E, Silva JM, Coco R, Le Breton A, Préat V. PLGA-based nanoparticles: An overview of biomedical applications. *J Control Release.* 2012;161(2):505–22.
172. Nagarwal RC, Kant S, Singh PN, Maiti P, Pandit JK. Polymeric nanoparticulate system: A potential approach for ocular drug delivery. *J Control Release.* 2009;136(1):2–13.
173. Kumari A, Yadav SK, Yadav SC. Biodegradable polymeric nanoparticles based drug delivery systems. *Colloids Surfaces B Biointerfaces.* 2010;75(1):1–18.
174. Kamaly N, Xiao Z, Valencia PM, Radovic-Moreno AF, Farokhzad OC. Targeted polymeric therapeutic nanoparticles: design, development and clinical translation. *Chem Soc Rev.* 2012;41(7):2971.
175. Krasia-Christoforou T, Georgiou TK. Polymeric theranostics: using polymer-based systems for simultaneous imaging and therapy. *J Mater Chem B.* 2013;1(24):3002.
176. Owens DE, Peppas NA. Opsonization, biodistribution, and pharmacokinetics of polymeric nanoparticles. *Int J Pharm.* 2006;307(1):93–102.
177. Hans M., Lowman A. Biodegradable nanoparticles for drug delivery and targeting. *Curr Opin Solid State Mater Sci.* 2002;6(4):319–27.
178. Fessi H, Puisieux F, Devissaguet JP, Ammoury N, Benita S. Nanocapsule formation by

- interfacial polymer deposition following solvent displacement. *Int J Pharm.* 1989;55(1):R1–4.
179. Cañadas C, Alvarado H, Calpena AC, Silva AM, Souto EB, Garcia ML, et al. *In vitro*, *ex vivo* and *in vivo* characterization of PLGA nanoparticles loading pranoprofen for ocular administration. *Int J Pharm.* 2016;511(2):719–27.
180. Patel A, Khanna S, Xavier GK, Khanna K, Goel B. Polymeric Nano-Particles for Tumor Targeting – A Review. *Int J Drug Dev Res.* 2017;9:50–9.
181. Lin P-C, Lin S, Wang PC, Sridhar R. Techniques for physicochemical characterization of nanomaterials. *Biotechnol Adv.* 2014;32(4):711–26.
182. van der Vossen AC, van der Velde I, Smeets OSNM, Postma DJ, Eckhardt M, Vermes A, et al. Formulating a poorly water soluble drug into an oral solution suitable for paediatric patients; lorazepam as a model drug. *Eur J Pharm Sci.* 2017;100:205–10.
183. van der Vossen AC, van der Velde I, Smeets OSNM, Postma DJ, Vermes A, Koch BCP, et al. Design and stability study of an oral solution of amlodipine besylate for pediatric patients. *Eur J Pharm Sci.* 2016;92:220–3.
184. Abrego G, Alvarado H, Souto EB, Guevara B, Bellowa LH, Parra A, et al. Biopharmaceutical profile of pranoprofen-loaded PLGA nanoparticles containing hydrogels for ocular administration. *Eur J Pharm Biopharm.* 2015;95:261–70.
185. Abrego G, Alvarado H, Souto EB, Guevara B, Bellowa LH, Garduño ML, et al. Biopharmaceutical profile of hydrogels containing pranoprofen-loaded PLGA nanoparticles for skin administration: *In vitro*, *ex vivo* and *in vivo* characterization. *Int J Phar.* 2016;501(1–2):350–61.
186. Mallandrich M, Fernández-Campos F, Clares B, Halbaut L, Alonso C, Coderch L, et al. Developing Transdermal Applications of Ketorolac Tromethamine Entrapped in Stimuli Sensitive Block Copolymer Hydrogels. *Pharm Res.* 2017;34(8):1728–40.
187. Sanz R, Clares B, Mallandrich M, Suñer-Carbó J, Montes MJ, Calpena AC. Development of a mucoadhesive delivery system for control release of doxepin with application in vaginal pain relief associated with gynecological surgery. *Int J Pharm.* 2018;535(1–2):393–401.
188. Beck-Broichsitter M, Rytting E, Lehardt T, Wang X, Kissel T. Preparation of nanoparticles by solvent displacement for drug delivery: A shift in the “ouzo region” upon drug loading. *Eur J Pharm Sci.* 2010;41(2):244–53.
189. Han J, Zhao D, Li D, Wang X, Jin Z, Zhao K. Polymer-based nanomaterials and applications for vaccines and drugs. *Polymers.* 2018;10(1):1–14.
190. El-Say KM, El-Sawy HS. Polymeric nanoparticles: Promising platform for drug delivery. *Int J Pharm.* 2017;528(1–2):675–91.
191. Kreuter J. Drug delivery to the central nervous system by polymeric nanoparticles: What do we know?. *Adv Drug Deliv Rev.* 2014;71:2–14.
192. Guo Y, Terazzi E, Seemann R, Fleury JB, Baulin VA. Direct proof of spontaneous translocation of lipid-covered Hydrophobic nanoparticles through a phospholipid bilayer. *Sci Adv.* 2016;2(11):38–40.
193. Vega E, Gamisans F, García ML, Chauvet A, Lacoulonche F, Egea MA. PLGA Nanospheres for the Ocular Delivery of Flurbiprofen: Drug Release and Interactions. *J Pharm Sci.* 2008;97:5306–17.

194. Abrego G, Alvarado HL, Egea MA, Gonzalez-Mira E, Calpena AC, Garcia ML. Design of nanosuspensions and freeze-dried PLGA nanoparticles as a novel approach for ophthalmic delivery of pranoprofen. *J Pharm Sci.* 2014;103(10):3153–64.
195. Ramos Yacasi GR, García Lopéz ML, Espina García M, Parra Coca A, Calpena Campmany AC. The influence of freeze drying and γ -irradiation in pre-clinical studies of flurbiprofen polymeric nanoparticles for ocular delivery using D-(+)-trehalose and polyethylene glycol. *Int J Nanomedicine.* 2016;11:4093–106.
196. Abdelhalim MAK. The rheological properties of different GNPs. *Lipids Health Dis.* 2012;11(1):1–5.
197. Parra A, Mallandrich M, Clares B, Egea MA, Espina M, García ML, et al. Design and elaboration of freeze-dried PLGA nanoparticles for the transcorneal permeation of carprofen: Ocular anti-inflammatory applications. *Colloids Surfaces B Biointerfaces.* 2015;136:935–43.
198. Sánchez-López E, Egea MA, Cano A, Espina M, Calpena AC, Ettcheto M, et al. PEGylated PLGA nanospheres optimized by design of experiments for ocular administration of dexibuprofen-in vitro, ex vivo and in vivo characterization. *Colloids Surfaces B Biointerfaces.* 2016;145:241–50.
199. Gonzalez-pizarro R, Silva-abreu M, Calpena AC, Egea A, Espina M, García ML. Development of Fluorometholone-loaded PLGA Nanoparticles for Treatment of Inflammatory Disorders of Anterior and Posterior Segments of the Eye. *Int J Pharm.* 2018.
200. Niwa T, Takeuchi H, Hino T, Kunou N, Kawashima Y. Preparations of biodegradable nanospheres of water-soluble and insoluble drugs with D,L-lactide/glycolide copolymer by a novel spontaneous emulsification solvent diffusion method, and the drug release behavior. *J Control Release.* 1993;25(1):89–98.
201. Sugita M, Kataoka M, Sugihara M, Takeuchi S, Yamashita S. Effect of Excipients on the Particle Size of Precipitated Pioglitazone in the Gastrointestinal Tract: Impact on Bioequivalence. *AAPS J.* 2014;16(5):1119–27.
202. Krishnaiah YSR, Raju V, Shiva Kumar M, Rama B, Raghumurthy V, Ramana Murthy K V. Studies on optimizing in vitro transdermal permeation of ondansetron hydrochloride using nerodilol, carvone, and limonene as penetration enhancers. *Pharm Dev Technol.* 2008;13(3):177–85.
203. Resende AP, Silva B, Braz BS, Nunes T, Gonçalves L, Delgado E. Ex vivo permeation of erythropoietin through porcine conjunctiva, cornea, and sclera. *Drug Deliv Transl Res.* 2017 Oct 21;7(5):625–31.
204. Araújo J, Garcia ML, Mallandrich M, Souto EB, Calpena AC. Release profile and transscleral permeation of triamcinolone acetonide loaded nanostructured lipid carriers (TA-NLC): *In vitro* and *ex vivo* studies. *Nanomedicine Nanotechnology, Biol Med.* 2012;8(6):1034–41.
205. Wen HE, Hao J, Li SK. Characterization of Human Sclera Barrier Properties for Transscleral Delivery of Bevacizumab and Ranibizumab. *J Pharm Sci.* 2013;102(3):892–903.
206. Khan AR, Liu M, Khan MW, Zhai G. Progress in brain targeting drug delivery system by nasal route. *J Control Release.* 2017;268 :364–89.
207. Lochhead JJ, Thorne RG. Intranasal delivery of biologics to the central nervous system. *Adv Drug Deliv Rev.* 2012;64(7):614–28.

208. Parra A, Clares B, Rosselló A, Garduño-Ramírez ML, Abrego G, García ML, et al. Ex vivo permeation of carprofen from nanoparticles: A comprehensive study through human, porcine and bovine skin as anti-inflammatory agent. *Int J Pharm.* 2016;501(1–2):10–7.
209. Draize, J; Woodard, G; Calvery H. Methods for the study of irritation and toxicity of substances applied topically to the skin and mucous membranes. *J Pharmacol Exp Ther.* 1944;82(3):377–90.
210. Vasconcelos A, Vega E, Pérez Y, Gómara MJ, García ML, Haro I. Conjugation of cell-penetrating peptides with poly(Lactic-co-glycolic acid)-polyethylene glycol nanoparticles improves ocular drug delivery. *Int J Nanomedicine.* 2015;10:609–31.
211. Doktorovova S, Souto EB, Silva AM. Nanotoxicology applied to solid lipid nanoparticles and nanostructured lipid carriers - A systematic review of in vitro data. *Eur J Pharm Biopharm.* 2014;87(1):1–18.
212. Fangueiro JF, Andreani T, Egea MA, Garcia ML, Souto SB, Silva AM, et al. Design of cationic lipid nanoparticles for ocular delivery: Development, characterization and cytotoxicity. *Int J Pharm.* 2014;461(1–2):64–73.
213. Sánchez-López E, Ettcheto M, Egea MA, Espina M, Calpena AC, Folch J, et al. New potential strategies for Alzheimer's disease prevention: pegylated biodegradable dexibuprofen nanospheres administration to APP^{swe}/PS1^{dE9}. *Nanomedicine Nanotechnology, Biol Med.* 2017;13(3):1171–82.
214. Neves AR, Queiroz JF, Weksler B, Romero IA, Couraud P-O, Reis S. Solid lipid nanoparticles as a vehicle for brain-targeted drug delivery: two new strategies of functionalization with apolipoprotein E. *Nanotechnology.* 2015 Dec 11;26(49):495103.
15. Wohlfart S, Gelperina S, Kreuter J. Transport of drugs across the blood–brain barrier by nanoparticles. *J Control Release.* 2012;161(2):264–73.
216. Pardridge WM. Drug transport across the blood-brain barrier. *J Cereb Blood Flow Metab.* 2012;32(11):1959–72.
217. Mastrofrancesco A, Kovacs D, Sarra M, Bastonini E, Cardinali G, Aspite N, et al. Preclinical Studies of a Specific PPAR γ Modulator in the Control of Skin Inflammation. *J Invest Dermatol.* 2014;134(4):1001–11.
218. Jiang Y, Thakran S, Bheemreddy R, Ye EA, He H, Walker RJ, et al. Pioglitazone normalizes insulin signaling in the diabetic rat retina through reduction in tumor necrosis factor and suppressor of cytokine signaling 3*. *J Biol Chem.* 2014;289(38):26395–405.
219. Searcy JL, Phelps JT, Pancani T, Kadish I, Popovic J, Anderson KL, et al. Long-Term Pioglitazone Treatment Improves Learning and Attenuates Pathological Markers in a Mouse Model of Alzheimer's Disease. *J Alzheimer's Dis.* 2012;30:943–61.
220. Mandrekar-Colucci S, Karlo JC, Landreth GE. Mechanisms Underlying the Rapid Peroxisome Proliferator-Activated Receptor- γ -Mediated Amyloid Clearance and Reversal of Cognitive Deficits in a Murine Model of Alzheimer's Disease. *J Neurosci.* 2012; 25;32(30):10117–28.
221. Chen J, Li S, Sun W, Li J. Anti-diabetes drug pioglitazone ameliorates synaptic defects in AD transgenic mice by inhibiting cyclin-dependent kinase5 activity. *PLoS One.* 2015;10(4):1–12.
222. Yin Q, Pei J, Xu S, Luo D, Dong S, Sun M-H, et al. Pioglitazone Improves Cognitive Function via Increasing Insulin Sensitivity and Strengthening Antioxidant Defense System in Fructose-Drinking Insulin Resistance Rats. Kline AE, editor. *PLoS One.* 2013;

- 20;8(3):e59313.
223. Papadopoulos P, Rosa-Neto P, Rochford J, Hamel E. Pioglitazone Improves Reversal Learning and Exerts Mixed Cerebrovascular Effects in a Mouse Model of Alzheimer's Disease with Combined Amyloid- β and Cerebrovascular Pathology. Ginsberg SD, editor. PLoS One. 2013;18;8(7):e68612.
224. Fernandez-Martos CM, Atkinson RAK, Chuah MI, King AE, Vickers JC. Combination treatment with leptin and pioglitazone in a mouse model of Alzheimer's disease. Alzheimer's Dement Transl Res Clin Interv. 2017;3(1):92–106.